Univerzita Karlova

Přírodovědecká fakulta

Studijní program: Fyzikální chemie



Mgr. Martin Dvořák

Matematické modelování lineárních a nelineárních jevů v kapilární elektroforéze

Mathematical modelling of linear and nonlinear phenomena in capillary electrophoresis

Disertační práce

Vedoucí disertační práce: Mgr. Pavel Dubský, PhD.

Praha, 2019

Prohlášení:

Prohlašuji, že jsem závěrečnou práci zpracoval samostatně a že jsem uvedl všechny použité informační zdroje a literaturu. Tato práce ani její podstatná část nebyla předložena k získání jiného nebo stejného akademického titulu.

Práce je postavena na čtyřech původních odborných publikacích a dvou přehledových odborných publikacích, jejichž jsem spoluautorem. V rámci své disertační práce jsem se věnoval zejména matematickému popisu studovaných systémů a teoretickým výpočtům. Můj podíl činí přibližně 2/3 na publikacích II, III, V a VI a 1/3 na publikacích I a IV.

V Praze dne ……. Podpis……..

Poděkování

Na tomto místě bych rád poděkoval svému školiteli Mgr. Pavlovi Dubskému, PhD. a konzultantovi prof. RNDr. Bohuslavu Gašovi, CSc. za jejich cenné rady, konzultace a připomínky při psaní této disertační práce.

Klíčová slova

kapilární zónová elektroforéza, afinitní kapilární elektroforéza, lineární teorie elektromigrace, elektromigrační disperze, rozlišení píků, matematické modelování

Keywords

capillary zone electrophoresis, affinity capillary electrophoresis, linear theory of electromigration, electromigration dispersion, peak resolution, mathematical modelling

Abstrakt

Kapilární elektroforéza je jedna z předních analytických separačních metod. V současné době existuje řada počítačových programů, které jsou schopny předpovědět výsledek elektroforetického experimentu. Jde jednak o programy založené na numerickém řešení příslušných rovnic kontinuity a rovnic chemické rovnováhy a jednak o programy založené na aproximativních modelech kapilární elektroforézy. Programy z první skupiny jsou použitelné pro širokou škálu módů kapilární elektroforézy a poskytují přesné řešení. Jejich nevýhodou je však jejich značná časová náročnost. Aproximativní modely naopak dávají výsledek téměř okamžitě a navíc poskytují teoretické vztahy užitečné při optimalizaci separační metody.

Tato disertační práce se zaměřuje na vylepšení a rozšíření oblasti platnosti stávajících aproximativních modelů kapilární elektroforézy. V rámci této práce je představen model vhodný pro plnohodnotný popis kapilární elektrokinetické chromatografie. Tento model je implementován do programu PeakMaster 6. Dále je pozornost věnována nelineárnímu modelu elektromigrace bez difúze. Tento model umožňuje velmi dobrý popis elektromigrační disperze včetně efektů spojených se vzájemnou interakcí mezi píky. Činí tak ovšem na úkor úplného zanedbání difúze. V této práci je nelineární model elektromigrace bez difúze formulován pro systémy obsahující libovolný počet složek a je uvedeno jeho analytické řešení pro systémy obsahující dva komigrující analyty. Model poskytuje teoretické vysvětlení pro řadu charakteristických tvarových deformací, ke kterým dochází při komigraci dvou analytů. Nelineární model elektromigrace bez difúze také poskytuje odpověď na otázku, zda a jakým způsobem je migrační čas analytů ovlivněn jejich komigrací v počáteční fázi separace.

Předkládaná disertační práce se rovněž věnuje procesu vyhodnocení experimentálních elektroferogramů. Je navržen parametr, který správně kvantifikuje rozsah separace dvojice píků v případě, kdy jsou píky výrazně deformovány nebo se podstatně liší svou plochou. Kapilární elektroforéza je často využívaná pro měření fyzikálně-chemických vlastností látek, jako jsou například konstanty stability komplexů. Primární měřenou veličinou při těchto měřeních bývá efektivní elektroforetická pohyblivost látky podílející se na tvorbě příslušného komplexu, respektive její migrační čas. V rámci této práce je navržen postup, jak určit migrační čas příslušející píku, který byl zdeformován elektromigrační disperzí, bez nutnosti provádět nelineární regresi.

Abstract

Capillary electrophoresis is one of the prominent analytical separation methods. Currently, many computer programs exist which are able to predict the result of an electrophoretic experiment. Firstly, there are programs based on numerical solving of corresponding continuity equations and equations of chemical equilibria. Secondly, there are programs based on approximative models of capillary electrophoresis. Programs belonging to the first group are applicable to a wide range of modes of capillary electrophoresis and provide a precise solution. Their disadvantage is though a considerable time demand. On the other hand, the approximative models give the results almost immediately and, in addition, provide some theoretical relationships which are useful for optimization of the separation process.

This dissertation thesis is focused on improvement and extension of validity of existing approximative models of capillary electrophoresis. As a part of this thesis, a model capable of a full-blown description of capillary electrokinetic chromatography is introduced. This model is implemented into program PeakMaster 6. The attention is also paid to a nonlinear model of electromigration without diffusion. This model enables a very good description of electromigration dispersion including effects related to mutual interaction between peaks. However, it does so at the expense of total neglection of diffusion. In this thesis, the nonlinear model of electromigration without diffusion is formulated for systems consisting of any number of constituents, and its analytical solution is presented in the case of two co-migrating analytes. The model provides a theoretical explanation of several characteristic shape deformations which occur due to the co-migration of analytes. The nonlinear model of electromigration without diffusion also answers the question if and in which way the migration time of analytes is influenced by their co-migration in the early stage of the separation process.

The presented dissertation thesis also pays attention to the process of evaluation of experimental electropherograms. A parameter is introduced which quantifies correctly the extent of separation of a pair of peaks when the peaks are substantially distorted or differ significantly in their area. Capillary electrophoresis is often used to determine physical-chemical properties of chemical species such as complexation constants. Then the primarily measured quantity is usually the effective electrophoretic mobility of the particular species which participates in the complex formation, respectively its migration

time. In this thesis, an approach is suggested how to determine the migration time of a peak distorted by electromigration dispersion without any need for nonlinear regression.

Obsah

Seznam použitých zkratek a symbolů **9**

1 Úvod **14**

1.1 Lineární teorie elektromigrace 14

1.2 Aproximativní nelineární teorie elektromigrace 18

1.3 Rozšíření modelu NLTEM o komplexační rovnováhy 20

1.4 Nelineární model elektromigrace bez difúze 21

1.5 Harrhoff – Van der Lindeho funkce 23

1.6 Rozlišení píků v kolonových a kapilárních separačních metodách 23

2 Cíle disertační práce **26**

3 Experimentální podmínky **27**

4 Výsledky a diskuze **28**

4.1 Afinitní kapilární elektroforéza: *Publikace I* 28

4.2 Zobecnění vztahu pro rozlišení dvou analytů: *Publikace II* 50

4.3 Určení parametrů Haarhoff-Van der Lindeho funkce z geometrických vlastností píku: *Publikace III* 64

4.5 Zobecněný model lineární teorie elektromigrace a jeho aplikace na elektrokinetickou chromatografii: *Publikace IV* 75

4.6 Nelineární model elektromigrace bez difúze a dynamika evoluce píků analytů v CZE: *Publikace V, VI* 90

5 Závěr **150**

Přílohy **152**

Seznam publikací **152**

Seznam konferenčních příspěvků **154**

Literatura **155**

Seznam použitých zkratek a symbolů

a	parametr charakterizující míru a povahu elektromigrační disperze v rámci modelu NEM
a_0	parametr HVL funkce mající význam plochy píku v časové doméně
a_1	parametr HVL funkce mající význam migračního času píku
a_2	parametr HVL funkce charakterizující rozšiřování píku v důsledku difúze
a_3	parametr HVL funkce charakterizující míru asymetrie píku
A_i	plocha postupné vlny w_i, respektive plocha *i*-tého píku
A_{12}	plocha vzájemného překryvu píků 1 a 2
BGE	základní elektrolyt (background electrolyte)
c_A	koncentrace analytu A
$c_{(g)}$	koncentrace iontové formy g
c_i	analytická koncentrace *i*-té složky
$\tilde{c}_i$	rozdíl aktuální koncentrace *i*-té složky a její koncentrace v neporušeném základním elektrolytu (porucha koncentrace *i*-té složky)
$\tilde{c}_i^{in}$	počáteční porucha koncentrace *i*-té složky
c_i^{BGE}	koncentrace *i*-té složky v základním elektrolytu
c_B^{BGE}	koncentrce koiontu analytu v základním elektrolytu
$c_{i,z}$	koncentrace iontové formy *i*-té složky, která má nábojové číslo z
c_{mo}	koncentrace analytu v mobilní fázi
c_{st}	koncentrace analytu ve stacionární fázi
c_D^0	počáteční koncentrace analytu D
c_S^0	počáteční koncentrace analytu S
CZE	kapilární zónová elektroforéza (capillary zone electrophoresis)
$\mathbb{D}$	matice shrnující příspěvky difúzních látkových toků do rovnic kontinuity v rámci modelu NLTEM
$\mathbb{D}_d$	pomocná matice sdružující v sobě difúzní koeficienty všech iontových forem v elektroforetickém systému

$d_d(i,h)$	prvek matice $\mathbb{D}_d$ stojící v i-tém řádku a h-tém sloupci
$D_{(h)}$	difúzní koeficient iontové formy h
$\delta(x)$	Diracova delta funkce
δ_i	efektivní difúzní koeficient postupné vlny w_i
E_{BGE}	intenzita elektrického pole v základním elektrolytu
EKC	elektrokinetická chromatografie (elektrokinetic chromatography)
EOF	elektroosmotický tok (electroosmotic flow)
ϵ	pórovitost náplně chromatografické kolony
F	Faradayova konstanta
f_q^{-1}	funkce popisující vztah mezi parametrem deformace q a parametrem HVL funkce a_3
H	výška píku
HVL	Haarhoff-Van der Lindeho funkce
HVLR	zobecnění HVL funkce pro počáteční podmínku ve tvaru obdélníkové zóny
j	proudová hustota
$J_{(g)}$	látkový tok iontové formy g
$J_{i,z}$	látkový tok iontové formy i-té složky, která má nábojové číslo z
$J_{i,z(em)}$	elektromigrační příspěvek k látkovému toku $J_{i,z}$
K_α	koeficient udávající vztah mezi šířkou píku $s_{(\alpha)}$, migračním časem maxima píku t_M a parametrem HVL funkce a_1
K_{ad}	adsorpční konstanta
KRF	Kohlrauschova regulační funkce (Kohlrausch regulating function)
κ	měrná elektrická vodivost
κ_{BGE}	měrná elektrická vodivost základního elektrolytu
κ_j	aproximace parciální derivace měrné elektrické vodivosti podle koncentrace j-tého analytu
κ_A	aproximace parciální derivace měrné elektrické vodivosti podle koncentrace analytu A

L_α	koeficient úměrnosti mezi šířkou píku $s_{(\alpha)}$ a parametrem HVL funkce a_2
L	počáteční šířka zóny dávkovaného vzorku
Λ_0	diagonální matice sestavená z vlastních čísel matice $\mathbb{M}_0$
$\lambda_{0,i}$	*i*-té vlastní číslo matice $\mathbb{M}_0$ (nazývané též *i*-tá eigenmobilita)
LTEM	lineární teorie elektromigrace (linear theory of electromigration)
$\mathbb{M}$	matice vystupující v maticovém zápisu elektromigračních rovnic kontinuity
$\mathbb{M}_0$	konstantní matice aproximující matici $\mathbb{M}$ v modelu LTEM
MBE	elektroforéza s pohyblivým rozhraním (moving boundary electrophoresis)
$\mathbb{M}_\mu$	pomocná matice sdružující v sobě elektroforetické mobility všech iontových forem v elektroforetickém systému a jejich závislost na iontové síle
$\mathbb{M}_\partial$	komunikační matice udávající vztah mezi koncentracemi jednotlivých složek a jednotlivých iontových forem v elektroforetickém systému
$m_\mu(i,h)$	prvek matice $\mathbb{M}_\mu$ stojící v *i*-tém řádku a *h*-tém sloupci
$m_\partial(h,q)$	prvek matice $\mathbb{M}_\partial$ stojící v *h*-tém řádku a *q*-tém sloupci
μ_A	elektroforetická mobilita analytu A
μ_B	elektroforetická mobilita koiontu analytu
μ_R	elektroforetická mobilita protiiontu analytu
$\mu_{\mathrm{eff},i}$	efektivní elektroforetická mobilita *i*-tého analytu
$\mu_{(g)}$	elektroforetická mobilita iontové formy g
$\mu_{i,z}$	elektroforetická mobilita iontové formy *i*-té složky, která má nábojové číslo z
N	počet složek elektroforetického systému
n_i	minimální nábojové číslo, kterého nabývá některá iontová forma *i*-té složky
N_A	počet analytů v elektroforetickém systému
N_b	koncentrace vazebných míst pro analyt ve stacionární fázi
NEM	nelineární model elektromigrace bez difúze (nonlinear electromigration model)
NLTEM	aproximativní nelineární teorie elektromigrace (nonlinear theory of electromigration)
Ω	překryvový integrál dvojice píků

P	relativní překryv dvojice píků
${}^{2}P_{1}$	relativní překryv dvojice píků 1 a 2 vztažený k ploše píku 1
${}^{1}P_{2}$	relativní překryv dvojice píků 1 a 2 vztažený k ploše píku 2
p_i	maximální nábojové číslo, kterého nabývá některá iontová forma *i*-té složky
ψ_i	parametr HVL funkce určující míru a typ asymetrie píku
q	parametr charakterizující deformaci píku na základě jeho geometrických vlastností
$\mathbb{Q}_L$	pomocná transformační matice
$\mathbb{Q}_R$	pomocná transformační matice
$r_{(g)(h)}$	pomocný koeficient použitý při konstrukci matice $\mathbb{M}_\mu$
R_Ω	ekvivalentní rozlišení definované na bázi překryvového integrálu Ω
R_P	ekvivalentní rozlišení definované na bázi relativního překryvu P
R_S	rozlišení dvojice identických píků s gaussovským koncentračním profilem
$s_{(\alpha)}$	šířka píku ve výšce rovnající se α-frakci jeho celkové výšky
$s_{L(\alpha)}$	levá dílčí šířka píku ve výšce rovnající se α-frakci jeho celkové výšky
$s_{R(\alpha)}$	pravá dílčí šířka píku ve výšce rovnající se α-frakci jeho celkové výšky
s_i	šířka *i*-tého píku při základní linii
$S_{(D)}$	šokové rozhraní analytu D
$S_{(S)}$	šokové rozhraní analytu S
S_X	relativní směrnice rychlosti analytu
σ	standardní směrodatná odchylka píku s Gaussovým rozdělením koncentračního profilu
Σ_{D}	parametr charakterizující intenzitu displacement efektu
Σ_{TA}	parametr charakterizující intenzitu tag along efektu
t	čas
t_i	retenční čas *i*-tého píku
t_{M}	migrační čas maxima píku
T_{USP}	parametr charakterizující míru asymetrie píku definovaný dle amerického lékopisu (*U.S. Pharmacopeia tailing factor*)
u	rychlost mobilní faze

$v_{0,i}$	rychlost šíření postupné vlny w_i kapilárou (též rychlost i-tého analytu při jeho nekonečném zředění)
v_A	rychlost analytu A při jeho nekonečném zředění
$v_{\mathrm{eff},i}$	efektivní rychlost i-tého analytu při jeho nekonečném zředění
$v_{\mathrm{eff},A}$	efektivní rychlost analytu A při jeho nekonečném zředění
$\nu_{(g)i}$	stechiometrický koeficient i-té složky v iontové formě g
w_i	funkce popisující i-tou postupnou vlnu šířící se kapilárou po vložení elektrického napětí
w_i^{in}	počáteční tvar funkce w_i
ΔW_i	počáteční výška funkce w_i
x	prostorová souřadnice probíhající podél separační kapiláry
X	množina všech iontů a neutrálních molekul přítomných v elektroforetickém systému
x_{det}	vzdálenost detektoru od počátku kapiláry
z	nábojové číslo
$z_{(h)}$	nábojové číslo iontové formy h

1 Úvod

1.1 Lineární teorie elektromigrace

Pohyb iontů v kapalných roztocích v důsledku působení vnějšího stacionárního elektrického pole je popsán rovnicemi kontinuity, jež jsou matematickým vyjádřením zákona zachování hmoty. Rovnice kontinuity byly formulovány již v roce 1897 Kohlrauschem [1]. Uvažujeme-li pohyb iontů pouze v jednom rozměru, mají rovnice kontinuity pro elektroforetický systém tvořený N složkami tvar:

$$\frac{\partial c_i(x,t)}{\partial t} = -\sum_{z=n_i}^{p_i} \frac{\partial J_{i,z}(x,t)}{\partial x} \qquad i = 1, \dots, N \qquad (1)$$

kde t je čas, x je prostorová souřadnice probíhající podél separační kapiláry, c_i je celková (analytická) koncentrace i-té složky, p_i a n_i je maximální a minimální nábojové číslo, kterého mohou iontové formy i-té složky nabývat a $J_{i,z}$ je látkový tok té iontové formy i-té složky, která má nábojové číslo z. Celková koncentrace i-té složky je svázána s koncentracemi $c_{i,z}$ jejích iontových forem s nábojovými čísly z rovnicí látkové bilance.

$$c_i = \sum_{z=n_i}^{p_i} c_{i,z} \qquad (2)$$

Látkové toky v rovnici (1) v sobě obecně zahrnují také reakční členy, které popisují ustavování chemických rovnováh mezi jednotlivými iontovými formami složek elektroforetického systému. Za předpokladu, že doba potřebná pro ustavení chemických rovnováh je mnohem kratší než typická časová škála charakterizující elektroforetický pobyb píků v kapiláře [2,3][1], je možné reakční členy v látkových tocích nahradit algebraickými rovnicemi, které popisují okamžité ustavení rovováhy na dané prostorové souřadnici systému. Okamžitá koncentrace každé iontové formy přítomné v elektroforetickém systému je potom funkcí pouze okamžitých celkových koncentrací všech složek.

[1] Za typickou časovou škálu elektroforetického pohybu píků v kapiláře můžeme považovat dobu, během níž pík urazí vzdálenost rovnou své šířce.

$$c_{i,z}(x,t) = c_{i,z}\big(c_1(x,t), \ldots, c_N(x,t)\big) \tag{3}$$

Kvůli silně nelineární povaze rovnic kontinuity (1) nebylo dodnes nalezeno jejich analytické řešení. Pro nalezení alespoň přibližného analytického řešení je nutné uplatnit některé zjednodušující předpoklady. Zjednodušení vycházející ze specifického experimentálního uspořádání kapilární zónové elektroforézy (CZE) dala vzniknout modelu, který je dnes znám jako lineární teorie elektromigrace (LTEM) [4-6]. V rámci modelu LTEM je v rovnicích kontinuity uvažována pouze elektromigrační část látkového toku $J_{i,z(em)}$ a je zcela zanedbána difúze:

$$J_{i,z(em)}(x,t) = \frac{j}{\kappa(x,t)} \mu_{i,z} c_{i,z}(x,t) \tag{4}$$

kde j je proudová hustota v kapiláře, $\kappa(x,t)$ je měrná elektrická vodivost v místě x uvnitř kapiláry a v čase t, $\mu_{i,z}$ je elektroforetická pohyblivost iontové formy i-té složky s nábojovým číslem z a $c_{i,z}$ je koncentrace této iontové formy. Zanedbání difúze umožňuje přepsat rovnice kontinuity (1) do přehledného maticového zápisu:

$$\frac{\partial \vec{c}(x,t)}{\partial t} = -\frac{j}{\kappa_{\mathrm{BGE}}} \mathbb{M}\big(\vec{c}(x,t)\big) \frac{\partial \vec{c}(x,t)}{\partial x} \tag{5}$$

kde κ_{BGE} je měrná elektrická vodivost základního elektrolytu (BGE). Prvky matice $\mathbb{M}\big(\vec{c}(x,t)\big)$, která vystupuje v rovnici (5), jsou obecně funkcí koncentrací všech složek elektroforetického systému a zahrnují v sobě též rovnovážné konstanty popisující acidobazické rovnováhy mezi jednotlivými iontovými formami složek elektroforetického systému včetně iontů H_3O^+ a OH^-. Další zjednodušení uplatněná v rámci modelu LTEM jsou založena na skutečnosti, že v CZE je úzká zóna vzorku dávkována do kapiláry naplněné homogenním roztokem BGE. Řešení modelu LTEM navíc předpokládá, že koncentrace jednotlivých složek ve vzorku se jen málo liší od svých hodnot v BGE. Definujeme-li poruchy koncentrací $\tilde{c}_i(x,t)$ jako rozdíl aktuální koncentrace i-té složky $c_i(x,t)$ a její koncentrace v BGE c_i^{BGE},

$$\tilde{c}_i(x,t) = c_i(x,t) - c_i^{\mathrm{BGE}} \tag{6}$$

je poslední tvrzení ekvivalentní podmínce $\tilde{c}_i(x,t) \cong 0$. V případě, že *i*-tá složka není přítomna v BGE, platí $c_i^{\mathrm{BGE}} = 0$ a $\tilde{c}_i(x,t) = c_i(x,t)$.

Poppe [7,8] jako první ukázal, že toto experimentální uspořádání CZE umožňuje provést linearizaci rovnic kontinuity (1). Štědrý a kol. následně v práci [4] proces linearizace podrobně rozpracovali a prezentovali s využitím moderního matematického zápisu. Klíčovou myšlenkou linearizace je představa, že na dávkovaný vzorek je možné pohlížet jako na malou poruchu v jinak homogenním prostředí BGE. V prvním přiblížení je potom možné v matici $\mathbb{M}\big(\vec{c}(x,t)\big)$ dosadit za koncentrace všech složek jejich koncentrace v neporušeném BGE, čímž se tato matice původně závislá na proměnných x a t změní na konstantní matici $\mathbb{M}_0 \equiv \mathbb{M}(\vec{c}^{\mathrm{BGE}})$. Autoři práce [4] ukázali, že po aplikaci teorému o diagonalizaci matic na matici $\mathbb{M}_0$ a přechodu od koncentrací $c_i(x,t)$ k novým vhodně zvoleným funkcím $w_i(x,t)$ se původně provázaná soustava diferenciálních rovnic (5) rozpadne na *N* nezávislých diferenciálních rovnic pro jednotlivé funkce $w_i(x,t)$.

$$\frac{\partial \vec{w}(x,t)}{\partial t} = -\frac{j}{\kappa_{\mathrm{BGE}}} \Lambda_0 \frac{\partial \vec{w}(x,t)}{\partial x} \tag{7}$$

Matice Λ_0 vystupující v rovnici (7) je diagonální matice, která má na diagonále vlastní čísla $\lambda_{0,i}$ matice $\mathbb{M}_0$. Jelikož tato vlastní čísla mají fyzikální rozměr elektroforetické mobility, bylo pro ně v práci [4] zavedeno označení eigenmobility (odvozeno od pojmu eigenvalue – vlastní číslo matice). Funkce $c_i(x,t)$, $w_i(x,t)$ a matice $\mathbb{M}_0$, Λ_0 jsou spolu svázány těmito vztahy:

$$\mathbb{M}_0 = \mathbb{Q}_R \, \Lambda_0 \, \mathbb{Q}_L \tag{8}$$

$$\vec{w}(x,t) = \mathbb{Q}_L \times (\vec{c}(x,t) - \vec{c}^{\mathrm{BGE}}) = \mathbb{Q}_L \times \vec{\tilde{c}}(x,t) \tag{9}$$

$\mathbb{Q}_R$ je transformační matice, jejíž řádky jsou tvořeny levými vlastními vektory matice $\mathbb{M}_0$, přičemž vlastní vektor na *i*-tém řádku matice $\mathbb{Q}_R$ odpovídá vlastnímu číslu na *i*-tém řádku matice Λ_0. Matice $\mathbb{Q}_L$ je inverzní maticí k matici $\mathbb{Q}_R$. Řešení rovnic (7) má tvar[4][2]:

[2] Rovnice (7) mají řešení ve tvaru (10) pouze za předpokladu, že všechna nenulová vlastní čísla matice $\mathbb{M}_0$ jsou navzájem různá [4]. Tento předpoklad je v naprosté většině elektroforetických systémů splněn.

$$w_i(x,t) = w_i^{in}\left(x - \frac{j}{\kappa_{\mathrm{BGE}}}\lambda_{0,i}t\right) \tag{10}$$

kde $w_i^{in}(x) = \mathbb{Q}_R \times \tilde{c}_i^{in}(x)$ a $\tilde{c}_i^{in}(x)$ jsou počáteční poruchy koncentrací jednotlivých složek. Z rovnice (10) vyplývá, jaký je význam funkcí $w_i(x,t)$. Každá z funkcí $w_i(x,t)$ představuje vlnu, která se kapilárou šíří rychlostí[3] $v_{0,i} = \frac{j}{\kappa_{\mathrm{BGE}}}\lambda_{0,i}$. Tvar této vlny se v čase nemění a zůstává totožný s jejím počátečním tvarem.

Celkový počet vln, které v kapiláře v důsledku působení vnějšího elektrického pole vzniknou, je roven celkovému počtu složek v elektroforetickém systému[4]. Některé z těchto vln představují píky analytů a jejich eigenmobility jsou rovny efektivní elektroforetické mobilitě příslušného analytu v limitě jeho nekonečného zředění, neboli v situaci, kdy je amplituda vlny analytu nekonečně malá[5]. Jiné vlny jsou tvořeny výhradně poruchami koncentrací složek BGE a jejich eigenmobility jsou funkcí pouze mobilit složek BGE a koncentrací těchto složek v neporušeném BGE. Takovéto vlny se označují jako systémové píky [4]. Model LTEM umí kromě elektroforetických mobilit jednotlivých vln předpovědět též jejich amplitudy, respektive poměr mezi koncentracemi jednotlivých složek v daném píku. V neposlední řadě model LTEM poskytuje alespoň základní představu o reálném tvaru píků analytů, neboť v rámci LTEM je možné určit parametr S_X nazývaný relativní směrnicí rychlosti a definovaný vztahem [9]:

$$S_X = \lim_{c_A \to 0} \frac{\kappa}{v_A}\frac{dv_A}{dc_A} \tag{11}$$

kde c_A je koncentrace příslušného analytu a v_A je jeho rychlost. Znaménko veličiny S_X určuje, zda bude pík analytu v důsledku elektromigrační disperze frontující či tailující. Je-li $S_X = 0$, k elektromigrační disperzi nedochází. Časový vývoj koncentračních profilů jednotlivých píků však model LTEM předpovědět nedokáže, neboť elektromigrační

[3] V podkapitolách 1.4 a 4.6 používáme pro rychlost $v_{0,i}$ označení $v_{\mathrm{eff},i}$ a nazýváme ji efektivní rychlost analytu při jeho nekonečném zředění.

[4] Některé z těchto vln ovšem mohou mít nulovou amplitudu. Tato situace nastane, pokud $w_i^{in}(x) = \mathbb{Q}_R \times \tilde{c}_i^{in}(x) = 0$. Často také dochází k tomu, že se vlny, jejichž elektroforetické mobility jsou si velmi blízké, vzájemně překrývají.

[5] To je pochopitelné, neboť eigenmobility jsou vlastní čísla matice $\mathbb{M}_0$, v níž byly koncentrace všech analytů položeny rovny nule. V kontextu modelů LTEM, NLTEM (podkapitola 1.2) a NEM (podkapitola 1.4) nazýváme analytem každou složku, která je přítomna ve vzorku, ale není přítomna v BGE.

disperse, která je hlavní příčinou deformace píků v průběhu kapilární elektroforézy, je jev ryze nelineární.

1.2 Aproximativní nelineární teorie elektromigrace

V roce 2012 se Hruškovi [10] podařilo rozšířit model LTEM o takový korekční nelineární člen, že rozšířený model, v této disertační práci nazývaný aproximativní nelineární teorie elektromigrace (NLTEM), byl stále analyticky řešitelný. Model NLTEM umožnil předpovídat nejen elektroforetické mobility píků a poměr koncentrací složek v jednotlivých pících, ale také tvary píků. Navíc, narozdíl od modelu LTEM, bere NLTEM v úvahu jak elektromigrační, tak difúzní příspěvek k látkovému toku jednotlivých iontových forem. Postup navržený v rámci modelu NLTEM pro separaci soustavy diferenciálních rovnic (5) je založen na předpokladu, že každý pík se v kapiláře pohybuje zcela nezávisle na ostatních pících. Jinými slovy jsou zanedbány veškeré interakce mezi píky, které se vzájemně překrývají. Přidání korekčního nelineárního členu spočívá v provedení Taylorova rozvoje matice $\mathbb{M}\big(\vec{c}(x,t)\big)$, která vystupuje v soustavě diferenciálních rovnic (5), v bodě $\vec{c}(x,t) = \vec{c}^{\,\mathrm{BGE}}$ a ponechání pouze prvních dvou členů tohoto rozvoje

$$\begin{aligned}\mathbb{M}\big(\vec{c}(x,t)\big) &= \mathbb{M}(\vec{c}^{\,\mathrm{BGE}}) + \sum_{k=1}^{N} \frac{\partial \mathbb{M}(\vec{c}^{\,\mathrm{BGE}})}{\partial c_k}\left(c_k(x,t) - c_k^{\mathrm{BGE}}\right) + \cdots \\ &= \mathbb{M}_0 + \sum_{k=1}^{N} \frac{\partial \mathbb{M}(\vec{c}^{\,\mathrm{BGE}})}{\partial c_k}\tilde{c}_k(x,t) + \cdots\end{aligned} \tag{12}$$

Zanedbání vyšších členů v rozvoji (12) je oprávněné pouze za předpokladu, že poruchy koncentrací $\tilde{c}_k(x,t)$ jsou dostatečně malé. Po provedení rozvoje (12) a doplnění soustavy diferenciálních rovnic (5) o člen, který aproximuje difúzi, získáme následující soustavu diferenciálních rovnic

$$\frac{\partial \vec{c}(x,t)}{\partial t} = -\frac{j}{\kappa_{\mathrm{BGE}}}\left(\mathbb{M}_0 + \sum_{k=1}^{N} \frac{\partial \mathbb{M}(\vec{c}^{\,\mathrm{BGE}})}{\partial c_k}\tilde{c}_k(x,t)\right)\frac{\partial \vec{c}(x,t)}{\partial x} + \mathbb{D}\frac{\partial^2 \vec{c}(x,t)}{\partial x^2} \tag{13}$$

Matice $\mathbb{D}$ byla sestavena z difúzních příspěvků k látkovým tokům. Její detailní vnitřní struktura však nebyla v práci [10] uvedena. Taktéž mnohé aproximace potřebné pro sestavení matice $\mathbb{D}$ byly v práci [10] pouze naznačeny. V práci [10] však Hruška navrhl postup, jak soustavu provázaných diferenciálních rovnic (13) separovat na N nezávislých diferenciálních rovnic, které mají tvar tzv. Burgesovy diferenciální rovnice a jsou analyticky řešitelné.

$$\frac{\partial w_i(x,t)}{\partial x} = -\frac{j}{\kappa_{\mathrm{BGE}}}\left(\lambda_{0,i} + \frac{\partial \lambda_i}{\partial w_i} w_i(x,t)\right)\frac{\partial w_i(x,t)}{\partial x} + \delta_i \frac{\partial^2 w_i(x,t)}{\partial x^2} \quad i = 1, \ldots, N \qquad (14)$$

V diferenciálních rovnicích (14) vystupují postupné vlny $w_i(x,t)$, které jsou stejně jako v modelu LTEM definovány vztahem (9). Kromě eigenmobility $\lambda_{0,i}$, známé již z modelu LTEM, vystupují v rovnicích (14) dva nové parametry, a sice $\frac{\partial \lambda_i}{\partial w_i}$ a δ_i. Derivace $\frac{\partial \lambda_i}{\partial w_i}$ je vyčíslena pro složení odpovídající neporušenému BGE. Součin $\frac{j}{\kappa_{\mathrm{BGE}}}\frac{\partial \lambda_i}{\partial w_i} w_i(x,t)$ potom v prvním přiblížení vyjadřuje odchylku rychlosti *i*-té vlny v čase t a na místě x, kde má vlna výšku $w_i(x,t)$, od limitní hodnoty $v_{0,i}$. Parametr δ_i je možné chápat jako efektivní difúzní koeficient *i*-té vlny, neboť charakterizuje míru, s jakou *i*-tá vlna podléhá difúzi. Matematická vyjádření zmíněných parametrů jsou následující

$$\delta_i = (\mathbb{Q}_L\, \mathbb{D}\, \mathbb{Q}_R)_{i,i} \qquad (15)$$

$$\frac{\partial \lambda_i}{\partial w_i} = \sum_{k=1}^{N} (\mathbb{Q}_R)_{k,i} \left(\mathbb{Q}_R \frac{\partial \lambda_i}{\partial w_i} \mathbb{Q}_L\right)_{i,i} \qquad (16)$$

Řešením rovnic (14) s počáteční podmínkou $w_i^{in}(x) = A_i \delta(x)$, kde $\delta(x)$ je Diracova delta funkce a A_i je plocha *i*-té vlny vyjádřená v jednotkách mol m^{-2}, je takzvaná Haarhoff-Van der Lindeho funkce (HVL) [11]:

$$\mathrm{HVL}_i(x,t) = \frac{A_i}{\sqrt{4\pi\delta_i t}} \frac{\exp\left[-\frac{\left(x - v_{0,i}t\right)^2}{4\delta_i t}\right]}{\psi_i \left\{\frac{1}{\exp(\psi_i) - 1} + \frac{1}{2}\left[1 + \mathrm{erf}\left(\frac{x - v_{0,i}t}{\sqrt{4\delta_i t}}\right)\right]\right\}} \qquad (17)$$

kde parametr ψ_i určuje míru a typ asymetrie HVL píku, tj. zda je pík frontující či tailující. Parametr ψ_i je dán vztahem:

$$\psi_i = -\frac{j}{\kappa_{\mathrm{BGE}}}\frac{\partial \lambda_i}{\partial w_i}\frac{\Delta W_i}{2\delta_i} \tag{18}$$

kde ΔW_i je počáteční výška *i*-té vlny. K empirickému zjištění, že HVL funkce popisuje velmi dobře tvar píků v CZE, pokud jsou tyto píky deformované elektromigrační disperzí, dospěli Erny a kol. ještě před formulací modelu NLTEM [12,13]. Model NLTEM později přinesl teoretické zdůvodnění tohoto pozorování. Samotná HVL funkce byla nicméně odvozena Haarhoffem a Van der Lindem v docela jiných souvislostech již v roce 1966, a to jako řešení neideálního modelu plynové chromatografie za podmínky dávkování velmi malého množství koncentrovaného vzorku [11].

Burgersovy rovnice (14) mají analytické řešení také pro počáteční podmínku ve tvaru pravoúhlé zóny o počáteční šířce L, tj.

$$\begin{aligned} w_i^{in}(x) &= \Delta W_i && \text{pro } x \in \left(-\tfrac{L}{2}, \tfrac{L}{2}\right) \\ w_i^{in}(x) &= 0 && \text{pro } x \notin \left(-\tfrac{L}{2}, \tfrac{L}{2}\right) \end{aligned} \tag{19}$$

Pro řešení s touto počáteční podmínkou bylo v práci [10] zavedeno označení HVLR funkce. Matematický zápis HVLR funkce je již značně komplikovaný (viz vztahy (37) – (41) v práci [10]). Narozdíl od HVL funkce je HVLR funkce schopna lépe vystihnout tvar píků krátce po vložení vnějšího elektrického pole, kdy je ještě částečně zachováno koncentrační plato pocházející z počátečního tvaru dávkované zóny.

1.3 Rozšíření modelu NLTEM o komplexační rovnováhy

Dosud popisované modely LTEM a NLTEM braly v úvahu pouze acidobazické chemické rovnováhy. V práci [14] byla do modelu NLTEM v omezené míře přidána také komplexační rovnováha. Rozšířený model byl proto kromě CZE schopen postihnout také některé speciální případy elektrokinetické chromatografie (EKC). Model se omezil na

komplexační rovnováhu mezi jedním ligandem v BGE a jedním analytem. Jedna z komplexujících složek musí být přítomna pouze ve formě neutrálních molekul, zatímco druhá je silným elektrolytem, a proto je plně disociována či plně protonována a přítomna pouze jako jedna nabitá iontová forma. Dále model předpokládal, že analyt a ligand vytvářejí komplex ve stechiometrickém poměru 1:1 a jiné komplexační rovnováhy, například mezi ligandem a složkami BGE, se neuplatňují. Rozšířený model NLTEM významně přispěl k objasnění mechanismu, kterým interakce mezi analytem a ligandem přispívá k elektromigrační disperzi píku analytu, avšak neumožňoval popis vlivu komplexačních rovnováh na systémové píky či popis systémů se složitějšími komplexačními a acido-bazickými rovnováhami.

Praktický význam aproximativních modelů CZE jako jsou LTEM a zejména NLTEM spočívá ve skutečnosti, že počítačové programy založené na těchto modelech dokáží s uspokojivou přesností předpovědět průběh elektroforetické separace během několika sekund [10] a mohou proto značně usnadnit a urychlit hledání optimálních separačních podmínek před provedením reálného experimentu. Naproti tomu analogický výpočet v programech jako je Simul [15], GENTRANSS [16,17] či SPRESSO [18], které jsou založené na numerickém řešení soustavy rovnic kontinuity (5), trvá obvykle hodiny až několik dní. Model NLTEM navíc poskytuje, alespoň pro některé jednoduché systémy, analytické vztahy pro řadu zajímavých a praktických veličin, jako jsou elektroforetické mobility systémových píků či relativní směrnice rychlosti píků S_X. Model NLTEM je tak velmi užitečný nástroj pro teoretické studium CZE.

1.4 Nelineární model elektromigrace bez difúze

V roce 1979 Mikkers a kol. představili analyticky řešitelný nelineární model CZE [19] založený na odlišných zjednodušujících předpokladech než model NLTEM. Ve zbytku této disertační práce se budeme na tento model odkazovat jako na nelineární model elektromigrace (NEM). V modelu NEM byl, stejně jako v modelu LTEM, zcela zanedbán příspěvek difúze k látkovému toku jednotlivých složek. Autoři práce [19] se dále omezili na elektroforetický systém tvořený výhradně silnými elektrolyty, a to speciálně analytem A a dvěma složkami BGE, B (koion analytu) a R (protiion analytu). Kombinací rovnice kontinuity bez difúzního členu a Kohlrauschovy regulační funkce (KRF) dospěli autoři k následující diferenciální rovnici popisující vývoj koncentračního profilu analytu:

$$\frac{\partial c_A}{\partial t} = -\mu_A E_{\mathrm{BGE}} \frac{\partial}{\partial x}\left(\frac{c_A}{1 - a c_A}\right) \tag{20}$$

kde E_{BGE} je intenzita elektrického pole v neporušeném BGE a a je parametr daný vztahem:

$$a = \frac{1}{c_B^{\mathrm{BGE}}} \frac{(\mu_A - \mu_R)(\mu_B - \mu_A)}{\mu_A(\mu_B - \mu_R)} \tag{21}$$

Ve vztahu (21) jsou μ_A, μ_B a μ_R po řadě elektroforetické mobility analytu, jeho koiontu a protiiontu. c_B^{BGE} je koncentrace koiontu v neporušeném BGE. Pro počáteční podmínku ve tvaru obdélníkové zóny o šířce L má rovnice (20) analytické řešení:

$$c_A(x,t) = \frac{1}{a}\left(1 - \sqrt{\frac{t v_{\mathrm{eff},A} - L}{x - L}}\right) \qquad \text{pro } a > 0 \tag{22}$$

$$c_A(x,t) = \frac{1}{a}\left(1 - \sqrt{\frac{t v_{\mathrm{eff},A}}{x}}\right) \qquad \text{pro } a < 0 \tag{23}$$

kde $v_{\mathrm{eff},A}$ je efektivní rychlost analytu A při jeho nekonečném zředění. Řešení pro koncentrační profil analytu (22) a (23) jsou platná pouze za předpokladu, že se pík analytu pohybuje nezávisle na systémových pících. Na stejném předpokladu je postaven i model NLTEM. V pozdější práci [20] Mikkers ukázal, že diferenciální rovnice analogická rovnici (20) popisuje také vývoj systémových píků, a prezentoval rozšíření modelu NEM na situace, kdy BGE obsahuje dva nebo tři koionty analytu. V práci [19] vystupuje ve vztahu (23) ještě korekční člen, který má za cíl postihnout změnu koncentrace analytu v důsledku jeho zakoncentrování na rozhraní dávkované zóny a neporušeného BGE. Tento člen byl ovšem do vztahu (23) přidán uměle a jeho existence nijak neplyne z diferenciální rovnice (20)[6].

[6] Zakoncentrování analytu na rozhraní dávkované zóny a neporušeného BGE je možné interpretovat jako důsledek interakce mezi píkem analytu a stacionárními systémovými píky, tj. těmi, jejichž mobilita je nulová či blízká nule. Jelikož řešení (23) předpokládá, že pík analytu neinteraguje se systémovými píky, nemůže postihnout jev zakoncentrovávání analytu.

1.5 Harrhoff – Van der Lindeho funkce

V CZE a EKC se často setkáváme s koncentračními profily deformovanými elektromigrační disperzí. Elektromigrační disperze vzniká jako důsledek lokálních změn rychlostí elektroforetického pohybu látek. Tyto změny rychlostí jsou vyvolány změnami pH, vodivosti či přítomností komplexačního činidla v základním elektrolytu [9,12,21]. V kapitole o modelu NLTEM bylo uvedeno, že píky deformované v CZE či EKC elektromigrační disperzí mají tvar velmi dobře popsaný HVL funkcí (17). Projde-li pík ve tvaru HVL funkce (17) detektorem umístěným ve vzdálenosti x_{det} od začátku kapiláry, má časový záznam tohoto píku na elektroferogramu tvar (odvození bylo provedeno autorem této disertační práce):

$$\mathrm{HVL}(x_{\mathrm{det}}, t) \equiv \mathrm{HVL}(t; a_0, a_1, a_2, a_3) = \frac{\frac{a_0}{a_2 a_3 \sqrt{2\pi}} \exp\left[-\frac{1}{2}\left(\frac{t-a_1}{a_2}\right)^2\right]}{\frac{1}{\exp(a_3)-1} + \frac{1}{2}\left[1 + \mathrm{erf}\left(\frac{t-a_1}{\sqrt{2}a_2}\right)\right]} \qquad (24)$$

Vztahem (24) byla zavedena funkce $\mathrm{HVL}(t; a_0, a_1, a_2, a_3)$ jedné proměnné t, která má formálně stejné pojmenování jako funkce $\mathrm{HVL}(x, t)$ dvou proměnných x a t[7]. Funkce $\mathrm{HVL}(t; a_0, a_1, a_2, a_3)$ má čtyři parametry: a_0, a_1, a_2 a a_3. Parametr a_0 má význam plochy píku vyjádřené v jednotkách s mol m^{-3} s^{-1}. Parametr a_1 určuje pozici píku na časové ose. Parametr a_2 charakterizuje rozšiřování píku v důsledku difúze a parametr a_3 popisuje rozšiřování a deformaci píku v důsledku elektromigrační disperze. Ještě v době před formulací modelu NLTEM Le Saux a kol. [22] ukázali, že parametr a_1 HVL funkce nafitované na pík analytu v časovém záznamu elektroferogramu odpovídá správnému migračnímu času, který je třeba použít pro výpočet efektivní elektroforetické pohyblivosti tohoto analytu. Toto tvrzení bylo následně potvrzeno modelem NLTEM [10].

1.6 Rozlišení píků v kolonových a kapilárních separačních metodách

V kolonových a kapilárních separačních metodách, jako například kapilární elektroforéze, kapalinové a plynové chromatografii, se k objektivní charakterizaci rozsahu

[7] Z matematického hlediska se jedná o dvě různé funkce, které však nesou stejné pojmenování HVL. Ačkoli toto nejednoznačné pojmenování může být někdy matoucí, je v chemické literatuře zvykem označovat obě funkce stejně a v této disertační práci se toho budeme držet.

separace dvojice píků analytů užívá veličiny zvané rozlišení. Jakožto objektivní míru rozsahu separace dvojice analytů je možné rozlišení využít v automatizovaných algoritmech pro optimalizaci separačních podmínek. První a dodnes široce užívaná definice rozlišení pochází z roku 1958, kdy Philips pro rozlišení dvojice analytů, jejichž koncentrační profily jsou dány Gaussovým rozdělením a mají stejný rozptyl a plochu, navrhl vztah [23]:

$$R_S = \frac{2(t_2 - t_1)}{s_1 + s_2} \tag{25}$$

kde t_i je retenční (migrační) čas *i*-tého analytu a s_i je šířka příslušného píku při základně, $i = 1,2$. Šířka píku je přitom určena jako vzdálenost průsečíků tečen vedených inflexními body daného píku se základní linií chromatogramu či elektroferogramu. V průběhu času byla hodnota $R_S = 1{,}5$ přijata jako kritérium úplné separace píků [24].

Vztah (25) byl odvozen pro dvojici píků s identickými gaussovskými koncentračními profily. Jak však bylo ukázáno v předchozích kapitolách, setkáváme se v analytické praxi běžně s píky, které mají výrazně odlišnou plochu či jejich koncentrační profil je různým způsobem zdeformován, v kapilární elektroforéze například v důsledku elektromigrační disperze. Ve snaze vyřešit první z těchto problémů zavedli Schoenmakers a kol. [25] veličinu nazvanou relativní překryv dvojice píků. Ten je pro analyt 1 definován vztahem

$${}^2P_1 = \frac{A_{12}}{A_1} \tag{26}$$

a pro analyt 2 vztahem

$${}^1P_2 = \frac{A_{12}}{A_2} \tag{27}$$

kde A_i je plocha píku *i*-tého analytu a A_{12} je plocha vzájemného překryvu píků obou analytů. Mají-li píky analytů rozdílnou plochu, jsou rozdílné též hodnoty relativních překryvů ${}^2P_1$ a ${}^1P_2$. Není-li podstatné, ke kterému analytu relativní překryv vztahujeme, značíme jej v této disertační práci pouze symbolem P bez indexů 1,2. Hodnota relativního překryvu, na rozdíl od rozlišení R_S, dokáže v případě nestejně velkých píků postihnout rozdílnou relativní míru znečištění píku analytu 1, respektive píku analytu 2 v důsledku

přítomnosti druhého nezcela separovaného analytu. Z definičních vztahů (26) a (27) je dále zřejmé, že relativní překryv nabývá hodnot od 0 do 1.

Ve snaze najít způsob, jak objektivně charakterizovat rozsah separace obecně nesymetrických píků, navrhli Dose a Guiochon v roce 1990 veličinu Ω [26]:

$$\Omega = \frac{\left[\int_{-\infty}^{+\infty} c_1(t)\, c_2(t) dt\right]^2}{\int_{-\infty}^{+\infty} c_1^2(t) dt \int_{-\infty}^{+\infty} c_2^2(t) dt} \tag{28}$$

kde $c_1(t)$ a $c_2(t)$ jsou koncentrační profily analytů 1 a 2 v časové doméně, tj. zaznamenané detektorem. Veličina Ω svou konstrukcí připomíná překryvový integrál jednorozměrných vlnových funkcí v kvantové mechanice. Od relativního překryvu P se Ω odlišuje ve dvou aspektech. Zaprvé hodnota Ω nezávisí na škálování koncentračních profilů analytů. Tato vlastnost může být v určitých situacích výhodná, neboť znamená, že hodnota Ω je invariantní vůči změně odezvového faktoru detektoru vůči analytům a do značné míry proto nezávisí na způsobu detekce[8]. Na druhou stranu činí tato vlastnost hodnotu Ω zcela necitlivou vůči rozdílům v plochách píků. V tomto směru je tedy Ω přesným opakem relativního překryvu P. Zadruhé hodnota Ω je určena úplnými koncentračními profily obou analytů, a proto lépe, ve srovnání s relativním překryvem P, odráží skutečný tvar píků. Autoři práce [26] rovněž ukázali, že v případě dvou identických gaussovských koncentračních profilů platí mezi veličinou Ω a rozlišením R_S vztah

$$\Omega = \exp(-8R_S^2) \tag{29}$$

Vztah (29) představuje přirozené pojítko mezi nově zavedenou veličinou Ω a tradiční definicí rozlišení R_S. Navzdory výhodám, které Ω a relativní překryv P přinášejí oproti tradičnímu rozlišení R_S, se ani jedna z nových veličin v experimentální praxi neujala. Důvodem může být přílišná abstraktnost veličiny Ω a v případě relativního překryvu P přílišná obtížnost, kterou v době zveřejnění práce [25] představovalo určení vzájemného překryvu dvojice píků z experimentálních dat.

[8] Vždy je třeba zvolit metodu detekce, která je citlivá na oba analyty. Tato citlivost však nemusí být pro oba analyty stejná.

2 Cíle disertační práce

Cílem této disertační práce bylo rozšíření a zobecnění matematických modelů vybraných módů kapilární elektroforézy, kapilární zónové elektroforézy a elektrokinetické chromatografie, a to s důrazem na popis nelineárních jevů.

(*i*) Rozšíření aproximativní nelineární teorie elektromigrace (NLTEM) tak, aby umožnila popis elektroforetických systémů tvořených multivalentními slabými elektrolyty, mezi nimiž se ustavují rychlé chemické rovnováhy (zejména rovnováha acidobazická a komplexační). (*Publikace I* a *IV*)

(*ii*) Nalezení vztahu mezi aproximativní nelineární teorií elektromigrace (NLTEM) a nelineárním modelem elektromigrace bez difúze (NEM) a rozšíření nelineárního modelu elektromigrace bez difúze (NEM) tak, aby umožnil popis vzájemné komigrace dvou analytů. (*Publikace V* a *VI*)

Další cíle disertační práce se vztahovaly k procesu vyhodnocení experimentálních elektroferogramů a jejich interpretaci.

(*i*) Navrhnout parametr, který by správně charakterizoval rozlišení dvojice píků, a to i v případě kdy jsou píky výrazně deformovány (nesymetrické) nebo se podstatně liší svou plochou. (*Publikace II*)

(*ii*) Nalézt vztahy mezi geometrickými vlastnostmi HVL funkce a jejími parametry a na základě těchto vztahů navrhnout postup stanovení migračního času, který odpovídá efektivní mobilitě analytu při jeho nekonečném zředění, bez nutnosti použít nelineární regresi. (*Publikace III*)

3 Experimentální podmínky

Elektroforetická měření byla prováděna na přístroji Agilent ^{3D}CE, který byl řízen softwarem ChemStation (Agilent Technologies, Waldbronn, Německo). Elektroferogramy byly zaznamenávány UV-VIS detektorem s diodovým polem. Kontrolní měření pH základních elektrolytů byla prováděna pH-metrem PHM 220 (Radiometer, Kodaň, Dánsko), který byl kalibrován standardními pufry IUPAC (Radiometer, Kodaň, Dánsko). Všechna měření byla prováděna v křemenných kapilárách o vnitřním průměru 50 μm (Polymicro Technologies, Phoenix, USA). Pro přípravu všech roztoků byla použita voda deionizovaná systémem Rowapur a Ultrapur (Watrex, San Francisco, USA). Detailní popis experimentálních podmínek jednotlivých měření je uveden v příslušných publikacích.

4 Výsledky a diskuze

4.1 Afinitní kapilární elektroforéza: *Publikace I*

V rámci teoretického studia elektroforetických systémů, v nichž se uplatňují komplexační rovnováhy (viz podkapitola 1.3), byla publikována přehledová *Publikace I*, která byla pojata jako shrnutí současného stavu poznání v oblasti experimentální metody zvané afinitní kapilární elektroforéza (ACE). Jedná se o metodu kapilární elektroforézy určenou pro stanovení konstant stability slabě vázaných komplexů. *Publikace I* se omezuje pouze na situace, kdy vznikají komplexy se stechiometriií 1:1, neboť tento případ je v praxi zdaleka nejběžnější. *Publikace I* shrnuje teoretické vztahy pro efektivní elektroforetickou mobilitu analytu podílejícího se na tvorbě komplexu, které byly v odborné literatuře publikovány mezi lety 1992 až 2015. Značná pozornost je věnována shrnutí a diskuzi různých přístupů k provádění korekce efektivní elektroforetické mobility analytu na změny viskozity BGE, které nastávají v důsledku přítomnosti často značně objemného komplexačního činidla v BGE. Na závěr *Publikace I* jsou shrnuty dosavadní poznatky o vlivu iontové síly na průběh experimentů v rámci metody ACE.

Publikace I

Affinity capillary electrophoresis: the theory of electromigration

Pavel Dubský, **Martin Dvořák**, Martin Ansorge

Analytical and Bioanalytical Chemistry 2016, *408*, 8623 – 8641

Anal Bioanal Chem (2016) 408:8623–8641
DOI 10.1007/s00216-016-9799-y

REVIEW

Affinity capillary electrophoresis: the theory of electromigration

Pavel Dubský[1] · **Martin Dvořák**[1] · **Martin Ansorge**[1]

Received: 26 May 2016 / Revised: 4 July 2016 / Accepted: 14 July 2016 / Published online: 24 August 2016
© Springer-Verlag Berlin Heidelberg 2016

Abstract We focus on the state-of-the-art theory of electromigration under single and multiple complexation equilibrium. Only 1:1 complexation stoichiometry is discussed because of its unique status in the field of affinity capillary electrophoresis (ACE). First, we summarize the formulas for the effective mobility in various ACE systems as they appeared since the pioneering days in 1992 up to the most recent theories till 2015. Disturbing phenomena that do not alter the mobility of the analyte directly but cause an unexpected peak broadening have been studied only recently and are also discussed in this paper. Second, we turn our attention to the viscosity effects in ACE. Change in the background electrolyte viscosity is unavoidable in ACE but numerous observations scattered throughout the literature have not been reviewed previously. This leads to an uncritical employment of correction factors that may or may not be appropriate in practice. Finally, we consider the ionic strength effects in ACE, too. Limitations of the current theories are also discussed and the tasks identified where open problems still prevail.

Published in the topical collection *Fundamental Aspects of Electromigrative Separation Techniques* with guest editors Carolin Huhn and Pablo A. Kler.

Electronic supplementary material The online version of this article (doi:10.1007/s00216-016-9799-y) contains supplementary material, which is available to authorized users.

✉ Pavel Dubský
dubsky@natur.cuni.cz

[1] Faculty of Science, Department of Physical and Macromolecular Chemistry, Charles University in Prague, Hlavova 8, 128 43 Prague 2, Czech Republic

Keywords Capillary electrophoresis/electrophoresis · Affinity capillary electrophoresis · Electrokinetic chromatography · Viscosity · Ionic strength · Separations/theory

Introduction

Affinity capillary electrophoresis (ACE) refers to a family of methods. These have in common that a sample reversibly interacts with one (or more) component(s) of the electrophoretic system while it is driven through the capillary or gel by the electric force [1, 2]. These methods are used for studies in proteomics, immunology, drug development, molecular biology, or microbiology, as well as in the separation sciences [1–5]. The interacting component is often referred to as a ligand since the purpose is to study analyte–ligand weak interactions. In separation sciences, however, the interacting component takes the role of a selector that interacts selectively with various components of the sample (analytes) thus affecting their separation. Although gel electrophoresis was first applied in the ACE mode, namely in biophysical studies, the free-solution ACE, where the interacting components are dissolved in the background electrolyte (BGE), has become a highly popular technique especially in the separation sciences. The term electrokinetic chromatography (EKC) became common for these kinds of separations [6, 7], while capillary EKC (cEKC) was suggested by other authors [8]. However, this terminology should not be confused with micellar electrokinetic chromatography (MEKC)—which is based on similar principles, yet described by a conceptually different approach—or even capillary electrochromatography (CEC), which is a completely diverse technique. Since cyclodextrins (CDs) belong to the most common selectors in EKC, CD-mediated EKC (CD-EKC) [9, 10] or CD-modified CZE

(CD-CZE) [6] are idioms that can also be encountered in the literature. Other authors [11] differentiate between ACE and EKC so that "[in EKC] the constituent(s) added to the electrophoresis buffer [BGE] is considered to form a separate phase as is the case for micelle, microemulsion and liposome forming excipients". Then they used the formalism of phase distribution equilibria in the case of the EKC (which applies to MEKC, too), while the weak chemical binding equilibria was considered characteristic for ACE. Specifically, the term mobility-shift ACE [2, 11] is used for the electrophoretic technique that we are going to discuss in this review paper. Although this differentiation between ACE and EKC is natural, it is not generally accepted. Historically, EKC has been used in the sense of what the authors would refer to as the mobility-shift ACE. For example, CD-EKC is a common term in spite of the fact that CDs do not form a separate phase in the BGE. The terminology may also differ upon the authors' perspective. When, for example, the prime interest is in determining the analyte–selector binding constants by means of capillary electrophoresis experiments, the (mobility-shift) ACE designation is sometimes preferred over the EKC, perhaps to put the stress from "chromatography" (resembling separation) back on "affinity" (resembling molecular binding). Since the separation principles in electrophoretic systems with weakly interacting selectors are not directly comparable to chromatography (as we also discuss later in this paper), we suggest to stick to the simple ACE acronym whenever the selectors (ligands) are (i) added to the BGE, (ii) do not form a separate phase, and (iii) affect the migration of the analyte(s) through the affinity interactions.

The detailed theory of the electromigration in ACE is reviewed in this paper. Its application is found namely in chiral separations or when the analyte–ligand weak interactions are to be studied carefully. Numerous review papers exist (we counted over 100 of them since 1993 but here give only those that appeared over the last decade) summarizing applications of ACE [8, 12–21], monitoring usage of various selectors [6, 7, 12, 14, 18, 20], others targeting CDs only [9, 22–27], or focusing on the weak interactions between analytes and selectors (ligands) [28–30]. Only a few out of the numerous review papers cover the fundamentals of the technique as (one of) their prime subject [8, 31–37], whereas some focus more on theoretical aspects of the separation principles [34, 36–40]. As far as we are concerned, the theory of electromigration under the influence of complexation equilibrium has never been summarized to the extent we do in this paper.

Effective mobility

Although it may seem that the effective mobility of an analyte in ACE is so well understood that it is not worth any special attention, the diversity of various equilibria that may take place in the ACE separation system gave rise to a variety of expressions in the mid-1990s and the research has still not subsided. Simultaneously, these expressions were sometimes derived by several authors in various forms but have apparently never been summarized in one place. This may cause difficulties when getting oriented in the subject. For this reason we summarize the theory in this section, placing especial emphasis on mutual relationships among the equations.

Simple systems

The theory of ACE is based on the fundamentals of electrophoresis as postulated by Tiselius in 1930 [41]. If a chemical species exists in various forms among which a chemical equilibrium establishes at fast reaction rate, the individual forms of the species do not migrate apart each other. Instead, they form a single zone whose effective mobility is given by the Tiselius equation:

$$\mu_{\mathrm{A,eff}} = \sum_i \chi_i \mu_{\mathrm{A},i} \tag{1}$$

where

$$\chi_i = \frac{n_i}{\sum_j n_j} \tag{2}$$

is the molar fraction of the i-th form of the species A, $\mu_{A,i}$ is its individual electrophoretic mobility, and n_i and $\sum_j n_j$ represent the amount of the i-th form and the total amount of the species A, respectively. (See the Electronic Supplementary Material (ESM) for more detailed explanation of the Tiselius equation.) Equation (1) is applicable to, e.g., the three ionic forms of phosphoric acid as well as the ACE scenario depicted in Fig. 1A. Here, an analyte (A) interacts with a selector (S); the selector is homogenously distributed in the BGE at a total concentration of c_S. Thus the analyte exists in two forms, as the free analyte (A0) and as the complex with the selector (AS). The fast equilibrium with 1:1 stoichiometry is assumed between the analyte and the selector. Noticeably, the selector also exists in two forms, as the free selector (S0) and as the complex with the analyte (AS). Nevertheless, it is the analyte that is of prime importance in the separation process; thus, the selector is generally considered as a uniform background. This is only appropriate if the selector is present in sufficient excess of the analyte. Violating this rule has consequences that we will discuss later in this paper. Under these circumstances (fast equilibria, large amount of selector), a constant molar ratio between the two forms of the analyte is kept across its migrating zone during the entire separation process,

$$\frac{n_{AS}}{n_{A0}} = K'_{AS} c_S, \tag{3}$$

where K'_{AS} is the apparent (in contrast to the true thermodynamic) binding constant,

$$K'_{AS} = \frac{c^{rel}_{AS}}{c^{rel}_{A0} c^{rel}_{S0}}. \tag{4}$$

In Eq. (4), c stands for concentrations, while the superscript *rel* reminds of the fact that the relative concentrations should appear in formulas regarding chemical equilibria. Equation (3) results from Eq. (4) after realizing that the relative concentrations are numerically equal to the absolute ones, that $n = cV$ in any finite volume element V, and that $c_{S0} \cong c_S$ under the assumption of $c_S \gg c_{AS}$.

The analyte migrates with its own mobility, μ_{A0}. The analyte–selector complex migrates with a mobility of μ_{AS}. In the simplest case of Fig. 1A, $\chi_{AS} = 1 - \chi_{A0}$ and the effective mobility of the analyte results as [34, 42]

$$\begin{aligned}\mu_{A,eff} &= \chi_{A0}\mu_{A0} + (1-\chi_{A0})\mu_{AS} \\ &= (1-\chi_{AS})\mu_{A0} + \chi_{AS}\mu_{AS},\end{aligned} \tag{5}$$

where χ_{A0} is the fraction of the uncomplexed analyte [42] or (equivalently) χ_{AS} is the degree of complexation [34]. After expressing the molar ratios by means of Eqs. (2) and (3), the well-known relation for the effective mobility of the analyte in the ACE results,

$$\mu_{A,eff} = \frac{\mu_{A0} + K'_{AS} c_S \mu_{AS}}{1 + K'_{AS} c_S}. \tag{6}$$

The binding constant, K'_{AS}, depends on the ionic strength (IS) of the BGE. The same applies to the mobilites of the free analyte and the analyte–selector

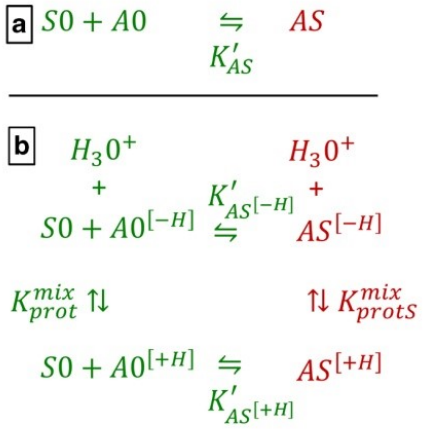


Fig. 1 Complexation scheme. **A** Simple complexation. **B** Coupled acid–base equilibrium

complex. Thus Eq. (6) is generally valid but the IS-conditional parameters must be entered into it. Typically, the parameters are determined at a certain IS and thus the IS must be kept while changing the selector concentration when applying Eq. (6). This causes difficulties especially when permanently or weakly acidic/basic selectors are used. Alternatively, the IS-conditional parameters can be calculated from the thermodynamic (binding constant) or limiting (mobilities) ones. We discuss the role of the IS of the BGE in more detail in "Ionic strength". Equation (6) is often ascribed to Wren and Row [43] (which has over 600 citations since 1992) but it was already published in this exact form by Guttman et al. in 1988 [42] in the context of the employment of cyclodextrins incorporated within a gel matrix. Explicit forms of Eq. (6) were given for neutral analytes ($\mu_{A0} = 0$) [44, 45] or neutral analyte–selector complexes ($\mu_{AS} = 0$) [46, 47]. In the former case the selector has to be charged ($\mu_{AS} \neq 0$) so as to mobilize the sample, while the latter case is a consequence of analyte and selector bearing the same but opposite charges. An alternative form of Eq. (6) can be encountered in the literature [48], although it does not seem to bring any advantage.

Studies that primarily aim to determine the binding constant, K'_{AS}, often start with Eq. (6) expressed as [49]

$$K'_{AS} c_S = \frac{\mu_{A0} - \mu_{A,eff}}{\mu_{A,eff} - \mu_{AS}}. \tag{7}$$

Other rearrangements lead to the so-called x-reciprocal, y-reciprocal, and double-reciprocal linearized expressions [49], respectively:

$$\frac{\mu_{A,eff} - \mu_{A0}}{c_S} = -K'_{AS}(\mu_{A,eff} - \mu_{A0}) + K'_{AS}(\mu_{AS} - \mu_{A0}), \tag{8a}$$

$$\frac{c_S}{\mu_{A.eff} - \mu_{A0}} = \frac{1}{\mu_{AS} - \mu_{A0}} c_S + \frac{1}{\mu_{AS} - \mu_{A0}} \cdot \frac{1}{K'_{AS}}, \text{ and} \tag{8b}$$

$$\frac{1}{\mu_{A,eff} - \mu_{A0}} = \frac{1}{\mu_{AS} - \mu_{A0}} \cdot \frac{1}{K'_{AS}} \cdot \frac{1}{c_S} + \frac{1}{\mu_{AS} - \mu_{A0}}. \tag{8c}$$

Another approach to the linearization of Eq. (6), which is somewhat similar to the x-reciprocal Eq. (8a) and enables specific statistical treatment that we discuss in "Other approaches", can be found in ref. [50]. Results (namely binding constants) obtained by the different linearization approaches, Eq. (8), and the nonlinear regression of Eq. (6) have been compared in several studies showing that the obtained values may or may not differ significantly [51–55]. Nevertheless, Bowser and Chen demonstrated by Monte Carlo simulations in 1998 that the data transformation causes a violation of statistical requirements on that data and thus is not recommended

[56, 57]. Linearization of the fundamental Eq. (6) seems rather obsolete with the contemporary computational power and statistical tools. We recently published freeware CEval (http://echmet.natur.cuni.cz/download) [58] that enables easy evaluation of data from ACE measurements, automatic estimation of the binding parameters by the linearized equations, and subsequent nonlinear regression of Eq. (6). On the other hand, the *x*-reciprocal rearrangement may be advantageous for data visualization since it is sensitive to possible nonlinearities, namely deviations from the 1:1 stoichiometry [59–61].

The existence of the weak interactions between the analyte and the selector makes ACE comparable to chromatography. This may bring about certain confusion reflected both in the nomenclature (as briefly demonstrated in the "Introduction") and the related theory. Bowser et al. [62] opened "a potential pathway to a unified separation science" in 1997. Virtually the same idea was published by Lelièvre et al. [63] that same year. The authors realized the common nature between the molar fraction, Eq. (2), and the chromatographic capacity (retention) factor

$$k' = \frac{n_{\mathrm{SF}}}{n_{\mathrm{MF}}}, \tag{9}$$

where n_{SF} represents the amount of the analyte adsorbed on the stationary phase and n_{MF} stands for that remaining in the mobile phase. Denoting $n_{\mathrm{MF}} \equiv n_0$ (aka the free analyte), it follows that

$$\chi_i = \frac{n_i}{\sum n_j} = \frac{(n_i/n_0)}{\left(\sum n_j/n_0\right)} = \frac{k_i'}{\sum k_j'}. \tag{10}$$

Consequently, Tiselius' Eq. (1) is of general applicability in separation sciences if k_i' is defined as

$$k_i' = \frac{[\text{Amount of analyte of species } i]}{[\text{Amount of free analyte}]}, \tag{11}$$

where the "species *i*" represents various analyte interactions that can appear in the separation system. Comparison between Eqs. (3) and (11) clearly shows that the product of $K'_{\mathrm{AS}} c_{\mathrm{S}}$ in ACE gives the counterpart to the retention factor, k', in chromatography. Consequently, Eq. (6) becomes

$$\mu_{\mathrm{A,eff}} = \frac{1}{1+k'}\mu_{\mathrm{A0}} + \frac{k'}{1+k'}\mu_{\mathrm{AS}} \tag{12}$$

as also explicitly derived by Peng et al. in one of their subsequent papers [64]. Although the chromatographic approach to the effective mobility provided its educative purpose in the early days of ACE, it seduces one to think of the ACE systems as chromatographic ones, which is not always appropriate [7, 8, 33, 38]. For this reason we consider it best avoided nowadays. See the ESM for additional information on the chromatographic concept in ACE.

Acid–base equilibria

Only rare analytes are permanently charged or neutral molecules. Usually they bear one or more ionizable (acidic or basic) groups. Monovalent analytes are common. Larger molecules can often be treated as "stepwise ionizable" in the entire pH range as long as the pK_{a} values of all individual ionizable groups are sufficiently different. Thus the natural extension of Eq. (6) is to account for monovalent weakly acidic and basic analytes. By "monovalent" we mean that only one ionizable group is considered at a time in the sense of the "stepwise ionization". Thus the protonated form of an acidic analyte does not necessarily need to be the neutral one and the same applies to the deprotonated form of a basic analyte. This situation is depicted in Fig. 1B. The protonated/deprotonated forms of the analyte are denoted by subscripts $[+H]$ / $[-H]$ respectively, so as not to impose a perception of any charge state.

The complete solution was published by Williams and Vigh in 1997 [65]. After expressing the molar fractions, x_i, for the individual forms of the weak acid or base in Fig. 1B, its effective mobility results as

$$\mu_{\mathrm{A,eff}} = \frac{\mu_{\mathrm{A}^{[-\mathrm{H}]}} + \mu_{\mathrm{AS}^{[-\mathrm{H}]}} K'_{\mathrm{AS}^{[-\mathrm{H}]}} c_{\mathrm{S}} + K^{\mathrm{mix}}_{\mathrm{prot}} a_{\mathrm{H_3O^+}} \cdot \left(\mu_{\mathrm{A}^{[+\mathrm{H}]}} + \mu_{\mathrm{AS}^{[+\mathrm{H}]}} K'_{\mathrm{AS}^{[+\mathrm{H}]}} c_{\mathrm{S}}\right)}{1 + K'_{\mathrm{AS}^{[-\mathrm{H}]}} c_{\mathrm{S}} + K^{\mathrm{mix}}_{\mathrm{prot}} a_{\mathrm{H_3O^+}} \cdot \left(1 + K'_{\mathrm{AS}^{[+\mathrm{H}]}} c_{\mathrm{S}}\right)}. \tag{13}$$

In Eq. (13), subscripts *A* and *AS* refer to the free analyte (acid or base) and the analyte–selector complex. μ and K' stand for electrophoretic mobilities and apparent equilibrium constants (cf. Fig. 1B), respectively. $K^{\mathrm{mix}}_{\mathrm{prot}}$ is the so-called

mixed protonation constant, either of the acid or the base. For acids, $K_{\mathrm{prot}}^{\mathrm{mix}} = 1/K_{\mathrm{A}}^{\mathrm{mix}}$, for bases, $K_{\mathrm{prot}}^{\mathrm{mix}} = K_{\mathrm{B}}^{\mathrm{mix}}/K_{\mathrm{W}}$, where $K_{\mathrm{A}}^{\mathrm{mix}}$ is a mixed acidity constant, $K_{\mathrm{B}}^{\mathrm{mix}}$ is a mixed basicity constant and $K_{\mathrm{W}} = a_{\mathrm{H_3O^+}} \cdot a_{\mathrm{OH^-}}$ is the ionic product of water. Finally, $a_{\mathrm{H_3O^+}}$ and $a_{\mathrm{OH^-}}$ are activities of hydroxonium and hydroxide ions in a BGE, respectively. Equation (13) does not originally contain the $K_{\mathrm{prot}}^{\mathrm{mix}} a_{\mathrm{H_3O^+}}$ product, but it was expressed in terms of $K_{\mathrm{prot}}^{'} c_{\mathrm{H_3O^+}}$, i.e., an apparent protonation constant and a concentration of hydroxonium ions. Using the product of $K_{\mathrm{prot}}^{\mathrm{mix}} a_{\mathrm{H_3O^+}}$ is more appropriate though [66], and thus we will use it throughout this paper (cf. the ESM). Notice that the mixed constant applies only in the context of the acid–base equilibrium. The complexation equilibria are described by apparent binding constants. The activity of the hydroxonium ions can be obtained directly from a measurement of $\mathrm{pH} = -\log a_{\mathrm{H_3O^+}}$. The only precaution is needed regarding IS of the BGE. As a matter of fact, $K_{\mathrm{prot}}^{\mathrm{mix}}$ actually results when the protonation constant is determined by means of the CE (a dependence of the effective mobility of a weakly acidic/basic analyte on *pH* at a constant IS) [66] and thus can be directly used for the purpose of Eq. (13). Another approach was adopted in one of our very recent studies [67]. From Eq. (15a) given below it follows that

$$K_{\mathrm{prot}}^{\mathrm{mix}} a_{\mathrm{H_3O^+}} = \frac{\mu_{\mathrm{A0}^{[-\mathrm{H}]}} - \mu_{\mathrm{A0}}^{\mathrm{pH}}}{\mu_{\mathrm{A0}}^{\mathrm{pH}} - \mu_{\mathrm{A0}^{[+\mathrm{H}]}}}, \tag{14}$$

where $\mu_{\mathrm{A0}}^{\mathrm{pH}}$ is the mobility of the analyte at the given *pH* (and IS) without presence of any selector. All mobilities in Eq. (14) are easily accessible experimentally and the resulting product of Eq. (14) can be input into Eq. (13) when the analysis is performed at defined *pH* and IS with changing c_{S} only. Derivation of Eq. (13) is a relatively simple task. For example Rizzi summarized the derivation process in a highly instructive way in his review paper in 2001 [34]. On the other hand, this enabled various authors to make this derivation from scratch; this resulted in numerous different-looking expressions, additionally depending on whether acids or basis were of interest [26, 65–70]. We explore these expressions and their mutual relations in the ESM.

Lelièvre, Gareil, and Jardy [63] expressed the dependence of the effective mobility of an analyte on its ionization state and the concentration of the selector in terms of *pH*-conditional parameters. The conditional constants were referred to as apparent ones in the original work. In one of our recent papers [67] we used a term "overall". However, the adjective "conditional" is the more appropriate from the physicochemical point of view [71]. In the frame of the last paragraph, the parameters were actually $c_{\mathrm{H_3O^+}}$ -conditional, i.e., requiring constant concentration of the hydroxonium ions. Nevertheless, we can adopt the concept of the mixed protonation constants, which will make the model truly *pH*-conditional. The resulting formula takes the same form as that for the effective mobility in simple systems, Eq. (6):

$$\mu_{\mathrm{A,eff}} \frac{\mu_{\mathrm{A0}}^{\mathrm{pH}} + \mu_{\mathrm{AS}}^{\mathrm{pH}} K_{\mathrm{AS}}^{\mathrm{pH}} c_{\mathrm{S}}}{1 + K_{\mathrm{AS}}^{\mathrm{pH}} c_{\mathrm{S}}}, \tag{15}$$

with

$$\mu_{\mathrm{A0}}^{\mathrm{pH}} = \frac{\mu_{\mathrm{A}^{[-\mathrm{H}]}} + \mu_{\mathrm{A}^{[+\mathrm{H}]}} K_{\mathrm{prot}}^{\mathrm{mix}} a_{\mathrm{H_3O^+}}}{1 + K_{\mathrm{prot}}^{\mathrm{mix}} a_{\mathrm{H_3O^+}}}, \tag{15a}$$

$$\mu_{\mathrm{AS}}^{\mathrm{pH}} = \frac{\mu_{\mathrm{AS}^{[-\mathrm{H}]}} K_{\mathrm{AS}^{[-\mathrm{H}]}}^{'} + \mu_{\mathrm{AS}^{[+\mathrm{H}]}} K_{\mathrm{AS}^{[+\mathrm{H}]}}^{'} K_{\mathrm{prot}}^{\mathrm{mix}} a_{\mathrm{H_3O^+}}}{K_{\mathrm{AS}^{[-\mathrm{H}]}}^{'} + K_{\mathrm{AS}^{[+\mathrm{H}]}}^{'} K_{\mathrm{prot}}^{\mathrm{mix}} a_{\mathrm{H_3O^+}}}, \text{ and} \tag{15b}$$

$$K_{\mathrm{AS}}^{\mathrm{pH}} = \frac{K_{\mathrm{AS}^{[-\mathrm{H}]}}^{'} + K_{\mathrm{AS}^{[+\mathrm{H}]}}^{'} K_{\mathrm{prot}}^{\mathrm{mix}} a_{\mathrm{H_3O^+}}}{1 + K_{\mathrm{prot}}^{\mathrm{mix}} a_{\mathrm{H_3O^+}}}. \tag{15c}$$

Notice that not only *pH* but also IS of the BGE must be kept constant to ensure the validity of Eq. (15). The IS-conditional equilibrium constants, $K_{\mathrm{AS}}^{'}$ and $K_{\mathrm{prot}}^{\mathrm{mix}}$, make the *pH*-conditional parameters, Eqs. (15a–15c), IS-conditional, too. Equations (15a–15c) appear in a different form from that in the original paper [63]. We deliberately applied some rearrangements to give them the shape resembling Eq. (13). See the ESM for details. Mofaddel et al. [54] further extended the *pH*-conditional model by considering two simultaneously dissociating acidic groups of binols. The prime message is that even such complicated systems can be treated from the *pH*-conditional perspective and the protonation equilibria can be omitted as long as the *pH* (and IS) stays constant.

The *pH*-conditional mobilities and binding constants can be obtained in yet another way, which is of general applicability for systems with multiple equilibria. For this reason we briefly introduce the rearrangement strategy in the ESM, too. On the other hand, when the *pH* dependency is taken into account but the concentration of the selector, c_{S}, is kept constant, the same rearrangement (ESM) can be applied to Eq. (13) with respect to the $a_{\mathrm{H_3O^+}}$, rather than c_{S}, yielding

$$\mu_{\mathrm{A,eff}} = \frac{\mu_{\mathrm{A}^{[-\mathrm{H}]}}^{c_{\mathrm{S}}} + \mu_{\mathrm{A}^{[+\mathrm{H}]}}^{c_{\mathrm{S}}} K_{\mathrm{prot}}^{\mathrm{mix},c_{\mathrm{S}}} a_{\mathrm{H_3O^+}}}{1 + K_{\mathrm{prot}}^{\mathrm{mix},c_{\mathrm{S}}} a_{\mathrm{H_3O^+}}}, \tag{16}$$

where

$$\mu_{\mathrm{A}^{[-\mathrm{H}]}}^{c_{\mathrm{S}}} = \frac{\mu_{\mathrm{A}^{[-\mathrm{H}]}} + \mu_{\mathrm{AS}^{[-\mathrm{H}]}} K_{\mathrm{AS}^{[-\mathrm{H}]}}^{'} c_{\mathrm{S}}}{1 + K_{\mathrm{AS}^{[-\mathrm{H}]}}^{'} c_{\mathrm{S}}}, \tag{16a}$$

$$\mu_{\mathrm{A}^{[+\mathrm{H}]}}^{c_{\mathrm{S}}} = \frac{\mu_{\mathrm{A}^{[+\mathrm{H}]}} + \mu_{\mathrm{AS}^{[+\mathrm{H}]}} K_{\mathrm{AS}^{[+\mathrm{H}]}}^{'} c_{\mathrm{S}}}{1 + K_{\mathrm{AS}^{[+\mathrm{H}]}}^{'} c_{\mathrm{S}}}, \text{ and} \tag{16b}$$

$$K_{\mathrm{prot}}^{\mathrm{mix},c_{\mathrm{S}}} = \frac{1 + K_{\mathrm{AS}^{[+\mathrm{H}]}}^{'} c_{\mathrm{S}}}{1 + K_{\mathrm{AS}^{[-\mathrm{H}]}}^{'} c_{\mathrm{S}}} \cdot K_{\mathrm{prot}}^{\mathrm{mix}} = Z_{\mathrm{prot}} K_{\mathrm{prot}}^{\mathrm{mix}} \tag{16c}$$

are the c_S -conditional parameters. Specifically, $K_{prot}^{mix,cS}$ is the c_S -conditional (mixed) protonation constant. Equation (16b) implies $pK_{prot}^{mix,cS} = pK_{prot}^{mix} + pZ_{prot}$. This means that the system behaves as if no selector was present but the pK_{prot}^{mix} value was shifted by a factor of pZ_{prot}. This effect is known as the complexation-induced pK_A shift. We recapitulate the key papers [72–77] in the ESM. More studies are summarized in the review paper [7]. A list of related studies (not limited to electrophoresis) is also provided in the introduction of ref. [78]. Yet again, the c_S -conditional constants, Eqs. (16a–16c) are simultaneously IS-conditional.

Multiple equilibria

Separation systems with two or more selectors, i.e., dual- or multi-selector systems, respectively, are often encountered in ACE. The former occurs in an attempt to increase the separation efficiency (cf., e.g., [35]), whereas the latter out of necessity since commercial derivatives of selectors (namely functionalized cyclodextrins) are usually produced as mixtures of isomers [40, 79–82]. We reviewed the theoretical aspects of ACE separations in such systems recently [31].

When an analyte interacts with a mixture of selectors and the requirements of the fast equilibria, the 1:1 stoichiometry, and the large amount of the selector are fulfilled for every analyte–selector interaction, the effective mobility of the analyte results as a straightforward extension of Eq. (6),

$$\mu_A^{eff} = \frac{\mu_{A0} + \mu_{AS^{[1]}} K'_{AS^{[1]}} c_{S^{[1]}} + \cdots + \mu_{AS^{[N]}} K'_{AS^{[N]}} c_{S^{[N]}}}{1 + K'_{AS^{[1]}} c_{S^{[1]}} + \cdots K'_{AS^{[N]}} c_{S^{[N]}}}. \quad (17)$$

Equation (16c) was expressed in terms of the capacity factors, Eq. (11), from the "unified separation science" approach by Bowser et al. [64] and derived by Lurie et al. earlier in 1994 [83] for dual-selector systems ($N = 2$). The indexes $[1]\ldots[N]$ refer to the first up to the N-th selector in the mixture. When all concentrations of the selectors in the mixture are kept constant except one, e.g., the first one ($c_{S^{[1]}}$), the rearrangement introduced in the ESM provides the $c_{S^{[1]}}$ -conditional parameters. Similarly to the previous cases, such parameters are IS-conditional, too. They were originally published for dual-selector systems [84] but we provide universal formulas here:

$$\mu_{A0}^{c_{S^{[1]}}} = \frac{\mu_{A0} + \sum_{q=2}^{N} \mu_{AS^{[q]}} K'_{AS^{[q]}} c_{S^{[q]}}}{1 + \sum_{q=2}^{N} K'_{AS^{[q]}} c_{S^{[q]}}}, \quad (18a)$$

$$\mu_{AS}^{c_{S^{[1]}}} = \mu_{AS^{[1]}}, \text{ and} \quad (18b)$$

$$K'^{c_{S^{[1]}}}_{AS} = \frac{K'_{AS^{[1]}}}{1 + \sum_{q=2}^{N} K'_{AS^{[q]}} c_{S^{[q]}}}. \quad (18c)$$

Alternatively, the mixture composition may be held constant while changing its total (analytical) concentration. So every selector concentration can be expressed as $c_{S^{[q]}} = \chi_q c_S$, where χ_q is the (constant) molar fraction of the q-th selector in the mixture and c_S now represents the total concentration of the mixture. Then, the same rearrangement yields the χ-conditional (and simultaneously IS-conditional) parameters [85, 86],

$$\mu_{A0}^{\chi} = \mu_{A0}, \quad (19a)$$

$$\mu_{AS}^{\chi} = \frac{\sum_{q=1}^{N} \mu_{AS^{[q]}} K'_{AS^{[q]}} \chi_q}{K'^{\chi}_{AS}}, \text{ and} \quad (19b)$$

$$K'^{\chi}_{AS} = \sum_{q=1}^{N} K'_{AS^{[q]}} \chi_q. \quad (19c)$$

We give preference to the χ-conditional perspective for two reasons. First, the χ parameter is well constrained between 0 and 1, which makes the inspection of the parametric space of the effective mobility easier in the case of dual-selector systems. Second, the χ-conditional perspective is natural to the multi-selector systems composed of a mixture of unknown but constant composition. The model can explain the extraordinary selectivity of randomly charged CDs as often encountered in practice [87]. Recently we showed that the χ-conditional perspective enables determination of relative enantiomer migration order of enantiomers using a racemic sample [88]. If an enantiomer A migrates first with one single selector, it is possible to decide whether the first migrating enantiomer with another selector is also the enantiomer A or it is the opposite one. Such a decision can be made without the need of having the pure enantiomers available if the two selectors are combined into a dual-selector mixture in a defined way. This allows for assigning the complexation parameters obtained in single-selector systems to the correct enantiomeric forms as necessary for computation of the χ-conditional parameters, Eq. (19), e.g., for subsequent method optimization.

For the "total concentration" of the mixture it applies

$$c_S = \sum_{q=1}^{N} c_{S^{[q]}} = \frac{\sum_{q=1}^{N} n_{S^{[q]}}}{V}. \quad (20)$$

Equation (19a) may come in useful especially when dealing with deliberately prepared mixtures, typically the dual-selector ones, for which the individual values of $n_{S^{[q]}}$ or $c_{S^{[q]}}$ are known. When, on the other hand, dealing with mixtures of constant, yet unknown, composition, it is best to express the total concertation, c_S, and the χ-contitional binding constants in terms of masses. Additionally, one may be unsure whether or not the χ-contitional parameters can be further combined into yet other χ-contitional parameters. To illustrate such a need, imagine that two

commercial mixtures of CD derivatives are to be combined into a final "dual-selector"-like mixture. Although intuitively accepted, this problem has apparently never been addressed in the literature explicitly. We provide a proof that it is indeed so in the ESM.

Another example of a multiple analyte–selector interaction is represented by chiral separations of *cis*-diols (and related compounds, such as saccharides) in borate buffers. The borate–diol interaction provides achiral resolution of analytes or mobilizes the neutral ones, while addition of a chiral selector, typically cyclodextrin, allows for the chiral recognition. We again provide detailed discussion on the key papers [89–92] in the ESM. The theoretical treatment of such coupled equilibria shows that the χ-conditional perspective has stronger limits than the $c_{S^{[i]}}$ -conditional (or any equivalent) one. The 1:1 stoichiometry is the only prerequisite for the latter, while no mixed complexes are an additional constrain put on the former. Apart from multiple interactions among one analyte and a mixture of selectors, one can imagine multiple interactions between one analyte and one selector, yet occurring among various binding sites. This issue was addressed by Asnin and Nikitina only recently in 2014 [93]. Their model aimed exclusively at the 1:1 complexation stoichiometry, which means that a certain portion of the molecules of the analyte interacts with the selector through an interaction "A", another portion through an interaction "B", etc., but these interaction modes are independent of each other and there is no space for a mixed mode. The model is also summarized in the ESM. In brief, the theory reveals that what manifests itself as a single analyte–selector interaction can actually be made up of more elementary equilibria (between one analyte and one selector) that, however, remain hidden and inaccessible.

Despite the long-term existence of the above equations, we identified in our recent review [31] that a model that would adequately describe both complexation equilibria with multiple selectors and acid–base equilibria was still missing. This led us to formulation of the so-called M_AM_S -conditional parameters in our recent work in 2015 [94]. The M_AM_S nomenclature shortens the "multi-analyte multi-selector" model and the parameters are also IS-conditional, as usual. The model is designed for an analyte that exists in L forms among which fast equilibria are established. The L forms are not specified but the protonated/deprotonated forms of a weakly acidic/basic/amphoteric compound are definitely of prime interest. Such compounds are no longer limited to monovalent or "stepwise ionizable" ones. These L forms of the analyte are allowed to interact with N selectors under the exclusive 1:1 stoichiometry and no mixed interactions. Noticeably, R out of the N selectors ($R \leq N$) may alternatively represent R (de)protonated forms of weakly acidic/basic selector(s). The conditional parameters read

$$\mu_{A0}^{M_AM_S} = \sum\nolimits_{i=1}^{L} \chi_{i0}\mu_{A0^{[i]}}, \tag{21a}$$

$$\mu_{AS}^{M_AM_S} = \frac{\sum\nolimits_{i=1}^{L} \chi_{i0} \sum\nolimits_{q=1}^{N} \mu_{AS^{[i][q]}} K'_{AS^{[i][q]}} \chi_q}{K'^{\chi}_{AS}}, \text{ and} \tag{21b}$$

$$K'^{M_AM_S}_{AS} = \sum_{i=1}^{L} \chi_{i0} \sum_{q=1}^{N} K'_{AS^{[i][q]}} \chi_q, \tag{21c}$$

where χ_{i0} is the molar fraction of the i-th form of the free (not complexed) analyte, $\mu_{A0^{[i]}}$ are their (the i-th forms') electrophoretic mobilities, $K_{AS^{[i]}}\,[q]'$ are apparent binding constants between the i-th form of the analyte and the q-th (form of the) selector, $\mu_{AS^{[i]}}\,[j]$ are the electrophoretic mobilities of such complexes, and χ_q are the molar fractions of each q-th (r-th form of the) selector.

The most important outcomes of the model—as discussed in more detail in the ESM—are the following. First, the molar fractions of the free analyte, χ_{i0}, can be evaluated, e.g., from the given pH without the need to take the complexation into account if the K_{prot}^{mix} constants are known for every ionization state (cf., e.g., [95, 96]). The same possibly holds true for the fractions of, χ_q (aka χ_r), if a weakly acidic/basic selector is present alone or in a mixture. The latter must be applied with caution that the selector—being present in a large amount—may participate in the buffering properties of the BGE and also significantly contribute to the IS of the BGE, which both would invalidate this approach. Having the values of χ_{i0} and χ_q in hand, one can deduce the M_AM_S-conditional parameters directly from Eq. (21). Similarly, pH-conditional parameters can be determined at defined pH (and IS) for several selectors (or several mixtures of selectors) and simply combined into the χ-conditional parameters, Eq. (19). Likewise, the χ-conditional parameters can be determined with a mixture of selectors and inserted into any of the pH-dependent models; this latter case is only applicable to mixtures of neutral or permanently charged selectors. Such a method was demonstrated in the experimental part of one study [67]. It was observed that the χ-conditional parameters can be evaluated from the pH-conditional ones (a partially dissociated weakly acidic analyte) with an excellent precision. The precision was not so perfect in the opposite case of inputting the χ-conditional parameters (of a mixture of selectors) into the pH-conditional model. This was attributed to the difficulties with which the complexation constant of the neutral form of the weakly acidic analyte are determined (regardless of whether the selector is a single compound or a mixture). Nevertheless the pH-conditional parameters were still satisfactory for practical use.

Violating the basic assumptions

Apart from the 1:1 complexation stoichiometry (which is taken as granted here), fast equilibrium rate, sufficient excess of the selector, and the requirement that the selector does not

interact with any component of the BGE are the prime prerequisites of the aforementioned models. We briefly summarize consequences of violating these assumptions in this section.

If the complexation equilibrium is not accomplished with fast enough rates, the peak (zone) of the analyte broadens, while it eventually splits into two peaks interconnected with an intermediate plateau at medium reaction rates, until the peaks become completely separated at slow reaction rates [97]. The process is characterized by two characteristic times,

$$t_{\mathrm{eq}} = \frac{1}{k_+ \cdot c_{S0} + k_-} \tag{22}$$

and

$$t_{\mathrm{sep}} = \frac{w}{|v_{A0} - v_{AS}|}, \tag{23}$$

where k_+ is the rate constant of the complex formation, k_- is that of the complex dissociation, w is the width of the initial zone, and v stands for velocities. (Other authors define t_{sep} as half of the value of Eq. (23) [98].) It is possible to determine the individual rate constants, k_+ and k_-, from the specific peak shape distribution caused by the slow kinetics. The most relevant outcome for our purposes, however, is that the peak shape distribution was indistinguishable from the one that would result if no complexation equilibrium took place by computer simulation with $t_{\mathrm{sep}}/t_{\mathrm{eq}} > 10$. This relation along with Eqs. (22) and (23) somewhat quantifies the adjective "fast" used to describe the equilibrium rates.

If the selector is present in small amounts, the effective mobility of the analyte is not affected but nonlinear peak dispersion occurs. Some authors tried to calculate the free amount of the selector, c_{S0}, in the sample zone in an attempt to compensate for the selector consumption in Eq. (6) [99–101] (see ESM). However, such a procedure is not adequate. Le Saux, Varenne, and Gareil [102] reported highly convincing experimental evidence that the analyte peak becomes HVL-distorted with decreasing selector/analyte concentration ratio, where HVL stands for the Haarhoff–Van der Linde function (see the ESM). The HVL function was proven to be an exact solution of the linearized governing equations of capillary zone electrophoresis (CZE) with a first-order nonlinear term (yet not concerning the complexation equilibrium) [103, 104]. We made the same conclusion as Le Saux et al. on the basis of a series of papers combining experiments, computer simulations, and computations by means of the linearized theory of CZE (newly partially accounting for the complexation equilibrium, too) [105–109]. The complexation-induced distortion in ACE can be understood when realizing that there is always low enough concentration of the analyte at the diffusive edges of its migrating zone (peak). Consumption of the selector can be severe only inside the zone. Thus the peak edges migrate with the expected mobility, Eq. (6), while the possible consumption of the selector pushes the peak apex out of its central position. More about this topic can be found in the ESM. These findings provide a strong reasoning for using the HVL function for peak evaluations in ACE. The a_1 parameter of the fitted HVL function is the proper migration time that should be used for the effective mobility calculations. To the contrary, the migration time should not be read from the peak apex since it can be shifted out of its expected position. The CEval software introduced above [58] performs automated estimates of the HVL parameters followed by a HVL fitting procedure and reading the effective mobility from the a_1 parameter.

Presence of any selector, even a neutral one, can alter the BGE properties if any of the BGE components interacts with it [78, 110]. The interacting component is possibly subject to the complexation-induced pK_A (generally pK_{prot}) shift (cf. "Acid–base equilibria" and the ESM). Consequently, the pH of the buffer may be compromised. pH shifts as high as 0.5 pH units were recently reported with some common buffer constituents (benzoic acid, CHES) and neutral CDs at a concentration as low as 10 mM. When complexation parameters are determined in such systems, they become conditional to that one particular system only (cf. Eq. (18a)). An almost 20-fold biased value of a binding constant determined in such an interacting BGE has been reported [110]. Additionally, the mobility of system peaks is affected in this way. The authors also demonstrated a complete deterioration of an otherwise promising separation as a result of these side effects. On the basis of these results it was concluded that clearly—but against the contemporary usual practice—the pH of the buffer should always be controlled after the addition of the complexation agent (even a neutral chiral selector) to reveal a possible complexation with the constituents of the buffer.

Noticeably, the complexation-induced distortion and deterioration of the BGE properties have been studied for a few neutral CDs only. The theory has not been completed for charged selectors, or mixtures of selectors. It is only partially completed for coupled complexation and acid–base equilibria. System peaks in ACE present yet another open problem.

Viscosity

Selectors in ACE are typically large molecules, such as cyclodextrins, macrocyclic antibiotics, or even polysaccharides and polycyclodextrins [111, 112]. The addition of such molecules into the BGE undoubtedly alters electrophoretic moblities of ions (including that of the analyte and the analyte–selector complex). The related theory is reviewed, e.g., in a book by Robinson and Stokes [113] and a paper by Sadek [114]. We recapitulate the

main ideas in the ESM. In brief, a correction factor, ν, is introduced,

$$\nu = \frac{\eta_s}{\eta_0}, \tag{24}$$

which provides conversion from the mobility measured in a BGE of viscosity η_s to the reference BGE of viscosity η_0 (the so-called Walden's rule [113], $\mu \cdot \eta = \text{const}$). Consequently, Eq. (6) becomes either

$$\nu \cdot \mu_{A,eff} = \frac{\mu_{A0} + \mu_{AS} K'_{AS} c_S}{1 + K'_{AS} c_S} \tag{25a}$$

or

$$\mu_{A,eff} = \frac{\mu_{A0} + \mu_{AS} K'_{AS} c_S}{1 + K'_{AS} c_S} \cdot \frac{1}{\nu} \tag{25b}$$

depending on whether the model parameters are to be determined from the effective mobility data or the effective mobility is to be predicted from the model parameters, respectively. The essential problem with the viscosity correction factor, Eq. (25), is that Walden's rule is by far not ultimate. This fact apparently did not prevent this correction from becoming uncritically popular in ACE applications, which inspires us to make a relatively detailed discussion on this topic herein.

The correction factor (aka the relative viscosity) is determined in several ways in ACE: directly, by determining the individual viscosities η_0 and η_S [115], or indirectly employing the CZE instrumentation. Typical indirect measurements consist in determination of (subscripts s and 0 refer to "with" and "without the addition of the selector", respectively): (i) t_S/t_0, where t is the time required to push the solution through the capillary by a defined pressure [116], (ii) I_0/I_S, where I is the current in the capillary at a constant voltage [43, 117], (iii) G_0/G_S and κ_0/κ_S where G is conductance, $G = I/U$, at constant power, U is voltage across the capillary, and κ is conductivity of the BGE [118], (iv) t_{MS}/t_{M0}, where t_M is a migration time of an indifferent marker [119]. When viscosity of the solution is determined by means of external instrumentation, the bulk viscosity is measured rather than its effect on the movement of ions. The same applies to method (i) above that effectively turns the CZE instrumentation into a viscometer. Using the CZE instrumentation for the viscosity measurements (in the role of a viscometer) was somewhat validated within the study by Shibukawa et al. [119] or Fanali and Boček (who weighed the vials rather than reading times t_0 and t_s) [120]. The relative viscosity generally increases with increasing concentration of the additive in a nonlinear manner [113, 115, 120]. Several studies [45, 58, 70 122, 123] nevertheless show that a linear dependence,

$$\nu = r \cdot c_S + 1, \tag{26}$$

is often obeyed with an excellent precision within the range of the selector concentrations used. In Eq. (26), r is an empirical constant that has to be determined. In some studies [70, 121, 122] the intercept of Eq. (26) was also subject to the linear regression. This is indeed unrealistic ($\nu|_{[c_S=0]} \equiv 1$) and the intercept should always be fixed to 1 during the regression.

Relations among the various correction factors

Østergaard et al. [118] investigated mobility ratios, μ_0/μ_S, for various analytes (pharmaceuticals and two bile salts) in glycerol-altered BGEs. Glycerol was supposed not to interact with the analytes. We reprocessed the data and provide a graphical comparison in Fig. 2A. If Walden's rule applied, the mobility ratios would equal the relative viscosities, whereas Fig. 2A clearly displays that it is not so. Interestingly, the graphical data reveal that not only are some compounds less affected by the viscosity changes than Walden's rule suggests but other compounds are influenced to a higher extent than the mere viscosity change can account for (which is inconsistent with the underlying theory recapped in the ESM). Aware of this discrepancy, the authors attributed it to an observed decrease in temperature or possible IS effects. Alternatively though, the data may just reflect the true nature of the problem since the theory of migration under the influence of a non-electrolyte is definitely not a closed issue yet. In any case, Fig. 2 in the original study demonstrates that the anticipated constancy of the Walden's product strongly improves if the relative viscosity or current is applied as the correction factor to the effective mobilities. Such an observation can be understood when realizing that the effective mobilities of the analytes drop roughly by 45 % (calculated as $(\mu_0 - \mu_S)/\mu_0 = 1 - (\mu_0/\mu_S)^{-1}$) as a result of the presence of glycerol, while they do not deviate from the relative viscosity trend by more than 8 % (cf. Fig. 2A).

The relative viscosity and current ratio worked comparably well in the case of glycerol in the study by Østergaard et al. The comparison between these two correction factors is depicted in Fig. 2B (we present the BGE dilution corrected values only; see the ESM for details). An agreement between the relative viscosity and current ratio was reported by other authors at low concentrations of cyclodextrins, too. A maximal relative viscosity of 1.32 (corresponding to 75 mM methylated-β-CD) was achieved in one study [43]; although this information was not available in another study [123], the hydroxypropyl-β-CD concentration did not exceed 20 mM in that case. Lemesle-Lamache et al. [117] reported a 1:1 relation between relative viscosity and current ratio up to concentrations of β-CD of

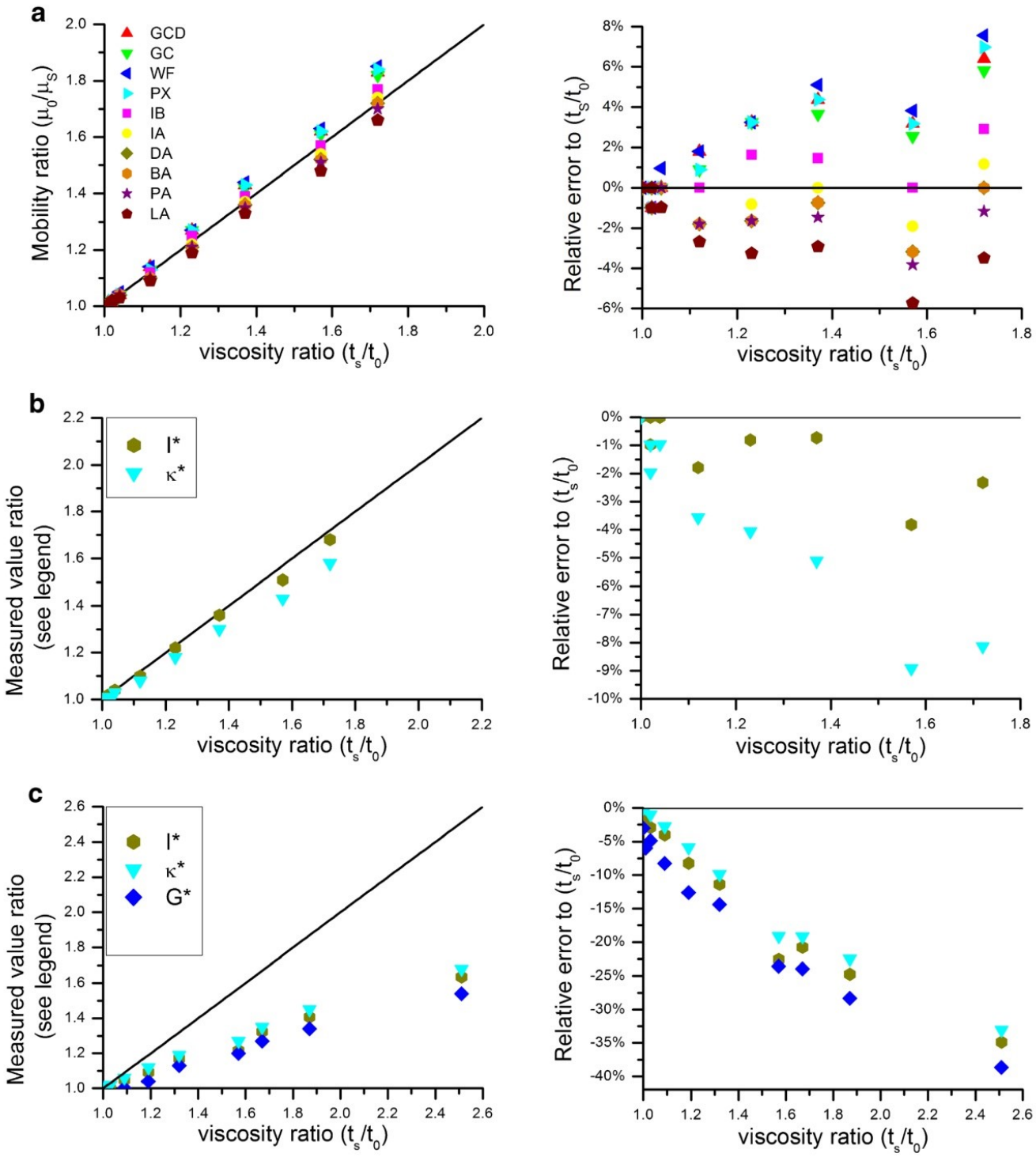


Fig. 2 Correlation of the (BGE dilution corrected) values of relative current (*I**), relative conductivity (*k**), relative conductance (*G**); and mobility ratios of non-interacting ions, lidocain (*LA*), propranolol (*PA*), benzoic acid (*BA*), Dibucaine (*DA*), imipramine (*IA*), ibuprofen (*IB*), piroxicam (*PX*), warfarin (*WF*), glycocholate (*GC*), glycodeoxycholate (*GDC*)—see ESM for chemical structures—with the relative viscosity measured by the ratio of times needed to push the solution through the capillary by a defined pressure. **A** viscosity altered by glycerol; **B** viscosity altered by glycerol; **C** viscosity altered by cyclodextrin. *Left* absolute values, *diagonal line* shows the ideal match; *Right* relative differences to the absolute match (*diagonal line* in the *right panel*). Data reprocessed from the study by Østergaard et al. (2009)

200 mM ($v \cong 2.2$). Nevertheless, a closer look at the data plot (Fig. 3 in the original paper) reveals that the current ratio might have followed the relative viscosity well up to the values of $v \cong 1.3$ while it possibly started

deviating at the higher values of the relative viscosity (however, there are not enough data points in the study to make a solid conclusion).

These results may seduce one to a conclusion that determining the current ratio is an equivalent alternative to the relative viscosity. It may well be so but only at rather low relative viscosities (selector concentrations). Taking the t_S/t_0 ratio as a reference, Østergaard et al. [118] also showed that other methods (current, conductivity, or conductance ratios) provided systematically lower correction factors than the relative viscosity when a CD (instead of glycerol) was present in the BGE. The results are less optimistic than the aforementioned studies, indicating that the current or conductivity ratios approximately match the relative viscosity at the lowest CD concentrations only (cf. Fig. 2C). The opposite conclusion made for glycerol (ν up to 1.7; equivalent CD concentration of 100 mM) was attributed to the fact that glycerol is a much smaller molecule than the CD, comparable in size to the BGE ions. Shibukawa et al. [119] provided highly convincing results that univocally prefer the current ratio over the relative viscosity. They determined both the current ratio and the mobility ratio of (presumably non-interacting) ascorbic acid in the presence of γ-CD. The current ratio started deviating from the relative viscosity at values of approx. 1.8 and the deviation grew up to $\nu \cong 4.5$, $I_0/I_s \cong 3.3$ (approximate values read from data plot) at 250 mM γ-CD. To the contrary, the mobility ratio of the acid followed the relative current nearly perfectly up to the highest CD concentrations.

The fact that the relative viscosity (or rather current ratio) accounts for a big portion of the change in the electrophoretic mobility of non-interacting ions not only justifies the application of such correction factors but even makes them essential especially for the weakly interacting analytes in ACE. Penn et al. discussed in 1994 [99] that if the binding constant is of the order of 100 M^{-1} or less, the relative viscosity as low as 1.02 easily overweighs the actual binding effect at low selector concentrations. At high selector concentrations the binding effect is significant enough but then so is the viscosity of the BGE [100] as well as the deviation of the effective mobility from Walden's rule [119]. Unfortunately though, the current ratio is only applicable when neutral selectors are used for obvious reasons, while the relative viscosity seems to be an appropriate choice only at low selector concentrations. Finally, Vespalec and Boček [71] pointed out that cyclodextrins are relatively small molecules (in contrast to, e.g., polymerized CDs) so that the bulk viscosity of the BGE should be sufficiently relevant. Figure 2 as well as the results by Shibukawa et al. indicate that the viscosity changes caused by the presence of CDs in the BGE do not fully correlate with mobility changes of small ions and the same can apply even to as small additives as glycerol.

Using a mobility standard

Britz-McKibbin and Chen used a non-interacting analyte as a mobility standard (MOS) for viscosity corrections in their attempt to accurately describe weak analyte–additive interactions by capillary electrophoresis [124]. When the effective mobilities were corrected to the relative viscosity only, the dependences of $\mu_{A,eff}$ vs. c_S did not follow the hyperbolic pattern of Eq. (6) and the product of $\mu_A \cdot \nu$ was by far not constant for non-interacting analytes. The situation substantially improved by applying a correction factor $\nu' = \mu_{MOS,S}/\mu_{MOS,0}$, i.e., a mobility ratio analogous to that depicted in Fig. 2A. The authors attributed the difference between ν and ν' to the fact that the selector alters both the viscosity and the dielectric properties of the BGE. They originally expressed ν' as $\nu' = \nu \cdot \nu_\delta$ where ν_δ is supposed to be the relative dielectric correction factor. Although this idea is consistent with the basic theory provided in the ESM and the ν_δ values were reported as closely matching those obtained for glucose in the literature, the study leaves the hypothesis of altering the dielectric properties of the BGE rather open. The way in which the parameter ν_δ was determined and used would be perhaps better reflected by concluding that a MOS helps in improving the results no matter what the real cause of $\nu' \neq \nu$ is. Similarly, the ascorbic acid used by Shibukawa et al. [59] was actually meant as a MOS.

Other authors realized that even the electroosmotic flow (EOF) can be used as the MOS since it is—similarly to the ion mobility (see the ESM)—inversely proportional to the viscosity of the solution,

$$\mu_{EOF} = \frac{\epsilon\zeta}{4\pi\eta}, \tag{27}$$

where is the dielectric constant of the BGE and ζ is the zeta potential of the capillary wall. Valkó et al. [125] reported a constant Walden's product for the EOF in a phosphate buffer up to concentrations of γ-CD of 100 mM and consequently used the EOF as a MOS for determination of binding constants of mandelic acid with the CD. The constant Walden's product for the EOF is in accordance with the study by Shibukawa et al. [59] who made the same observation in the same buffer up to 250 mM of γ-CD. Interestingly, Lemesle-Lamache et al. [117] reported just the opposite. They claimed the EOF mobility ratio did not correspond to the relative viscosity (β-CD, maximal ν of 2.5). Unfortunately, the data are not really convincing in this case since they are rather scattered, and what manifests itself as a nonlinear relationship might be alternatively seen as a high variance caused by an unstable EOF. However, the constant Walden's product for the EOF up to the highest relative viscosities simultaneously raises doubts about using the EOF as a MOS. It rather

indicates that the EOF happens to be an excellent marker of the bulk viscosity (which seems reasonable), whereas the bulk viscosity is not always decisive for the small ions (analytes) as discussed in the previous section. This is perfectly demonstrated in the aforementioned study by Shibukawa et al. [59].

Yang, Bose, and Hage [126] showed (both theoretically and experimentally) that the reproducibility of the moblities and migration times in general CE improves significantly by considering a mobility ratio $M = \mu'_A/\mu_{MOS}$ or migration time ratio $R_t = t_A/t_{MOS}$ where the subscripts A and MOS refer to the analyte and the mobility standard, respectively. The MOS has a similar role here as in the previous cases but it is used in a different manner now. The mobility of the analyte is not multiplied by a correction factor based on the mobilities of the MOS with and without the addition of the selector, but a new parameter is introduced that is evaluated instead of the analyte's mobility. Furthermore, the correction is applied to the apparent mobility of the analyte, μ'_A, not the effective one, $\mu_{A,eff}$, in the original paper by Yang, Bose, and Hage. The EOF is also applicable as a MOS in general but we already discussed that such practice is doubtful in ACE. The two ratios not only account for the viscosity effects but also do not depend on the experimental setup (capillary length, detector position, voltage, temperature), thereby making the method more robust. It is not completely independent of other effects that alter the EOF, though. The authors also stated that "*M* can be used… where it is desirable to relate… migration to fundamental parameters of the system, such as… binding to agents that have been added to the running buffer". Nevertheless, the meaning of this statement actually was—as demonstrated experimentally—that the *M* or R_t parameter compensates the effects the additives have on non-interacting analytes. Kawaoka and Gomez [127] realized that the *x*-reciprocal transformation of Eq. (6) can be equivalently expressed in terms of the mobility ratio, *M*, and they determined some binding constants (though using the EOF as the MOS) in this way. We give a more general proof in the ESM showing that the *M* parameter obeys Eq. (6) exactly. The resulting binding constant, K'_{AS}, is identical to that obtained in the standard way but the related mobility of the free analyte, μ_{A0}, and that of the analyte–selector complex, μ_{AS}, result in terms of the *M* parameter. Subsequently, the original mobilities must be back-calculated from these parameters. (The situation is not so simple in the case of the R_t parameter as shown in the ESM.) Two mobility standards are required to take advantage of the robustness of the *M* and R_t parameters and simultaneously work with the mobilities directly [128]. Such an approach also has general applicability in CE, and the inventors demonstrated its applicability in ACE measurements, too [129, 130]. In our opinion this latter approach better accounts for various instabilities in CE, including the EOF; however, it requires two MOSs, which can cause difficulties in ACE. If the *M* parameter is to be used, we would additionally suggest to base it on the effective mobility, $\mu_{A,eff}$, rather than the apparent one, μ'_A (cf. ESM).

The use of a MOS may seem the best idea to cope with the side effects caused be the presence of the selector. Unfortunately even this cannot be applied without caution. The problem with using the EOF as a MOS has been already discussed. The selector may further alter the zeta potential of the capillary wall [131], which would make the entire approach of no use. If an internal standard is used as the MOS, it should resemble the analyte as much as possible, which contradicts the requirement of the MOS not to interact with the selector. Additionally, another interesting finding results from the study by Østergaard et al. [121]. The visual similarity of tested compounds does not imply their similar sensitivity to the presence of an additive. When data in Fig. 2A are compared to chemical structures of the compounds (available in the ESM) it turns out that, for example, benzoic acid (orange hexagons) does not follow ibuprofen (violet squares), its closest molecule by visual comparison, but it perfectly overlaps with dibucaine (green diamonds), a molecule that looks somewhat different. Similarly, benzoic acid is the smallest of the tested compounds but lidocaine (brown pentagons) is the least affected by the viscosity changes whereas ibuprofen, the smallest molecule but one, approaches the largest ones. Several observations of this kind can be made. Only the very large molecules (triangles) somewhat cluster together, but again piroxicam and warfarin (rightward and leftward triangles) are the most sensitive to the viscosity changes even though they are apparently smaller than the bile salts (upward and downward triangles). In fact, using, e.g., benzoic acid as a MOS for ibuprofen (under the conditions of Fig. 2A) would even worsen the situation compared to the simple relative viscosity correction as benzoic acid deviates systematically negatively while ibuprofen deviates positively from the relative viscosity.

Other approaches

Barták et al. [132, 133] took advantage of the linearization of Eq. (6) and applied an advanced statistical approach to the evaluation of binding constants in ACE. A perfect linear dependence would result after linearization if the effective mobility of an analyte was influenced by nothing but the mere interaction with the selector. Further, only a slight deviation from linearity is expected if the effective mobility is not disturbed by the viscosity (or other) effects too much. On the other hand, real experimental data are always of a random nature so that the nonlinearity cannot be easily uncovered and compensated. The statistical approach introduced by Barták et al. allows for estimating the extent of nonlinearity of experimental data on the basis of the expected function (the linearized form of Eq. (6)), which leads to corrected

estimates of the parameters, i.e., μ_{A0}, μ_{AS}, and K'_{AS}. Although the method can handle only minor nonlinearities [71] and it requires rather sophisticated mathematical treatment, it can be advantageous for evaluation of the corrected binding constants. On the other hand, it leaves the question of the source(s) of such nonlinearity open and thus it is not useful for predicting the effective mobility in the separation system, e.g., for the purpose of further method optimization.

Inspired by the fact that the viscosity changes caused by large selectors should mostly influence similarly sized moving particles, we adopted a practice of correcting only the mobility term of the complex in some of our studies [45, 70],

$$\mu_{A,eff} = \frac{\mu_{A0} + \frac{\mu_{AS}}{\nu} K'_{AS} c_S}{1 + K'_{AS} c_S}. \quad (28)$$

Equation (28) requires an explicit formula for the relative viscosity, ν, as a function of the selector concentration, c_S, (cf., e.g., Eq. (26)) and can no longer be linearized. This correction is also implemented in the CEval software [58]. Although this idea is becoming rather dubious in the light of the just reviewed evidence that small ions are affected by the presence of large additives as well, applying the relative viscosity in Eq. (28) provided a complete match between the fitting function, Eq. (28), and the experimental data, further supported by a perfect agreement between the binding constants determined in this way and those determined independently by NMR [70]. To the contrary, biased fitting curve and binding constants resulted without any viscosity correction. Perhaps, the best practice would be to use different correction factors for the two mobilities on the right-hand side of Eq. (6) (alike Eq. (28)). Such an approach has not been tested in the literature yet. As a final note let us point out that the χ-conditional mobility, Eq. (19) or generally Eq. (21), can be corrected in the same way only under the—yet most likely reasonable—assumption that the correction factor, ν, is common to all selectors in the mixture.

Ionic strength

The IS influences the effective mobility of an analyte in ACE in two ways: (i) it governs the complexation and the acid–base equilibria, (ii) it affects the movement of ions in the BGE

Complexation and acid–base equilibria

We advise the reader to refer to the review by Vespalec and Boček [71] who summarized the related physicochemical concept of apparent vs. true thermodynamic binding equilibrium in a highly educative way. The true thermodynamic binding constant is related to the apparent one through the activity coefficients, γ, according to

$$K^{th}_{AS} = K'_{AS} \frac{\gamma_{AS}}{\gamma_{A0}\gamma_{S0}} = K'_{AS} \cdot K^{\gamma}_{AS}, \quad (29)$$

where we use the superscript *th* to emphasize the thermodynamic constant and the subscripts AS, A0, and S0 in their usual meanings. The activity coefficients can be expressed from the given IS of the BGE using the Debye–Hückel extended law,

$$-\log\gamma_i = \frac{0.509 z_i^2 \sqrt{I}}{1 + 3.287 a \sqrt{I}}, \quad (30)$$

where the two numerical constants are valid for water solutions at 25 °C, z_i is the charge of the species i (AS, A0, or S0), parameter a represents the distance of closest approach of ions (in nanometers), and I is the IS, $I = \sum c_i z_i^2$, where the summation extends over all ions in the system and the concentrations are expressed in moles per cubic decimeter. The logarithm of the activity coefficient quantifies (but not equals) an extra potential energy that the species i attains in the solution owing to its interactions with surrounding molecules (including those of the species i itself). It is generally accepted that electrostatic interactions are the prime source of such energy in electrolyte solutions as reflected by Eq. (30). At this point we have to distinguish among three cases. The first one is a neutral analyte interacting with a charged selector. The potential energy of neutral analytes is not affected by the electrostatic interactions and thus its activity coefficient equals one (the logarithm being zero). The analyte–selector complex bears the same charge as the selector itself and it is reasonable to assume that the two are of similar sizes as well, thus sharing the same value of the parameter a. Consequently, the activity coefficients of the selector and the complex are likely similar. Under all these assumptions, $K^{\gamma}_{AS} \cong 1$, and, $K^{th}_{AS} \cong K'_{AS}$ [134]. The opposite case happens when a charged analyte interacts with a neutral selector. Then the activity coefficient of the (neutral) free selector is equal to one. The parameter a of small ions is generally close to 0.5 nm, which gives the McInnes approximation of the product $3.287a \cong 1.5$. Taking the same value for the analyte–selector complex is not appropriate for most selectors, which are generally much bigger than the "small ions", but the correct value is hardly available and so one is left with using a rough estimate (cf. [70]). Alternatively, the value can be estimated from the dependency of the effective mobility of an analyte (either the free ion or the selector) on the IS [45, 135]. The final case is that of both charged analyte and selector. The McInnes approximation can be used for the analyte, and the same parameter a would possibly apply to a large selector and its complex with the analyte. The activity

coefficients of the free selector and the complex do not cancel each other this time since the free selector and the analyte–selector complex have different charges. As far as we are concerned, no data have been published that would deal with the IS correction in such systems.

Next, let us consider the χ-conditional binding constant, Eq. (19c), of a (presumably commercial) mixture of selectors. In the case of neutral analytes, $K'_{\mathrm{AS}^{[q]}} \cong K^{\mathrm{th}}_{\mathrm{AS}^{[q]}}$, and consequently, $K'^{\chi}_{\mathrm{AS}} \cong K^{\mathrm{th}\chi}_{\mathrm{AS}}$, regardless of the nature of the selectors used. In the case of a mixture of neutral selectors, the constant, K^{χ}_{AS}, reduces to, $\gamma_{\mathrm{AS}}/\gamma_{\mathrm{A0}}$, which factors out of the summation in Eq. (19c) only if all the selectors in the mixture have similar sizes, i.e., they share a common parameter a. The same applies to a mixture of selectors that all have the same charge (and a charged analyte) if additionally the size of the complex is comparable to the size of the selector ($a_{\mathrm{AS}} \cong a_{\mathrm{S0}}$), which is often a reasonable assumption, though. Lastly, the χ-conditional binding constant cannot be corrected to the IS as if it were a binding constant of a single selector when the mixture consists of selectors of different charges (and the analyte is also a charged molecule). Instead, an individual correction constant, $K^{\gamma}_{\mathrm{AS}^{[q]}}$, applies to each individual selector that cannot be separated out of the summation, Eq. (19c). Unfortunately, this is often the case with commercial mixtures of CDs and so attention must be paid to this fact when analyzing charged solutes. Combinations of charged and neutral CDs in dual systems are also common but often employed for neutral analytes or the individual constants, $K^{\gamma}_{\mathrm{AS}^{[q]}}$, can be utilized since the composition of such artificial mixtures of selectors is known (unless being composed of commercial mixtures of selectors, for which the above stated limitations apply).

Concerning the mixed protonation constant, it results [66] that

$$K^{\mathrm{th}}_{\mathrm{prot}} = K^{\mathrm{mix}}_{\mathrm{prot}} \frac{\gamma_{\mathrm{A}^{[+\mathrm{H}]}}}{\gamma_{\mathrm{A}^{[-\mathrm{H}]}}}. \tag{31}$$

The activity coefficients can be calculated according to Eq. (30), e.g., using the McInnes approximation. The two activity coefficients do not cancel each other because of obviously different charges of the two protonated states of the analyte.

Effective mobility

Correction of the ionic moblities to the IS poses a convoluted problem that involves recursive formulas as results from the theory by Onsager and Fuoss [136] (cf. namely Eqs. (4.6.8), (4.7.11), (4.7.12), (4.8.1)–(4.8.3) in the reference). The formulas must be solved numerically as implemented, e.g., in our software PeakMaster [137] (available for free at http://echmet.natur.cuni.cz/download), though only for non-interacting analytes and BGE constituents. The equations have not been solved for analytes interacting with a selector in the BGE yet. The IS mobility correction is considerably simplified when only two species (an ion and its counterion) are present in the solution (cf. Eq. (4.9.1) in [136]). Then,

$$\mu^0_A - \left(0.7853 \cdot \mu^0_A |z_A z_B| \frac{q}{1+\sqrt{q}} + 3.138 \cdot 10^{-8} \cdot |z_A|\right) \frac{\sqrt{I}}{1 + 3.287 a \sqrt{I}} \tag{32a}$$

where z_{A} is the charge of the ion of interest, z_{B} is its counterion, and the numeric constants are valid for water solution at 25 °C if the IS is expressed in moles per cubic decimeter, the parameter a in nanometers, and the electrophoretic mobility in meters squared per volt per second. μ^0_{A} is the limiting electrophoretic mobility of the ion A (at infinite dilution of the solution) and

$$q = \frac{|z_{\mathrm{A}} z_{\mathrm{B}}|}{|z_{\mathrm{A}}| + |z_{\mathrm{B}}|} \frac{\mu^0_{\mathrm{A}} + \mu^0_{\mathrm{B}}}{|z_{\mathrm{A}}|\mu^0_{\mathrm{A}} + |z_{\mathrm{B}}|\mu^0_{\mathrm{B}}}. \tag{32b}$$

Specifically, $q = 0.5$, for uni-univalent electrolytes. One may be aware of a simplified version of Eq. (32a), which takes only the square root of the IS on the right-hand side, thus not requiring the parameter a. Unfortunately, this simplification is not appropriate in CE [135]. Electrophoretic mobility of an analyte, A, can be corrected to the IS of the BGE using Eq. (32) while the counterion of the BGE is taken for the ion B. This results in a somewhat hybrid approach when only analyte–counterion interaction is assumed on the one hand, but all present ions are accounted for in the calculation of the IS on the other hand. Nevertheless, such an approximation is preferred over not performing the IS correction at all [138]. It has been further justified experimentally in a rather unique study by Beneš et al. [45]. The authors studied electromigration of a neutral analyte in the presence of a defined monovalent charged CD. When the simple Eq. (6) was employed, the fitting curve did not match the experimental points very well but the situation improved dramatically when viscosity and IS corrections were applied. Additionally, the data were obtained in two ways. First the IS was kept constant by decreasing buffer concentration while increasing the (charged) selector concentration. Second, the IS was not adjusted manually but the IS correction, Eq. (32a), was employed to account for it. The parameter a of the selector was estimated experimentally in the study and the authors introduced a simple verification that the same value applies to the analyte–selector complex, too. A perfect agreement between binding constants determined at the constant IS and the variable IS was reported. Equation (32a) has been applied by other authors even in methanol/water solvent systems (after accommodating the numerical constants properly) [139]. Other approaches to the IS

correction can be found in the literature [135] but they have not been apparently transferred to ACE.

When a highly charged selector is employed in the separation system, it influences the IS of the BGE to a great extent and simultaneously the mobility of the (highly charged) complex is especially sensitive to the IS (cf. Eq. (32a)). In such systems, the dependence of the effective mobility of the analyte on the selector concentration may completely violate the hyperbolic pattern prescribed by Eq. (6). Instead it may exhibit a local maximum, which would be much unexpected if not observed for several highly charged CDs ($z > 7$) by the group of Vigh [140–143]. The authors explained their observation by the mechanism that we reproduce in the ESM. Additionally, the large multiply charged selectors (as typical for several widely used CD derivatives) definitely do not satisfy assumptions required for the validity of the Onsager–Fuoss theory. As a matter of fact, the entire concept of the IS is questionable in such systems. So even the compensation for the increasing IS is not fully justifiable, notwithstanding the usually unknown composition of commercial mixtures. Whatever else might be said about it, the problem of large highly charged selectors and their impact on the (effective) mobilities of ions remains an open issue.

Conclusion

Various equations describing the dependence of the effective mobility of an analyte on the selector concentration, pH, and composition of a mixture of selectors have been reviewed and their mutual relationships explored. Equation (6) is the fundamental equation in ACE, originally developed for interactions with a single selector in systems where neither the analyte nor the selector is involved in the acid–base equilibria. Several authors extended this formula in an attempt to account for the pH dependence of the effective mobility of a monovalent weakly acidic/basic analyte interacting with a neutral or permanently charged selector. The resulting expressions are not always easily seen as being actually identical but they are all covered by Eq. (13). If pH is kept constant, the analyte obeys Eq. (6) with the pH-conditional parameters regardless of its actual ionization state. If the selector is present at a constant amount, the analyte behaves as a standard weakly acidic/basic compound possibly with a complexation-induced shifted pK_A value.

The most recently published multi-analyte multi-selector model discloses that Eq. (6) with conditional parameters, $\mu_{A0}^{M_A M_S}$, $\mu_{AS}^{M_A M_S}$, $K_{AS}^{'M_A M_S}$, i.e., Eq. (21), retains its validity if (i) the external conditions (typically pH) are maintained so that the distribution of the analyte into its possible (typically ionic) forms does not change; and (ii) a mixture of selectors of constant composition is employed. The pH-conditional and the χ-conditional parameters can be further combined into the $M_A M_S$-conditional ones. Specifically, in any of the previously published models any mixture of selectors can be treated as a single selector with the χ-conditional parameters, including the case when χ-conditional parameters of several mixtures of selectors are combined into subsequent χ-conditional parameters of yet another mixture. This justifies the usual practice of treating commercial mixtures of selectors as a single one. Nonetheless, the χ-conditional parameters may (or may not) lose their validity when the selectors alter the viscosity of the BGE or when it comes to the ionic-strength-related effects. Also, attention must be paid to the fact that the fundamental Eq. (6) as well as any of its various conditional alternatives are always additionally IS-conditional.

Apart from the 1:1 complexation stoichiometry several further requirements apply, namely fast equilibrium rate, sufficiently abundant amount of the selector in comparison with the amount of the analyte, and no interaction between the selector and the BGE components. Violation of these requirements has diverse consequences. Slow equilibrium makes the peak wider, while it can eventually split into two. Low selector concentration does not alter the effective mobility of the analyte but rather leads to an unexpected dispersion of its migrating zone. The Haarhoff–Van der Linde (HVL) function seems to describe the dispersed peak well. Finally, if the selector interacts with any of the BGE components, conditional parameters valid in the particular separation system only appear in Eq. (6). Such side interactions can also considerably alter the basic BGE properties such as its pH. pH of the buffer should always be checked after the addition of a selector (even a neutral one). If the buffer pH changes upon addition of the selector, it indicates undesirable side interactions of the BGE component(s) with the selector (but the stabile pH does not guarantee a lack of such side interactions).

Both viscosity of the BGE and its ionic strength have a significant impact on the effective mobility of the analyte. None of these effects can be treated in an ultimately exact way. Viscosity effects are unavoidable in ACE but few studies can be found in the literature on this topic, sometimes with contrary conclusions. Different ions exhibit different sensitivity to the addition of large particles (selectors) into the BGE, perhaps regardless of their visual structural resemblance on paper. An observation has been made that large ions are influenced by the addition of glycerol to a larger extent than the bulk viscosity can account for, which is in contradiction with the standard theory. Using the current ratio (neutral selectors only) as a "viscosity" correction factor or adopting different correction factors for the mobility of the free analyte and the

mobility of the complex, perhaps employing a mobility standard (MOS), seems the best practice in the light of current studies. Further investigations are needed, though. Nonetheless, using the EOF as the MOS is not advisable. Few studies examined the IS-related effects in ACE. The binding constant is (under reasonable assumptions) not affected by the IS if a neutral analyte interacts with any selector or their mixture. Otherwise it can be approximately recalculated to the thermodynamic one, but mixtures of charged selectors of unknown composition cannot be generally treated in this way. IS correction of the effective mobility is a complex task that has not been fully accomplished in the literature yet. The Onsager–Fuoss formula for two interacting ions (the free analyte and the BGE counterion and/or the complex and the BGE counterion) was reported to work with sufficient precision for this purpose. In general, it is best to keep the IS constant in the separation system. The BGE can be appropriately diluted upon addition of a well-defined charged selector. This practice is, however, hard to meet specifically in systems with highly charged selectors or a mixture of selectors. A suitable treatment of the IS remains an open problem there.

When (possibly conditional) complexation parameters are to be extracted from the experimental data, linearization of Eq. (6)—as often applied in practice—is neither advisable nor needed with current computational power and tools. We kindly encourage the reader to download our recently published freeware CEval (http://echmet.natur.cuni.cz/download) for this purpose. The software accounts for HVL distortion of the peaks, viscosity corrections, nonlinear regression of Eq. (6), and statistical evaluations.

Acknowledgements Acknowledged is the financial support of this work from the grant no. 15-18424Y of the Czech Science Foundation and from the Charles University grants UNCE204025/2012 and GAUK no.726716.

Compliance with ethical standards

Conflict of interest All authors declare no conflicts of interest.

References

1. Heegaard NHH, Kennedy R. Identification, quantitation, and characterization of biomolecules by capillary electrophoretic analysis of binding interactions. Electrophoresis. 1999;20:3122–33.
2. Heegaard NHH. Affinity in electrophoresis. Electrophoresis. 2009;30:S229–39.
3. Vuignier K, Schappler J, Veuthey JL, Carrupt PA, Martel S. Drug–protein binding: a critical review of analytical tools. Anal Bioanal Chem. 2010;398:53–66.
4. Heegaard NHH. Applications of affinity interactions in capillary electrophoresis. Electrophoresis. 2003;24:3879–91.
5. Colton IJ, Carbeck JD, Rao J, Whitesides GM. Aflinity capillary electrophoresis: a physical-organic tool for studying interactions in biomolecular recognition. Electrophoresis. 1998;19:367–82.
6. Tsioupi DA, Stefan-van Staden RI, Kapnissi-Christodoulou CP. Chiral selectors in CE: recent developments and applications. Electrophoresis. 2013;34:178–204.
7. Scriba GKE. Fundamental aspects of chiral electromigration techniques and application in pharmaceutical and biomedical analysis. J Pharm Biomed Anal. 2011;55:688–701.
8. Chankvetadze B. Enantioseparations by using capillary electrophoretic techniques. The story of 20 and a few more years. J Chromatogr A. 2007;1168:45–70.
9. Terabe S, Otsuka K, Nishi H. Separation of enantiomers by capillary electrophoretic techniques. J Chromatogr A. 1994;666:295–319.
10. Cucinotta V, Contino A, Giuffrida A, Maccarrone G, Messina M. Application of charged single isomer derivatives of cyclodextrins in capillary electrophoresis for chiral analysis. J Chromatogr A. 2010;1217:953–67.
11. Jensen H, Larsen SW, Larsen C, Østergaard J. Physicochemical profiling of drug candidates using capillary-based techniques. J Drug Delivery Sci Technol. 2013;23:333–45.
12. Stavrou IJ, Mavroudi MC, Kapnissi-Christodoulou CP. Chiral selectors in CE: recent developments and applications (2012–mid 2014). Electrophoresis. 2015;36:101–23.
13. Ali I, Al-Othman ZA, Al-Warthan A, Asnin L, Chudinov A. Advances in chiral separations of small peptides by capillary electrophoresis and chromatography. J Sep Sci. 2014;37:2447–66.
14. Jáč P, Scriba GKE. Recent advances in electrodriven enantioseparations. J Sep Sci. 2013;36:52–74.
15. Pérez-Fernandez V, García MÁ, Marina ML. Chiral separation of agricultural fungicides. J Chromatogr A. 2011;1218:6561–82.
16. Horáková H, Grüner B, Vespalec R. Emerging subject for chiral separation science: cluster boron compounds. Chirality. 2011;23:307–19.
17. Lu H, Chen G. Recent advances of enantioseparations in capillary electrophoresis and capillary electrochromatography. Anal Methods. 2011;3:488–508.
18. Mikuš P, Maráková K. Advanced CE for chiral analysis of drugs, metabolites, and biomarkers in biological samples. Electrophoresis. 2009;30:2773–802.
19. Poinsot V, Rodat A, Gavard P, Feurer B, Couderc F. Recent advances in amino acid analysis by CE. Electrophoresis. 2008;29:207–23.
20. Kašička V. Recent developments in capillary electrophoresis and capillary electrochromatography of peptides. Electrophoresis. 2006;27:142–75.
21. Eeckhaut AV, Michotte Y. Chiral separations by capillary electrophoresis: Recent developments and applications. Electrophoresis. 2006;27:2880–95.
22. Řezanka P, Navrátilová K, Řezanka M, Král V, Sýkora D. Application of cyclodextrins in chiral capillary electrophoresis. Electrophoresis. 2014;35:2701–21.
23. Chankvetadze B. Separation of enantiomers with charged chiral selectors in CE. Electrophoresis. 2009;30:S211–21.
24. Fanali S. Chiral separations by CE employing CDs. Electrophoresis. 2009;30:S203–10.
25. Tang W, Ng SC. Monosubstituted positively charged cyclodextrins: synthesis and applications in chiral separation. J Sep Sci. 2008;31:3246–56.
26. Scriba GKE. Cyclodextrins in capillary electrophoresis enantioseparations – recent developments and applications. J Sep Sci. 2008;31:1991–2011.
27. Juvancz Z, Kendrovics RB, Iványi R, Szente L. The role of cyclodextrins in chiral capillary electrophoresis. Electrophoresis. 2008;29:1701–12.

28. Jiang C, Armstrong DW. Use of CE for the determination of binding constants. Electrophoresis. 2010;31:17–27.
29. Schou C, Heegaard NHH. Recent applications of affinity interactions in capillary electrophoresis. Electrophoresis. 2006;27:44–59.
30. Tanaka Y, Terabe S. Estimation of binding constants by capillary electrophoresis. J Chromatogr B. 2002;768:81–92.
31. Müllerová L, Dubský P, Gaš B. Twenty years of development of dual and multi-selector models in capillary electrophoresis: a review. Electrophoresis. 2014;35:2688–700.
32. Scriba GKE. Selected fundamental aspects of chiral electromigration techniques and their application to pharmaceutical and biomedical analysis. J Pharm Biomed Anal. 2002;27:373–99.
33. Chankvetadze B. Enantiomer migration order in chiral capillary electrophoresis. Electrophoresis. 2002;23:4022–35.
34. Rizzi A. Fundamental aspects of chiral separations by capillary electrophoresis. Electrophoresis. 2001;22:3079–106.
35. Fillet M, Hubert P, Crommen J. Enantiomeric separations of drugs using mixtures of charged and neutral cyclodextrins. J Chromatogr A. 2000;875:123–34.
36. Fanali S. Controlling enantioselectivity in chiral capillary electrophoresis with inclusion–complexation. J Chromatogr A. 1997;792:227–67.
37. Vespalec R, Boček P. Chiral separations by capillary electrophoresis: present state of the art. Electrophoresis. 1994;15:755–62.
38. Chankvetadze B, Blaschke G. Enantioseparations in capillary electromigration techniques: recent developments and future trends. J Chromatogr A. 2001;906:309–63.
39. Vespalec R, Boček P. Chiral separations in capillary electrophoresis. Chem Rev. 2000;100:3715–53.
40. Chankvetadze B. Separation selectivity in chiral capillary electrophoresis with charged selectors. J Chromatogr A. 1997;792:269–95.
41. Tiselius A. Nova Acta Regiae Soc Sci Ups, Ser IV 7. 1930;4:1-107. pp. 26.
42. Guttman A, Paulus A, Cohen S, Grinberg N, Karger BL. Use of complexing agents for selective separation in high-performance capillary electrophoresis; chiral resolution via cyclodextrins incorporated within polyacrylamide gel columns. J Chromatogr. 1988;448:41–53.
43. Wren SAC, Rowe RC. Theoretical aspects of chiral separation in capillary electrophroesis I. Initial evaluation of a model. J Chromatogr. 1992;603:235–41.
44. Porras SP, Jussila M. Electromigration of a heteroconjugated imidazole–acetate complex in ACN. Electrophoresis. 2007;28:3590–9.
45. Beneš M, Zusková I, Svobodová J, Gaš B. Determination of stability constants of complexes of neutral analytes with charged cyclodextrins by affinity capillary electrophoresis. Electrophoresis. 2012;33:1032–9.
46. Bjørnsdottir I, Hansena SH, Terabe S. Chiral separation in nonaqueous media by capillary electrophoresis using the ion-pair principle. J Chromatogr A. 1996;745:37–44.
47. Hedeland Y, Haglöf J, Beronius P, Pettersson C. Effect of alkali metal hydroxides on the enantioseparation of amines using di-O-isopropylidene-keto-L-gulonic acid as the selector in NACE. Electrophoresis. 2006;27:4469–79.
48. Pang N, Zhang Z, Bai Y, Liu H. A study of the interaction between enantiomers of zolmitriptan and hydroxypropyl-beta-cyclodextrin by capillary electrophoresis. Anal Bioanal Chem. 2009;393:313–20.
49. Rundlett KL, Armstrong DW. Examination of the origin, variation, and proper use of expressions for the estimation of association constants by capillary electrophoresis. J Chromatogr A. 1996;721:173–86.
50. Horáková H, Vespalec R. Influence of substituents on selectivity and efficiency of chiral separations of anions containing single nido-7,8-dicarbaundecaborane cluster with α-cyclodextrin. J Chromatogr A. 2007;1143:143–52.
51. Šolínová V, Mikysková H, Kaiser MM, Janeba Z, Holý A, Kašička V. Estimation of apparent binding constant of complexes of selected acyclic nucleoside phosphonates with β-cyclodextrin by affinity capillary electrophoresis. Electrophoresis. 2016;37:239–47.
52. Baudelet D, Ghinet A, Furman C, Dezitter X, Gautret P, Rigo B, et al. Antagonists of the P2X7 receptor: mechanism of enantioselective recognition using highly sulfated and sulfobutylether cyclodextrins by capillary electrokinetic chromatography. Electrophoresis. 2014;35:2892–9.
53. Al Azzama KM, Saad B, Aboul-Enein HY. Determination of the binding constants of modafinil enantiomers with sulfated β-cyclodextrin chiral selector by capillary electrophoresis using three different linear plotting methods. Electrophoresis. 2010;31:2957–63.
54. Mofaddel N, Krajian H, Villemin D, Desbène PL. Enantioseparation of binaphthol and its monoderivatives by cyclodextrin-modified capillary zone electrophoresis: a mathematical approach. Talanta. 2009;78:631–7.
55. Danel C, Azaroual N, Brunel A, Lannoy D, Vermeersch G, Odou P, et al. Study of the complexation of risperidone and 9-hydroxyrisperidone with cyclodextrin hosts using affinity capillary electrophoresis and ^{1}H NMR spectroscopy. J Chromatogr A. 2008;1215:185–93.
56. Bowser MT, Chen DDY. Monte Carlo simulation of error propagation in the determination of binding constants from rectangular hyperbolae. 1. Ligand concentration range and binding constant. J Phys Chem A. 1998;102:8063–71.
57. Bowser MT, Chen DDY. Monte Carlo simulation of error propagation in the determination of binding constants from rectangular hyperbolae. 2. Effect of the maximum-response range. J Phys Chem A. 1999;103:197–202.
58. Dubský P, Ördögová M, Malý M, Riesová M. CEval: all-in-one software for data processing and statistical evaluations in affinity capillary electrophoresis. J Chromatogr A. 2016;1445:158–65.
59. Bowser MT, Chen DDY. Higher order equilibria and their effect on analyte migration behavior in capillary electrophoresis. Anal Chem. 1998;70:3261–70.
60. Progent F, Taverna M, Le Potier I, Gopée F, Ferrier D. A study of the binding between polymers and peptides, using affinity capillary electrophoresis, applied to polymeric drug delivery systems. Electrophoresis. 2002;23:938–44.
61. Karakasyan C, Taverna M, Millot MC. Determination of binding constants of hydrophobically end-capped poly(ethylene glycol)s with β-cyclodextrin by affinity capillary electrophoresis. J Chromatogr A. 2004;1032:159–64.
62. Bowser MT, Bebault GM, Peng X, Chen DDY. Redefining the separation factor: a potential pathway to a unified separation science. Electrophoresis. 1997;18:2928–34.
63. Lelievre F, Gareil P, Jardy A. Selectivity in capillary electrophoresis: application to chiral separations with cyclodextrins. Anal Chem. 1997;69:385–92.
64. Peng X, Bowser MT, Britz-McKibbin P, Bebault GM, Morris JR, Chen DDY. Quantitative description of analyte migration behaviour based on dynamic complexation in capillary electrophoresis with one or more additives. Electrophoresis. 1997;18:706–16.
65. Williams BA, Vigh G. Dry look at the CHARM (charged resolving agent migration) model of enantiomer separations by capillary electrophoresis. J Chromatogr A. 1997;777:295–309.
66. Včeláková K, Zusková I, Kenndler E, Gaš B. Determination of cationic mobilities and pKa values of 22 amino acids by capillary zone electrophoresis. Electrophoresis. 2004;25:309–17.
67. Müllerová L, Dubský P, Gaš B. Generalized model of electromigration with 1:1 (analyte:selector) complexation stoichiometry: Part II. Application to dual systems and experimental verification. J Chromatogr A. 2015;1384:147–54.

68. Rwjee YY, Staerk DU, Gyula V. Capillary electrophoretic chiral separations with cyclodextrin additives; I. Acids: chiral selectivity as a function of pH and the concentration of β-cyclodextrin for fenoprofen and ibuprofen. J Chromatogr A. 1993;635:291–306.
69. Rwjee YY, Williams RL, Gyula V. Capillary electrophoretic chiral separations using β-cyclodextrin as resolving agent; II. Bases: chiral selectivity as a function of pH and the concentration of β-cyclodextrin. J Chromatogr A. 1993;652:233–45.
70. Riesová M, Svobodová J, Ušelová K, Tošner Z, Zusková I, Gaš B. Determination of thermodynamic values of acidic dissociation constants and complexation constants of profens and their utilization for optimization of separation conditions by Simul 5 Complex. J Chromatogr A. 2014;1364:276–88.
71. Vespalec R, Boček P. Calculation of stability constants for the chiral selector–enantiomer interactions from electrophoretic mobilities. J Chromatogr A. 2000;875:431–45.
72. Righetti PG, Ettori C, Chafey P, Wahrmann JP. Enantiomer resolution in immobilized pH gradient gels via inclusion of a chiral discriminator. Electrophoresis. 1990;11:1–4.
73. Yoshida N, Seiyama A, Fujimoto M. Stability and structure of the inclusion complexes of alkyl-substituted hydroxyphenylazo derivatives of sulfanilic acid with alpha-cyclodextrin and beta-cyclodextrin. J Phys Chem. 1990;94:4254–9.
74. Rizzi AM, Kremser L. pKa shift-associated effects in enantioseparations by cyclodextrin-mediated capillary zone electrophoresis. Electrophoresis. 1999;20:2715–22.
75. Li JJ, Waldron KC. Estimation of the pH-independent binding constants of alanylphenylalanine and leucylphenylalanine stereoisomers with beta-cyclodextrin in the presence of urea. Electrophoresis. 1999;20:171–9.
76. Hammitzsch-Wiedemann M, Scriba GKE. Influence of buffer substances and urea on the β-cyclodextrin-mediated chiral separation of dipeptides in CE. Electrophoresis. 2007;28:2619–28.
77. Hammitzsch-Wiedemann M, Scriba GKE. Mathematical approach by a selectivity model for rationalization of pH- and selector concentration-dependent reversal of the enantiomer migration order in capillary electrophoresis. Anal Chem. 2009;81:8765–73.
78. Riesová M, Svobodová J, Tošner Z, Beneš M, Teařová E, Gaš B. Complexation of buffer constituents with neutral complexation agents: Part I. Impact on common buffer properties. Anal Chem. 2013;85:8518–25.
79. Linnemayr K, Rizzi A, Allmaier G. Characterization of modified cyclodextrins applied in capillary electrophoresis and high-performance liquid chromatography as chiral selectors by matrix-assisted laser desorption ionization curved field reflectron mass spectrometry. J Chromatogr A. 1997;791:299–306.
80. Chen FTA, Shen G, Evangelista RA. Characterization of highly sulfated cyclodextrins. J Chromatogr A. 2001;924:523–32.
81. Schmitt U, Ertan M, Holzgrabe U. Chiral capillary electrophoresis: facts and fiction on the reproducibility of resolution with randomly substituted cyclodextrins. Electrophoresis. 2004;25:2801–7.
82. Amini A, Rundl T, Rydberg MBG, Arvidsson T. Characterization of sulfated b-cyclodextrins and determination of enantiomeric purity of (1R,2S)-ephedrine by capillary zone electrophoresis. J Sep Sci. 2004;27:1102–8.
83. Lurie IS, Klein RFX, Dal Cason TA, LeBelle MJ, Brenneisen R, Weinberger RE. Chiral resolution of cationic drugs of forensic interest by capillary electrophoresis with mixtures of neutral and anionic cyclodextrins. Anal Chem. 1994;66:4019–26.
84. Bowser MT, Kranack AR, Chen DDY. Properties of multivariate binding isotherms in capillary electrophoresis. Anal Chem. 1998;70:1076–84.
85. Kranack AR, Bowser MT, Britz-McKibbin P, Chen DDY. The effects of a mixture of charged and neutral additives on analyte migration behavior in capillary electrophoresis. Electrophoresis. 1998;19:388–96.
86. Dubský P, Svobodová J, Gaš B. Model of CE enantioseparation systems with a mixture of chiral selectors Part I. Theory of migration and interconversion. J Chromatogr B. 2008;875:30–4.
87. Dubský P, Svobodová J, Tesařová E, Gaš B. Enhanced selectivity in CZE multi-chiral selector enantioseparation systems: proposed separation mechanism. Electrophoresis. 2010;31:1435–41.
88. Müllerová L, Dubský P, Ördögová M, Gaš B. Determination of relative enantiomer migration order using a racemic sample. J Chromatogr A. 2015;1242:139–43.
89. Novotný M, Stefansson M. Electrophoretic resolution of monosaccharide enantiomers in borate-oligosaccharide complexation media. J Am Chem Soc. 1993;115:11573–80.
90. Tadey T, Purdy WC. Capillary electrophoretic separation of nucleotide isomers via complexation with cyclodextrin and borate. J Chromatogr B. 1994;657:365–72.
91. Lin CE, Lin SL, Liao WS, Liu YC. Enantioseparation of benzoins and enantiomer migration reversal of hydrobenzoin in capillary zone electrophoresis with dual cyclodextrin systems and borate complexation. J Chromatogr A. 2004;1032:227–35.
92. Svobodová J, Dubský P, Tesařová E, Beneš M, Gaš B. Methods for determination of all binding parameters in systems with simultaneous borate and cyclodextrin complexation. J Chromatogr A. 2011;1218:7211–8.
93. Asnin LD, Nikitina Y. Effect of competing binding modes on retention in chromatography and capillary electrophoresis. A theoretical consideration. J Sep Sci. 2014;37:390–2.
94. Dubský P, Müllerová L, Dvořák M, Gaš B. Generalized model of electromigration with 1:1 (analyte:selector) complexation stoichiometry: Part I Theory. J Chromatogr A. 2015;1384:142–6.
95. Šolínová V, Kašička V. Determination of acidity constants and ionic mobilities of polyprotic peptide hormones by CZE. Electrophoresis. 2013;34:2655–65.
96. Koval D, Kašička V, Jiráček J, Collinsová M. Determination of pKa values of diastereomers of phosphinic pseudopeptides by CZE. Electrophoresis. 2006;27:4648–57.
97. Kanoatov M, Cherney LT, Krylov SN. Extracting kinetics from affinity capillary electrophoresis (ACE) data: a new blade for the old tool. Anal Chem. 2014;86:1298–305.
98. Mironov GG, Okhonin V, Gorelsky SI, Berezovski MV. Revealing equilibrium and rate constants of weak and fast noncovalent interactions. Anal Chem. 2011;83:2364–70.
99. Boonleang J, Stobaugh JF. New single isomer negatively charged β-cyclodextrin derivatives as chiral selectors in capillary electrophoresis. Electrophoresis. 2013;34:1232–40.
100. Penn SG, Bergstrijm ET, Knights I, Liu G, Ruddick A, Goodall DM. Capillary electrophoresis as a method for determining binding constants: application to the binding of cyclodextrins and nitrophenolatest. J Phys Chem. 1995;99:3875–80.
101. Penn SG, Bergstrom ET, Goodall DM, Loran JS. Capillary electrophoresis with chiral selectors: optimization of separation and determination of thermodynamic parameters for binding of tioconazole enantiomers to cyclodextrins. Anal Chem. 1994;66:2866–73.
102. Le Saux T, Varenne A, Gareil P. Peak shape modeling by Haarhoff-Van der Linde function for the determination of correct migration times: a new insight into affinity capillary electrophoresis. Electrophoresis. 2005;26:3094–104.
103. Hruška V, Riesová M, Gaš B. A nonlinear electrophoretic model for PeakMaster: I. Mathematical model. Electrophoresis. 2012;33:923–30.
104. Riesová M, Hruška V, Gaš B. A nonlinear electrophoretic model for PeakMaster: II. Experimental verification. Electrophoresis. 2012;33:931–7.
105. Dubský P, Dvořák M, Müllerová L, Gaš B. Determination of the correct migration time and other parameters of the Haarhoff–van

der Linde function from the peak geometry characteristics. Electrophoresis. 2015;36:655–61.
106. Hruška V, Svobodová J, Beneš M, Gaš B. A nonlinear electrophoretic model for PeakMaster: Part III. Electromigration dispersion in systems that contain a neutral complex-forming agent and a fully charged analyte. Theory. J Chromatogr A. 2012;1267:102–8.
107. Beneš M, Svobodová J, Hruška V, Dvořák M, Zusková I, Gaš B. A nonlinear electrophoretic model for PeakMaster: Part IV. Electromigration dispersion in systems that contain a neutral complex-forming agent and a fully charged analyte. Experimental verification. J Chromatogr A. 2012;1267:109–15.
108. Hruška V, Beneš M, Svobodová J, Zusková I, Gaš B. Simulation of the effects of complex formation equilibria in electrophoresis: I. Mathematical model. Electrophoresis. 2012;33:938–47.
109. Svobodová J, Hruška V, Beneš M, Ušelová K, Gaš B. Simulation of the effects of complex formation equilibria in electrophoresis: II. Experimental verification. Electrophoresis. 2012;33:948–57.
110. Beneš M, Riesová M, Svobodová J, Tesařová E, Dubský P, Gaš B. Complexation of buffer constituents with neutral complexation agents: Part II. Practical impact in capillary zone electrophoresis. Anal Chem. 2013;85:8526–34.
111. Nishi H. Enantioselectivity in chiral capillary electrophoresis with polysaccharides. J Chromatogr A. 1997;792:327–47.
112. Gübitz G, Schmid MG. Chiral separation principles in capillary electrophoresis. J Chromatogr A. 1997;792:179–225.
113. Robinson RA, Stokes RH. Electrolyte solutions. 2nd ed. Mineola: Dover; 2002. p. 125–31, p. 303–13.
114. Sadek H. Walden product, Stocke's law and water structure. J Electroanal Chem. 1983;144:11–32.
115. Penn SG, Goodall DM, Loran JS. Differential binding of tioconazole enantiomers to hydroxypropyl-b-cyclodextrin studied by capillary electrophoresis. J Chromatogr. 1993;636:149–52.
116. Peng X, Bebault GM, Sacks SL, Chen DDY. Quantitative description of analyte migration behavior based on the dynamic complexation model in capillary electrophoresis. Can J Chem. 1997;75: 507–17.
117. Lemesle-Lamache V, Taverna M, Wouessldjewe D, Duchêne D, Ferrier D. Determination of the binding constant of salbutamol to unmodified and ethylated cyclodextrins by affinity capillary electrophoresis. J Chromatogr A. 1996;735:321–31.
118. Østergaard J, Jensen H, Holm R. Use of correction factors in mobility shift affinity capillary electrophoresis for weak analyte – ligand interactions. J Sep Sci. 2009;32:1712–21.
119. Shibukawa A, Lloyd KD, Wainer IW. Simultaneous chiral separation of leucovorin and its major metabolite 5-methyltetrahydrofolate by capillary electrophoresis using cyclodextrins as chiral selectors: estimation of the formation constant and mobility of the solute-cyclodextrin complexes. Chromatographia. 1993;35:419–29.
120. Fanali S, Boček P. A practical procedure for the determination of association constants of the analyte-chiral selector equilibria by capillary zone electrophoresis. Electrophoresis. 1996;17:1921–4.
121. Østergaard J, Jensen H, Holm R. Affinity capillary electrophoresis method for investigation of bile salts complexation with sulfobutyl ether-β-cyclodextrin. J Sep Sci. 2012;35:2764–72.
122. Fonslow BR, Bowser MT. Fast electrophoretic separation optimization using gradient micro free-flow electrophoresis. Anal Chem. 2008;80:3182–9.
123. Holm R, Nicolajsen HV, Harvig RA, Westh P, Østergaard J. Complexation of tauro- and glyco-conjugated bile salts with three neutral β-CDs studied by ACE. Electrophoresis. 2007;28:3745–52.
124. Britz-McKibbin P, Chen DDY. Accurately describing weak analyte-additive interactions by capillary electrophoresis. Electrophoresis. 2002;23:880–8.
125. Valkó IE, Billiet HAH, Frank J, Luyben KCAM. Factors affecting the separation of mandelic acid enantiomers by capillary electrophoresis. Chromatographia. 1994;38:730–6.
126. Yang J, Bose S, Hage DS. Improved reproducibility in capillary electrophoresis through the use of mobility and migration time ratios. J Chromatogr A. 1996;735:209–20.
127. Kawaoka J, Gomez FA. Use of mobility ratios to estimate binding constants of ligands to proteins in affinity capillary electrophoresis. J Chromatogr B. 1998;715:203–10.
128. Vespalec R, Gebauer P, Boček P. Identification of peaks in capillary zone electrophoresis based on actual mobilities. Electrophoresis. 1992;13:677–82.
129. Vespalec R, Barták P, Šimánek V, Vlčková M. Electrophoretic investigation of interactions of sanguinarine and chelerythrine with molecules containing mercapto group. J Chromatogr B. 2003;797:357–66.
130. Barták P, Šimánek V, Vlčková M, Ulrichová J, Vespalec R. Interactions of sanguinarine and chelerythrine with molecules containing a mercapto group. J Phys Org Chem. 2003;16:803–10.
131. Annstrong DW, Nair UB. Capillary electrophoretic enantioseparations using macrocyclic antibiotics as chiral selectors. Electrophoresis. 1997;18:2331–42.
132. Barták P, Bednář P, Kubáček L, Stránský Z. Advanced statistical evaluation of complex formation constant from electrophoretic data. Anal Chim Acta. 2000;407:327–36.
133. Barták P, Bednář P, Kubáček L, Lämmerhofer M, Lindner W, Stránský Z. Advanced statistical evaluation of the complex formation constants from electrophoretic data II Diastereomeric ion-pairs of (R, S)-N-(3,5-dinitrobenzoyl)leucine and tert-butylcarbamoylquinine. Anal Chim Acta. 2004;506:105–13.
134. Svobodová J, Beneš M, Dubský P, Vigh G, Gaš B. Simulation of the effects of complexformation equilibria in electrophoresis: III. Simultaneous effects of chiral selector concentration and background electrolyte pH. Electrophoresis. 2012;33:3012–20.
135. Friedl W, Reijenga JC, Kenndler E. Ionic strength and charge number correction for mobilities of multivalent organic anions in capillary electrophoresis. J Chromatogr A. 1995;709:163–70.
136. Onsager L, Fuoss M. Irreversible processes in electrolytes. Diffusion, conductance, and viscous flow in arbitrary mixtures of strong electrolytes. J Phys Chem. 1932;36:2689–778.
137. Jaroš M, Včeláková K, Zusková I, Gaš B. Optimization of background electrolytes for capillary electrophoresis: II. Computer simulation and comparison with experiments. Electrophoresis. 2002;23:2667–77.
138. Ušelová-Včeláková K, Zusková I, Gaš B. Stability constants of amino acids, peptides, proteins, and other biomolecules determined by CE and related methods: recapitulation of published data. Electrophoresis. 2007;28:2145–52.
139. Ehala S, Makrlík E, Toman P, Kašička V. ACE applied to the quantitative characterization of benzo-18-crown-6-ether binding with alkali metal ions in a methanol–water solvent system. Electrophoresis. 2010;31:702–8.
140. Maynard DK, Vigh G. Hepatakis(2-O-methyl-3,6-di-O-sulfo)-beta-cyclodextrin: a single-isomer, 14-sulfated beta-cyclodextrin for use as a chiral resolving agent in capillary electrophoresis. Electrophoresis. 2001;22:3152–62.
141. Zhu W, Vigh G. A family of single-isomer, sulfated γ-cyclodextrin chiral resolving agents for capillary electrophoresis: octa(6-O-sulfo)-γ-cyclodextrin. Electrophoresis. 2003;24:130–8.
142. Busby MB, Lim P, Vigh G. Synthesis, analytical characterization and use of octakis(2,3-di-O-methyl-6-O-sulfo)-γ-cyclodextrin, a novel, single-isomer, chiral resolving agent in low-pH background electrolytes. Electrophoresis. 2003;24:351–62.
143. Nzeadibe K, Vigh G. Synthesis of mono-6-deoxy-6-N, N, N', N', N'-pentamethylethylenediammoniocyclomaltoheptaose, a single-isomer, monosubstituted, permanently dicationic β-CD and its use for enantiomer separations by CE. Electrophoresis. 2007;28: 2589–605.

Analytical & Bioanalytical Chemistry is a copyright of Springer, 2016. All Rights Reserved.

4.2 Zobecnění vztahu pro rozlišení dvou analytů: *Publikace II*

V *Publikaci II* byla hledána nová funkce, která by objektivně kvantifikovala rozsah separace dvojice píků, zachovávala zažitou škálu hodnot charakteristickou pro tradiční rozlišení R_S (dané vztahem (25)), ale současně na rozdíl od tradičního rozlišení zohledňovala možnou asymetrii či různou velikost píků. Tato funkce byla nazvána ekvivalentní rozlišení. V *Publikaci II* byly formulovány požadavky, které by měla taková funkce splňovat: *i*) ekvivalentní rozlišení bere v úvahu celé koncentrační profily píků, *ii*) v případě dvojice identických píků s Gaussovým rozdělením koncentračních profilů splývá ekvivalentní rozlišení s tradičním rozlišením R_S, *iii*) ekvivalentní rozlišení je rostoucí funkcí rozsahu separace píků a *iv*) v případě zcela separovaných píků je hodnota ekvivalentního rozlišení větší nebo rovna 1,5.

Výchozím bodem pro konstrukci ekvivalentního rozlišení se staly vztahy (26) – (28). Jak relativní překryv P, tak veličina Ω totiž přirozeně splňují požadavek *i*). Pro splnění požadavku *ii*) bylo třeba nalézt vztah mezi P, respektive Ω a tradičním rozlišením R_S pro případ, kdy je dvojice píků dána identickými koncentračními profily s Gaussovým rozdělením. Takový vztah mezi Ω a R_S byl publikován již v práci [26], viz vztah (28). V *Publikaci II* byl odvozen analogický vztah mezi P a R_S.

$$P = 1 - \mathrm{erf}\left(\sqrt{2}R_S\right) \tag{30}$$

Inverzní vztahy ke vztahům (28) a (30) byly vzaty jakožto definice ekvivalentních rozlišení R_Ω a R_P.

$$R_\Omega = \sqrt{-\frac{1}{8}\ln\Omega} \tag{31}$$

$$R_P = \frac{1}{\sqrt{2}}\mathrm{inverf}(1 - P) \tag{32}$$

Výše popsaná konstrukce přirozeně zajišťuje splnění požadavků *i*) – *iv*). Splnění požadavku *iii*) bylo ilustrováno grafem, který znázorňuje závislost R_P a R_Ω na rozsahu separace vyjádřeném prostřednictvím relativního překryvu P, respektive veličiny Ω

(*Publikace II*, Figure 2). Název ekvivalentní rozlišení vychází ze skutečnosti, že nově definované veličiny R_Ω a R_P udávají, jaká by byla hodnota tradičního rozlišení R_S hypotetické dvojice píků, které by měly jednak identické koncentrační profily dané Gaussovým rozdělením a jednak jim příslušná hodnota relativního překryvu P, respektive hodnota veličiny Ω by byla stejná jako v případě reálných píků. Zřejmým důsledkem předchozího tvrzení je skutečnost, že v případě dvojice identických píků s koncentračním profilem daným Gaussovým rozdělením obě definice ekvivalentního rozlišení splývají s tradičním rozlišením R_S.

Jelikož pro zcela obecnou dvojici píků existují dvě odlišné hodnoty relativního překryvu, ${}^2P_1$ a ${}^1P_2$ (viz vztahy (26) a (27)), bylo zapotřebí upřesnit, která hodnota relativního překryvu se má dosadit do definičního vztahu (32). V *Publikaci II* bylo navrženo vyjadřovat relativní překryv píků vzhledem k ploše menšího z píků, tedy

$$P = \frac{A_{12}}{\min(A_1, A_2)} \tag{33}$$

neboli vyjádřeno pomocí koncentračních profilů,

$$P = \frac{\int_{-\infty}^{+\infty} \min[c_1(t), c_2(t)]dt}{\min\left[\left(\int_{-\infty}^{+\infty} c_1(t)dt\right), \left(\int_{-\infty}^{+\infty} c_2(t)dt\right)\right]} \tag{34}$$

Definice relativního překryvu dle vztahu (33), respektive (34) totiž zajistí, že ekvivalentní rozlišení R_P dobře popisuje znečištění minoritního píku dominantní složkou, což je z hlediska analytické praxe výhodnější volba.

Na několika příkladech dvojic neidentických píků, jejichž koncentrační profily měly Gaussovo rozdělení, byly ilustrovány rozdíly mezi hodnotami R_S, R_Ω a R_P (*Publikace II*, Figure 3). Bylo ukázáno, že v případě, kdy oba píky v dané dvojici mají stejné plochy (liší se tedy výškou a šířkou), jsou si hodnoty R_P a R_S vzájemně blíže než hodnoty R_Ω a R_S (*Publikace II*, Figure 3A a 3B). Dále bylo demonstrováno, že hodnota R_P je citlivá na poměr ploch obou píků, zatímco hodnoty R_Ω a R_S jsou invariantní vůči změnám ploch píků (*Publikace II*, Figure 3C a 3D). V případě nestejných ploch píků rozlišení R_S výrazně podhodnocuje rozsah vzájemného překryvu píků. Byla též ilustrována rozdílná citlivost R_S, R_Ω a R_P na poměr ploch píků (*Publikace II*, Figure 4A).

Ačkoli obě nové definice rozlišení, R_Ω a R_P, mají mnohé vlastnosti společné, například obě splňují požadavky *i*) – *iv*), v mnoha dalších ohledech se podstatným způsobem liší. Rozdíly mezi R_Ω a R_P přitom vyplývají z rozdílných vlastností Ω a P, viz definiční vztahy (31) a (32). V *Publikaci II* byl značný prostor věnován diskuzi výhod a nevýhod, které z těchto rozdílů vyplývají pro aplikaci R_Ω a R_P v analytických či preparativních metodách. První významnou vlastností R_Ω je skutečnost, že nezávisí na odezvových faktorech detektoru vůči jednotlivým analytům, a tudíž nezávisí ani na zvolené metodě detekce. Tato vlastnost je však současně nevýhodou, neboť R_Ω narozdíl od R_P není schopné postihnout rozdíl v kvantitativním zastoupení obou analytů, tj. rozdíl v plochách obou píků. Zajímavou vlastností jak R_Ω, tak R_P je jejich schopnost do jisté míry postihnout situace, kdy se jeden úzký pík nachází uvnitř píku mnohem širšího. S takovou situací se můžeme setkat například v preparativních metodách. Tato situace byla ilustrována pro speciální případ, kdy maxima obou píků nejsou vůči sobě časově posunutá (*Publikace II*, Figure 4B). Bylo demonstrováno, že v případě, kdy je úzký pík vyšší než pík široký, mají nenulovou hodnotu obě rozlišení R_Ω i R_P. V opačném případě je nenulová pouze hodnota R_Ω. Nenulová hodnota rozlišení je přitom žádoucí, neboť správně postihuje skutečnost, že izolováním zóny úzkého píku je možné získat směs obohacenou o komponentu, která je zastoupena pouze v úzkém píku. V tomto smyslu se jeví R_Ω výhodnější než R_P. Na druhou stranu vzhledem k necitlivosti R_Ω na vzájemný poměr ploch píků nevypovídá hodnota R_Ω nic o míře tohoto obohacení. Rozlišení R_S má nulovou hodnotu nezávisle na poměru výšek obou píků ve všech výše zmíněných případech.

S ohledem na výše diskutované vlastnosti ekvivalentních rozlišení R_Ω a R_P byl vysloven závěr, že pro účely preparativních metod není ani jedna z těchto definic ekvivalentního rozlišení univerzálně použitelná. Pro účely analytických metod se pouze ekvivalentní rozlišení R_P jeví jako vhodné zobecnění vztahu pro tradiční rozlišení R_S.

Na závěr byla ověřena aplikovatelnost konceptu ekvivalentního rozlišení na reálné experimentální elektroferogramy. Na příkladu dvou experimentálních elektroferogramů obsahujících vždy dvojici částečně separovaných píků, jejichž koncentrační profily měly Gaussovo rozdělení, avšak rozdílné plochy, bylo demonstrováno, že metodou nelineární regrese je možné rozložit elektroferogram na součet dvou gaussovských píků a určit rozlišení R_S, veličinu Ω i relativní překryv P, a tudíž také hodnoty ekvivalentních rozlišení R_Ω a R_P. Tradiční rozlišení R_S bylo určeno jednak z parametrů obou gaussovských píků získaných nelineární regresí a jednak vyhodnocením elektroferogramu v softwaru

ChemStation, který je dodáván firmou Agilent Technologies spolu s přístrojem pro kapilární elektroforézu. Hodnoty R_S získané oběma zmíněnými přístupy se velmi dobře shodovaly, což potvrdilo správnost nelineární regrese (*Publikace II*, Table 2). Porovnání hodnot R_S, R_Ω a R_P potvrdilo teoretické závěry, že pouze ekvivalentní rozlišeni R_P je schopné správně postihnout míru separace menšího píku od většího (*Publikace II*, Table 2).

Publikace II

Equivalent peak resolution: Characterization of the extent of separation for two components based on their relative peak overlap

Martin Dvořák, Jana Svobodová, Pavel Dubský, Martina Riesová, Gyula Vigh, Bohuslav Gaš

Electrophoresis 2015, *36*, 646-654

Martin Dvořák[1]
Jana Svobodová[1,2]
Pavel Dubský[1]
Martina Riesová[1]
Gyula Vigh[3]
Bohuslav Gaš[1]

[1]Department of Physical and Macromolecular Chemistry, Faculty of Science, Charles University in Prague, Prague, Czech Republic
[2]Ruprecht-Karls-Universität Heidelberg, Organisch-Chemisches Institut, Heidelberg, Germany
[3]Department of Chemistry, Texas A&M University, College Station, TX, USA

Received October 14, 2014
Revised December 1, 2014
Accepted December 2, 2014

Research Article

Equivalent peak resolution: Characterization of the extent of separation for two components based on their relative peak overlap†

Although the classical formula of peak resolution was derived to characterize the extent of separation only for Gaussian peaks of equal areas, it is often used even when the peaks follow non-Gaussian distributions and/or have unequal areas. This practice can result in misleading information about the extent of separation in terms of the severity of peak overlap. We propose here the use of the equivalent peak resolution value, a term based on relative peak overlap, to characterize the extent of separation that had been achieved. The definition of equivalent peak resolution is not constrained either by the form(s) of the concentration distribution function(s) of the peaks (Gaussian or non-Gaussian) or the relative area of the peaks. The equivalent peak resolution value and the classically defined peak resolution value are numerically identical when the separated peaks are Gaussian and have identical areas and SDs. Using our new freeware program, Resolution Analyzer, one can calculate both the classically defined and the equivalent peak resolution values. With the help of this tool, we demonstrate here that the classical peak resolution values mischaracterize the extent of peak overlap even when the peaks are Gaussian but have different areas. We show that under ideal conditions of the separation process, the relative peak overlap value is easily accessible by fitting the overall peak profile as the sum of two Gaussian functions. The applicability of the new approach is demonstrated on real separations.

Keywords:
Extent of separation / Peak resolution / Quality of separation / Relative peak overlap
DOI 10.1002/elps.201400475

1 Introduction

1.1 Background

Selection of the right separation criterion is crucial in at least two main aspects. In the first aspect, the criterion serves as an objective measure of the extent (quality) of separation, as required by national and international regulatory authorities in drug, food and environmental analysis. Currently, the classically defined peak resolution value plays a key role as a separation criterion in method validation and system suitability tests. In the second—and just as important—aspect, the separation criterion serves as an objective function for the algorithms that are used to optimize the separation conditions. As reviewed by Schoenmakers and Mulholland [1], a large number of different criteria have been used for the optimization of chromatographic separations to achieve either the resolution of a critical pair of peaks or an adequate resolution of all the peaks (or most of the peaks, or many of the peaks) in a chromatogram (global resolution).

In a seminal early paper, Glueckauf [2] characterized the extent of separation by the term impurity fraction, η_2, defined as:

$$\eta_2 = \frac{\Delta m_1}{m_2 - \Delta m_2}, \quad (1)$$

where m_2 is the amount of Component 2, and Δm_1 and Δm_2 are the amounts of Component 1 and 2 that contaminate the collected portions of Component 2 and 1, respectively. When $\Delta m_2 << m_2$, the impurity fraction expression can be simplified to $\eta_2 = \Delta m_1 / m_2$. Despite its clear and informative meaning, the term impurity fraction has not gained widespread use in chromatography, possibly due to the difficulties involved in the calculation of Δm_1 and Δm_2 from the chromatographic data.

In 1958, Phillips proposed the use of the term peak resolution, R_S, to characterize the extent (quality) of separation

Correspondence: Dr. Pavel Dubský, Department of Physical and Macromolecular Chemistry, Faculty of Science, Charles University in Prague, Albertov 2030, CZ-128 40 Prague 2, Czech Republic
E-mail: dubsky@natur.cuni.cz

† Dedicated to the memory of Professor Georges Guiochon without whose work and life separation science would not be the same as we know it now.

Colour Online: See the article online to view Figs. 1–3 and 5 in colour.

© 2014 WILEY-VCH Verlag GmbH & Co. KGaA, Weinheim

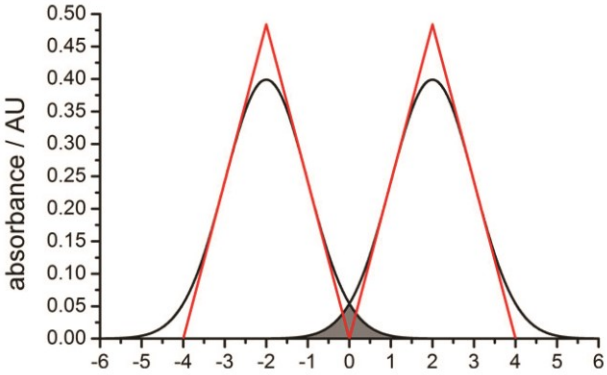


Figure 1. Two overlapping Gaussian peaks having a classical resolution of $R_S = 1$ with the tangential isosceles triangle approximation of the Gaussian distributions (in red). The relative peak-overlap integral *P* shadowed [7].

for a pair of analytes that had Gaussian concentration distributions and equal peak areas [3]. He defined R_S as:

$$R_S = \frac{2\,(t_2 - t_1)}{(w_2 + w_1)}, \tag{2}$$

where t_1 and t_2 were the elution times of Component 1 and 2 and w_1 and w_2 were the widths of the peaks measured between the baseline intercepts of the inflection point tangents of the peaks (see Fig. 1). The logic behind this formula is that when the two Gaussian peaks are approximated by the two tangential isosceles triangles, an R_S value of 1 indicates that the two triangles touch each other at their basis. If (and only if) the two Gaussian peaks have the same areas and SDs, this corresponds to the situation that the first peak overlaps 4.55% of the area of the second peak and vice versa (Fig. 1, shaded area). Over time, an R_S value of 1.5 became the widely accepted threshold for "baseline" separation [4], and corresponds to a mutual peak overlap of 0.27% for the two identical Gaussians. For Gaussian distributions with SDs of σ_1 and σ_2, $w_i = 4\sigma_i$ ($i = 1$ and 2), Eq. (2) becomes:

$$R_S = \frac{(t_2 - t_1)}{2\,(\sigma_2 + \sigma_1)}. \tag{3}$$

However, R_S—by definition—was not meant to describe the quality of separation for peaks that have non-Gaussian distributions and/or have different areas [5]. Therefore, other parameters were introduced to characterize the extent (quality) of separation for analyte peak pairs that had one of, or the other of, or both of the problems. In 1960, Giddings defined the term separation function, *F*, as:

$$F = \frac{(t_2 - t_1)^2}{8\,(\sigma_2^2 + \sigma_1^2)}, \tag{4}$$

and related *F* to the common chromatographic operational variables [6]. While *F* lost the intuitive meaning of the classical definition of *Rs*, it kept the disadvantage of being applicable, strictly speaking, only to symmetrical peaks.

To rectify this problem, Schoenmakers et al. [7] introduced the term relative peak overlap and defined it for the earlier eluting Component *i* contaminated by the later eluting Component *j* as:

$${}^{j}P_i = \frac{A_{ij}}{A_i}, \tag{5}$$

where ${}^{j}P_i$ (originally denoted in [7] as ${}^{j}RO_i$) was the relative peak overlap value for Component *i* that reflected the influence of Component *j*, A_i was the total peak area of Component *i*, and A_{ij} was the area overlap of the peaks (*cf.* the shaded area in Fig. 1). The corresponding relative peak overlap value for Component *j* was defined in the same way. Schoenmakers et al. [7] pointed out that when the sizes of the two peaks were different, the ${}^{j}P_i$ and ${}^{i}P_j$ values were also different and a single R_S value did not—and could not—reflect the differing purities of the separated components. The authors concluded that relative peak overlap is not a practical resolution criterion, because it is very difficult to calculate its value from a chromatogram. Instead, they modified the resolution expression Eq. (2) to reflect the effects of area and asymmetry differences of the peaks. The modified definition, ${}^{i}Rs_{ji}$, was based solely on the geometrical properties of the peaks without explicite reference to the relative peak overlap, ${}^{j}P_i$.

In 1990, Dose and Guiochon proposed that another normalized measure of peak overlap, Ω, be used to characterize the extent (quality) of separation for two peaks of any distribution [8]. Ω was related to the overlap integral between two one-dimensional wave functions in a quantum mechanical sense:

$$\Omega = \frac{\left[\int_{-\infty}^{+\infty} c_1(\tau)\, c_2(\tau)\, d\tau\right]^2}{\int_{-\infty}^{+\infty} c_1^2(\tau)\, d\tau \int_{-\infty}^{+\infty} c_2^2(\tau)\, d\tau}, \tag{6}$$

where $C_1(\tau)$ and $C_2(\tau)$ are the concentration profiles (distributions) of the 1st and the 2nd peak in the time domain. Similarly to relative peak overlap, values of Ω always lie between 0 and 1 (for completely separated and completely overlapped peaks, respectively) [8]. In contrast to the relative peak overlap value, where only the intersection area is normalized by the area of the first or the second peak, the concentration profiles of both peaks in their entirety contribute to the value of Ω. The desirable mathematical properties of Ω include invariance (independence of the horizontal and vertical scales), continuity and monotonicity. Neither the normalized overlap nor its derivative has discontinuities (in contrast to the classical definition of peak resolution). The authors specifically emphasize the signal intensity scaling invariance, which is valid for both peaks individually. Thus, if the two components have, e.g. different response factors at various UV wavelengths, or even are measured with different detection techniques, Ω keeps its value irrespectively of the response factors or the detection technique used.

Analytical expressions to calculate the Ω values for chromatographically meaningful distributions were derived in [8]. Specifically, it was shown that Ω is closely related to

© 2014 WILEY-VCH Verlag GmbH & Co. KGaA, Weinheim

Giddings' separation factor F, Eq. (4), and that for two Gaussians with equal σ values, Ω and R_S are related as:

$$\Omega = \exp\left(-8\,R_S^2\right). \tag{7}$$

(Equation (7) differs from Eq. (15) in [8] due to a mistyped factor of 1/2 in Eq. (11) in the original paper that propagated to Eq. (15) (in [8]).

Additionally, the authors concluded that Ω as a measure of the extent of separation is especially convenient for preparative separation techniques, because the entire peak profiles enter into the definition of Ω. Thus, Ω does not measure the extent to which the two peaks are separated from each other, rather it indicates the extent to which the peaks mutually contaminate each other.

Unfortunately, despite the compelling logic and thorough analysis of the benefits of the new approaches to the characterization of the extent of the separation of two peaks, as briefly reviewed above, the use of the modified resolution expressions did not become widespread among chromatographers due to, possibly, the simplicity of the classical R_S formula (2) and its long-lasting, uncritical use irrespectively of the properties of the peak pair it was applied to. This paper proposes an approach that relies on the use of the peak-overlap integrals ${}^jP_i$ or Ω, as objective measures of the extent of separation to obtain a parameter called the equivalent peak resolution value. The equivalent peak resolution function is invariant, monotonous, continuous, and differentiable, all of which are important requirements for optimization algorithms. For two identical Gaussian peaks of equal area and SD, the equivalent peak resolution function yields values that are the same as the classical peak resolution values, R_S. For any other situation, the equivalent resolution value states what would be the value of R_S if the two peaks were identical Gaussians (e.g. an equivalent peak resolution value of 1.5 suggests "baseline separation" just as an R_S = 1.5 value does). The equivalent peak resolution function can be applied either as a separation optimization criterion or as a quality control parameter that characterizes a particular analytical method, or both.

1.2 Software

Simultaneously, we present a new freeware software, Resolution Analyzer, which can be used to calculate both the classical peak resolution values and the equivalent peak resolution values. The software is written in C++ and compiled by RAD Studio XE3 Professional, providing a complete graphical user interface under MS Windows operating systems. It can be downloaded for free from echmet.natur.cuni.cz.

Peak positions, widths, area ratios, and asymmetries can be adjusted in Resolution Analyzer to explore and plot their influences on the calculated characteristics of a pair of peak distribution functions and study various measures of their separation. If the experimental error (SD) of the input parameters is also entered into Resolution Analyzer, the related asymptotic SDs of the calculated characteristics are estimated through a first-order approximation of the error propagation law under the assumption of zero covariance among the input parameters [9]. The calculation procedures are described in detail in a Help file distributed with the software.

1.3 Theory

Any resolution function is expected to reflect the extent of separation of the peaks and provide a clear threshold value at which—and above which—the two peaks are baseline separated. The core problem lies in the term "baseline separated" as this term is not well defined in a mathematical sense. In search of an alternative approach to R_S to quantify the extent of peak separation, we were looking for a resolution function that meets the following constraints:

(1) It properly reflects the form of the peak distribution functions and the areas of the peaks.
(2) For identical Gaussian peaks, it gives the same resolution value as the classical definition Eq. (2) does.
(3) The resolution function is monotonous—the higher the resolution value, the greater the extent of separation of the peaks.
(4) For clearly baseline separated peaks, the calculated resolution value is equal to or greater than 1.5, matching the commonly expected R_S value.

The first point was elegantly addressed by the peak-overlap integrals ${}^jP_i$ or Ω, as discussed by Schoenmakers et al. [7] or Dose and Guiochon [8]. However, both ${}^jP_i$ and Ω lost the visual immediacy and familiarity of the classical R_S value. Finding the overlap area for two partially separated peaks does not pose a problem for the currently available data processing algorithms. Even if peak-specific detection is not available, the peak cluster can be decomposed to the individual components as, for instance, demonstrated recently by Grisales et al. [10]. Thus, the second constraint put on the resolution function sought can be solved by finding a reasonable mapping from the peak-overlap integrals into a measure similar to the classical resolution value, *Rs*. This task is solved straightforwardly in the case of the Ω integral (6). According to Eq. (7), for two Gaussian distributions having the same SDs,

$$R_S = \sqrt{-\frac{1}{8}\ln(\Omega)}. \tag{8}$$

Equation (8) seems a reasonable candidate for the resolution function sought. Explicitly, we wish to set:

$$R_\Omega = \sqrt{-\frac{1}{8}\ln(\Omega)}. \tag{9}$$

This resolution function, R_Ω, tells us what would be the classical resolution, R_S, if the two peaks were identical Gaussians having the same peak-overlap integral, Ω, as the actual peaks (Gaussian or non-Gaussian) do. Thus, R_Ω is an equivalent resolution value (with respect to Ω).

© 2014 WILEY-VCH Verlag GmbH & Co. KGaA, Weinheim

Similarly, we wish to define R_P, the equivalent resolution function with respect to the relative peak overlap, ${}^{j}P_i$, Eq. (5). To do so, first consider two Gaussian distributions, Gauss(τ;t_i,σ) that have equal SDs, $\sigma_1 = \sigma_2 = \sigma$, and are positioned at different positions, $t_2 > t_1$. Second, consider that the two Gaussian peaks with the same SDs have the same areas, $A_1 = A_2 = A$. Thus, the peak distribution function becomes A*Gauss (τ; t_i, σ). The point of intersection of the two peaks is at time $t_{\text{int}} = (t_2 + t_1)/2$ and their overlap area, A_{12}, is (*cf.* Fig. 1):

$$A_{12} = \int_{-\infty}^{t_{\text{int}}} \text{A} * \text{Gauss}\,(\tau; t_2, \sigma)\, d\tau + \int_{t_{\text{int}}}^{\infty} \text{A} * \text{Gauss}\,(\tau; t_1, \sigma)\, d\tau$$
$$= A\left\{1 - \text{erf}\left(\frac{t_2 - t_1}{2\sqrt{2}\sigma}\right)\right\}. \quad (10)$$

With that, the expression for the relative peak overlap for the two peaks, P (${}^{2}P_1 = {}^{1}P_2 = P = A_{12}/A$), becomes:

$$P = \left\{1 - \text{erf}\left(\frac{t_2 - t_1}{2\sqrt{2}\sigma}\right)\right\} \quad (11)$$

Clearly, the classical definition of peak resolution, Eq. (3), is contained in the argument of the error function. So, we can write the relationship between the relative peak overlap, P, and the classical definition of resolution, R_S, as:

$$P = 1 - \text{erf}\left(\sqrt{2}\,R_S\right) \quad (12)$$

By inverting this relation (12), the final expression for resolution as a function of the relative peak overlap of the separated peaks is obtained as:

$$R_S = \frac{1}{\sqrt{2}}\text{inverf}\,(1 - P) \quad (13)$$

So, analogously to R_Ω, we wish to set:

$$R_P = \frac{1}{\sqrt{2}}\text{inverf}\,(1 - P) \quad (14)$$

This resolution function, R_P, tells us what would be the classical resolution, R_S, if the two peaks were identical Gaussians having the same relative peak overlap, P, as the actual peaks (Gaussian or non-Gaussian) do. Thus, R_P is an equivalent resolution value (with respect to P).

Similarly to the original concept of Schoenmakers et al. [7], two equivalent resolution values R_P result when the two peaks have different areas, since in ${}^{2}P_1$ and ${}^{1}P_2$, the peak overlap area is normalized by the area of the first and the second peak, respectively. In order to eliminate any ambiguity, we further define the relative peak overlap, P, as normalized to the minor of the two areas, min (A_1, A_2). In our eyes, the R_P value obtained for the minor peak is of greater practical relevance because, often, the separation and accurate quantitation of the minor peak is the main concern. Finally, we provide the definition of the area overlap A_{12}, which was not provided in [7] and which may not be clear (especially for distributions and positionings of the peaks where several intersection points exist) as (*cf.* Fig. 1 and Fig. 4):

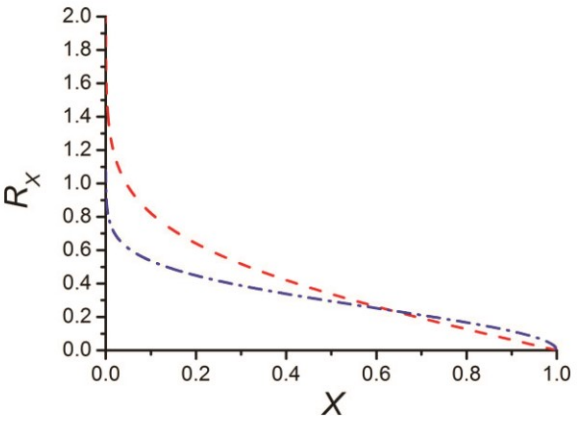


Figure 2. Dependence of the equivalent resolution value, R_X, on the extent of the relative peak-overlap integral X, for any type of peaks. X represents either Ω (Eq. (9); blue dashed-dot line) or P (Eq. (16); red dashed line).

$$A_{12} = \int_{-\infty}^{+\infty} \min(c_1(\tau), c_2(\tau))d\tau \quad (15)$$

In combination with normalizing the relative peak overlap to the minor peak, the final formula for P becomes:

$$P = \frac{\int_{-\infty}^{+\infty} \min(c_1(\tau), c_2(\tau))d\tau}{\min\left[\left(\int_{-\infty}^{+\infty} c_1(\tau)d\tau\right), \left(\int_{-\infty}^{+\infty} c_2(\tau)d\tau\right)\right]} \quad (16)$$

Both equivalent resolution functions, R_Ω and R_P, naturally fulfill all the expectations of a resolution function stated above:

(1) The functions are valid for any distribution for which the area-overlap integrals Ω and P are defined as objective measures of the extent of peak overlap for any form of the peak distribution functions and the areas of the peaks.
(2) The equivalent resolution functions and the classical resolution function provide the same numerical values for identical Gaussian peaks.
(3) The numerical values of equivalent resolutions R_Ω or R_P increase with decreasing values of the peak-overlap integrals, see Fig. 2.
(4) $R_\Omega = 1.5$ and $R_P = 1.5$ always correspond to the same peak-overlap integrals that one observes for "baseline separated" identical Gaussian peaks for which the classical resolution value is $R_S = 1.5$. Specifically, $R_\Omega = 1.5$ indicates $\Omega = 1.5 \times 10^{-6}$% and $R_P = 1.5$ indicates $p = 0.27$% (the latter being more familiar).

Specifically, the functions described by Eqs. (9) and (14) are defined over a domain of $X \in (0; 1\rangle$ (where X stands for either Ω or P), corresponding to a relative peak overlap of 0–100%, where they are invariant and monotonous, with a limit of $\lim_{X\to 0+} R_X = \infty$. These properties follow directly from the

© 2014 WILEY-VCH Verlag GmbH & Co. KGaA, Weinheim

definitions, Eqs. (9) and (14), and the properties of the ln and inverse error functions. Additionally, the equivalent resolution functions are continuous and differentiable as are the peak-area overlap integrals Ω and P (for a thorough discussion of the various distributions, see Dose and Guiochon [8]).

2 Materials and methods

2.1 Chemicals

All chemicals were of analytical grade purity. Buffer constituents 3-phenylpropionic acid (hydrocinnamic acid), lithium hydroxide monohydrate, tris(hydroxymethyl)-aminomethane (Tris), and *N*-[tris(hydroxymethyl) methyl]glycine (Tricine) and analytes (*S*)-2-(6-methoxy-2-naphthyl)propionic acid ((*S*)-naproxen) and the racemic mixture of (*R*)-(-)- and (*S*)-(+)-2-fluoro-α-methyl-4-biphenylacetic acid (flurbiprofen) were all purchased from Sigma Aldrich (Prague, Czech Republic). Water used for preparation of all solutions was purified by a Rowapur and an Ultrapur water purification system (Watrex, Prague, Czech Republic).

2.2 Instrumentation

All experiments were performed using an Agilent 3D CE capillary electrophoresis equipment operated under ChemStation software (Agilent Technologies, Waldbronn, Germany) control. Fused silica capillaries (50 μm id, 375 μm od) were provided by Polymicro Technologies (Phoenix, AZ, USA). The 240 pH/ion meter instrument (Radiometer, Copenhagen, Denmark), calibrated with standard IUPAC buffers pH 4.005 and pH 7.000 (Radiometer, Lyon, France), was used for pH measurements.

2.3 Experimental conditions

New capillaries were flushed with deionized water and 0.1 M sodium hydroxide. Prior to each run, the capillary was conditioned with the running buffer for 5 min. All solutions used in the experiments were filtered with a syringe filter, pore size 0.45 μm (Sigma-Aldrich, Prague, Czech Republic).

The BGE in both experiments was 12.7 mM hydrocinnamic acid and 9.0 mM lithium hydroxide, measured pH 5.05. The ionic strength of the BGE, calculated by PeakMaster 5.3, was 9.01 mM. Due to their poor solubility in the BGE, the analytes were first dissolved at a concentration of 3 mM in a buffer that contained 20 mM Tris and 20 mM Tricine, measured pH 8.10. The injected sample was a mixture of 0.9 mM (*S*)-naproxen and 0.3 mM racemic mixture of (*R*)- and (*S*)-flurbiprofen, prepared by mixing appropriate amounts of the respective stock solutions and the BGE. Detection was performed with the DAD at a wavelength of 240 nm. The samples were injected hydrodynamically for 9 s at 10 mbar. The total length of the capillary and its effective length to the detector were 50.0 and 41.5 cm, respectively. The applied voltage was 20 kV. During the separation process the analytes were pushed to the detector side by an applied pressure of 30 or 40 mbar. The operating temperature was 25°C. The Origin Ver. 8.1 software (OriginLab, Northhampton, USA) was used for data evaluation.

3 Results and discussion

3.1 Selection of the peak distribution functions

In practice, unless component-specific detection is available, the peak cluster must be decomposed in order to calculate the peak-overlap integrals, Ω or P. Once the decomposition is done, the calculation of the respective integrals, Eqs. (6) or (16), is straightforward. However, in order to be able to do so, the forms of the expected individual peak distributions must be known a priori. Several such candidates exist. Schoenmakers et al. [7] used in their approach Gaussian and exponentially modified Gaussian distributions. Dose and Guiochon [8] took several other distributions into account. HVL and HVLR functions seem to be other reasonable candidates, especially in CE [11].

Although one may be tempted to inspect the equivalent resolution values for various combinations of such distributions, Guiochon pointed out that it is not generally valid to assume that a cluster of unresolved peaks is formed by a simple sum of two distributions belonging to independently migrating individual peeks [12, 13]. Such decomposition is only possible in special cases, when the migrating components do not interact with each other and Gaussian peaks evolve from the very beginning of the separation process (linear or ideal separations). In capillary electrophoresis, one such case is when (*i*) the conductivity of the BGE is much higher than the conductivity perturbation in the sample zone and (*ii*) the initial width of the sample zone is much shorter than the effective length of the capillary [14]. In chromatography, such conditions typically require a linear adsorption isotherm, injection of a small sample and efficient columns (high plate numbers) [15, 16]. In this paper (Part 1 of a planned series), we will deal with such systems and restrict ourselves to the exploration of the equivalent resolution function in the case of two Gaussian peaks.

3.2 Comparison of the equivalent resolution function and the classical resolution function

In Fig. 3, we plotted the classical resolution values, R_S (black solid curves), the Ω-based equivalent resolution values, R_Ω (blue dot-dashed curves), and the P-based equivalent resolution values, R_P (red dashed curves) calculated with Resolution Analyzer for a pair of Gaussian peaks as a function of various parameters of the underlying Gaussian distributions.

In Fig. 3A, the dependence of the resolution value on the distance between the peaks is inspected. Both peak areas

© 2014 WILEY-VCH Verlag GmbH & Co. KGaA, Weinheim

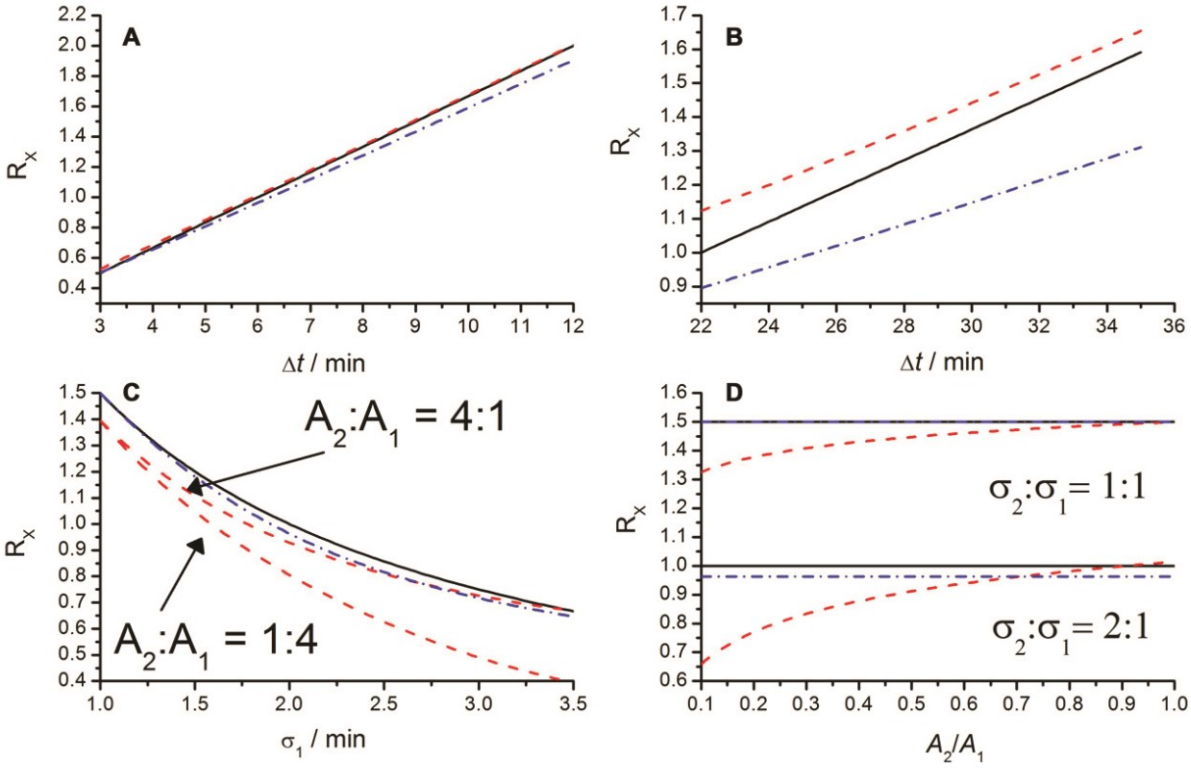


Figure 3. Dependencies of the resolution value, R_X on various parameters of a pair of Gaussian peaks. R_X stays for the classical resolution value R_S (Eq. (2); black solid curve), the Ω-based equivalent resolution value, R_Ω (Eq. (9); blue dashed-dot curve), and the *P*-based equivalent resolution, R_P (Eq. (14); red dashed curve). (Panel A) Both peaks have an area of 1, their SDs are 1 min and 10 min, respectively, and the distance of the peaks changes from 3 min to 12 min; (Panel B) both peaks have an area of 1, their SDs are 1 min and 10 min, respectively, and the distance of the peaks changes from 22 to 36 min; (Panel C) the distance of the peaks is 6 min, their areas are either 1 and 0.25 or 1 and 4, respectively, and the SD of the first peak changes from 1 to 3.5 min; (Panel D) the distance of the peaks is 6 min, the peaks have SDs of either 1 and 1 min, or 1 and 2 min, respectively, and their area ratio changes from 0.1 to 1.

are fixed at 1, the SDs are 1 min and 2 min, respectively. In this case, the difference between R_S and R_P is negligible. R_Ω increases with $\Delta t = t_2 - t_1$ at a slightly lower rate than either R_S or R_P. If both the areas and the SDs were the same for both peaks, all three resolution measures would, by definition, coincide, *cf.* Eqs. (2), (9) and (14). In Fig. 3B, the peak areas are the same as in Fig. 3A (fixed at 1), but the ratio of the SDs is increased to σ_2:$\sigma_1 = 10$:1 (10 min and 1 min, respectively). The positioning of the peaks was adjusted such that there is only one intersection point between the narrower and the wider peak. Now, R_S, R_Ω, and R_P are all different and R_Ω differs from R_S more than R_P does. The R_Ω values diverge from the R_S values, while the R_P values converge to the R_S values as the distance between the two peaks increases.

Figure 3C describes the dependence of the resolution measures on the SD of the first peak, σ_1, when σ_2 is fixed at 1 min. The distance of the peaks is fixed at 6 min. Two sets of cases were inspected for $A_2/A_1 = 4$:1 and 1:4 as parameters. Since R_S does not depend on the peak areas, only one black solid curve is observed for both area ratios. The peak-overlap integral, Ω, and the related resolution, R_Ω, are also invariant in the peak area ratios, therefore only one blue dash-dot curve is observed for both area ratios. Additionally, the values of R_Ω and R_S coincide at $\sigma_1 = \sigma_2 = 1$, since the two peaks differ only in their areas at this point. On the other hand, $R_P < R_S$ (even in the $\sigma_1 = \sigma_2 = 1$ case), because any time A_2/A_1 differs from unity, the relative peak overlap value, *P* (normalized to the minor peak), is larger than that at $A_2/A_1 = 1$.

The effects of peak area differences are illustrated in Fig. 3D with σ_2:σ_1 serving as parameter. The distance of the two peaks is fixed at 6 min, σ_1 is fixed at 1 min, while σ_2 is set at either 1 min or 2 min. Since both R_S and R_Ω are invariant in the peak areas, the black solid line and the blue dash-dot line are parallel to the A_2/A_1 axis. When σ_2:$\sigma_1 = 1$, the values of R_S and R_Ω coincide, when σ_2:$\sigma_1 = 2$, $R_\Omega < R_S$. Only R_P reflects the effects of the peak areas. When $\sigma_2 = \sigma_1$, $R_P = R_S$ at $A_2 = A_1$, as expected. When $\sigma_2 = 2\sigma_1$, R_P becomes equal to R_S at $A_2 < A_1$, properly indicating that the wider peak must have lower area in order to achieve the same extent of separation at the given peak distance, $t_2 - t_1$. The top, middle and bottom panels in Fig. 4A visually compare the separation of two peaks for which σ_1 and σ_2 are the same, but the peak area ratio A_2/A_1 goes from 1:1 through 1:2 to 1:20. While Ω, R_Ω, and R_S remain the same, *P* increases from 4.55%

© 2014 WILEY-VCH Verlag GmbH & Co. KGaA, Weinheim

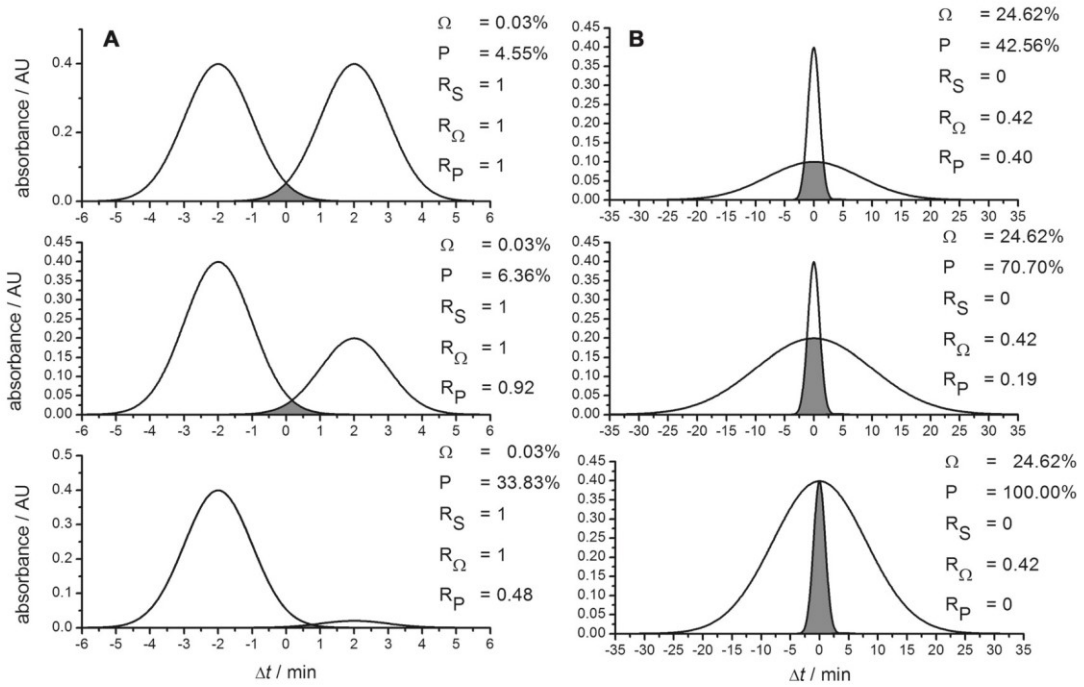


Figure 4. Two overlapping Gaussian peaks. (A) Classical resolution $R_S = 1$ with consecutively decreasing area ratio $A_2/A_1 = \{1; 0.5; 0.05\}$. (B) Coincident peaks (classical resolution $R_S = 0$) with SDs of $\sigma_2 = 1$ and $\sigma_1 = 8$ and with consecutively decreasing area ratios of $A_2/A_1 = \{0.5; 0.25; 0.125\}$. The measures are calculated as follows: Ω by Eq. (6), P by Eq. (16), R_S by Eq. (3), R_Ω by Eq. (9), and R_P by Eq. (14). The relative peak-overlap integrals, P, are shadowed.

through 6.36 to 33.83%, and R_P decreases from 1 through 0.92 to 0.48.

3.3 The Ω-based versus the *P*-based equivalent resolution functions

Having two equivalent resolutions defined, one may wonder what is the key difference between the two measures of the extent of separation and which one is suited better for what purpose. The most obvious difference between Ω and P is that Ω is a rather abstract measure, while P has a clear physical meaning. In Figs. 1 and 4, the areas corresponding to the P integrals are shadowed, but no such interpretation can be found for the Ω integral. This difference though, in itself, does not make one measure preferable over the other.

The more essential difference lies in the invariance of the Ω integral to the Y (response) scale. If Ψ_i is the distribution function and f_i the respective (constant) response factor of the ith component ($i = 1, 2$), then substituting $c_i = f_i^* \Psi_i$ into Eq. (6) readily reveals that the Ω integral attains the same value irrespectively of the response factors f_i of the individual components. As already stated in the Introduction, Dose and Guiochon [8] found this property to be of advantage since it makes the Ω measure uniquely independent of the detection technique(s) used. On the other hand, this property simultaneously makes Ω incapable of handling quantitative relationships between the peaks, in contrast to the P-integral, which indicates how much of the signal of one component is "contaminated" by the signal of the other component.

Secondly, Dose and Guiochon [8] suggested that the Ω integral may be a suitable measure of the quality of the separation in preparative chromatography since, in contrast to the classical resolution, R_S, it properly reflects the fact that one component (with a narrower distribution) can be successfully isolated (enriched) from a broader component even if the two components technically coelute (Fig. 4B, inspired by Fig. 7A in [8]). From the top through the middle to the bottom panel in Fig. 4B, Ω and R_Ω remain constant at 24.62% and 0.42, while P goes from 42.56%, through 70.70% to 100% and R_P goes from 0.40 through 0.19 to 0. In case of the nested peaks (Fig. 4B is an extreme example) the P integral for instance becomes one (and thus the R_P equivalent resolution value becomes zero) as soon as the minor peek is completely covered by the major peak. Thus, in the bottom panel of Fig. 4B, while isolation of the minor peak would still lead to its enrichment, the minor peak is completely covered by the major peak and the R_P equivalent resolution value becomes zero. The Ω integral (and the related R_Ω value) correctly reflect the fact that the two peaks do not completely overlap in any of the cases in Fig. 4B. However, due to the lack of its sensitivity to response factors, the Ω integral (and the related R_Ω value) remain constant irrespectively of the fact that the possible enrichment of the minor component by its isolation from the major one clearly decreases as going from the situation depicted at the

© 2014 WILEY-VCH Verlag GmbH & Co. KGaA, Weinheim

Table 1. Parameters of the fitted Gaussian functions for the experimentally obtained peaks shown in Fig. 5

Case	Naproxen			Flurbiprofen		
	A_1 (min·AU)	t_1 (min)	σ_1 (min)	A_2 (min·AU)	t_2 (min)	σ_2 (min)
A	1.919 ($4{\cdot}10^{-3}$)	5.7420 ($9{\cdot}10^{-5}$)	0.0393 ($8{\cdot}10^{-5}$)	0.543 ($4{\cdot}10^{-3}$)	5.8796 ($3{\cdot}10^{-4}$)	0.0388 ($3{\cdot}10^{-4}$)
B	2.309 ($8{\cdot}10^{-3}$)	7.2492 ($1{\cdot}10^{-4}$)	0.0434 ($1{\cdot}10^{-4}$)	0.692 ($8{\cdot}10^{-3}$)	7.4543 ($4{\cdot}10^{-4}$)	0.0434 ($4{\cdot}10^{-4}$)

SDs of the parameter estimates are in parenthesis.

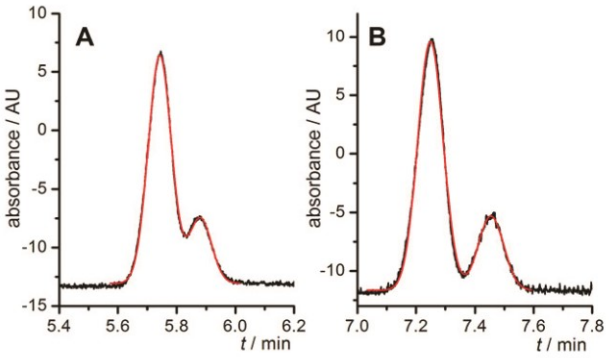


Figure 5. Experimental electropherograms (black line) detected at 240 nm. The fitted sum of the two Gaussian functions is depicted in red. The resulting parameters of the fit are in Table 2. First peak: naproxen, second peak: flurbiprofen.

top most panel of Fig. 4B down to the situation depicted in the bottom panel.

Generally, the argument in Eq. (14), (1–*P*), measures how well the signal of one component can be differentiated from the signal of another component. Thus, we suggest that the *P* integral—along with the *P*-based equivalent resolution function, R_P—be used in analytical chemistry as a measure of the extent of separation. For preparative chromatography neither the *P* integral nor the Ω integral seem to satisfy all the needs.

3.4 Experimental examples

In this section, electrophoresis was used as the separation technique and naproxen and flurbiprofen as the model analytes. The background electrolyte was chosen such that linear electrophoretic conditions were met, as verified both theoretically by computing the PeakMaster software [11] the relative velocity slope of the analytes, S_x [17] (which is a measure of the tendency of the analyte to undergo electromigration dispersion) and experimentally, since the two peaks had Gaussian shapes when fully separated. The two measured electropherograms containing the two incompletely separated analyte peaks are shown in Fig. 5 (zoomed to the time interval of interest).

The nonlinear curve fitting method was applied to detector traces obtained in actual separations in order to illustrate the applicability of the peak-overlap based equivalent resolution concept on real separations. The analyte peaks in both electropherograms were fitted by the sum of two Gaussian functions. Parameters of the fits are summarized in Table 1.

The resolution values for each pair of peaks were determined in four ways. First using the ChemStation software, which is the software provided with the electrophoretic instrument by the manufacturer. The ChemStation software calculates resolution on the basis of Eq. (3) employing the approximate relation $\sigma = w_{50}/2.35$, where w_{50} is the full width of the peak at 50% of its height (also referred to as FWHM). Next, the detector trace was decomposed into two Gaussian components by a nonlinear fitting procedure with 6 parameters (A_i, t_i, and σ_i with $i = \{1;2\}$ for the first and the second component, respectively) in the Origin software. Based on the resulting parameters, the R_S, R_Ω, and R_P values were calculated using Resolution Analyzer. Resolution Analyzer employs numerical integration to calculate the relative peak-overlap integrals Ω and *P*, and applies the first-order error propagation law approximation in order to make a rough estimate of the error (asymptotic SD) of the calculated parameters based on the SDs of the input data (fitting parameters). The calculated resolution values corresponding to the electropherograms shown in Fig. 5 are summarized in Table 2.

The classical resolution value provided by the ChemStation software is comparable to that obtained from the fitted Gaussian peaks. This indicates that the fitting procedure is equivalent to the FWHM method, as expected. As follows from Table 2, the two peaks have the same SDs, σ, which can be generally expected for two nearly comigrating zones under linear electrophoretic conditions. They only differ in their areas. Thus, both the classical resolution value, R_S, and the Ω-based equivalent resolution value, R_Ω, result in exactly the same number and neither of them reflect the peak area overlap properly (*cf.* Fig. 3D). Only the *P*-equivalent resolution value, R_P, describes correctly the extent of separation of the minor component from the major one, resulting in significantly smaller values than classical resolution would indicate. These *P*-equivalent peak resolution values, R_P, tell us what would be the classical resolution value for the two peaks under the standardized frame of reference of two identical Gaussian peaks.

© 2014 WILEY-VCH Verlag GmbH & Co. KGaA, Weinheim

Table 2. Comparison of the peak resolution values obtained by the various approaches as described in detail in the text.

Case	Classical resolution, R_S		Ω Integral		*P* Integral	
	ChemStation	Gaussian fit	Ω (%)	R_Ω	*P* (%)	R_P
A	0.84	0.881 (0.002)	0.20 (10^{-16})	0.881 (10^{-14})	14.10 (0.10)	0.736 (0.002)
B	1.17	1.181 (0.004)	10^{-3} (10^{-15})	1.181 (10^{-13})	3.228 (0.04)	1.070 (0.002)

ChemStation: Automated peak detection by the instrument-controlling software. Gaussian fit: Equation (3). Ω Integral: Equations (6) and (9). *P* Integral: Equations (14)–(16).

4 Concluding remarks

A new resolution function, called the equivalent resolution function, was introduced as an objective measure of the quality of an analytical separation of two peaks. The equivalent resolution function maps the relative peak-overlap integral—an objective measure of the extent of separation—into the scale of classical resolution, R_S, so that, e.g. an equivalent resolution value of 1.5 always corresponds to baseline separated peaks, independently of their distributions or areas. Two candidates for the equivalent resolution function, R_P and R_Ω, were considered, the former based on the relative peak-overlap integral (*P*) introduced by Schoenmakers et al. [8], the latter based on an analogous integral (Ω) introduced by Dose and Guiochon [8]. It was concluded that the *P* integral reflects the extent of separation in ways the Ω integral does not. Thus, the R_P equivalent resolution is suggested for use in analytical practice. The traditional definition of peak resolution, R_S, is only acceptable when two Gaussian peaks have similar areas and their SDs do not differ more than roughly ten times. In all other cases, R_S may seriously underestimate the actual extent of peak overlap. Finally, it was demonstrated that when both individual peaks have Gaussian distributions, the relative peak overlap and thus the corresponding equivalent resolution value can be easily obtained by fitting the overall peak profile by the sum of two Gaussian functions. This opens a way to an objective characterization of the extent of separation, both for regulatory and optimization purposes.

The support by the Grant Agency of the Czech Republic, Grant no. P206/12/P630, the Grant Agency of the Charles University, Grant No. 570213, project Kontakt LH11018, and Alexander von Humboldt Foundation (Research Fellowship for postdoctoral researchers of Jana Svobodova), as well as the TAMU Gradipore Chair in Separation Science Endowment are gratefully acknowledged.

The authors have declared no conflict of interest.

5 References

[1] Schoenmakers, P. J., Mulholland, M., *Chromatographia* 1988, *25*, 737–748.

[2] Glueckauf, E., *Trans. Faraday Soc.* 1955, *51*, 34–44.

[3] Desty, D. H., *Proceedings of the second symposium/organized by the Gas Chromatography Discussion Group under the auspices of the Hydrocarbon Research Group of the Institute of Petroleum and the Koninklijke Nederlandse Chemische Vereniging*, held at the Royal Tropical Institite, Amsterdam, 19–23 May 1958; Butterworths Scientific, London 1958.

[4] Snyder, L. R., Kirkland, J. J., Glajch, J. L. (Eds.), *Practical HPLC*, 2nd edition, John Wiley & Sons, Inc., New York 1997, pp. 22–24.

[5] Giddings, J. C., *Unified Separation Science*, John Wiley & Sons, Inc., New York 1991, pp. 86–108.

[6] Giddings, J. C., *Anal. Chem.* 1960, *32*, 1707–1711.

[7] Schoenmakers, P. J., Strasters, J. K, Bartha, A., *J. Chromatogr.* 1988, *458*, 355–370.

[8] Dose, E. V., Guiochon, G., *Anal. Chem.* 1990, *62*, 174–181.

[9] Ku, H. H., *J. Res. Nat. Bur. Stand. C* 1966, *70C*, 263–273

[10] Grisales, J. O., Arancibia, J. A., Castells, C. B., Olivieri, A. C., *J. Chromatogr. B* 2012, *910*, 78–83

[11] Hruška, V., Riesová, M., Gaš, B., *Electrophoresis* 2012, *33*, 923–930.

[12] Golshan-Shirazi, S., Guiochon, G., *J. Phys. Chem.* 1989, *93*, 4143–4157.

[13] Golshan-Shirazi, S., Guiochon, G., *Chromatographia* 1990, *30*, 613–617.

[14] Khaledi, M. G. (Ed.), *High Performance Capillary Electrophoresis, volume 146*, John Wiley & Sons, Inc., New York 1998, pp 48–50

[15] Golshan-Shirazi, S., Guiochon, G., *Anal. Chem.* 1989, *61*, 462–467.

[16] Golshan-Shirazi, S., Guiochon, G., *J. Phys. Chem.* 1990, *94*, 495–500.

[17] Horká, M., Šlais, K., *Electrophoresis* 2000, *21*, 2814–2827.

© 2014 WILEY-VCH Verlag GmbH & Co. KGaA, Weinheim

4.3 Určení parametrů Haarhoff-Van der Lindeho funkce z geometrických vlastností píku: *Publikace III*

Je-li pík analytu deformován elektromigrační disperzí, je třeba pro správné stanovení elektroforetické mobility analytu znát hodnotu parametru a_1 HVL funkce, která popisuje daný pík. Parametr a_1, stejně jako další parametry HVL funkce, lze určit metodou nelineární regrese. Nutnost provádět nelineární regresi však do značné míry zpomaluje vyhodnocení experimentálních dat, neboť je obvykle nutné experimentální data nejprve vyexportovat do vhodného softwaru a v něm následně provést nelineární regresi. Vzhledem k numerickým vlastnostem HVL funkce je navíc třeba pro dosažení správné konvergence fitu dobře odhadnout počáteční hodnoty všech parametrů HVL funkce.

Cílem *Publikace III* bylo nalézt vztah mezi parametry HVL funkce a_1, a_2 a a_3 a jejími geometrickými vlastnostmi jako je poloha jejího maxima či její šířka měřená v určité frakci její výšky. Analogické vztahy jsou známé pro píky s koncentračním profilem daným Gaussovým rozdělením, kde například šířka píku v polovině jeho výšky $s_{(0.5)}$ a standardní směrodatná odchylka píku σ jsou spolu svázány vztahem:

$$s_{(0.5)} = 2\sqrt{2\ln 2}\sigma \tag{35}$$

V *Publikaci III* byly pro parametry a_1, a_2 a a_3 HVL funkce nalezeny následující vztahy:

$$a_1 = t_{\mathrm{M}} - s_{(\alpha)} K_\alpha \left(f_q^{-1}(q) \right) \tag{36}$$

$$a_2 = s_{(\alpha)} L_\alpha \left(f_q^{-1}(q) \right) \tag{37}$$

$$a_3 = f_q^{-1}(q) \tag{38}$$

kde t_{M} je čas (poloha na časové ose) maxima píku, $s_{(\alpha)}$ je šířka píku ve výšce αH, kde H je výška píku, $K_\alpha \left(f_q^{-1}(q) \right)$, $L_\alpha \left(f_q^{-1}(q) \right)$ a $f_q^{-1}(q)$ jsou jisté funkce parametru q, který je geometrickou charakteristikou míry deformace píku. Parametr q je možné definovat mnoha způsoby, například těmito vztahy:

$$q = \frac{s_{(\alpha)}}{s_{(\beta)}} \tag{39}$$

$$q = \frac{s_{(\alpha)}}{s_{L(\alpha)}} \tag{40}$$

$$q = \frac{s_{R(\alpha)}}{s_{L(\alpha)}} \tag{41}$$

kde $s_{L(\alpha)}$ a $s_{R(\alpha)}$ jsou levá a pravá dílčí šířka[9] píku měřená ve výšce αH. Taktéž za α ve vztazích (36) – (38) je v principu možné zvolit libovolnou hodnotu z intervalu (0,1). Funkční předpisy $K_\alpha\left(f_q^{-1}(q)\right)$, $L_\alpha\left(f_q^{-1}(q)\right)$ a $f_q^{-1}(q)$ se samozřejmě liší v závislosti na volbě hodnoty α a definici parametru q, jak je naznačeno spodními indexy α a q. Nicméně rovnosti (36) – (38) zůstávají platné bez ohledu na konkrétní definici parametru q či volbu α. Parametry HVL funkce a_1, a_2 a a_3 je tedy možné jednoznačně určit na základě rovnic (36) – (38) ze tří geometrických charakteristik píku, a to t_M, $s_{(\alpha)}$ a q.

Funkce K_α, L_α a f_q^{-1} je možné získat pouze numerickým výpočtem. Jednou vypočtené hodnoty však můžeme tabelovat a následně opakovaně použít pro vyhodnocení různých HVL píků. V *Publikaci III* je uveden příklad průběhu funkcí K_α, L_α a f_q^{-1}, a to pro volbu $\alpha = 0{,}5$ a $q = T_\mathrm{USP}$ (viz vztah (42) níže) (*Publikace III*, Figure 1). Použitelnost vztahů (36) – (38) pro určení parametrů HVL funkce byla ilustrována na jednom reálném elektroferogramu a třech modelových pících vygenerovaných v simulačním programu Simul 5 Complex [27], přičemž tyto modelové píky vykazovaly různou míru elektromigrační disperze. Detailní popis experimentálních podmínek a nastavení simulací je uvedeno v *Publikaci III*. Pík analytu v reálném elektroferogramu byl nejprve analyzován v softwaru ChemStation, který je firmou Agilent Technologies dodáván spolu s přístrojem pro kapilární elektroforézu.

Software ChemStation provádí automatické vyhodnocení vlastností píku analytu, jehož výstupem jsou mimo jiné čas maxima píku t_M, šířka píku v polovině jeho výšky $s_{(0.5)}$ a parametr T_USP (*U.S. Pharmacopeia tailing factor*) definovaný vztahem [28]:

$$T_{USP} = \frac{s_{(0.05)}}{2s_{L(0.05)}} \tag{42}$$

[9] Levou, respektive pravou dílčí šířkou píku rozumíme časovou vzdálenost mezi levým, respektive pravým okrajem píku a migračním časem maxima píku.

Parametr T_{USP} přitom představuje jednu z možných definic geometrické charakteristiky q. Na druhou stranu software ChemStation neprovádí fitování píku analytu HVL funkcí, a tak neumožňuje stanovení parametrů HVL funkce nelineární regresí.

Parametry HVL funkce popisující experimentální pík byly vypočteny podle vztahů (36) – (38) z hodnot t_{M}, $s_{(0.5)}$ a T_{USP} poskytnutých softwarem ChemStation. Následně byly parametry HVL funkce stanoveny také nelineární regresí v softwaru Origin 8.1. Vyhodnocení simulovaných píků napodobovalo tento postup s tím rozdílem, že hodnoty t_M, $s_{(0.5)}$ a T_{USP} byly odečteny manuálně (s použitím softwaru Origin 8.1). V případě všech studovaných píků se hodnoty parametrů a_1 a a_2 vypočtené podle vztahů (36) a (37) a získané nelineární regresí velmi dobře shodovaly (*Publikace III*, Table 1 a Table 2). Shoda parametrů a_3 byla poněkud horší (zejména v případě symetrického píku), což bylo způsobeno jednak konečnou vzorkovací frekvencí detektoru[10] a jednak tím, že tvar studovaných píků neodpovídal zcela přesně tvaru HVL funkce[11]. Velmi dobrá shoda mezi HVL funkcí získanou nelineární regresí a HVL funkcí sestrojenou na základě parametrů a_1, a_2 a a_3 získaných výpočtem podle vztahů (36) – (38) byla ilustrována též graficky (*Publikace III*, Figure 3).

Z výsledků dále plyne (*Publikace III*, Table 1 a Table 2), že v případě výrazně nesymetrického píku se hodnoty t_{M} a a_1 liší řádově o procenta. Pro přesné určení elektroforetické mobility analytu je proto v takovém případě nutné vycházet z parametru a_1 (vypočteného dle vztahu (36)) a nikoli migračního času maxima píku t_{M}.

[10] Negativní vliv konečné vzorkovací frekvence detektoru se nejvýrazněji projeví v případě symetrického píku.

[11] HVL funkce není přesným řešením rovnic kontinuity, nýbrž pouze řešením aproximativním. HVL funkce nepostihuje veškeré nelineární jevy, ke kterým může v průběhu kapilární elektroforézy docházet. [10]

Publikace III

Determination of the correct migration time and other parameters of the Haarhoff-van der Linde function from the peak geometry characteristics

Pavel Dubský, **Martin Dvořák**, Ludmila Müllerová, Bohuslav Gaš

Electrophoresis 2015, *36*, 655 – 661

Pavel Dubský
Martin Dvořák
Ludmila Můllerová
Bohuslav Gaš

Department of Physical and Macromolecular Chemistry, Faculty of Science, Charles University in Prague, Prague, Czech Republic

Received October 1, 2014
Revised November 14, 2014
Accepted November 14, 2014

Research Article

Determination of the correct migration time and other parameters of the Haarhoff–van der Linde function from the peak geometry characteristics

For Gaussian peaks, the migration time of the analyte results as the position of the top of the peak and the zone variance is proportional to the peak width. Similar relations have not yet been derived for the Haarhoff–van der Linde (HVL) function, which appears as a fundamental peak-shape function in electrophoresis. We derive the relations between the geometrical measures of the HVL-shaped peak, that is the position of its maximum, its width and a measure of its asymmetry, and the respective parameters a_1, a_2, and a_3, of the corresponding HVL function. Under the condition of the HVL-shaped peak, the a_1 parameter reflects the true migration time of the analyte, which may differ from the peak top position significantly. Our procedure allows us to express the parameters without the need of any external data processing (nonlinear regression). We demonstrate our approach on simulated peaks and on experimental data integrated by the ChemStation software (delivered with the CE instrumentation by Agilent Technologies). A significant improvement is achieved reading the migration time of the experimental and simulated peaks, which draws the error of the HVL-shaped peak migration time evaluation down to the resolution of the data sampling rate.

Keywords:
Electromigration dispersion / Haarhoff–van der Linde / Migration time
DOI 10.1002/elps.201400463

1 Introduction

In CZE measurements, asymmetrical peaks are often observed due to electromigration dispersion (EMD). EMD is caused by local changes in electrophoretic mobility of a substance/analyte in the zone of the corresponding peak. These changes in electrophoretic mobility may be related to changes in pH or conductivity in the zone of the particular peak or to the presence of complex-forming constituents in BGE [1–3]. Erny et al. [4, 5] showed that the Haarhoff–van der Linde (HVL) function [6] often correctly describes peak shapes observed in CZE and is very suitable for fitting CZE peaks. The HVL function was also found to be the solution of the linearized model of electromigration with a small nonlinear disturbance [7].

Other peak-shape functions have been proposed. While the HVL function is exactly valid only for an infinitely narrow injection zone, the so-called HVLR function additionally results as the solution of the linearized model of electromigration as the injection zone grows in width [7]. The situation further complicates if the conditions of the linearized model are not satisfied. In such cases some semiempirical approaches succeeded in finding a suitable peak-shape function [8, 9].

In this we focus on the HVL peak function, mainly for the following two reasons. First, we intend to provide a fundamental mathematical analysis of the HVL function that results in formulas that relate the geometrical properties of the function to its parameterization given in the theoretical section. This practice is similar to that applied on the Gaussian-shaped peaks, where the peak variance is estimated, for example from its FWHM. Second, the linearized theory of electromigration shows that as far as the peak of the analyte obeys the HVL shape, the a_1 parameter of the HVL function gives the correct migration time of the analyte (as expected from its electrophoretical mobility). The herein-introduced relations will provide a correction term that allows the analysts to find the (unobservable) a_1 position of the peak from its directly observable properties, such as the peak top position, width, and asymmetry. Unfortunately though, the relations cannot be found in the closed form. Instead, a lookup table of a set of coefficients is introduced. This procedure is still generally more convenient compared to the otherwise needed

Correspondence: Dr. Pavel Dubský, Department of Physical and Macromolecular Chemistry, Faculty of Science, Charles University in Prague, Albertov 2030, CZ-128 40 Prague 2, Czech Republic
E-mail: pavel.dubsky@natur.cuni.cz

Abbreviations: **EMD**, electromigration dispersion; **HVL**, Haarhoff–van der Linde

Colour Online: See the article online to view Figs. 1–3 in colour.

© 2014 WILEY-VCH Verlag GmbH & Co. KGaA, Weinheim

data export and nonlinear curve fitting. It allows us to utilize the output of the standard data integration software and a simple tool such as MS Excel for a_1 calculation as we will demonstrate in the experimental section.

It should be pointed out that there are two different parameterizations of the HVL function in the literature. The older type of parameterization, which was first used in the software PeakFit® (www.sigmaplot.com) and thereafter adopted by Erny et al. [4] and many other authors, is defined by the following formula:

$$HVL(t; a_0, a_1, a_2, a_3) = \frac{\frac{a_0 a_2}{a_1 a_3 \sqrt{2\pi}} \exp\left[\frac{-1}{2}\left(\frac{t-a_1}{a_2}\right)^2\right]}{\frac{1}{\exp\left(\frac{a_1 a_3}{a_2^2}\right)-1} + \frac{1}{2}\left[1 + \operatorname{erf}\left(\frac{t-a_1}{\sqrt{2}a_2}\right)\right]}, \tag{1}$$

where a_0 is the area of the peak. Although not explicitly stated in Eq. (1), parameters a_1 and a_2 are dependent on time, namely $a_1 = v_0 t$ and $a_2 = \sqrt{2\delta t}$, where v_0 is the linear velocity and δ the diffusion coefficient of the electromigration zone corresponding to the particular peak. These two terms, v_0 and δ, are explained in [7] in more detail. The parameter a_2 describes diffusional (symmetrical) broadening of the peak and as we shall see later, it is directly proportional to the peak width. The parameter a_3 is usually said to be a measure of the peak distortion and is defined as the ratio $-v_{EMD}/v_0$, where v_{EMD} is the difference in the electromigration velocity at the base and at the top of the peak. It can be indeed shown that the HVL function becomes a symmetrical Gaussian function if $a_3 = 0$ regardless of the choice of the remaining parameters and it becomes asymmetric as $a_3 \neq 0$. The parameter a_3 enters the definition of the HVL function in two ways. First, it appears in the numerator of the HVL function where it plays only a role of a multiplicative factor having no influence on the asymmetry of the HVL function. Hence, the asymmetry of the HVL function must be governed by the term $\exp(\frac{a_1 a_3}{a_2^2})$ in the denominator. However, the value of this asymmetry-determining term depends not only on a_3 but also on a_1 and a_2. Therefore, the value of a_3 itself is not deterministic for the peak distortion (asymmetry). From the physical perspective, the parameter a_3, although closely related to the EMD, does not take into account the effect of the diffusion. Yet, it is the counterbalance of the EMD and diffusion that determines the final peak shape. At this point, the second type of parameterization of the HVL function naturally follows from the linear model of electromigration and was introduced in the aforementioned paper by Hruška et al. [7]. The related formula is:

$$HVL_\delta(t; a_0, a_1, a_2, a_{3\delta}) = \frac{\frac{a_0}{a_2 a_{3\delta}\sqrt{2\pi}} \exp\left[-\frac{1}{2}\left(\frac{t-a_1}{a_2}\right)^2\right]}{\frac{1}{\exp(a_{3\delta})-1} + \frac{1}{2}\left[1 + \operatorname{erf}\left(\frac{t-a_1}{\sqrt{2}a_2}\right)\right]}. \tag{2}$$

The definition of the parameters a_0, a_1, and a_2 remains unchanged. The only difference lies in the definition of the parameter $a_{3\delta}$, which now equals $-v_{EMD}/2\delta$ and includes both effects of the EMD and the diffusion (therefore the δ subscript). After this redefinition of the a_3 parameter, the asymmetry-determining term depends only on $a_{3\delta}$ (see Eq. (2)), so the geometrical distortion (asymmetry) of the peak is given solely by the $a_{3\delta}$ value. Later in this article, we will use this latter parameterization (Eq. (2)). Notice, however, that both the parameterizations describe exactly the same HVLi peak shape and result in the same a_0, a_1 , and a_2 parameters. The $a_{3\delta}$ is given by substitution $a_{3\delta} = \frac{a_1 a_3}{a_2^2}$. Therefore we will further omit the δ subscript in HVL_δ (Eq. (2)) and stay on the general term "HVL function."

If the peaks are significantly distorted due to the EMD, a question arises what is the "true" migration time as expected from the effective electrophoretic mobility of the analyte. The analyte migration time is usually measured at the top of the electrophoretic peak. Nevertheless, Le Saux et al. [10] have proven that the peak apex position, t_M, shifts with increasing the analyte concentration leading to over- or underestimation of the analyte effective mobility. Instead, the parameter a_1 of the HVL function fitted to the peak is proposed as the accurate migration time, which does not depend on the analyte concentration. This is later substantiated by the linear theory of electromigration [7], which stays that the a_1 parameter of the HVL function be the expected migration time of the analyte. Based on this justification we will use the a_1 parameter in the meaning of the parameter of the HVL function as well as the correct migration time of the analyte interchangeably throughout this article. For the sake of clarity, we will further refer to the migration time of the top of the peak, t_M, as to the "experimental" migration time, while the expected migration time of the analyte, a_1, will be denoted as the "theoretical" migration time. Notice that if there is no EMD, $a_3 \to 0$, the peak has a Gaussian shape, and the parameter a_1 coincides with t_M. Finally, we should mention that the HVL function accounts only for the EMD-related shift of the peak apex out of the expected migration time, a_1. Namely in the case of highly overloaded samples, higher order nonlinear (de)stacking effects may arise in an electrophoretic system that affect both the peak shape and observed velocity (migration time) of the analyte [11, 12].

2 Theory

2.1 General

In order to investigate the geometrical properties of the HVL function in more detail, it is useful to introduce its normalized form $hvl(\tau; a_{3\delta}) \equiv HVL(\tau; a_0 = 1, a_1 = 0, a_2 = 1, a_{3\delta})$ of one independent variable, τ, and the single parameter, $a_{3\delta}$:

$$hvl(\tau; a_{3\delta}) = \frac{\frac{1}{a_{3\delta}\sqrt{2\pi}} \exp\left(\frac{-\tau^2}{2}\right)}{\frac{1}{\exp(a_{3\delta})-1} + \frac{1}{2}\left\{1 + \operatorname{erf}\left(\frac{\tau}{\sqrt{2}}\right)\right\}}. \tag{3}$$

© 2014 WILEY-VCH Verlag GmbH & Co. KGaA, Weinheim

Using this new auxiliary function we can simplify the HVL function to the form of

$$HVL(t; a_0, a_1, a_2, a_{3\delta}) = F\,hvl(\tau; a_{3\delta}) \tag{4}$$

where the constant F is defined as a_0/a_2 and the substitution:

$$\tau = \frac{t - a_1}{a_2} \tag{5}$$

applies. In the rest of this section we shall denote the maximum of $hvl(\tau; a_{3\delta})$ by θ and the position of the maximum by τ_Θ. Realize (see Eq. (3)) that both θ and τ_Θ depend only on $a_{3\delta}$. Likewise the hvl function, quantities θ and τ_Θ have only an auxiliary role in this text and their physical meaning, if any, is not significant here. In addition to introducing the hvl function, we need to solve the inverse problem of finding τ for a specified h such that $hvl(\tau; a_{3\delta}) = h$. Since the hvl has one maximum at τ_Θ, the inverse problem results in two solutions in the domains $(-\infty;\tau_\Theta\rangle$ and $\langle\tau_\Theta;\infty)$. Thus we introduce restrictions of function $hvl(\tau; a_{3\delta})$ to the respective intervals by defining $hvlL(\tau; a_{3\delta}) = hvl(\tau; a_{3\delta})|_{(-\infty;\tau_\Theta\rangle}$ and $hvlR(\tau; a_{3\delta}) = hvl(\tau; a_{3\delta})|_{\langle\tau_\Theta;\infty)}$. This allows us to express the values of $\tau_L = hvlL^{-1}(h; a_{3\delta})$ and $\tau_R = hvlR^{-1}(h; a_{3\delta})$ for an arbitrary $h \in (0, \Theta\rangle$ so that $hvl(\tau_L; a_{3\delta}) = hvl(\tau_R; a_{3\delta}) = h$. It indeed applies $hvlL^{-1}(\Theta; a_{3\delta}) = hvlR^{-1}(\Theta; a_{3\delta}) = \tau_\Theta$.

From Eq. (4) it follows that the maximum, M, of the original HVL function equals to $M = F\Theta$. This maximum is situated at a position of t_M, which can be expressed as:

$$t_M = a_1 + \tau_\Theta a_2. \tag{6}$$

This is a simple consequence of Eqs. (4) and (5) and the fact that τ_Θ is the position of the maximum of $hvl(\tau; a_{3\delta})$. Equation (6) provides the first relationship between the (yet unknown) parameters of the HVL function and the physical characteristics of the peak, that is its experimental migration time, t_M. In order to get further, we will get rid of the parameter a_1 in Eq. (6) and show that the a_2 parameter is proportional to the geometrical width of the HVL peak.

Let α be an arbitrary number from (0, 1) and denote w_α the full width of the HVL peak at α-fraction of its height, αM. It is easy to think over that there exist just one $\tau_{L\alpha} \in (-\infty, \tau_\Theta)$ and one $\tau_{R\alpha} \in (\tau_\Theta, \infty)$ such that:

$$\alpha\Theta = hvl(\tau_{L\alpha}; a_{3\delta}) = hvl(\tau_{R\alpha}; a_{3\delta}). \tag{7}$$

Both $\tau_{L\alpha}$ and $\tau_{R\alpha}$ depend only on $a_{3\delta}$. Using Eqs. (5) and (4) this translates into the physical time domain as:

$$t_{L\alpha} = a_2\tau_{L\alpha} + a_1 \tag{8a}$$

$$t_{R\alpha} = a_2\tau_{R\alpha} + a_1 \tag{8b}$$

$$HVL(t_{L\alpha}; a_0, a_1, a_2, a_{3\delta}) = HVL(t_{R\alpha}; a_0, a_1, a_2, a_{3\delta}) = \alpha M \tag{8c}$$

The difference between $t_{L\alpha}$ and $t_{R\alpha}$ is the width, w_α:

$$w_\alpha \equiv t_{R\alpha} - t_{L\alpha} = a_2(\tau_{R\alpha} - \tau_{L\alpha}). \tag{9}$$

The subtraction (9) gives the a_1 parameter vanished and shows that the HVL peak width is directly proportional to the a_2 parameter, and vice versa.

$$a_2 = w_\alpha L_\alpha(a_{3\delta}) \tag{10}$$

The constant of proportionality, L_α, depends only on the $a_{3\delta}$ parameter. This means that HVL functions that may differ in their sizes, heights, widths, and peak top positions share the same set of L_α coefficients as only the function of their distortions (asymmetries) determined by the $a_{3\delta}$ parameter.

The remaining task is thus to find the relation between the $a_{3\delta}$ value and the distortion (asymmetry) of the HVL peak. This can be easily done by realizing that the ratio of the two w_α values is independent of a_2 as follows directly from Eq. (10). In this way we are left with a formula depending solely on $a_{3\delta}$:

$$q_{\alpha\beta} = \frac{w_\alpha}{w_\beta} = \frac{L_\beta}{L_\alpha} = f_q(a_{3\delta}). \tag{11}$$

If the function f_q is continuous and monotonous, the $a_{3\delta}$ parameter is obtained from the measure of the peak widths ratio, $q_{\alpha\beta}$, as:

$$a_{3\delta} = f_q^{-1}(q_{\alpha\beta}). \tag{12}$$

The α and β fractions of the peak height at which the peak distortion (asymmetry) is measured can, in principle, be chosen arbitrarily. Alternatively, t_M (resp. τ_M) can stay for either $t_{R\alpha}$ or $t_{L\alpha}$ (resp. $\tau_{R\alpha}$ or $\tau_{L\alpha}$) in Eq. (9) resulting in the peak half-widths, $w_{L\alpha}$ or $w_{R\alpha}$. In this way, the ratio of the peak half-width to the full-width as well as the ratio of the two (rightward and leftward) half-widths at the same α-fraction of the peak height may serve the purpose.

Finally, let us summarize the entire procedure of finding the individual parameters of the HVL function from its geometrical properties. Apart from the experimental migration time, w_α is used as a measure of the peak width and $q_{\alpha\beta}$ as a measure of its distortion (asymmetry). Parameter $a_{3\delta}$ of the corresponding HVL function then results as the function $f_q^{-1}(q_{\alpha\beta})$(Eq. (12)). Next, the L_α coefficient relates the w_α measure of the peak width to its actual a_2 parameter (Eq. (10)). Since the L_α is only the function of $a_{3\delta}$, which itself is a function of $q_{\alpha\beta}$, the L_α coefficients can be advantageously related to the $q_{\alpha\beta}$ directly rather than through the $a_{3\delta}$ parameter, $L_\alpha \equiv L_\alpha(q_{\alpha\beta})$. As the last step, the a_1 parameter is determined from the peak top position, t_M, and Eq. (6). For the practical purposes, Eq. (6) can be rearranged as:

$$a_1 = t_M - \tau_\Theta a_2 = t_M - \tau_\Theta w_\alpha L_\alpha = t_M - w_\alpha K_\alpha, \tag{13}$$

where K_α forms yet another set of coefficients dependent on $a_{3\delta}$ (τ_Θ is an $a_{3\delta}$-dependent constant that need not to be specified). Similarly to the previous case of the L_α coefficients, K_α can be related to the $q_{\alpha\beta}$ directly, $K_\alpha \equiv K_\alpha(q_{\alpha\beta})$.

Unfortunately, none of the f_q^{-1}, L_α, and K_α functions of $q_{\alpha\beta}$ can be found in the closed form. Instead, they can be easily solved numerically for a chosen $q_{\alpha\beta}$ parameter by modeling the normalized $hvl(\tau; a_{3\delta})$ function for various values of $a_{3\delta}$. Once generated for the normalized function, the

© 2014 WILEY-VCH Verlag GmbH & Co. KGaA, Weinheim

coefficients can serve for any HVL-shaped peak since they are fully determined by the peak distortion (asymmetry), regardless of its actual size, that is height, width, or area. We finally emphasize that although the entire procedure is based on the δ-parameterization of the HVL function (Eq. (2)) this fact only concerns the $a_{3\delta}$ parameter, that is the values derived for the $f_q^{-1}(q_{\alpha\beta})$ function, because parameters a_1 and a_2 are the same in both parameterizations.

Equations (10), (12), and (13) form a unique mapping from the parametric space of the HVL function (a_1, a_2, $a_{3\delta}$) to the physical domain of the HVL peak (t_M, w_α, $q_{\alpha\beta}$) and vice versa. It is evident that one may choose (fix) the a_1, a_2, and $a_{3\delta}$ parameters of the HVL function while the physical characteristics t_M, w_α, and $q_{\alpha\beta}$ will result. Similarly though, one may now fix the experimental time (peak top position), width, and asymmetry (at a certain peak–height ratio) of the HVL peak and the Eqs. (10), (12), and (13), or effectively the coefficients K_α and L_α, secure that the parameters a_1, a_2 and $a_{3\delta}$ adjust themselves so that the resulting HVL function will exhibit the exact top position, width, and asymmetry as desired. This has a practical consequence that may not be apparent at the first sight but will be discussed in the experimental part of this article.

2.2 Application to the ChemStation software output

We will illustrate the above-introduced relations on determining the HVL parameters of the electrophoretic peaks analyzed by the ChemStation software. The ChemStation is a standard software package supplied with the CE equipment by Agilent Technologies, Waldbronn, Germany. As many other data analysis software packages, ChemStation provides an automated peak analysis with detailed report on peak properties, including system performance parameters such as peak width, asymmetry, number of theoretical plates (equivalent to chromatography), etc. Nevertheless, the HVL fit is not available, which primarily affects the reading of the migration time, which is attributed to t_M rather than a_1. This may result in misleading assessments of the electrophoretic mobilities of the analytes if EMD is present. In order to overcome this problem, the data are to be exported into a third-party software tool and then reprocessed manually with the HVL nonlinear regression, including the peak detection, baseline definition and its subtraction. This procedure tends to be laborious and needs a certain level of experience especially in order to supply a reasonable estimate for the initial values of the HVL parameters. Our proposed procedure not only aims to provide such estimates but should enable the analysts to completely avoid the need of the external data processing.

Of the parameters reported by the ChemStation software, t_M denotes here the peak top position, $w_{0.5}$ the full width at the 50% of the peak height, and T_{USP} the U.S. Pharmacopeia (USP) tailing factor: [13]

$$T_{USP} = \frac{w_{0.05}}{2\, w_{L0.05}}, \tag{14}$$

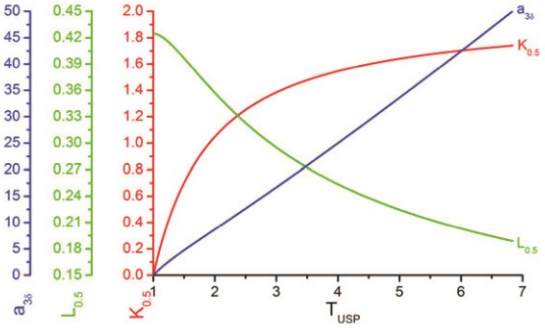


Figure 1. Dependencies of the $a_{3\delta}$ parameter, $K_{0.5}$ coefficient, and $L_{0.5}$ coefficient on the USP tailing factor, T_{USP}. See discussion with Eq. (14). Each dependency has its own *y*-axis.

where $w_{L0.05}$ and $w_{0.05}$ are the left half-width and full-width of the peak measured at 5% of its height, respectively. The USP tailing factor is used as the measure of the peak asymmetry (cf. Eq. (11)). We generated the $f_q^{-1}(T_{USP})$, $L_{0.5}(T_{USP})$, and $K_{0.5}(T_{USP})$ dependencies by means of our software ResolutionAnalyzer (http://echmet.natur.cuni.cz, paper accepted for publication in this special issue). Unambiguous functions have been observed (Fig. 1). Specifically, for $T_{USP} = 1$(symmetrical peak), the $a_{3\delta} = 0$ and the HVL function becomes a Gaussian. Thus also the $K_{0.5}$ coefficient becomes zero as there is not shift of the a_1 parameter out of the peak apex, t_M, regardless of the peak width. Finally, the $L_{0.5}$ coefficient becomes equal to 0.425 ($\frac{1}{2\sqrt{2\ln(2)}}$), the well-known coefficient of proportionality between the peak FWHM measure and the Gaussian $a_2 \equiv \sigma$ parameter. As the peak asymmetry grows, the $a_{3\delta}$ parameter increases (by definition) as well as the $K_{0.5}$ coefficient does. On the other hand, the $L_{0.5}$ coefficient decreases with the increasing asymmetry of the peak. This can be easily understood when realizing that the EMD (asymmetrical peak distortion, reflected by the $a_{3\delta}$ parameter) contributes to the overall peak width apart from the diffusion (symmetrical peak dispersion, reflected by the a_2 parameter). Thus if two peaks have the same overall widths, $w_{0.5}$, while the first is more EMD-distorted than the other, then the first one must be less diffusion-dispersed than the latter. Since $L_{0.5}$ coefficient is the coefficient of proportionality between the diffusional dispersion, a_2, and the peak width, $w_{0.5}$, it naturally decreases with the peak distortion, $a_{3\delta}$ (or equivalently T_{USP}).

The values were generated with the discretization of $a_{3\delta} = 0.01$, in the interval of $a_{3\delta} \in \langle 0; 50\rangle$ (equivalent to $T_{USP} \in \langle 1;$ approx. $6.836\rangle$. The resulting discretization of the L_α and K_α coefficients is $max(\Delta L_{0.5}) = 1.7 \times 10^{-5}$, and $max(\Delta K_{0.5}) = 1.7 \times 10^{-3}$. The HVL function is dissymmetrical with respect to the $a_{3\delta}$ parameter (tailing for $a_{3\delta} > 0$ and fronting for $a_{3\delta} < 0$), so it results:

$$a_{3\delta}(T_{USP}) = -a_{3\delta}\left(\frac{T_{USP}}{2T_{USP} - 1}\right) \tag{15}$$

Equation (15) extends the applicability of the numerical solution to $a_{3\delta} \in \langle -50; 50\rangle$ (T_{USP} approx. $\langle 0.146; 6.836\rangle$).

© 2014 WILEY-VCH Verlag GmbH & Co. KGaA, Weinheim

We implemented the calculation into a simple excel sheet that can be downloaded for free at our website (http://echmet.natur.cuni.cz). t_M, $w_{0.5}$, and T_{USP} serve as the input parameters based on which the a_1, a_2, and $a_{3\delta}$ parameters of the HVL peak are obtained as an output. The ResolutionAnalyzer software can be used in order to generate the f_q^{-1}, L_α, and K_α dependencies for other than $w_{0.5}$ and T_{USP} geometrical measures of the peak width and asymmetry.

3 Materials and methods

Experimental conditions of the real experiment were as follows. The experiment was performed using an Agilent ^{3D}CE equipment operated under the ChemStation software (Agilent Technologies, Waldbronn, Germany) control. Fused-silica capillaries (50 μm id, 375 μm od) were provided by Polymicro Technologies (Phoenix, AZ, USA). The total length of the capillary and the effective length to the detector were 52.0 and 43.5 cm, respectively. The PHM 220 instrument (Radiometer, Copenhagen, Denmark) calibrated with the standard IUPAC buffers, pH 7.000 and pH 10.012, (Radiometer, Lyon, France) was used for the pH measurements. The BGE contained 50 mM Tris and 50 mM Tricine, experimental pH 8.13. The ionic strength of the BGE was 25.76 mM according to the PeakMaster calculation. The complexation agent β-CD was dissolved directly in the running buffer at a concentration of 0.1 mM. The injected sample was 0.3 mM analyte ((*R*)-(–)-2-fluoro-α-methyl-4-biphenylacetic acid) and 0.07% v/v DMSO, which served as the EOF marker, both dissolved directly in the running buffer. Detection was performed with the DAD at the wavelength of 214 nm. The samples were injected hydrodynamically for 30 mbar·s. The applied voltage was 20 kV (cathode at the detector side). The operating temperature was 25°C.

Simulations were performed for the β-CD concentration of 1.0 mM in the running buffer and three different concentrations of the analyte ((*R*)-(–)-2-fluoro-α-methyl-4-biphenylacetic acid) in the injected sample: 0.01, 0.3, and 1.5 mM. In this way we were able to model systems with no, medium, and high EMD of the analyte peak. Other experimental conditions used in the simulations were similar to those in the experiment but it was not our intention to mimic the experiment with simulation exactly (as we are only interested in generating various shapes of the resulting peaks). Our SIMUL Complex software [14] was used for the simulations. The number of nodes in the *x*-axis was 50 000. The simulations were performed by means of the Intel® Core™ i7–960 processor, 3.40 GHz. The simulation time was in the range of hours.

4 Results and discussion

In order to verify the accuracy and applicability of the proposed method for determining the parameters of the HVL function, we tested this method on several peaks generated using our simulation program Simul 5 Complex [14] and on a real experiment. As a model system we chose a system with complexing constituents where the EMD of the analyte peak occurs due to the complexation [15, 16]. The ChemStation software allows the user to gain values of FWHM, $w_{0.5}$, and the USP tailing factor, T_{USP}. The calculation procedure is described in detail in Section 2.2 above. For the simulated peaks, the t_M, $w_{0.5}$, and T_{USP} were determined manually by means of the Origin 8.1 software. For the experimental peak, the integration was performed in the ChemStation software and the resulting values of t_M, $w_{0.5}$, and T_{USP} were used. The Origin 8.1 software was also utilized for the HVL nonlinear regression.

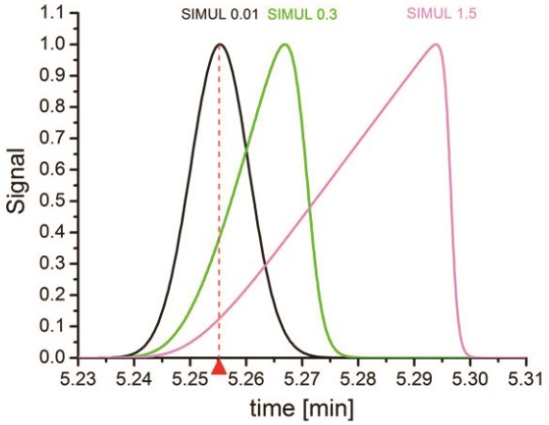


Figure 2. Simulated electropherograms of *R*-flurbiprofen in concentrations of 0.01, 0.3, and 1.5 mM with β-CD in the BGE. BGE consists of 50 mM Tris, 50 mM Tricine buffer, and 1 mM β-CD. See Section 3 for other simulation details. Theoretical migration time is depicted by the vertical line and the arrow at the *x*-axis. *y*-Axis is depicted on a normalized scale. See Table 1 for peak asymmetries and other characteristics.

Simulated electropherograms are shown in Fig. 2. If a low concentration of the analyte is injected (SIMUL 0.01) almost completely symmetrical Gaussian peak is observed. At the midrange concentration (SIMUL 0.3), the peak becomes medium distorted. A highly distorted peak is observed at the highest concentration of the analyte (SIMUL 1.5). The experimental migration times, t_M, and the parameters a_1 of the HVL fits of the peaks are given in Table 1. As expected, the experimental migration times, t_M, differ significantly for the individual peaks, while the a_1 parameter stays at the original position of the symmetrical (undistorted) peak (SIMUL 0.01). The estimate, denoted as $\tilde{a}_1$ in Table 1, results as the corrected experimental migration time, t_M, by Eq. (13). It is evident that the correction (13) significantly reduces the difference between the migration time read and the theoretical migration time of the peak, a_1. For all the EMD-dispersed peaks the estimated values, $\tilde{a}_1$, are much closer to the theoretical migration time, a_1, than is the experimental migration time, t_M. The correction factor to the migration time $w_\alpha K_\alpha$ in Eq. (13) is in the order of several percent. For the highly symmetrical peak (SIMUL 0.01) however, the correction

© 2014 WILEY-VCH Verlag GmbH & Co. KGaA, Weinheim

Table 1. Simulated data of *R*-flurbiprofen in concentrations of 0.01, 0.3, and 1.5 mM with 1 mM β-CD in the BGE

Name	Peak characteristics			HVL fit				HVL estimate			
	t_M (min)	$w_{0.5}$ (min)	T_{USP}	a_1 (min)	a_2 (min)	$a_{3\delta}$	R^2	$\tilde{a}_1$ (min)	$\tilde{a}_2$ (min)	$\tilde{a}_{3\delta}$	R^2
SIMUL 0.01	5.255	0.0123	0.9894	5.2552	0.00522	–0.032	0.99996	5.2547	0.00522	–0.135	0.99637
SIMUL 0.3	5.267	0.0139	0.6928	5.2542	0.00521	–6.905	0.99997	5.2541	0.00518	–7.115	0.99948
SIMUL 1.5	5.294	0.0244	0.5520	5.2538	0.00542	–33.95	0.99976	5.2534	0.00531	–36.25	0.99905

Experimental migration time, t_M; FWHM, $w_{0.5}$; and USP tailing factor, T_{USP} of peaks of *R*-flurbiprofen in various concentrations. a_1, a_2, and $a_{3\delta}$ parameters of the HVL fit of the individual peaks with Eq. (2). $\tilde{a}_1$, $\tilde{a}_2$, and $\tilde{a}_{3\delta}$ estimates of the respective HVL parameters by Eqs. (13), (10), and (12).

factor is so small (less than 0.006%) that it does not have any real impact.

The $\tilde{a}_2$ and $\tilde{a}_{3\delta}$ estimates are also summarized in Table 1. Although the $\tilde{a}_{3\delta}$ estimate differs from the actual $a_{3\delta}$ parameter of the HVL fit by an error as low as 5%, this error is significantly higher than the discretization with which the $a_{3\delta} = f_q^{-1}(T_{USP})$ dependence was generated. We attribute this discrepancy to either the data sampling rate, which affects the precision of the T_{USP} reading, or the fact that the HVL shape does not match the simulated peaks exactly. It seems (data not shown) that the former applies mostly to the symmetrical peaks with low $a_{3\delta}$ values while the latter becomes marginally significant for the highly distorted peaks with high $a_{3\delta}$ values. With the real data, the data noise would moreover most probably overweight both these effects. Fortunately though, the L_α and K_α coefficients are not too much sensitive to the exact T_{USP} value so that the $\tilde{a}_2$ and namely $\tilde{a}_1$ estimates are made precisely enough.

Additionally, the R^2 (coefficient of determination) is reported in Table 1 that quantifies how well the fitted/estimated function reflects the simulated data. The coefficients of determination are nearly 1 for the HVL fits indicating that the HVL function really evolves under the ideal conditions of the simulation (narrow injection zone, EMD, and diffusion effects only). Only negligibly lower coefficients of determination are observed when the HVL function is constructed using the $\tilde{a}_1$, $\tilde{a}_2$, and $\tilde{a}_{3\delta}$estimates. At high EMD peak distortion, the quality of the estimate is just as good as the actual fit, since the $K_{0.5}$ and $L_{0.5}$ coefficients become less sensitive to the peak asymmetry and neither the HVL function fits the peak absolutely perfectly. At low EMD peak distortion, the difference in the quality of the HVL fit and the estimate is the most significant, since even the smallest change in the $\tilde{a}_{3\delta}$estimate results in a slightly different HVL function shape. This, however, does not significantly affect the $\tilde{a}_1$ and $\tilde{a}_2$ estimates as discussed above.

The experimental electropherogram is shown in Fig. 3. The fitted and estimated a_1, a_2, and $a_{3\delta}$ parameters of the corresponding HVL functions are also given in Table 2. Figure 3 reveals a tiny shift of the estimated HVL function (green dashed line) from the fitted HVL function (red line) to the lower times. This is also reflected in the R^2 value of the estimate, which is 0.9779 compared to the 0.9992 by the fitting procedure. A deeper analysis reveals that this is primarily caused by the data sampling rate and the noise. The

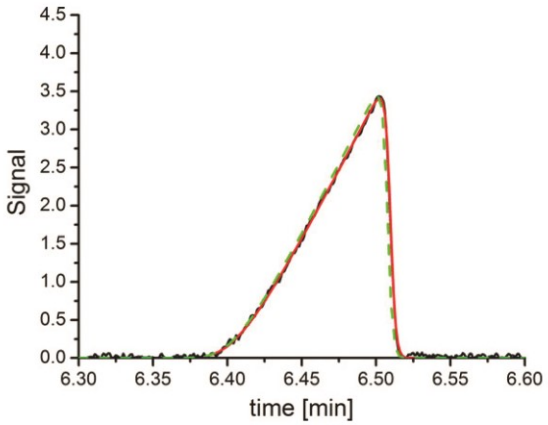


Figure 3. Peak of *R*-flurbiprofen in a concentration of 0.3 mM with 0.1 mM β-CD in the BGE. Black trace: experimental record; red solid line: HVL fit; green dashed line: HVL constructed from the $\tilde{a}_1$, $\tilde{a}_2$, and $\tilde{a}_{3\delta}$ estimates. BGE consists of 50 mM Tris, 50 mM Tricine buffer, and 0.1 mM β-CD. See Section 3 for other experimental details. See Table 1 for the characteristics of the experimental peak and the HVL functions.

ChemStation software reads the experimental peak top position, t_M, at the highest point of the measured peak, which is influenced both by the sampling rate and the noise. The HVL fit is primarily driven by the data points at the inclination and the declination edges of the peak, while the very few data points at the top of the peak does not have any significant influence. In our case, the apex of the HVL fit is shifted rightward from the experimental top position, t_M. The difference is $+1.5 \times 10^{-3}$ min, which is equivalent to approximately two data points with the sampling rate of 8.4×10^{-4}min. The fitting procedure makes the HVL fit robust against the data sampling rate and noise, so that the HVL peak overlaps the experimental peak well on the expense of (or possibly with the benefit of) adjusting its apex as needed. To the contrary, the apex of the HVL function resulting from the $\tilde{a}_1$, $\tilde{a}_2$, and $\tilde{a}_{3\delta}$ estimates must be located exactly at the predefined position of t_M as discussed at the very end of Section 2.1. Simultaneously, width, $w_{0.5}$, and asymmetry, T_{USP}, of the HVL peak are also kept by the estimating procedure. This may result in the shift of the entire HVL function towards the experimental peak top position compared to the HVL fit. Hence, the difference of the $\tilde{a}_1$ estimate from the actual a_1 parameter of the HVL fit equals -1.6×10^{-3}min (two data points), which is in

© 2014 WILEY-VCH Verlag GmbH & Co. KGaA, Weinheim

Table 2. Experimental data of *R*-flurbiprofen in a concentration of 0.3 mM with 0.1 mM β-CD in the BGE

Name	Peak characteristics			HVL fit				HVL estimate			
	t_M (min)	$w_{0.5}$ (min)	T_{USP}	a_1 (min)	a_2 (min)	$a_{3\delta}$	R^2	$\tilde{a}_1$ (min)	$\tilde{a}_2$ (min)	$\tilde{a}_{3\delta}$	R^2
Experiment	6.501	0.0554	0.5574	6.4123	0.0132	−30.10	0.9992	6.4107	0.01265	−32.325	0.9779

BGE consists of 50 mM Tris, 50 mM Tricine buffer and 0.1 mM β-CD. See Section 3 for other experimental details. Experimental migration time, t_M; FWHM, $w_{0.5}$; and USP tailing factor, T_{USP} of the peak of *R*-flurbiprofen. a_1, a_2, and $a_{3\delta}$ parameters of the HVL fit of the peak with Eq. (2). $\tilde{a}_1$, $\tilde{a}_2$, and $\tilde{a}_{3\delta}$ estimates of the respective HVL parameters by Eqs. (13), (10), and (12).

accordance with the $+1.5 \times 10^{-3}$ min shift of the fitted HVL apex out of the t_M position. When the tops of the estimated and fitted HVL functions are synchronized, no observable difference between the two is present and the R^2 value of the estimate grows up to 0.9983. It is important to note that such a bias has a negligible effect when compared to the error introduced if the uncorrected migration time were read from its experimental value, t_M. In our case the difference of $(t_M - a_1)$ is as large as 8.9×10^{-2} min (106 data points), which is over 50 times larger than that of $(\tilde{a}_1 - a_1)$. In conclusion, the correction of the experimental migration time, t_M, introduced by Eq. (13) is reasonably significant and made within the actual precision of the data sampling rate.

As a final point, let us underscore the fact that the migration time correction, that is the shift of the peak maximum, t_M, out of its theoretical position, a_1, does not only depend on the K_α parameter, that is the distortion (asymmetry) of the peak, but is directly proportional to its actual width, w_α (Eq. (13)). Thus although the experimental peak has its distortion comparable to, or even slightly less than, that of the simulated peak SIMUL 1.5 (cf. the respective coefficients $a_{3\delta}$ in Tables 1 and 2), the migration time shift is twice as significant for the experimental peak as for the simulated one since the former is twice as wide (Tables 1 and 2, parameter $w_{0.5}$).

5 Concluding remarks

We derived relations between the geometrical characteristics of the HVL function and its a_1, a_2, and $a_{3\delta}$ parameters. The relations require a set of coefficients that cannot be expressed analytically but were generated numerically for the FWHM, $w_{0.5}$, as a measure of the peak width, and the USP tailing factor, T_{USP}, as a measure of the peak distortion (asymmetry). The relations were successfully applied on simulated electropherograms of various peak distortions and an experimental electropherogram. The theoretical migration time of the peak was estimated as a corrected experimental migration time that would be otherwise falsely assigned to the position of the top of the peak. It was demonstrated that the procedure is directly applicable to the output of automated data integration software, such as ChemStation (CE instrumentation by Agilent Technologies). The correction of the migration time provided the accurate value comparable to that obtained by the HVL fit within the precision of the data sampling rate. Thus, the herein-introduced procedure may serve as a quick and easy alternative to the HVL fitting of the data that requires external data processing. Alternatively, it can provide a very precise estimate of the initial values of the HVL fit in an automated manner.

The authors acknowledge the financial support for this work from the grant agency of the Charles University, grants 669412 and 570213, and the grant agency of the Czech Republic, grant number P206/12/P630.

The authors have declared no conflict of interest.

6 References

[1] Xu, X., Kok, W. T., Poppe, H., *J. Chromatogr. A* 1996, *742*, 211–227.

[2] Horká, M., Šlajs, K., *Electrophoresis* 2000, *21*, 2814–2827.

[3] Hruška, V., Svobodová, J., Beneš, M., Gaš, B., *J. Chromatogr. A* 2012, *1267*, 102–108.

[4] Erny, G. L., Bergström, E. T., Goodall, D. M., *Anal. Chem.* 2001, *73*, 4862–4872.

[5] Erny, G. L., Bergström, E. T., Goodall, D. M., *J. Chromatogr. A* 2002, *959*, 229–239.

[6] Haarhoff, P. C., van der Linde, H. J., *Anal. Chem.* 1966, *38*, 573–582.

[7] Hruška, V., Riesová, M., Gaš, B., *Electrophoresis* 2012, *33*, 923–930.

[8] García-Alvarez-Coque, M. C., Simó-Alfonso, E. F., Sanchis-Mallols, J. M., Baeza-Baeza, J. J., *Electrophoresis* 2005, *26*, 2076–2085.

[9] Zhang, J., Huang, Q., Jin, J., Chang, J., Li, S., Fan, L., *Cao, C., Talanta* 2013, *105*, 278–286.

[10] Le Saux, T., Varenne, A., Gareil, P., *Electrophoresis* 2005, *26*, 3094–3104.

[11] Gebauer, P., Thormann, W., Boček, P., *Electrophoresis* 1995, *16*, 2039–2050.

[12] Gebauer, P., Boček, P., *Electrophoresis* 2009, *30*, S27–S33.

[13] Chapter <621> in United States Pharmacopeia 34, 2011, United States Pharmacopeia Convention, ISBN 37-692-5390-6.

[14] Hruška, V., Beneš, M., Svobodová, J., Zusková, I., Gaš, B., *Electrophoresis* 2012, *38*, 938–947.

[15] Hruska, V., Svobodova, J., Benes, M., Gas, B., *J. Chromatogr. A* 2012, *1267*, 102–108.

[16] Benes, M., Svobodova, J., Hruska, V., Dvorak, M., Zuskova, I., Gas, B., *J. Chromatogr. A* 2012, *1267*, 109–115.

© 2014 WILEY-VCH Verlag GmbH & Co. KGaA, Weinheim

4.5 Zobecněný model lineární teorie elektromigrace a jeho aplikace na elektrokinetickou chromatografii: *Publikace IV*

V *Publikaci IV* byl model NLTEM rozšířen takovým způsobem, aby dokázal popsat libovolné chemické rovnováhy mezi složkami elektroforetického systému, které vyhovují požadavku, že rychlost ustavení dané chemické rovnováhy je mnohonásobně vyšší než rychlost elektromigračního pohybu píků. Speciálním případem takových chemických rovnováh jsou rovnováhy komplexační. Rozšířený model NLTEM neklade žádná omezení na acidobazické chování složek BGE či analytů. Komplexační činidla mohou vytvářet komplex jak se složkami BGE, tak s analyty, přičemž stechiometrie těchto komplexů není nijak omezená. Stejně tak není omezený ani počet komplexačních činidel přítomných v elektroforetickém systému. Rozšíření modelu NLTEM o libovolný druh chemické rovnováhy si vyžádalo přepracování formálního popisu elektroforetického systému, a to zejména proto, aby bylo možné udržet kompaktní, přehledný a snadno interpretovatelný zápis celého odvození. Například rovnice látkové bilance pro *i*-tou složku má v novém formalismu tvar:

$$c_i = \sum_{g \in \mathrm{X}} \nu_{(g)i} c_{(g)} \tag{43}$$

kde X je množina všech iontů a neutrálních molekul, které jsou přítomné v elektroforetickém systému, včetně iontů H_3O^+ a OH^-. Pro prvky množiny X bylo v *Publikaci IV* zavedeno označení „formy“. $c_{(g)}$ je koncentrace formy g. Koeficient $\nu_{(g)i}$ je roven stechiometrickému koeficientu *i*-té složky ve formě g. Pokud se *i*-tá složka na tvorbě formy g nepodílí, je $\nu_{(g)i} = 0$. Ionty H_3O^+ a OH^- nejsou přiřazeny k žádné složce, a proto $\nu_{(H_3O^+)i} = 0$ a $\nu_{(OH^-)i} = 0$ pro každou složku i. Odvození rozšířeného modelu NLTEM v *Publikaci IV* sleduje postup uplatněný v práci [10]. Hlavní pozornost byla v *Publikaci IV* věnována vyjasnění a podrobné interpretaci dílčích kroků v průběhu odvození. Výchozím bodem odvození se opět staly rovnice kontinuity, které v uvažovaném obecném modelu mají následující tvar:

$$\frac{\partial c_i(x,t)}{\partial t} = -\sum_{g \in \mathrm{X}} \nu_{(g)i} \frac{\partial J_{(g)}(x,t)}{\partial x} \tag{44}$$

kde $J_{(g)}(x,t)$ značí látkový tok formy g. Elektromigrační příspěvek k látkovému toku $J_{(g)}(x,t)$ je dán vztahem analogickým k rovnici (4):

$$J_{(g)em} = \frac{j}{\kappa(x,t)}\mu_{(g)}(x,t)c_{(g)}(x,t) \tag{45}$$

Na rozdíl od práce [10] byla v *Publikaci IV* uvažována závislost elektroforetických mobilit $\mu_{(g)}$ jednotlivých forem g na x a t, neboť elektroforetická mobilita závisí na iontové síle a ta nemá v celé kapiláře konstantní hodnotu. Bylo ukázáno, že při uvažování pouze elektromigračního příspěvku k látkovému toku mohou být rovnice kontinuity přepsány do maticového zápisu, který je analogický rovnici (5). Jelikož v dřívějších pracích zabývajících se LTEM [4-6] byla vnitřní struktura matice $\mathbb{M}\left(\vec{c}(x,t)\right)$ prezentována vždy jen pro určitý speciální případ elektroforetického systému, byl v *Publikaci IV* značný prostor věnován právě diskuzi a interpretaci vnitřní struktury této matice. V doplňujícím materiálu *Publikace IV* bylo podrobně ukázáno, že matici $\mathbb{M}$ lze rozložit na součin dvou matic s jasnou fyzikální interpretací.

$$\mathbb{M} = \mathbb{M}_{\mu} \times \mathbb{M}_{\partial} \tag{46}$$

Matice $\mathbb{M}_{\mu}$ má počet řádků rovný počtu složek a počet sloupců rovný počtu forem přítomných v elektromigračním systému. Její prvky mají fyzikální rozměr elektroforetické mobility. Pro prvek $m_{\mu}(i,h)$ stojící v *i*-tém řádku a *h*-tém sloupci matice $\mathbb{M}_{\mu}$ platí:

$$m_{\mu}(i,h) = \frac{\kappa_{\mathrm{BGE}}}{\kappa}\left(\nu_{(h)i}\mu_{(h)} - \frac{F}{\kappa}\sum_{g\in \mathrm{X}}\nu_{(g)i}\mu_{(g)}c_{(g)}r_{(g)(h)}\right) \tag{47}$$

kde

$$r_{(g)(h)} = \left(z_{(h)}\mu_{(h)} - \frac{\kappa}{F}\frac{\partial \ln\mu_{(g)}}{\partial c_{(h)}} + \sum_{f\in \mathrm{X}} z_{(f)}c_{(f)}\frac{\partial \mu_{(f)}}{\partial c_{(h)}}\right) \tag{48}$$

Zahrnutí obecných chemických rovnováh do modelu NLTEM se projevilo přítomností koeficientů $\nu_{(g)i}$ a $\nu_{(h)i}$ ve výrazu pro $m_{\mu}(i,h)$. Přítomnost členů obsahujících derivace $\frac{\partial \ln\mu_{(g)}}{\partial c_{(h)}}$ a $\frac{\partial \mu_{(f)}}{\partial c_{(h)}}$ je potom odrazem uvažované závislosti elektroforetické mobility na iontové

síle. Matice $\mathbb{M}_\partial$ má počet řádků rovný počtu forem a počet sloupců rovný počtu složek přítomných v elektromigračním systému. Její prvky představují parciální derivace koncentrace jednotlivých forem podle celkové koncentrace jednotlivých složek. Pro prvek stojící v h-tém řádku a q-tém slouci matice $\mathbb{M}_\partial$ platí:

$$m_\partial(h,q) = \frac{\partial c_{(h)}}{\partial c_q} \tag{49}$$

V *Publikaci IV* byla matice $\mathbb{M}_\partial$ nazvána „komunikační“, neboť zprostředkovává vazby mezi jednotlivými iontovými formami tak, jak je určují chemické rovnováhy a rovnice látkové bilance. Při konstrukci matice $\mathbb{M}_\partial$ byl uplatněn předpoklad o rychlém ustavování chemických rovnováh zmíněný v úvodu komentáře k *Publikaci IV*. Bez splnění tohoto předpokladu by rovnice kontinuity nemohly být převedeny do maticového tvaru.

Difúze byla do rozšířeného modelu NLTEM zahrnuta stejným způsobem jako do základního modelu NLTEM v práci [10], viz rovnice (13). V doplňujícím materiálu *Publikace IV* bylo ukázáno, včetně rozboru všech provedených aproximací, že difúzní matici $\mathbb{D}$ lze vyjádřit jako součin jisté matice $\mathbb{D}_d$ a komunikační matice $\mathbb{M}_\partial$

$$\mathbb{D} = \mathbb{D}_d \times \mathbb{M}_\partial \tag{50}$$

$$d_d(i,h) = \left(\nu_{(h)i} D_{(h)} - \frac{F z_{(h)} D_{(h)}}{\kappa} \sum_{g \in \mathrm{X}} \nu_{(g)i} \mu_{(g)} c_{(g)} \right) \tag{51}$$

kde $d_d(i,h)$ je prvek matice $\mathbb{D}_d$ stojící v i-tém řádku a h-tém sloupci. Prvky matice $\mathbb{D}_d$ mají fyzikální rozměr difúzního koeficientu. Struktura matice $\mathbb{D}$ je tedy analogická struktuře elektroforetické matice $\mathbb{M}_\mu$. V *Publikaci IV* je dále stručně diskutován postup diagonalizace a přidání korekčního nelineárního členu, který je již zcela totožný s postupem prezentovaným v práci [10]. Na závěr teoretické části je v *Publikaci IV* konstatováno, že analytickým řešením zobecněného modelu NLTEM je pro počáteční podmínku ve tvaru Diracovy delta funkce opět HVL funkce, zatímco pro počáteční podmínku ve tvaru obdélníkové zóny (s konečnou šířkou) je řešením HVLR funkce.

Ačkoli na úrovni matic $\mathbb{M}$ a $\mathbb{D}$ je rozšířený model NLTEM totožný se starším modelem NLTEM, ve vnitřní struktuře těchto matic panují mezi oběma modely značné

rozdíly. Z tohoto důvodu bylo nutné přistoupit ke zcela novému způsobu implementace rozšířeného modelu NLTEM do softwarového kódu. Nový software s implementovaným rozšířeným modelem NLTEM byl s odkazem na software založený na starším modelu NLTEM nazván PeakMaster 6. Část *Publikace IV* týkající se implementace NLTEM do softwarového kódu je ovšem mimo rozsah předkládané disertační práce.

Pro ověření správnosti rozšířeného modelu NLTEM a správnosti jeho následné implementace do softwarového kódu bylo provedeno porovnání elektroferogramů předpovězených softwarem PeakMaster 6 pro modelový elektroforetický systém a simulací, tj. numerického řešení rovnic kontinuity (5), téhož elektroforetického systému v programu Simul 5 [27] (*Publikace IV*, Figure 3). V modelovém elektroforetickém systému tvořilo komplexační činidlo komplex jak s analytem, tak s jednou složkou BGE. Podrobný popis složení modelového elektroforetického systému je uvedeno v *Publikaci IV*, Table 1. Byla pozorována velmi dobrá shoda mezi elektroferogramy předpovězenými softwarem PeakMaster 6 a simulacemi.

Publikace IV

Generalized model of the linear theory of electromigration and its application to electrokinetic chromatography: Theory and software PeakMaster 6 – Next Generation

Michal Malý, Magda Dovhunová, **Martin Dvořák**, Gabriel S. Gerlero, Pablo A. Kler, Vlastimil Hruška, Pavel Dubský

Electrophoresis 2019, *40*, 683 – 692

Michal Malý[1]
Magda Dovhunová[1]
Martin Dvořák[1]
Gabriel S. Gerlero[2]
Pablo A. Kler[2,3]
Vlastimil Hruška[4]
Pavel Dubský[1]

[1]Faculty of Science, Department of Physical and Macromolecular Chemistry, Charles University in Prague, Prague, Czech Republic
[2]Centro de Investigación de Métodos Computacionales (CIMEC, UNL-CONICET), Santa Fe, Argentina
[3]Departamento de Ingeniería en Sistemas de Información, FRSF-UTN, Santa Fe, Argentina
[4]Liquid Phase Separations Division, Agilent Technologies Deutschland GmbH & Co. KG, Waldbronn, Germany

Received September 22, 2018
Revised December 4, 2018
Accepted December 5, 2018

Research Article

Generalized model of the linear theory of electromigration and its application to electrokinetic chromatography: Theory and software PeakMaster 6—Next Generation

The linear theory of electromigration, including the first-order nonlinear approximation, is generalized to systems with any equilibria fast enough to be considered instantaneous in comparison with the timescale of peak movement. For example, this theory is practically applied in the electrokinetic chromatography (EKC) mode of the CZE. The model enables the calculation of positions and shapes of analyte and system peaks without restricting the number of selectors, the complexation stoichiometry, or simultaneous acid–base equilibria. The latest version of our PeakMaster software, PeakMaster 6—Next Generation, implements the theory in a user-friendly way. It is a free and open-source software that performs all calculations and shows the properties of the background electrolyte and the expected electropherogram within a few seconds. In this paper, we mathematically derive the model, discuss its applicability to EKC systems, and introduce the PeakMaster 6 software.

Keywords:
Capillary zone electrophoresis / Electrokinetic chromatography / Linear theory of electromigration / PeakMaster

DOI 10.1002/elps.201800400

Additional supporting information may be found online in the Supporting Information section at the end of the article.

1 Introduction

Continuity laws, which describe the motion of charged particles under electric field effects in a one-dimensional channel, are not particularly difficult to formulate. The basic set of continuity equations was introduced by Kohlrausch [1], in 1897. Kohlrausch discovered the existence of specific conservation laws that may apply in electrophoretic systems [2]. Unfortunately, these laws have a limited scope of applicability and cannot be used to describe the behavior of an arbitrary electromigration system. The complete set of electromigration continuity equations is inherently nonlinear and must be numerically solved because no analytical closed form of the equations is known. Various computer implementations of numerical solvers of electromigration continuity laws have been developed since 1980s. Currently, advanced simulators such as Simul 5 [3], GENTRANS [4], and SPRESSO [5] are capable of solving 1D CE equations.

Finding an approximate solution to the continuity equations, valid under restrictions applicable to a given electromigration system, is an alternative to performing computer simulations. When available, an approximate solution provides the advantage of fast computation and often enables drawing more general conclusions about the given mode of electrophoresis. As first suggested by Poppe [6, 7], electromigration continuity equations can be linearized, and the solution leads to a matrix eigenvalue problem in CZE experimental setups. Using this approach, Štědrý et al. [8–10] later developed the linear theory of electromigration (LTEM). Štědrý et al. introduced the term *eigenmobility*, which is a number obtained as an eigenvalue of a mobility matrix. *Eigenmobility* means the true electromigration mobility of an

Correspondence: Dr. Pavel Dubský, Faculty of Science, Department of Physical and Macromolecular Chemistry, Charles University in Prague, Faculty of Science, Albertov 6, CZ-128 43 Prague 2, Czech Republic
E-mail: pavel.dubsky@natur.cuni.cz

Abbreviations: **EKC**, electrokinetic chromatography; **EMD**, electromigration dispersion; **HVL**, Haarhoff–van der Linde; **IS**, ionic strength; **LTEM**, linear theory of electromigration; **NLTEM**, first-order nonlinear theory of electromigration; **PDE**, partial differential equation; **PM6**, PeakMaster 6—Next Generation software; **R-FLU**, R-Flurbiprofen

Color online: See the article online to view Figs. 1–3 in color.

© 2018 WILEY-VCH Verlag GmbH & Co. KGaA, Weinheim

analyte or a system peak detectable in a CZE experiment. The model was able to predict the positions of all peaks in a CZE system containing an arbitrary number of analytes and a BGE consisting of any number of electrolytes. All constituents in a system could be general ampholytes. The model was implemented in PeakMaster 5 [11] software.

The linearized model provides previously unavailable insight into the behavior of CZE systems and can be fully resolved in a matter of seconds on an ordinary PC. Hruška et al. [12] later expanded the original model by including first nonlinear term in the linearized equation, herein referred to as the first-order nonlinear theory of electromigration (NLTEM) model. This enabled the model to predict not only the positions of all peaks but also their shapes. Although the practice of fitting distorted peaks by electromigration dispersion (EMD) with the Haarhoff–van der Linde (HVL) function [13, 14] was already recommended [15], the NLTEM model provided mathematical bases for such an approach. In addition, this practice demonstrated the time dependence of the fitted parameters that should be considered when analyzing peaks naturally detected in the time domain. The HVL function is a solution for an initial condition of an infinitely narrow injection plug. The function therein referred to as a HVLR function was shown to be the solution for a rectangular pulse initial condition. This model was included in PeakMaster 5.3.

Analytical demands of high-performance separations have led to the development of CZE techniques that achieve or improve separation through interactions between an analyte and an agent present in the background buffer. In electrokinetic chromatography (EKC) setups, the agent, usually referred to as the *selector*, forms a complex with the analyte, altering its electromigration properties. The equation used to calculate the expected change in analyte mobility as a function of its affinity to the selector and of the selector concentration was first proposed by Wren and Rowe [16]. The original Wren–Rowe equation was expanded by Rawjee, Williams, and Vigh [17] and Lelièvre and Gareil [18] to account for weak monovalent analytes and later by Dubský et al. [19, 20] to account for a mixture of selectors competing with each other for an analyte. All these models assume 1:1 stoichiometry and overlook possible interferences caused by interactions between a selector and other BGE constituents.

In terms of computer simulations, both GENTRANS [4] and Simul 5 [21] have been updated to simulate systems with one selector interacting with an arbitrary number of other constituents in a 1:1 stoichiometric ratio. All complexing components can be general ampholytes or neutral compounds. The complex-forming equilibria, nevertheless, also demands longer computational times for simulations. A limited complex-forming equilibrium model was also implemented in PeakMaster 5.3 Complex [22]. The model can handle a single selector that exclusively interacts with an analyte in a 1:1 ratio. Interactions between the selector and other BGE constituents are not allowed. Another constraint is that both analyte and selector can only be either neutral or fully charged species. In spite of these limitations, the model demonstrated for the first time that interactions between an analyte and a selector can have additional EMD-like effects on the analyte [23], and PeakMaster 5.3 Complex software can predict the extent of this dispersion.

The primary aim of this paper is to develop a comprehensive NLTEM model that describes complexation equilibria along with acid–base equilibria in CZE and EKC. In order to complete the theory, we further generalize the NLTEM model by formulating it in terms of any equilibria in which chemical species in solution decay or assemble to various forms with rates fast enough to consider that the equilibrium state is instantaneously achieved in comparison to the timescale of peak movement [23]. Generalized NLTEM is described in the first part of the paper, whereas PeakMaster 6—Next Generation software (PM6) is introduced in the second part of this paper.

The numerical implementation of the new model requires adopting a strategy different from that used in previous versions of PeakMaster in many aspects. This has led us to completely reimplementing the computational core and to developing an entirely new version of the PeakMaster software. PM6 is inevitably limited to a subset of the virtually unlimited number of chemical systems covered by the generalized NLTEM model. Nevertheless, our new model can handle all practically relevant systems of complex-forming equilibria with a 1:L stoichiometry in EKC, without restricting the number of selectors, wherein all BGE and analyte constituents can be general ampholytes, and any selector can interact with any number of analytes or other BGE constituents. Therefore, our new model makes it possible to characterize analyte and system peaks in a wide range of common EKC systems for the first time.

2 Theory

The original LTEM was built entirely around acid–base equilibria. In that case, the mutual relationships between partial differential equations (PDEs) that describe mass transport of every individual constituent in the system can be traced down to a single independent variable of the concentration of hydroxonium ions. This significantly simplifies the way in which (N)LTEM is formulated. The simplicity cannot be maintained in EKC where other equilibria can affect the system besides the acid–base ones. Addition of a neutral selector and the influence it has on analyte peak mobility and concentration distribution (peak shape) as revealed by PeakMaster 5.3 Complex calculations [22] is a particular example of an EKC system where complexation-related effects act independently of the acid–base-related effects.

On the other hand, when a single neutral/ fully charged selector interacts with a fully charged/neutral analyte (and no BGE constituents) in EKC—as previously implemented in the "5.3 Complex" version of PeakMaster—system peaks remain unaffected (up to a presence of the fully charged selector as a noninteracting species, if applicable), and the chemical equilibrium between the analyte and the selector

© 2018 WILEY-VCH Verlag GmbH & Co. KGaA, Weinheim

can be easily solved. Hence, an extension of the classical (N)LTEM model to such systems required only redefining a few analyte peak parameters [21]. The implementation of a more advanced complex-forming model was deemed complicated [21] due to the need for a new formulation of the theory and to the technical nature of the equilibrium solver used by the software at that time. Therefore, the implementation of the whole NLTEM model had to be changed to receive the general complex-forming equilibria solver.

2.1 Continuity equations

A one-dimensional model of electromigration consists of N continuity equations in which N is the number of chemical constituents of the system. Constituents can be general ampholytes or strictly neutral species, any of which can be present in various forms. The perception of forms is intuitive in simple CZE systems, as covered by the original theory, wherein every form belongs to exactly one constituent, such as the four (including neutral) forms of phosphoric acid, which belong to the phosphoric acid constituent. The only exceptions are water ions, H_3O^+ and OH^-, which are treated separately. The simple assignment of forms and constituents is lost when other equilibria compete with acid–base equilibria. For example, if both forms of a monovalent weak acid (A^- and HA) form complexes with a neutral selector S, all possible forms, SA^-, SAH, A^-, and AH, belong to the acid constituent, while the two forms, SA^- and SAH, simultaneously belong to the selector constituent.

Thus, a set (Ω) of all forms present in the system must be defined, regardless of constituent to which they belong. Additionally, the set (Ω) must now also include the water ions, herein referred to as H and OH. In contrast to simple CZE systems, a constituent may appear more than once in a single form; for example, the constituent S appears two times in a hypothetical complex form S_2A. We signify this with a coefficient $\nu_{(g)i}$, wherein the subscript (g) refers to the form g and the subscript i refers to the i-th constituent. If, for example, the selector, S, and the analyte, A, constituents are referred to with indexes $i = \{1;2\}$, respectively, then $\nu_{(S_2A)1} = 2$ and $\nu_{(S_2A)2} = 1$. Thus the coefficient $\nu_{(g)i}$ is equivalent to the stoichiometric coefficient of the i-th constituent in the form g, although its definition is extended for the purpose of this theory so that

$$\nu_{(g)i} = 0\text{, if the form } g \text{ does not belong to the } i\text{-}th \text{ constituent.} \quad (1)$$

For example, $\nu_{(S_2A)3} = 0$, provided that we add a third constituent to the aforementioned example system. The relationships between the constituents and their forms can be thus generally expressed by the mass balance relation

$$c_i = \sum_{g\in\Omega} \nu_{(g)i} c_{(g)}\ , \quad (2)$$

where c_i stands for the net (analytical) concentration of the i-th constituent, $c_{(g)}$ stands for the concentration of the form g, and the summation includes the entire set of forms, Ω. Importantly, the forms that do not belong to the i-th constituent are inevitably excluded from the summation due to Eq. (1), which is a principle that applies to various equations throughout this article.

A concise introduction to continuity equations describing the mass conservation in electrophoresis can be found in the original paper on NLTEM [12]. The spatiotemporal development of concentration profile of each constituent, $c_i \equiv c_i(x,t)$, is given by

$$\frac{\partial c_i}{\partial t} = -\frac{\partial J_i}{\partial x} = -\sum_{g\in\Omega} \nu_{(g)i} \frac{\partial J_{(g)}}{\partial x}, \quad (3)$$

where $J_i \equiv J_i(x,t)$ is the mass flux[1] of the i-th constituent consisting of the mass fluxes, $J_{(g)}$, of the individual forms g that belong to this constituent in accordance with Eq. (2). Every mass flux is decomposed into three components,

$$J_{(g)} = J_{(g)em} + J_{(g)D} + J_{(g)emdiff}, \quad (4)$$

the electromigration component, the diffusion component, and the diffusion-potential-related component, respectively. It should be noted that the last component is somewhat artificial because it emerged from the electromigration flux by excluding a part that accounts for the diffusion potential (cf. [12]). A previous study [12] has demonstrated that merging the diffusion-potential-related term of the resulting continuity equation with the diffusion term is more advantageous than hiding it within the original electromigration term. Nevertheless, for the purposes of our discussion, we will continue differentiating all three contributors to the overall mass flux, according to Eq. (4).

The electromigration flux reads

$$J_{(g)em} = \frac{j}{\kappa} \mu_{(g)} c_{(g)}, \quad (5)$$

where j is the current density (cf. footnote 1), $\kappa \equiv \kappa(x,t)$ is the conductivity, and $\mu_{(g)} \equiv \mu_{(g)}(x,t)$ is the electrophoretic mobility of the form g. In contrast to the original theory [8–12], we do not work with electrophoretic mobility as a constant. We rather consider it a spatiotemporal variable because electrophoretic mobility depends on IS. We discuss this issue in more detail in Supporting Information. For mathematical convenience, we also switch from using unsigned mobilities, $u_{(g)}$, to using signed mobilities $\mu_{(g)} = sign(z_{(g)})u_{(g)}$, where $z_{(g)}$ is the charge of the form g. The diffusion flux is given by

$$J_{(g)D} = -D_{(g)} \frac{\partial c_{(g)}}{\partial x}, \quad (6)$$

where $D_{(g)}$ is the diffusion coefficient of the form g, which is considered constant (i.e., independent of IS, cf. Supporting information) herein. Finally,

$$J_{(g)emdiff} = \frac{j_{diff}}{\kappa} \mu_{(g)} c_{(g)}, \quad (7)$$

[1]Technically, mass flux, as shown in Eq. (2), is a signed quantity numerically equal to the only component of the one-dimensional vector $\vec{J}_i$.

© 2018 WILEY-VCH Verlag GmbH & Co. KGaA, Weinheim

where $j_{diff} \equiv j_{diff}(x, t)$ is the diffusion current density. The conductivity and the diffusion current density equal

$$\kappa = F \sum_{f \in \Omega} z_{(f)} c_{(f)} \mu_{(f)}, \tag{8}$$

where F is the Faraday constant, and

$$j_{diff} = -F \sum_{f \in \Omega} z_{(f)} D_{(f)} \frac{\partial c_{(f)}}{\partial x}. \tag{9}$$

2.2 Generalization of the linear theory of electromigration beyond the acid–base equilibria

Eq. (3) and Eqs. (4)–(9) form a set of N vastly interrelated nonlinear partial differential equations for N constituents. LTEM aims to decoupling the set of PDEs. This is primarily achieved by focusing on the migration flux only and by expressing the resulting PDEs in a matrix form of

$$\left(\frac{\partial \vec{\mathbf{C}}}{\partial t}\right)_{em} = -\frac{j}{\kappa_{BGE}} \mathbf{M} \times \frac{\partial \vec{\mathbf{C}}}{\partial x}, \tag{10}$$

where $\vec{\mathbf{C}} \equiv (c_1, \ldots, c_N)^T$ is a column vector of the concentrations of all constituents, κ_{BGE} is the conductivity of the BGE, and $\mathbf{M} \equiv \mathbf{M}(\vec{\mathbf{C}}(x, t))$ is the target matrix.

The elements of the matrix $\mathbf{M}$ were evaluated by Štědrý et al. for strong [8], weak univalent [9], and multivalent [10] electrolytes. Nevertheless, these derivations were always specialized to the inspected case of weak electrolytes, and no derivation concerned complex-forming equilibria in CZE. The general structure of the matrices is also unclear in the original papers. Using the generalized form of the continuity equations (cf. Section 2.1) allows us to reformulate LTEM to cover electrophoretic systems comprising any chemical equilibrium so that equilibrium reactions are fast enough to instantaneously reach equilibrium. In practical terms, the time scale of every reaction is negligible in comparison with that of the separation process (notice that the latter is measured as the time needed for a peak to travel the peak width, and not as the time of the entire separation [24]). Therefore, at any time and position in the capillary, the concentration of every form can be expressed as an algebraic function of concentrations of all constituents

$$f \in \Omega: \; c_{(f)} \equiv c_{(f)}(c_1, \ldots, c_N). \tag{11}$$

Because $J_{i,em}$ is a function of only concentrations of individual forms, which in turn are functions of concentrations of constituents, Eq. (11), we can easily assume, based on Eq. (10), that the elements of the matrix, $\mathbf{M}$, become

$$\mathbf{M}: m(i, q) = \left(\frac{\kappa_{BGE}}{j} \frac{\partial J_{i,em}}{\partial c_q}\right). \tag{12}$$

We provide a more detailed analysis in Supporting Information in which we further show that Eq. (12) leads to the matrix $\mathbf{M}$ decomposition into two matrices $\mathbf{M}_{\boldsymbol{\mu}}$ and $\mathbf{M}_{\partial}$,

$$\mathbf{M} = \mathbf{M}_{\boldsymbol{\mu}} \times \mathbf{M}_{\partial}. \tag{13}$$

The first matrix

$$\mathbf{M}_{\boldsymbol{\mu}}: \; m_{\mu}(i, h) = \frac{\kappa_{BGE}}{\kappa} \left(\nu_{(h)i} \mu_{(h)} - \frac{F}{\kappa} \sum_{g \in \Omega} \nu_{(g)i} \mu_{(g)} c_{(g)} r_{(g)(h)}\right) \tag{14}$$

$$r_{(g)(h)} = \left(z_{(h)} \mu_{(h)} - \frac{\kappa}{F} \frac{\partial \ln \mu_{(g)}}{\partial c_{(h)}} + \sum_{f \in \Omega} z_{(f)} c_{(f)} \frac{\partial \mu_{(f)}}{\partial c_{(h)}}\right)$$

has an $N \times |\Omega|$ size, its elements have a dimension of electrophoretic mobility, and its i-th row can be regarded as referring to the i-th constituent, whereas its h-th column can be regarded as referring to the h-th form in the separation system. For this purpose, the set Ω is presumed arbitrarily, albeit uniquely, ordered, and we use the symbol h to express either the form h or its index in set Ω. Importantly, every i-th row of the matrix contains columns for all forms (h), even if that form does not belong to the i-th constituent, in which case $\nu_{(h)i} = 0$, in accordance with Eq. (1). Additionally, the matrix contains two special columns for the water ion "forms," which do not belong to any constituent, that is, $\nu_{(H)i} = 0$, $\nu_{(OH)i} = 0$ for every i.

The second matrix

$$\mathbf{M}_{\partial}: \; m_{\partial}(h, q) = \frac{\partial c_{(h)}}{\partial c_q} \tag{15}$$

has a size $|\Omega| \times N$ and its elements are dimensionless. We call it the "communication matrix" because it describes how constituents communicate with each other through the various equilibria present in the system. The communication matrix can be viewed as the central point in the linearization procedure because it reflects interconnections between individual mass conservation equations, Eq. (3), and thus is prerequisite for extracting the matrix, $\mathbf{M}$, Eq. (10), from the coupled set of PDEs. Simultaneously, the communication matrix could not be extracted from the coupled set of PDEs if Eq. (11) did not apply to every form $f \in \Omega$. Accordingly, the need for formulating the communication matrix limits the generalized LTEM model to infinitely fast equilibria.

The communication matrix converts the constituent concentration vector, $\vec{\mathbf{C}}$, into a vector of form concentrations, $(c_{(1)}, \ldots, c_{(|\Omega|)})^T = \mathbf{M}_{\partial} \times \vec{\mathbf{C}}$. Thus, the communication matrix is equivalent to the matrix $\mathbf{M}_2$ introduced for weak monovalent electrolytes in the appendix of [9] and further used in [10] for general ampholytes. Consequently, the matrix $\mathbf{M}_{\boldsymbol{\mu}}$ is equivalent to that therein referred to as the matrix $\mathbf{M}_1$. Nevertheless, matrices $\mathbf{M}_{\boldsymbol{\mu}}$ and $\mathbf{M}_{\partial}$ are not expressed identically to matrices $\mathbf{M}_1$ and $\mathbf{M}_2$, respectively, and the latter pair of matrices cannot be straightforwardly applied to complex-forming or similar equilibria.

Matrices $\mathbf{M}_{\boldsymbol{\mu}}$ and $\mathbf{M}_{\partial}$, as prescribed by Eqs. (14) and (15), respectively, enable us to express the LTEM matrix, $\mathbf{M}$, for systems with arbitrary fast equilibria. The diagonalization procedure and the introduction of the first-order nonlinear term, and thus the formulation of NLTEM for such systems, are identical to a previously published procedure [8–10, 12]. We refer the reader to Supporting Information for a complete theory, including several essential technical details that may not be clear in the original papers. Our second paper published in this special issue [25] provides a concise

© 2018 WILEY-VCH Verlag GmbH & Co. KGaA, Weinheim

summary of (N)LTEM (yet in simple CZE systems only). In short, the mathematical analysis reveals that BGE forms an environment in which N independent wave functions, $\tilde{w}_i$, tend to propagate with velocities $(\frac{j}{\kappa_{BGE}}\lambda_i)$. λ_i are eigenvalues of a matrix $\mathbf{M}_0 = \mathbf{M}(\vec{\mathbf{C}}_{\mathrm{BGE}})$ evaluated at the composition of BGE. It should be noted that the vector $\vec{\mathbf{C}}_{\mathrm{BGE}}$ also contains analyte constituents, whose concentration is set to zero therein. Wave functions represent system peaks and analyte peaks, whose position can be easily obtained from the velocities. The chemical composition of the peaks can also be calculated from LTEM [26]. Peak concentration distributions are approximated through NLTEM as the HVL or HVLR function [12].

NLTEM requires expressing a few additional terms that we provide below for consistency purposes. The key step in NLTEM is the Taylor expansion of matrix $\mathbf{M}$. Taylor expansion approximates the matrix in a specific region, $\vec{\mathbf{C}}_{\mathrm{BGE}} + \vec{\tilde{c}}$, wherein $\vec{\tilde{c}}$ is a sufficiently small disturbance in the otherwise homogeneous distribution of the BGE. In the frame of NLTEM, the matrix $\mathbf{M}_0$ is understood as a zero-order Taylor term of the expansion of the matrix $\mathbf{M}$, and the first-order term is added to the electromigration expression as

$$\left(\frac{\partial \vec{\mathbf{C}}}{\partial t}\right)_{em} \cong -\frac{j}{\kappa_{BGE}}\left(\mathbf{M}_0 + \sum_{k=1}^{N}\mathbf{M}_{1,k}\tilde{c}_k\right) \times \frac{\partial \vec{\mathbf{C}}}{\partial x}, \tag{16}$$

where

$$\mathbf{M}_{1,k} = \frac{\partial \mathbf{M}}{\partial c_k}\left(\vec{\mathbf{C}}_{BGE}\right) \tag{17}$$

Solving Eq. (16) requires additionally extending it with the diffusion term

$$\frac{\partial \vec{\mathbf{C}}}{\partial t} \cong -\frac{j}{\kappa_{BGE}}\left(\mathbf{M}_0 + \sum_{k=1}^{N}\mathbf{M}_{1,k}\tilde{c}_k\right) \times \frac{\partial \vec{\mathbf{C}}}{\partial x} + \mathbf{D}\frac{\partial^2 \vec{\mathbf{C}}}{\partial x^2}, \tag{18}$$

where $\frac{\partial^2 \vec{\mathbf{C}}}{\partial x^2} = (\frac{\partial^2 c_1}{\partial x^2}, \ldots, \frac{\partial^2 c_N}{\partial x^2})^T$, and $\mathbf{D}$ is the constant matrix to be approximated from the diffusion and from the diffusion-potential-related fluxes, which originate from Eq. (3). When generalized to the fast equilibria, the diffusion matrix results in a form that differs from that formulated in simple CZE systems, namely by the $\nu_{(g)i}$ coefficients (cf. Supporting Information)

$$\mathbf{D} = \mathbf{D}_d \times \mathbf{M}_\partial, \tag{19}$$

where

$$\mathbf{D}_d : d_d\ (i,h) = \left(\nu_{(h)i}\, D_{(h)} - \frac{F z_{(h)}\, D_{(h)}}{\kappa}\sum_{g\in\Omega}\nu_{(g)i}\,\mu_{(g)}c_{(g)}\right) \tag{20}$$

and $\mathbf{M}_\partial$ is the communication matrix given by Eq. (15). Finally, the matrix $\mathbf{D}$ is evaluated at the composition of BGE, $\mathbf{D} \equiv \mathbf{D}(\vec{\mathbf{C}}_{\mathrm{BGE}})$.

LTEM transforms the original set of coupled electromigration-term PDEs in the concentration domain, Eq. (5), into a fully equivalent set of decoupled PDEs in the domain of the wave functions, $\tilde{w}$. In contrast, NLTEM requires discarding some higher-order nonlinear terms when deriving Eq. (19). Moreover, the diagonalization procedure is incomplete when applied to the first-order Taylor expansion term and to the diffusion term. Thus, for diagonalization purposes, the effects of propagating waves on each other are disregarded. This assumption—termed the assumption of an immediate separation of zones [12]—is equivalent to discarding the off-diagonal elements of the two "diagonalized" matrices that originate from NLTEM. All approximations adopted within NLTEM are elaborated to detail in Supporting Information.

This suggests that the HVL and HVLR distributions can represent the exact solution to the set of PDEs, Eq. (3), only to a limited extent. Nevertheless, NLTEM has thus far proved to be in a very good agreement with both experimental data and numerical solutions to the factual set of equations (Eq. (3)) [22, 27], and—in contrast to full numerical solutions—it provides results straightforwardly. When a more exact solution of the peak shape is required, the disturbances $\tilde{c}_i$ are too large to satisfy the Taylor expansion limits, or the assumption of the immediate separation of waves (i.e., analyte or system peaks) is far from reality, the full numerical solution, for example, by means of Simul [20], has to be used.

3 Results and discussion

Despite the strong formal similarities between the old and the new formulations of the NLTEM model, the evaluation of the new model requires adopting a strategy significantly different from that used in the case of simple CZE systems. The original PeakMaster was written as a monolithic piece of code, which allowed the rapid development and quick addition of new features. However, such design made it difficult to introduce changes at a more fundamental level. PM6 involves a completely new implementation of NLTEM, which now includes general complex-forming equilibria. The code has been split into modules to facilitate code reuse and long-term maintainability. The entire code base is now built on top of free and open source tools and is available to the scientific community from https://github.com/echmet/PeakMasterNG (https://doi.org/10.5281/zenodo.1461507).

3.1 Computation engine

The inclusion of complex-forming equilibria in the model requires a different approach to calculating the equilibrium composition of a solution. In the former version of PeakMaster, the concentration of the hydroxonium ions, $c_{(H)}$, was first evaluated as the only positive root of the *G-polynomial* [10]. Consequently, the individual concentrations of all other ionic forms at a given pH of the system can be easily calculated when considering only acid–base equilibria. However, the *G-polynomial* can no longer be used because the equilibrium is now a function of more than one variable. Our new equilibrium solver instead constructs a system of equations in which each equation represents an individual equilibrium.

© 2018 WILEY-VCH Verlag GmbH & Co. KGaA, Weinheim

The system is numerically solved using the Newton–Raphson method. To prevent the solver from reaching mathematically correct but physically meaningless solutions with negative concentrations, we transform all equations into their logarithmic forms.

However, this transition to a numerical solver has a considerable disadvantage: the loss of the ability to analytically express the concentration derivatives of equilibrium composition (cf. the communication matrix, Eq. (15), and the first-order Taylor term, Eq. (17)). This was a problem because the *double floating*-point precision (per IEEE754 naming) turned out to be insufficient to correctly and consistently calculate the concentration derivatives. Thus, we calculate these derivatives using an arbitrary-precision floating-point arithmetic provided by GNU GMP library [28] (https://gmplib.org/). Higher-level mathematical functions operating with arbitrary precision are supplied by GNU MPFR library [29] (https://www.mpfr.org) and MPReal C++ wrapper [Holoborodko, P., MPFR C++, 2008] (http://www.holoborodko.com/pavel/mpfr/). Matrix algebra is provided by Eigen library [Benoît J., Gaël G., et al., Eigen v3, 2010] (http://eigen.tuxfamily.org/). Although the use of arbitrary-precision arithmetic decreases performance, and even though all numeric derivatives must be done in software, the computation is still completed within a few seconds.

The equilibrium solver is implemented as a separate module within a package termed ECHMETCoreLibs (https://github.com/echmet/ECHMETCoreLibs). The ECHMETCoreLibs package is a more general set of libraries for calculating the properties of chemical solutions with no particular focus on CZE. IS correction can be applied to the equilibrium composition through an iterative calculation. The NTLEM itself is implemented in another module termed LEMNG (https://github.com/echmet/LEMNG, https://doi.org/10.5281/zenodo.1461522). The LEMNG module uses ECHMETCoreLibs to create an internal description of a chemical system, to solve its equilibrium composition, and then it calculates the true ionic mobilities applying Onsager–Fuoss [30] IS correction. These data are used to generate the respective NTLEM matrices and to calculate the electrophoretic properties of the system, as described in the Section 2.

3.2 Complexation mode

The most prominent improvement in PM6 over its predecessors is the inclusion of a very general complex-forming model. However, some design compromises had to be made because developing a completely general complex-forming model is a daunting task, in terms of computer implementation. The logic of the complex-forming model implemented in ECHMETCoreLibs is based on a "nucleus-ligand" scheme designed with the specifics of EKC experimental setups in mind.

In this scheme, the tree of complex forms is built around ionic forms of nuclei, which can bind an arbitrary amount of ionic forms of any ligands. The rationale of this scheme is shown in Fig. 1. The allowed stoichiometry of complex-forming relationships between nucleus and "ligand" ionic forms is 1:L in which L is an arbitrary natural number. In other words, a specific complex form may contain only one ionic form of a nucleus and an arbitrary number of ligand ionic forms of multiple ligands. Relationships between two ionic forms of a nucleus or ligand type are not allowed. We illustrate how these rules work in practice in a few other examples given in Supporting Information.

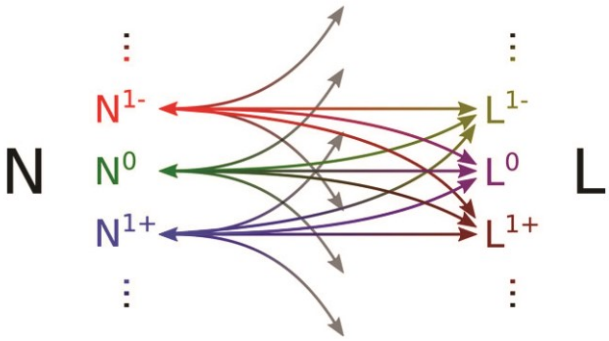


Figure 1. Schematic depiction of interactions allowed within ECHMETCoreLibs nucleus-ligand scheme.

The nucleus-ligand scheme allows the formation of mixed complexes with multiple ligand ionic forms simultaneously bound to a single nucleus. EKC experimental setups typically do not involve these complexes. Instead, selectors compete for analytes or BGE constituents and exclusively bind to them. To simplify the user interface, PM6 currently prevents users from entering systems in which mixed complexes would occur.

3.3 PeakMaster 6 software

The basic layout of the UI remained similar to that of Peakmaster 5. The most notable changes include the possibility to enter the exact composition of BGE and sample solutions directly from the main window, the simplification of the chart (shapes of system peaks are directly displayed in the main window), and the rearrangement of some control elements.

Limiting ionic mobilities and dissociation constants are available in a database based on Hirokawa's data [31–35]. There is no database available for complexation parameters—the number of possible interactions is exceedingly high, and the complexation parameters are often measured for specific conditions only. However, user can save the composition of their system, including the entered complexation parameters.

PeakMaster 6 offers several corrections for nonideal ionic behavior in solution, including corrections for IS, specifically the Onsager–Fuoss and Debye–Hückel model [36]. Both of these are enabled by default. In addition, correction for viscosity can be enabled [23]. Importantly, the applicability of any of these corrections may be compromised in systems containing bulky and/or highly charged selectors, especially

© 2018 WILEY-VCH Verlag GmbH & Co. KGaA, Weinheim

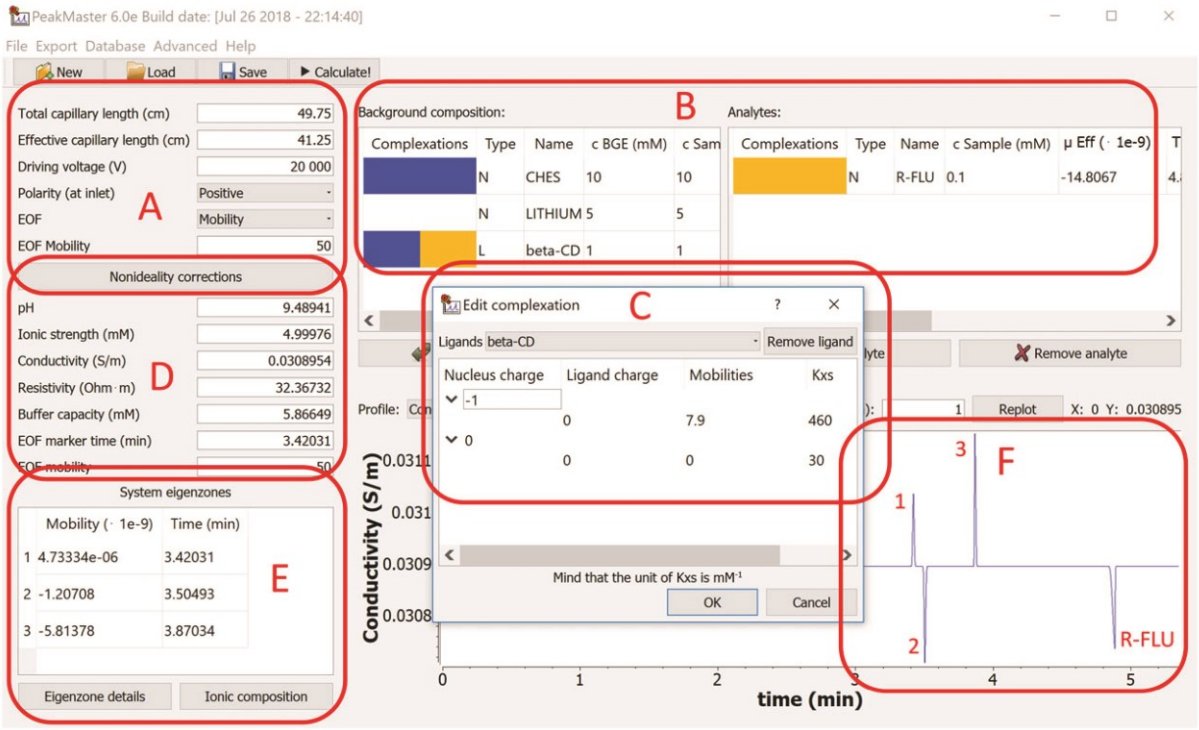


Figure 2. Screenshot of the PM 6 software. Model system described in Table 1. See text for detailed description of regions (A) to (F).

Table 1. Model system composition and characteristics

Composition	BGE	Sample
CHES concentration (mM)	10	10
Lithium concentration (mM)	5	5
β-CD concentration (mM)	1	1
R-FLU concentration (mM)	0.00	0.1
Electrophoretic properties (charge)	Mobility/ 10^{-9} m^2 s^{-1} V^{-1}	pK_a
CHES (–1)	25	9.55
Lithium (+1)	40.1	13.8
R-FLU (–1)	22.23	4.19
Complexes with β-CD	Mobility/ 10^{-9} m^2 s^{-1} V^{-1}	Complexation constant
CHES (–1)	7.9	460
CHES (0)	0	30
R-FLU (–1)	10.14	5 000
R-FLU (0)	0	10 000[a)]

a) The complexation constant of R-FLU(0)/β-CD complex was set to an arbitrary number. The true value does not matter because R-FLU exists almost exclusively in the (–1) acid–base form at the pH of 9.5.

at high selector concentrations. Such selectors (typically cyclodextrins) are quite common in EKC applications, although the relevant theory that would allow for exact IS or viscosity effects corrections has not been formulated yet [23].

Figure 2 shows the PM6 user interface. The model system specified in Table 1 is inspected. The mobilities and dissociation constants of CHES and Lithium were taken from the PM6 database, and those of R-Flurbiprofen (R-FLU) and the complexation parameters for R-FLU/β-CD complex and CHES/β-CD complex were taken from our previous study [37, 38]. System parameters are entered into region A and chemical composition into region B. Color coding in region B indicates constituents that form complexes. In our case, β-CD is considered the "ligand" that forms a complex with the R-FLU "nucleus" (orange) and another complex with the CHES "nucleus" (blue). The complexation parameters are specified in the complexation dialog, in region C. We show the complexation dialog for the CHES/β-CD complex (cf. Table 1). The dissociation constants of the complex forms require no specification [39]. After the calculation, basic characteristics of the analyte zone are further displayed in region B, and physical–chemical properties of BGE can be found in region D. Region E shows the emerging system peaks and their (eigen)mobilities, whereas a detailed description of zones and equilibria is provided in separate dialogs. Lastly, the predicted electropherogram is displayed in region F. We added numbers matching the system eignezones table (region E) and the name of the analyte to the peaks in the electropherogram.

The same model system from Table 1 was also simulated using Simul [20] (a developer version that numerically solves the full set of continuity equations, cf. Section 2.1, and utilizes the ECHMETCoreLibs for calculations of chemical equilibria at every simulation step). Figure 3 compares the calculated and simulated results without (A) and with (B) complexation between β-CD and the other constituents (CHES and R-FLU) applied. β-CD is present in BGE in both cases but is not set to form any complex in (A). Predicted

© 2018 WILEY-VCH Verlag GmbH & Co. KGaA, Weinheim

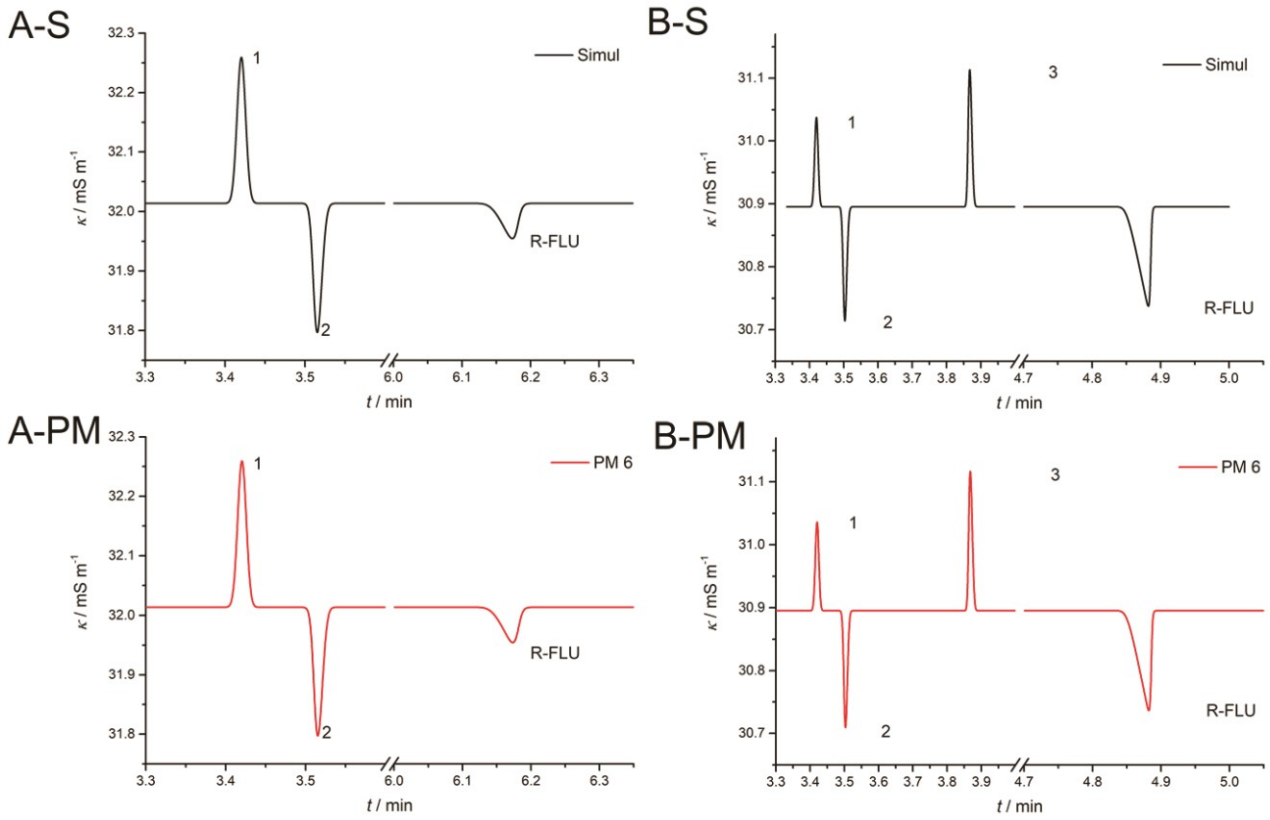


Figure 3. Electropherograms predicted by PM 6 (A-PM and B-PM) and by Simul (A-S and B-S) for the model system described in Table 1. (A-PM and A-S) Complexation between β-CD and CHES and β-CD and R-FLU is temporarily switched off. (B-PM and B-S) Complexation between β-CD and CHES and β-CD and R-FLU is switched on. Time axis is split for betted visibility of the peak shapes. Evaluation of the electropherogram is provided in Table 2.

electropherograms were evaluated using our software CEval [40] (https://echmet.natur.cuni.cz/software/download#ceval) and their numerical characteristics are given in Table 2.

Because β-CD is a neutral compound, the results (A) are equivalent to those observed in the previous versions of PeakMaster in simple CHES/Lithium buffer. Without the complexation, only two system peaks are apparently present, whereas three system peaks are actually present (as expected in systems with three BGE constituents), although two of them have exactly zero and almost zero mobilities (cf. Table 2) and thus coalesce. The system peak with exactly zero mobility arises due to the presence of the neutral noninteracting constituent (β-CD) in BGE. When the selector starts forming a complex with another BGE constituent (CHES), the system peak may become mobilized and visible (case (B)). Similarly, the effective mobility of the R-FLU analyte is altered by complexation with β-CD, as expected. As shown in Table 2 and Fig. 3, PM6 findings perfectly match the simulations. A detailed inspection of EKC systems using the generalized NLTEM and the verification of PM6 calculations will be reported in another paper (under preparation).

4 Concluding remarks

The generalized linear theory of electromigration was developed, including the first-order nonlinear approximation. The new theoretical model describes the behavior of electrophoretic systems with any equilibrium as long as the equilibrium reaction rates are fast enough to instantaneously reach the equilibrium state. The applicability of the model is shown, specifically in electrokinetic chromatography, which requires using complexing agents (selectors). Adding selectors to the system introduces additional complex equilibria that had not been implemented in the theory yet. Our model can describe the behavior of electrophoretical systems with any number of complexing agents, regardless of their charge or complexation stoichiometry. This model was implemented in the new generation of the PeakMaster software, which allows users to calculate the properties of electrophoretic systems and to predict the resulting electropherograms.

This work was supported by the Czech Science Foundation, under Grant No. 15–18424Y, by the Charles University Research Centre, under program No. UNCE/SCI/014, by the Charles

© 2018 WILEY-VCH Verlag GmbH & Co. KGaA, Weinheim

Table 2. BGE properties predicted by PM 6 for the model system specified in Table 1. Coding ((A-PM), (B-PM), (A-S), and (B-S)) corresponds to subparts of Figure 3

BGE characteristics (PM6)	Without complexation[c)]	With complexation[c)]
pH	9.54	9.49
Ionic Strength (mM)	5.00	5.00
Conductivity (mS/m)	32.0	30.9
Signed [a)] mobilities (PM6) (10^{-9} m^2 s^{-1} V^{-1})	Without complexation (A-PM)[c)]	With complexation (B-PM)[c)]
System peak 1	4.89×10^{-6}	4.73×10^{-6}
System peak 2	−1.38	−1.21
System peak 3	0.00	−5.81
Analyte peak R-FLU	−22.23	−14.81
Signed[a)] mobilities (Simul) (10^{-9} m^2 s^{-1} V^{-1})	Without complexation (A-S)[d)]	With complexation (B-S)[d)]
System peak 1	0.00	0.00
System peak 2	−1.38	−1.22
System peak 3	0.00	−5.83
Analyte peak R-FLU	−22.228	−14.77
Asymmetry[b)] (PM6)	Without complexation (A-PM)[d)]	With complexation (B-PM)[d)]
System peak 1	0.03	0.13
System peak 2	1.10	1.16
System peak 3	0.03	1.94
Analyte peak R-FLU	−5.30	−16.54
Asymmetry[b)] Simul	Without complexation (A-S)[d)]	With complexation (B-S)[d)]
System peak 1	0.01	−0.08
System peak 2	1.22	1.14
System peak 3	0.01	1.92
Analyte peak R-FLU	−5.13	−17.33

a) Positive/negative mobility corresponds to a movement of the peak toward the cathode/anode, respectively.
b) Measured as the a_{38} parameter of the HVL function [14].
c) PM6 output.
d) Evaluation of predicted electropherogram by means of CEval software [40].

University Grant Agency, through grants No. GA UK 726716 and No. GA UK 116217, Czech Republic, by the National Scientific and Technical Research Council (Agencia Nacional de Promoción Científica y Tecnológica – ANPCyT), through grant PICT-2016-0640, and by the National Technological University (Universidad Tecnológica Nacional – UTN), through grant PID ASUT-NFE0004475), Argentina.

The authors have declared no conflict of interest.

5 References

[1] Kohlraush, F., *Ann. Phys.* 1897, *62*, 209–239.

[2] Hruška, V., Gaš, B., *Electrophoresis* 2007, *28*, 3–14.

[3] Hruška, V., Jaroš, M., Gaš, B., *Electrophoresis* 2006, *27*, 984–991.

[4] Breadmore, M. C., Kwan, H. Y., Čáslavská, J., Thormann, W., *Electrophoresis* 2012, *33*, 958–969.

[5] Bercovici, M., Lele, S. K., Santiago, J. G., *J. Chromatogr. A* 2009, *1216*, 1008–1018.

[6] Poppe, H., *J. Chromatogr. A* 1990, *506*, 45–60.

[7] Poppe, H., *Anal. Chem.* 1992, *64*, 1908–1919.

[8] Štědrý, M., Jaroš, M., Gaš, B., *J. Chromatogr. A* 2002, *960*, 187–198.

[9] Štědrý, M., Jaroš, M., Včeláková, K., Gaš, B., *Electrophoresis* 2003, *24*, 536–547.

[10] Štědrý, M., Jaroš, M., Hruška, V., Gaš, B., *Electrophoresis* 2004, *25*, 3071–3079.

[11] Jaroš, M., Hruška, V., Štědrý, M., Zusková, I., Gaš, B., *Electrophoresis* 2004, *25*, 3080–3085.

[12] Hruška, V., Riesová, M., Gaš, B., *Electrophoresis* 2012, *33*, 923–930.

[13] Haarhoff, P. H., Van der Linde, H. J., *Anal. Chem.* 1966, *38*, 573–582.

[14] Dubský, P., Dvořák, M., Müllerová, L., Gaš, B., *Electrophoresis* 2015, *36*, 655–661.

[15] Erny G. L., Bergström, E. T., Goodall, D. M., *Anal. Chem.* 2001, *73*, 4862–4872.

[16] Wren, S. A. C., Rowe, R. C., *J. Chromatogr. A* 1992, *603*, 235–241.

[17] Rawjee, Y. Y., Williams, R. L., Vigh., G., *J. Chromatogr. A* 1993, *652*, 233–245.

[18] Lelièvre, F., Gareil, P., *Anal. Chem.* 1997, *69*, 385–392.

[19] Dubský, P., Svobodová, J., Gaš B., *J. Chromatogr. B* 2008, *875*, 30–34.

[20] Dubský, P., Müllerová, L., Dvořák, M., Gaš B., *J. Chromatogr. A* 2015, *1384*, 142–146.

[21] Hruška, V., Beneš, M., Svobodová, J., Zusková, I., Gaš, B., *Electrophoresis* 2012, *33*, 938–947.

[22] Hruška, V., Svobodová, J., Beneš, M., Gaš, B., *J. Chromatogr. A* 2012, *1267*, 102–108.

[23] Beneš, M., Svobodová, J., Hruška, V., Dvořák, M., Zusková, I., Gaš, B., *J. Chromatogr. A* 2012, *1267*, 109–115.

[24] Dubský P., Dvořák M., Ansorge M., *Anal. Bioanal. Chem.* 2016, *408*, 8623–8641.

[25] Dvořák, M., Dubský, P., Dovhunová, M., Gaš, B., *Electrophoresis*. https://doi.org/10.1002/elps.201800444

[26] Hruška, V., Štědrý, M., Včeláková, K., Lokajová, J., Tesařová, E., Jaroš, M, Gaš, B., *Electrophoresis* 2006, *27*, 4610–4617.

[27] Riesová, M., Hruška, V., Gaš, B., *Electrophoresis* 2012, *33*, 931–937.

[28] Granlund, T., GMP Development Team, GNU MP 6.0 Multiple Precision Arithmetic Library, Samurai Media Limited, Hong Kong 2015.

[29] Fousse, L., Guillaume, H., Lefévre, V., Pélissier, P, Zimmermann, P., *ACM Trans. Math. Softw.* 2007, *33*, 13.

[30] Onsager, L., Fuoss, R.M., *J. Phys. Chem.* 1932, *36*, 2689–2778.

[31] Hirokawa, T., Kiso, Y., *J. Chromatogr.* 1982, *248*, 341–362.

[32] Hirokawa, T., Nishimo, M., Aoki, N., Kiso, Y., Sawamoto, Y., Yagi, T., Akiyama, J., *J. Chromatogr.* 1983, *271*, D1–D106.

© 2018 WILEY-VCH Verlag GmbH & Co. KGaA, Weinheim

[33] Hirokawa, T., Gojo, T., Kiso, Y., *J. Chromatogr.* 1986, *369*, 59–81.

[34] Hirokawa, T., Gojo, T., Kiso, Y., *J. Chromatogr.* 1987, *390*, 201–223.

[35] Hirokawa T., Kiso Y., Gaš B., Zusková I., Vacík J., *J. Chromatogr.* 1993, *628*, 283–308.

[36] Bahga S. S., Bercovici M., Santiago J. G., *Electrophoresis* 2010, *31*, 910–919.

[37] Beneš M., Riesová M., Svobodová J., Tesařová E., Dubský P., Gaš B., *Anal. Chem.* 2013, *85*, 8526–8534.

[38] Riesová M., Svobodová J., Ušelová K., Tošner Z., Zusková I., Gaš B., *J. Chromatogr. A* 2014, *1364*, 276–288.

[39] Lelièvre F., Gareil P., Jardy A., *Anal. Chem.* 1997, *69*, 385–392.

[40] Dubský, P., Ördögová, M., Malý, M., Riesová M., *J. Chromatogr. A* 2016, *1445*, 158–165.

© 2018 WILEY-VCH Verlag GmbH & Co. KGaA, Weinheim

4.6 Nelineární model elektromigrace bez difúze a dynamika evoluce píků analytů v CZE: *Publikace V, VI*

Publikace V je věnována diskuzi teoretických modelů CZE, které jsou schopné popsat vývoj tvaru píků v průběhu CZE, a zejména pak deformaci píků v důsledku elektromigrační disperze. První polovina *Publikace V* je pojata jako přehled současného stavu poznání a jsou v ní představeny model pohybujícího se rozhraní (MBE), aproximativní nelineární teorie elektromigrace (NLTEM) a Mikkersův nelineární model elektromigrace bez difúze (NEM).

Druhá polovina *Publikace V* se zabývá hledáním souvislostí mezi modely NLTEM a NEM jakožto dvěma nejdůležitějšími nelineárními modely CZE. Bylo ukázáno, že základní rovnici modelu NEM (20) je možné odvodit s pomocí konceptu LTEM i bez použití KRF či jiného zákona zachování. Byl uvažován elektroforetický systém tvořený celkem N složkami, z nichž N_A složek jsou analyty, tj. jedná se o složky přítomné pouze v dávkovaném vzorku. Podle LTEM vznikne v kapiláře po aplikaci vnějšího elektrického pole celkem N píků, přičemž v N_A z těchto píků je přítomný některý z analytů.

Výchozím bodem odvození modelu NEM se stala soustava rovnic kontinuity (5). Na tomto místě je vhodné připomenout, že rovnice (5) byly sestaveny pouze z elektromigračních příspěvků k látkovým tokům, a tudíž podobně jako model NEM nezahrnují difúzi. Hlavní myšlenka odvození spočívá v provedení transformace (9) a přechodu k postupným vlnám $w_i(x,t)$. Narozdíl od LTEM je však tato transformace provedena i uvnitř matice $\mathbb{M}\big(\vec{c}(x,t)\big)$. V *Publikaci V* je dále ukázáno, že v důsledku vnitřní struktury transformačních matic $\mathbb{Q}_R$ a $\mathbb{Q}_L$ splývá v případě píků analytů příslušná postupná vlna s koncentrací daného analytu. Jelikož rovnice (20) v modelu NEM popisuje pouze evoluci píku analytu, soustředilo se i odvození v *Publikaci V* na píky analytů. Byl proto učiněn zjednodušující předpoklad, že systémové píky přítomné v kapiláře nijak neovlivňují vývoj píků analytů. Uvedený předpoklad je možné interpretovat také tak, že požadujeme, aby se systémové píky separovaly od píků analytů ihned po aplikaci vnějšího elektrického pole. Matematicky tento předpoklad znamená, že funkce reprezentující postupné vlny systémových píků pokládáme rovné nule všude, kde se překrývají s píky analytů. Ačkoli se tento předpoklad může jevit jako značně omezující, existují systémy, v nichž systémové píky mají nulovou amplitudu a požadavek na vzájemné neovlivňování se mezi

systémovými píky a píky analytů je v nich přirozeně splněn[12]. Příklad takového systému je uveden v *Publikaci VI*.

Prvky matice $\mathbb{M}\left(\vec{c}(x,t)\right)$ v sobě obsahují výraz pro měrnou elektrickou vodivost. Bylo ukázáno, že při splnění předpokladu, že systémové píky přítomné v kapiláře nijak neovlivňují vývoj píků analytů, je měrná elektrická vodivost v částech kapiláry, kde se vyskytují píky analytů, pouze funkcí koncentrací těchto analytů. Nicméně závislost měrné elektrické vodivosti na koncentracích analytů je velmi komplikovaná. Aby bylo možné rovnice kontinuity dále upravit do tvaru analogického modelu NEM, musel být učiněn dodatečný předpoklad, že pH je ve všech zónách analytů rovné pH neporušeného BGE. Tímto způsobem byly v zónách analytů zafixovány molární zlomky všech iontových forem všech složek, a tudíž byly zafixovány i efektivní mobility všech analytů. Zafixovaná hodnota efektivní elektroforetické mobility příslušného analytu je přitom rovna jeho efektivní elektroforetické mobilitě v limitě nekonečného zředění. Po uplatnění zmíněného předpokladu o konstantním pH v zónách všech analytů bylo možné vyjádřit měrnou elektrickou vodivost jako lineární funkci koncentrací analytů.

$$\kappa(x,t) = \kappa_{BGE} + \sum_{j=1}^{N_A} \kappa_j c_j(x,t) \tag{52}$$

kde

$$\kappa_j = F \sum_{i=1}^{N} \sum_{z=n_i}^{p_i} z\mu_{i,z} h_{i,z} (\mathbb{Q}_R)_{ij} \tag{53}$$

$(\mathbb{Q}_R)_{ij}$ je prvek transformační matice $\mathbb{Q}_R$ stojící v *i*-tém řádku a *j*-tém sloupci. Konstantní koeficienty $h_{i,z}$ v rovnici (53) mají význam molárního zlomku iontové formy *i*-té složky, která má nábojové číslo z, vztaženého k celkové koncentraci *i*-té složky.

$$c_{i,z} = h_{i,z} c_i \tag{54}$$

Koeficienty κ_j v rovnici (52) mají fyzikální rozměr Sm^2mol^{-1} a v první aproximaci udávají hodnotu parciální derivace měrné vodivosti podle koncentrace daného analytu, a to v limitním případě nekonečně malé koncentrace analytu. Na tomto místě je vhodné připomenout, že také v Mikkersově původní práci byly molární zlomky všech iontových

[12] Stejný předpoklad byl učiněn i v práci [10] při odvozní NLTEM.

forem pevně zafixovány, neboť Mikkers uvažoval pouze silné elektrolyty. Odvození modelu NEM v *Publikaci V* bylo zakončeno dosazením za měrnou elektrickou vodivost z rovnice (52) do matice $\mathbb{M}\big(\vec{c}(x,t)\big)$, což umožnilo upravit rovnice kontinuity (5) na soustavu N_A vzájemně provázaných kvazilineárních parciálních diferenciálních rovnic.

$$\frac{\partial c_i(x,t)}{\partial t} + \frac{\partial}{\partial x}\left(\frac{v_{\mathrm{eff},i}\, c_i(x,t)}{1 + \sum_{j=1}^{N_A} \frac{\kappa_j}{\kappa_{\mathrm{BGE}}} c_j(x,t)}\right) = 0 \qquad i = 1, \ldots, N_A \qquad (55)$$

V případě, kdy je v elektroforetickém systému přítomen pouze jeden analyt A, přejde soustava rovnic (55) na jedinou diferenciální rovnici ve tvaru:

$$\frac{\partial c_A(x,t)}{\partial t} + \frac{\partial}{\partial x}\left(\frac{v_{\mathrm{eff},A}\, c_A(x,t)}{1 + \frac{\kappa_A}{\kappa_{\mathrm{BGE}}} c_A(x,t)}\right) = 0 \qquad (56)$$

Tato diferenciální rovnice je totožná s Mikkersovou rovnicí (20), přičemž roli parametru a vystupujícím v Mikkersově rovnici hraje nyní podíl $-\frac{\kappa_A}{\kappa_{\mathrm{BGE}}}$. Znaménko koeficientu κ_A, viz rovnice (53), určuje, zda pík analytu bude frontující či tailující.

Zbylá část *Publikace V* se zabývá detailním rozborem rovnice (56). Byla diskutována pozoruhodná podobnost rovnice (56) a rovnice popisující ideální model kapalinové chromatografie pro jeden analyt [29]:

$$\frac{\partial c_{mo}}{\partial t} + \frac{1-\epsilon}{\epsilon}\frac{\partial c_{st}}{\partial t} + u\frac{\partial c_{mo}}{\partial x} = 0 \qquad (57)$$

V rovnici (57) představuje ϵ pórovitost náplně chromatografické kolony, u je rychlost mobilní fáze, c_{mo} je koncentrace analytu v mobilní fázi a c_{st} je koncentrace analytu ve stacionární fázi. V případě, kdy se adsorpce analytu na stacionární fázi řídí Langmuirovou izotermou, nabývá rovnice (57) tvaru téměř identického s rovnicí (56):

$$\frac{\partial c_{mo}}{\partial t} + \frac{1-\epsilon}{\epsilon}\frac{\partial}{\partial t}\left(\frac{N_b K_{ad} c_{mo}}{1 + K_{ad} c_{mo}}\right) + u\frac{\partial c_{mo}}{\partial x} = 0 \qquad (58)$$

kde N_b je koncentrace vazebných míst pro analyt ve stacionární fázi a K_{ad} je adsorpční konstanta. Z porovnání obou rovnic vyplynulo, že parametr a, respektive $-\frac{\kappa_A}{\kappa_{\mathrm{BGE}}}$ má v modelu NEM stejnou úlohu jako adsorpční konstanta K_{ad} v chromatografické rovnici

(58). Na rozdíl od adsorpční konstanty K_{ad} může ovšem parametr a nabývat jak kladných, tak záporných hodnot. To má za následek, že množina řešení rovnice (56) obsahuje píky tailující i frontující, zatímco řešením rovnice (58) mohou být pouze píky tailující[13].

V roce 1970 bylo publikováno úplné řešení chromatografické rovnice (58) nalezené pomocí takzvané metody charakteristik [30]. V situaci, kdy uvažujeme pouze jeden analyt, lze řešení rovnice (20), resp. (58) nalézt i bez použití pokročilé metody charakteristik, jak tomu bylo například v práci Mikkerse [20]. S ohledem na navazující *Publikaci VI*, která se zabývá systémy se dvěma analyty, byla v *Publikaci V* prezentace řešení rovnice (56) zopakována. Přitom byla ovšem důsledně používána terminologie, která vyplývá právě z metody charakteristik. V *Publikaci V* je uvedena ukázka řešení rovnice (56) pro případ $\kappa_A < 0$ (*Publikace V*, Figure 2). Zde je zobrazen jednak koncentrační profil analytu (*Publikace V*, Figure 2B) a jednak takzvaný *x*-*t* diagram (*Publikace V*, Figure 2A), který slouží jako pomůcka při konstrukci řešení a znázorňuje pohyb charakteristických bodů řešení v rovině se souřadnicovými osami *x* a *t*.

Zjednodušení uplatněná při odvození modelu NEM postupem prezentovaným v *Publikaci V* spočívala v zanedbání difúze a požadavku na konstantní pH uvnitř píku analytu. Nelinearita pramenící ze změn měrné elektrické vodivosti v místě píku analytu však zůstala v modelu NEM plně zachována. Model NLTEM zahrnuje tuto nelinearitu pouze v jisté aproximaci (první člen Taylorova rozvoje matice $\mathbb{M}(\vec{c}(x,t))$), na druhou stranu však zahrnuje též difúzi a připouští změny pH uvnitř píku analytu. Bylo proto zajímavé oba modely porovnat podrobněji a najít mezi nimi hlubší souvislosti. V *Publikaci V* bylo ukázáno, že po provedení Taylorova rozvoje v rovnici (56), doplnění modelu NLTEM o požadavek na konstantní pH uvnitř píku analytu a vynechání členu odpovídajícího difúzi v modelu NLTEM vedou modely NLTEM a NEM na stejnou diferenciální rovnici. Z hlediska nelinearity způsobené změnami měrné vodivosti uvnitř píku analytu tak můžeme model NLTEM považovat za aproximaci prvního řádu k modelu NEM.

Jak bylo zmíněno již v úvodu této disertační práce, je funkce HVL, jakožto řešení modelu NLTEM s počáteční podmínkou ve tvaru Diracovy delta funkce, hojně využívána v praxi pro popis tvaru píku v CZE. Správnější by ovšem bylo využití HVLR funkce, neboť počáteční šířka píku je v reálném experimentu vždy nenulová. Vyvstává proto otázka, zda po uplynutí dostatečně dlouhého času, kdy již zcela vymizí počáteční

[13] Pojmy tailující a frontující pík se vztahují k tvaru píku, jak je zaznamenán detektorem.

koncentrační plato HVLR funkce, přejde HVLR funkce na tvar popsatelný funkcí HVL. Důkaz či vyvrácení tohoto tvrzení je vzhledem ke složitosti funkčního předpisu HVLR funkce (viz rovnice (37) – (41) v práci [10]) nesmírně komplikované. Určitý vhled do této problematiky však vnáší model NEM. V *Publikaci V* bylo ukázáno, že píky analytů, které mají různé počáteční šířky, ale stejnou plochu, tj. stejnou hodnotu součinu počáteční šířky a počáteční koncentrace, v rámci modelu NEM navzájem splývají od okamžiku, kdy vymizí počáteční plato nejširšího z nich. Schematicky je tuto skutečnost možné znázornit pomocí *x-t* diagramů (*Publikace V*, Figure 3). Závěr přitom platí pro libovolnou počáteční šířku píku, tedy i pro velmi úzký pík, který libovolně přesně aproximuje Diracovu delta funkci. Na tento výsledek lze nahlížet jako na argument ve prospěch výše uvedeného tvrzení o přechodu HVLR funkce na HVL funkci. Model NEM dokonce poskytuje explicitní vztah pro kritický čas, kdy počáteční plato píku vymizí. Aby byl náš argument ještě více podpořen, byl využit simulační software Simul a pro několik různých počátečních šířek píku analytu byl z nasimulovaného elektroferogramu odhadnut čas, od kterého lze pík analytu dobře popsat HVL funkcí. Byla pozorována velmi dobrá shoda tohoto odhadnutého času s kritickým časem předpovězeným modelem NEM (*Publikace V*, Figure 4A). V *Publikaci V* je též ilustrován postup pro získání odhadu času konvergence HVLR funkce k HVL funkci z nasimulovaného elektroferogramu (*Publikace V*, Figure 4B). Podrobný popis zvoleného modelového elektroforetického systému je uveden v *Publikaci V*.

V *Publikaci VI* bylo představeno a diskutováno řešení soustavy rovnic (55) pro případ dvou analytů, kdy se tato soustava redukuje na dvě provázané kvazilineární parciální diferenciální rovnice.

$$\begin{aligned}\frac{\partial c_1(x,t)}{\partial t}+\frac{\partial}{\partial x}\left(\frac{v_{\mathrm{eff},1}c_1(x,t)}{1+\frac{\kappa_1}{\kappa_{\mathrm{BGE}}}c_1(x,t)+\frac{\kappa_2}{\kappa_{\mathrm{BGE}}}c_2(x,t)}\right)=0\\ \frac{\partial c_2(x,t)}{\partial t}+\frac{\partial}{\partial x}\left(\frac{v_{\mathrm{eff},2}c_2(x,t)}{1+\frac{\kappa_1}{\kappa_{\mathrm{BGE}}}c_1(x,t)+\frac{\kappa_2}{\kappa_{\mathrm{BGE}}}c_2(x,t)}\right)=0\end{aligned} \tag{59}$$

S velmi podobnou, nikoli však zcela shodnou, soustavou diferenciálních rovnic se opět můžeme setkat v rámci ideálního modelu chromatografie s Langmuirovou izotermou popisujícího separaci dvou analytů [31]. Teorie daného typu diferenciálních rovnic byla

dále rozvinuta v pracích [30,32]. Ačkoli jsou si rovnice popisující chromatografický a elektroforetický separační proces podobné, jedná se pouze o formální podobnost matematického popisu dvou rozdílných separačních mechanismů.

Jelikož teorie řešení kvazilineárních parciálních diferenciálních rovnic již byla podrobně vypracována v rámci ideálního modelu chromatografie, soustředí se *Publikace VI* pouze na zdrůraznění odlišností od chromatografie. Jako počáteční podmínka pro řešení soustavy (59) byla v *Publikaci VI* uvažována obdélníková zóna vzorku, neboť pro takovou počáteční podmínku lze nalézt analytické řešení. Bez újmy na obecnosti se v *Publikaci VI* dále předpokládá, že elektroforetická mobilita analytu 1 je v absolutní hodnotě menší než elektroforetická mobilita analytu 2. *Publikace VI* se věnuje popisu systémů, v nichž jsou oba píky analytů buď tailující, tj. $\kappa_1 < 0$, $\kappa_2 < 0$, nebo naopak frontující, tj. $\kappa_1 > 0$, $\kappa_2 > 0$. Tyto případy jsou do značné míry vzájemně symetrické, což umožňuje zavést jednotný formalismus pro jejich popis a diskutovat je současně. Na obrázku (*Publikace VI*, Figure 1) je uveden schématický *x*-*t* diagram znázorňující pohyb význačných bodů řešení v rovině se souřadnicovými osami *x* a *t,* a to pro elektroforetický systém, v němž $\kappa_1 < 0$, $\kappa_2 < 0$. V *Publikaci VI* je uvedena ukázka samotného řešení pro konkrétní elektroforetický systém tohoto typu (*Publikace VI*, Figure 2), kde jsou znázorněny koncentrační profily analytů pro několik separačních časů, které byly zvoleny tak, aby postihly celý průběh separace analytů. Bylo odvozeno, že po vložení elektrického napětí na kapiláru se na jedné straně počáteční obdélníkové zóny vzorku začne vyvíjet oblast disperzního rozhraní (D), zatímco na její druhé straně vznikne šokové rozhraní $S_{(S)}$. Pro analyt, který se nachází na straně disperzního rozhraní, bylo v *Publikaci VI* zavedeno označení D, zatímco pro analyt, který se nachází na straně šokového rozhraní, bylo zavedeno označení S. V případě $\kappa_1 < 0$, $\kappa_2 < 0$ odpovídá analyt D pomalejšímu analytu 1 a analyt S rychlejšímu analytu 2. Naopak, je-li $\kappa_1 > 0$, $\kappa_2 > 0$, odpovídá analyt D rychlejšímu analytu 2 a analyt S pomalejšímu analytu 1. Mezi disperzním rozhraním (D) a šokovým rozhraním $S_{(S)}$ mohou v průběhu separace existovat dvě další oblasti, které mají charakter disperzního rozhraní (oblasti (SD) a (DS)), tři oblasti, které mají konstantní složení (oblasti (Z), (V) a (R)) a jedno šokové rozhraní $S_{(D)}$ (viz *Publikace VI*, Figure1 a Figure 2). Oblasti (Z), (V), (R) a (SD) mají pouze dočasný charakter a po určitém separačním čase zaniknou. Disperzní rozhraní (D) a (DS) a obě šoková rozhraní mají trvalý charakter a existují i po dosažení úplné separace analytů. Po dosažení úplné separace analytů je pík analytu D tvořen

disperzním rozhraním (D) a šokovým rozhraním $S_{(D)}$ a pík analytu S je tvořen disperzním rozhraním (DS) a šokovým rozhraním $S_{(S)}$. Vztahy pro výpočet koncentrace analytů v jednotlivých oblastech byly uvedeny v doplňujícím materiálu *Publikace VI*. Rovněž vztahy pro rychlosti pohybu význačných bodů řešení (viz křivky na *x*-*t* diagramu, *Publikace VI*, Figure 1) a vztahy pro kritické časy, kdy některá oblast řešení zaniká, byly uvedeny v doplňujícím materiálu. V doplňujícím materiálu *Publikace VI* byly též uvedeny varianty obrázků Figure 1 a Figure 2 pro případ $\kappa_1 > 0$, $\kappa_2 > 0$ a příslušné vztahy pro rychlosti význačných bodů a kritické časy. Tyto vztahy a obrázky ilustrují, že z hlediska teoretického popisu není mezi elektroforetickými systémy $\kappa_1 < 0$, $\kappa_2 < 0$ a $\kappa_1 > 0$, $\kappa_2 > 0$ podstatný rozdíl a je možné je chápat jako vzájemné zrcadlové obrazy.

Nejcennější vlastností modelu NEM je jeho schopnost kvalitativně i kvantitativně předpovědět deformace píků analytů, jejichž příčinou je vzájemná interakce mezi píky a jež jiné současné modely, například LTEM a NLTEM, předpovědět nedokáží. Vzhledem ke značné formální podobnosti modelu NEM a ideálního modelu chromatografie s Langmuirovou izotermou mají deformace, s nimiž se můžeme setkat v kapilární elektroforéze, svou chromatografickou analogii. V *Publikaci VI* byla proto pro popis zmíněných deformací přejata již zažitá chromatografická terminologie, a sice termíny displacement efekt a tag along efekt (pro tyto pojmy výjimečně zachováváme anglické názvy). Displacement efekt je označení pro vznik oblasti, v níž je koncentrace analytu S vyšší než je jeho počáteční koncentrace ve vzorku. V důsledku změny vodivosti ve smíšené zóně analytů oproti vodivosti neporušeného BGE je pro analyt S splněna podmínka zakoncentrování a analyt S je vytlačován (angl. displaced) analytem D ze smíšené oblasti a zároveň zakoncentrován. Jak bylo ukázáno v *Publikaci VI*, platí tento závěr pro oba diskutované případy $\kappa_1 < 0$, $\kappa_2 < 0$ i $\kappa_1 > 0$, $\kappa_2 > 0$. Pro účely kvantifikace displacement efektu byla zavedena veličina Σ_D, definovaná jako podíl koncentrace analytu S na jedné a druhé straně šokového rozhraní $S_{(D)}$. Pomocí stejné veličiny se displacement efekt kvantifikuje i v chromatografii.

V *Publikaci VI* bylo ukázáno, že v případě, kdy jsou si efektivní mobility analytů velmi blízké, je možné vztah pro Σ_D zjednodušit na tvar

$$\Sigma_D \approx 1 + \frac{c_D^0}{c_S^0} \tag{60}$$

v němž vystupují pouze počáteční koncentrace analytů c_D^0 a c_S^0. Ze vztahu (60) plyne, že čím větší je počáteční koncentrace analytu D oproti počáteční koncentraci analytu S, tím je displacement efekt silnější.

Tag along efekt se vztahuje ke vzniku koncentračního plata obsahujícího pouze analyt D (viz oblast (V), *Publikace VI*, Figure 2A, 2B). Příčinou tag along efektu je rozdíl ve vodivosti mezi smíšenou oblastí disperzního rozhraní, kde se nacházejí oba analyty, a oblastí disperzního rozhraní čistého analytu D. Tento rozdíl způsobuje, že analyt D setrvává delší dobu ve smíšené oblasti a jen neochotně ji opouští. Pro kvantifikaci tag along efektu byla navržena veličina Σ_{TA}, jejíž definice byla opět inspirována přístupem v chromatografii. Závislost Σ_{TA} na počátečních koncentracích analytů je uvedena v doplňujícím materiálu *Publikace VI*. Bylo dokázáno, že tag along efekt je maximální v případě, kdy analyt S je přítomen ve velkém nadbytku oproti analytu D. Veličina Σ_{TA} potom závisí pouze na efektivních elektroforetických mobilitách analytů.

$$\lim_{c_S^0 \to \infty} \Sigma_{\mathrm{TA}} = \lim_{c_D^0 \to 0} \Sigma_{\mathrm{TA}} = \frac{\mu_{\mathrm{eff},2} - \mu_{\mathrm{eff},1}}{\mu_{\mathrm{eff},D}} \tag{61}$$

Je-li naopak analyt D přítomen v nadbytku oproti analytu S, je tag along efekt potlačen.

$$\lim_{c_S^0 \to 0} \Sigma_{\mathrm{TA}} = \lim_{c_D^0 \to \infty} \Sigma_{\mathrm{TA}} = 0 \tag{62}$$

Z praktického hlediska je velmi zajímavá otázka, zda a jakým způsobem se vzájemná interakce mezi píky analytů, ke které dochází v počátcích separačního procesu, projeví na tvaru a pozici píků analytů v okamžiku detekce, kdy jsou případně již analyty úplně separovány. Pomocí modelu NEM bylo dokázáno, že je-li doba trvání separačního procesu delší než kritický čas t_V (viz *Publikace VI*, Figure 1), nenese již pík analytu D žádné známky předchozí interakce s analytem S. Jinými slovy tvar i pozice píku analytu D jsou zcela identické s tvarem a pozicí, jaké by měl tento pík, pokud by analyt D byl jediným analytem přítomným ve vzorku. Naproti tomu pík analytu S je v důsledku interakce s analytem D v elektroferogramu posunut buďto k vyšším, je-li $\kappa_1 < 0$, $\kappa_2 < 0$, nebo nižším, je-li $\kappa_1 > 0$, $\kappa_2 > 0$, hodnotám migračního času[14] a jeho tvar je v obou případech nevratně ovlivněn počáteční interakcí s analytem D.

[14] Tento závěr platí za předpokladu, že neuvažujeme EOF a polarita napětí vloženého na kapiláru je zvolena tak, aby se analyty pohybovaly směrem k detektoru.

Na závěr *Publikace VI* byla správnost rozšíření modelu NEM na dva analyty ověřena porovnáním elektroferogramů (zobrazených v doméně prostorové souřadnice x)předpovězených modelem NEM a elektroferogramů, které byly výsledkem numerického řešení soustavy rovnic kontinuity (5) v programu Simul 5 [15] (*Publikace VI*, Figure 4). Prorovnání bylo provedeno pro dva separační časy, které odpovídaly různé míře vzájemné separace analytů. Podrobný popis složení modelového elektroforetického systému je uvedeno v *Publikaci VI*. Bylo prokázáno, že model NEM je schopen správně předpovědět všechny charakteristické deformace píků způsobené vzájemnou interakcí mezi píky analytů. Jmenovitě jde o předpověď existence tag along efektu, předpověď skokového zvýšení koncentrace analytu S na šokovém rozhraní $S_{(D)}$, tj. displacement efektu, a předpověď odlišné směrnice koncentračního profilu analytu S napravo a nalevo od šokového rozhraní $S_{(D)}$.

Elektroferogram předpovězený modelem NEM byl též porovnán s experimentálním elektroferogramem (*Publikace VI*, Figure 5). Byla pozorována dobrá shoda mezi předpovědí modelu NEM a experimentálním elektroferogramem. Koncentrační profily jednotlivých analytů v experimentálním elektroferogramu byly získány zaznamenáním elektroferogramu UV-VIS detektorem při vlnových délkách 220 nm a 250 nm a následnou lineární kombinací obou záznamů. Při tomto postupu bylo využito skutečnosti, že použité analyty mají při vlnových délkách 220 nm a 250 nm odlišné absorpční koeficienty.

Publikace V

The dynamics of band (peak) shape development in capillary zone electrophoresis in light of the linear theory of electromigration

Martin Dvořák, Pavel Dubský, Magda Dovhunová, Bohuslav Gaš

Electrophoresis 2019, *40*, 668 – 682

Martin Dvořák
Pavel Dubský
Magda Dovhunová
Bohuslav Gaš

Faculty of Science, Department of Physical and Macromolecular Chemistry, Charles University in Prague, Prague, Czech Republic

Received October 18, 2018
Revised November 20, 2018
Accepted November 21, 2018

Review

The dynamics of band (peak) shape development in capillary zone electrophoresis in light of the linear theory of electromigration

The continuity equations that describe the movement of ions in liquid solutions under the influence of an external stationary electric field, as it is utilized in electrophoresis, were introduced a long time ago starting with Kohlrausch in 1897. From that time on, there have been many attempts to solve the equations and to discuss the results. In electrophoresis, special attention has always been devoted to the peak shapes obtained by the detector since the shapes have a tight connection with the phenomena taking place during electromigration and influence the efficiency and selectivity of the separation. Among these phenomena, the most important is electromigration dispersion. In this commented review paper, we compare various models of electromigration, try to find points that connect them, and discuss the range of their validity in light of the linear and nonlinear theory of electromigration.

Keywords:
Capillary zone electrophoresis / Electromigration dispersion / Linear theory of electromigration
DOI 10.1002/elps.201800444

1 Introduction

CZE is one of the most popular modes of CE. This might be attributed to the fact that this method requires only the simplest possible experimental setup and results in a detector trace similar to its chromatographic counterpart. Just as in chromatography, it is fundamentally important to know how the shape of an analyte band (peak) develops in a given BGE during the separation process.

Although several disturbing phenomena can contribute to band shape development in CZE [1], diffusion and electromigration dispersion (EMD) are of the utmost importance, since they originate from the electromigration processes itself. Whereas diffusion is common to all transport phenomena, EMD is typical of CZE where it has been studied for decades resulting in a gradual progress of theory that still continues today. In this commented review paper, we first provide a detailed overview of the existing theories, then continue with a new mathematical treatment that creates a missing link between the two most significant CZE models, and end with a thorough discussion of band shape development in CZE under the influence of EMD.

Correspondence: Dr. Pavel Dubský, Charles University in Prague, Faculty of Science, Albertov 6, CZ-128 43 Prague 2, Czech Republic.
E-mail: pavel.dubsky@natur.cuni.cz

Abbreviations: **EKC**, electrokinetic chromatography; **EMD**, electromigration dispersion; **HVL**, Haarhoff-Van der Linde; **KRF**, Kohlrausch regulating function; **LTEM**, linear theory of electromigration; **MBE**, moving boundary electrophoresis; **NEM**, nonlinear electromigration model; **NLTEM**, nonlinear theory of electromigration; **PDE**, partial differential equation

1.1 Governing equations

A basic set of continuity equations describing the movement of ions in liquid solutions under the influence of an external stationary electric field was introduced by Kohlrausch [2]. The equations are expressed in the form of mass conservation laws that apply to each species in the system (capillary). The term "species" needs some clarification since chemical entities can exist in several forms as witnessed by the use of terms such as "radical" [3], "ion constituent" (as cited in [4]), and "subspecies" [4] that were introduced by some authors beginning in 1933. We prefer the terminology of "constituents" and their "forms" as it can be dated back to a paper by Alberty in 1950 [5]. We provide a detailed commentary on the perception of constituents and forms in a separate paper in this special issue [6], where we also examine general equilibria that exist in electrophoretic systems such as in electrokinetic chromatography (EKC) ones. We limit our discussion to simple acid–base equilibria in this paper.

The key relation that assigns individual forms to individual constituents is the mass balance equation, which in CZE systems reads

$$c_i = \sum_{z=n_i}^{p_i} c_{i,z} \quad (1)$$

Color online: See the article online to view Figs. 2–4 in color.

© 2018 WILEY-VCH Verlag GmbH & Co. KGaA, Weinheim

where $c_i \equiv c_i(x, t)$ and $c_{i,z} \equiv c_{i,z}(x, t)$ are concentrations of the i-th constituent and its individual ionic forms, respectively, x is the spatial coordinate in the separation channel, and t is time. The sum goes over all charges of the ionic forms of the i-th constituent, including the neutral one. The most negative/positive charge the i-th constituent can gain due to its de-protonization/protonization is denoted by the indexes n_i / p_i, respectively. The mass balance is expressed for general ampholytes in this way.

Electric current constitutes mass fluxes of each individual ionic form in the capillary and the fluxes, in principle, include reactive terms of all chemical equilibria involving the forms. These individual mass fluxes sum up to an overall mass flux for each constituent due to Eq. (1). The reactive terms can be omitted and replaced by a set of coupled algebraic equilibrium equations, provided the equilibrium state is achieved instantaneously compared to the timescale of band movement [7]. Under such conditions, concentration of each form in the system becomes a function of only analytical (overall) concentrations of all constituents. In the simple CZE systems, where acid–base equilibria are the only ongoing reactions, this translates into concentration of each form be a function of pH, which itself is a function of local concentrations of all constituents,

$$c_{\mathrm{i,z}} \equiv c_{\mathrm{i,z}}(\mathrm{pH}(c_1, \ldots, c_{\mathrm{N}})) \tag{2}$$

where we consider a system consisting of N constituents in total. Consequently [8],

$$\begin{aligned} \frac{\partial c_{\mathrm{i}}}{\partial t} &= \left(\frac{\partial c_i}{\partial t}\right)_{\mathrm{em}} + \left(\frac{\partial c_{\mathrm{i}}}{\partial t}\right)_{\mathrm{dif}} \\ \left(\frac{\partial c_i}{\partial t}\right)_{\mathrm{em}} &= -\frac{\partial}{\partial x}\sum_{z=n_{\mathrm{i}}}^{p_{\mathrm{i}}} \frac{j}{\kappa} c_{\mathrm{i,z}}\mu_{\mathrm{i,z}} \\ \left(\frac{\partial c_{\mathrm{i}}}{\partial t}\right)_{\mathrm{diff}} &= \frac{\partial}{\partial x}\sum_{z=n_{\mathrm{i}}}^{p_{\mathrm{i}}}\left(D_{\mathrm{i,z}}\frac{\partial c_{\mathrm{i,z}}}{\partial x} - \frac{j_{\mathrm{diff}}}{\kappa} c_{\mathrm{i,z}}\mu_{\mathrm{i,z}}\right) \end{aligned} \tag{3}$$

where j is the current density, $\mu_{i,z}$ is the signed electrophoretic mobility of the given form, $D_{i,z}$ is its diffusion coefficient, and $\kappa \equiv \kappa(x, t)$ and $j_{diff} \equiv j_{diff}(x, t)$ are (local) conductivity and diffusion current density, respectively. The signed electrophoretic mobility, $\mu_{i,z}$, is defined so that $\mu_{i,z} = \mathrm{sgn}(z) * |\mu_{i,z}|$. Further,

$$\kappa = F\left(\sum_{\mathrm{i}=1}^{N}\sum_{z=n_{\mathrm{i}}}^{p_{\mathrm{i}}} z\mu_{\mathrm{i,z}}c_{\mathrm{i,z}} + \mu_{\mathrm{H}}c_{\mathrm{H}} - \mu_{\mathrm{OH}}c_{\mathrm{OH}}\right) \tag{4}$$

where F is the Faraday constant and the subscripts H and OH refer to the H_3O^+ and OH^- ions, respectively, and

$$j_{\mathrm{diff}} = -F\left(\sum_{\mathrm{i}=1}^{N}\sum_{z=n_{\mathrm{i}}}^{p_{\mathrm{i}}} zD_{\mathrm{i,z}}\frac{\partial c_{\mathrm{i,z}}}{\partial x} + D_{\mathrm{H}}\frac{\partial c_{\mathrm{H}}}{\partial x} - D_{\mathrm{OH}}\frac{\partial c_{\mathrm{OH}}}{\partial x}\right) \tag{5}$$

1.2 Moving boundary electrophoresis

The theory of moving boundary electrophoresis (MBE) can valuably contribute to the understanding of the origin of many phenomena in electrophoresis as aptly pointed out, e.g., in monographs on the dynamics of electrophoresis in general [9], and CZE in particular [10]. Specifically, the initial CZE setup with an injected plug of sample surrounded by the BGE is similar to the original MBE setup dated back to the beginning of the 20th century [11]. It soon became recognized that two fundamental types of boundaries exist: A self-sharpening one that forms a sudden jump in the concentration profiles fighting the diffusion process during the electromigration process, and a diffusive one that tends to smear out any initial sharp boundary at the junction of two electrolytes more than mere diffusion would.

This notion was proven by Weber already in 1897 [12]. The author transformed a problem of electrophoretic movement of three strong electrolyte monovalent ions, i.e., ion (A), co-ion (B), and counter-ion (R), into a single partial differential equation describing the spatiotemporal development of a quantity $\eta = \frac{\omega}{\kappa}$, where ω is a regulating function equivalent to the Kohlrausch regulating function (KRF) [2] (exactly speaking, the function by Weber equals the KRF multiplied by mobility of the counter-ion, R). Weber showed that if a discontinuity exists in the system, it develops as either a self-sharpening or diffusive boundary as η_{backward} is higher or lower than η_{forward}, respectively, where "forward" and "backward" refer to the side of the discontinuity with respect to the movement of the boundary. He additionally treated a special case of the ion A be present exclusively on one side of the discontinuity and the co-ion B be present on the other side, showing that the above mentioned condition is equivalent to whether mobility of the ion A, μ_A, is lower (in its absolute value) or higher than that of the co-ion B, μ_B, respectively. Thus, the self-sharpening boundary develops in the former case ($|\mu_A| < |\mu_B|$), and the two co-ions are never mixed. To the contrary, the diffusive boundary develops in the latter case ($|\mu_A| > |\mu_B|$), and the ion A penetrates into the zone of the ion B. Interestingly, Weber pointed out that this process is not fully reversible since the diffusive boundary became the self-sharpening one and vice versa upon switching the voltage polarity.

In 1933, Henry and Brittain [13] studied the same model setup and introduced a function (we use different notations compared to original papers in order to stay consistent within this paper)

$$\Phi_* = 1 \mp F\frac{(\mu_{\mathrm{A}} - \mu_{\mathrm{B}})(\mu_{\mathrm{A}} - \mu_{\mathrm{R}})}{\mu_{\mathrm{A}}}\frac{c_{\mathrm{A},*}}{\kappa_*} \tag{6}$$

where subscript * refers either to the forward or the backward side of the boundary (with respect to its movement), $c_{A,*}$ is a (local) concentration of ion A at that side of the boundary, and the "–" or "+" signs apply to cationic or anionic species A, respectively. Similarly to Weber's quantity η, it was shown that if $\Phi_{\mathrm{backward}} > \Phi_{\mathrm{forward}}$, the backward region of the boundary tends to overcome the forward region and a moving discontinuity develops in the system, which manifests itself as

© 2018 WILEY-VCH Verlag GmbH & Co. KGaA, Weinheim

a self-sharpening boundary. Additionally, the velocity of the self-sharpening boundary was expressed as

$$v_{\mathrm{MBE}} = \frac{j}{\kappa_{\mathrm{forward}}} \mu_{\mathrm{A}} \Phi_{\mathrm{backward}} \tag{7}$$

If the opposite applies, i.e., $\Phi_{\mathrm{backward}} < \Phi_{\mathrm{forward}}$, the backward region lags behind the forward region and a continuous transition is established between the two regions in the concentration profiles so that the boundary, however, sharp at the beginning, becomes more and more diffuse. Finally, the authors showed that a single moving boundary is physically composed of overlapping discontinuities in more than one constituent.

Later on, Dole [14] developed a general theory of MBE for strong electrolytes and showed that a moving boundary across which the concentration of constituent *S* drops to zero propagates with a velocity (Eq. (8) is not expressed explicitly in the original work by Dole, though)

$$v_{\mathrm{MBE}} = \frac{j}{\kappa_{\mathrm{backward}}} \mu_{\mathrm{S}} \tag{8}$$

where $\kappa_{\mathrm{backward}}$ is the conductivity in the region adjacent to the boundary where constituent *S* is present. This signifies that such a boundary moves with the same velocity as constituent *S* in the region of its presence. Notice that both Eqs. (7) and (8) describe the same quantity, v_{MBE}, and that the latter is a special case of the former.

Svensson first commented on the problem of weak electrolytes in MBE in 1948 [4], and Alberty [5] completed the theory of MBE for weak electrolytes 2 years later. Alberty demonstrated that the equations introduced by Dole remain valid when the total concentrations of constituents and their effective mobilities are used in place of the ionic concentrations and ionic mobilities of strong electrolytes. This also applies to Eq. (8) as proposed earlier by Svensson. Additionally, Svensson pointed out that acid–base equilibria can be viewed as complex formation equilibria between various forms of weak electrolyte constituents and water ions, similarly to other possible complex-formation equilibria between a constituent and other constituent(s), including non-electrolytes, provided all of the reactions involved are fast enough. Although we are not aware of an explicit proof of this statement in MBE, its validity has been proven very recently in our group in the context of the EKC systems [6].

1.3 Mikkers' model for strong electrolytes

In 1979, Mikkers, Everaerts, and Verheggen [15] formulated the problem of CZE in terms of three strong electrolyte ions A, B, and R (originally C, A, and B, respectively; we again translate the symbols and terminology used in the original papers into a form that is consistent with the rest of this paper), similarly to the previous formulation of the MBE problem by Weber or Henry and Brittain (cf. above). Here, A is an analyte, and B and R are BGE co-ion and counter-ion, respectively. By combining a non-diffusional continuity equation (the *em* term in Eq. (3)) and the KRF [2], the authors arrived at the following differential equation for the concentration profile of the analyte

$$\frac{\partial c_{\mathrm{A}}}{\partial t} = -\mu_{\mathrm{A}} E_{\mathrm{BGE}} \frac{\partial}{\partial x} \left(\frac{c_{\mathrm{A}}}{1 - a c_{\mathrm{A}}} \right) \tag{9}$$

where E_{BGE} is the intensity of the electric field in the BGE. Constant a can be written in the form of

$$a = \frac{1}{c_{\mathrm{B,\ BGE}}} \frac{(\mu_{\mathrm{A}} - \mu_{\mathrm{R}})(\mu_{\mathrm{B}} - \mu_{\mathrm{A}})}{\mu_{\mathrm{A}}(\mu_{\mathrm{B}} - \mu_{\mathrm{R}})} \tag{10}$$

The same approach was adopted by Thormann [16], who augmented his calculations with experimental observations of peak development using a 255-channel detector located alongside the capillary.

The solution to Eq. (9) is summarized in Thormann's paper [17] and in another paper published by Mikkers [17]. The Thormann's paper [17] provides a concise list of mathematical formulae. Mikkers' paper [18] is interesting in two ways. First, it clearly illustrates the interrelation between the KRF, MBE, and CZE of strong electrolytes. Second, the author extended the theory to systems with an arbitrary number of strong electrolytes and demonstrated that the same mathematical model can be utilized for understanding the origin, mobilities, and approximate shapes of system peaks [18] in CZE. (The phenomenon of system peaks goes beyond the scope of this paper and we will stick to the results relevant to analyte peaks only.)

The most important outcome of Mikkers' model of CZE was that the originally rectangular concentration distribution of the sample plug develops into a triangular-like one with a self-sharpening front or back and a diffusive back or front, respectively. This can be easily understood in the frame of MBE since the sample plug surrounded by the BGE forms two antisymmetrical boundaries, one of which is self-sharpening and the other necessarily diffusive. We reproduce (with permission) the original illustration of the resulting peak shapes as provided by Mikkers [15] in Fig. 1. The solution itself is presented later in this paper, Eq. (40). Based on this solution, the famous "mobility match rules" have been established that state

$$\begin{aligned} &\mu_A > \mu_B \Rightarrow E_S < E_{BGE} \Rightarrow sharp\ back\ \&\ tailing\ front \\ &\mu_A < \mu_B \Rightarrow E_S > E_{BGE} \Rightarrow sharp\ front\ \&\ tailing\ back \\ &\mu_A = \mu_B \Rightarrow E_S = E_{BGE} \Rightarrow no\ triangulation \end{aligned} \tag{11}$$

where E_S and E_{BGE} is the strength of the electric field in the zone of the sample and in the BGE, respectively. The terms *back* and *front* refer to the direction of the movement of the band. The rules given in Eq. (11) are naturally consistent with Eq. (6) and can, in fact, be traced back to the work by Weber [12] (cf. 1.2 Moving boundary electrophoresis). It can be further noticed that the rules translate into the positive or negative value of parameter a, Eq. (10), since the sign of parameter a is fully determined by that of the difference $(\mu_B - \mu_A)$.

© 2018 WILEY-VCH Verlag GmbH & Co. KGaA, Weinheim

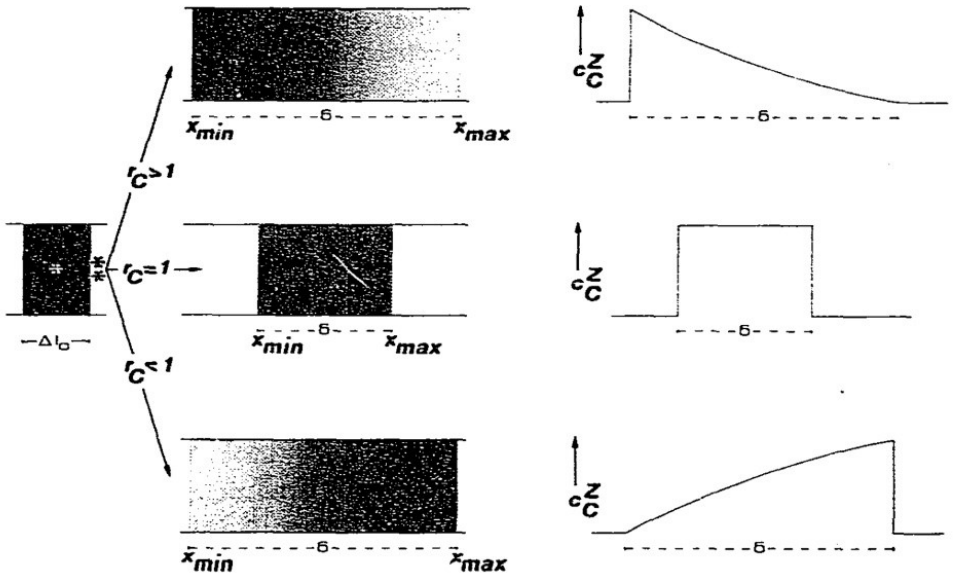


Figure 1. The original scheme of the solution to NEM, Eq. (9), as provided by Mikkers et al. in ref [15] (reproduced with permission). *Sampling compartment; **separation compartment; $\Delta l_0 = L$, the length of the injection zone; $r_c = \frac{\mu_A}{\mu_B}$, mobility ration between the analyte and its co-ion; x_{min}, x_{max} mark out the boundary of the region (X); δ determines the width of that region; $c_C^Z = c_A$, analyte concentration. (The equality signs relate original notation [15] to that used in this paper).

1.4 Weak electrolytes and mobility slope measures

Mikkers et al. pointed out in their original paper that most of the theory could be extended to weak electrolytes without troubles [15]. The EMD of weak electrolytes was studied by Foret, Boček, Fanali, Ossicin, and Šustáček [19, 20] around 1990 who concluded that the mobility match rules are applicable to weak electrolytes, when effective mobilities are used in place of ionic mobilities in Eq. (11); generalizing them as "effective mobility match rules".

In contrast to that, Xu et al. [21] proposed that systems with weak electrolytes are much more complex than systems with strong electrolytes. The authors adopted an approximation of the analyte velocity as directly proportional to its concentration with a constant of proportionality, the so-called EMD constant, k_{EMD},

$$v_{\mathrm{A}} = v_{\mathrm{A},0} + k_{\mathrm{EMD}} E_{\mathrm{BGE}} \frac{C_{\mathrm{A}}}{C_{\mathrm{BGE}}} \tag{12}$$

where v_A is the velocity of the analyte (taken as the velocity of the self-sharpening boundary as suggested by the authors), $v_{A,0}$ is its assumed velocity in the BGE (at infinite dilution), C_A is the concentration of the analyte at the self-sharpening boundary, and C_{BGE} is a certain concentration characteristic to the BGE, the choice of which is not relevant for this discussion (ref. the original paper [22]). The authors claimed their assumption to be justified by means of computer simulations and we will get back to it later (Section 2.1 From the Linear Theory of Electromigration Approach to Mikker's Equation). Subsequently, they were able to decompose the constant k_{EMD} into conductivity and pH-related terms in weak-electrolyte systems and proved that the (effective) mobility match rule may easily lose its validity in such systems. The conductivity change and the pH change can either have a synergistic effect on EMD or oppose each other when weak electrolytes are present.

Gebauer and Boček further developed their theory for systems consisting of univalent weak electrolyte analyte and univalent weak electrolyte co-ion and counter-ion in the BGE [22], in the pH region where the generalized KRF for univalent weak electrolytes applies [23, 24]. Using the generalized KRF allowed them to avoid the need for making an explicit assumption about the dependency of the analyte velocity on its concentration. The velocity of the analyte was shown not to be a simple linear function of its concentration (not even necessarily monotonous). It was argued and demonstrated by means of computer simulations that whatever the character of this function is, it is its derivative as the concentration of the analyte approaches zero that determines the final peak shape.

Consequently, Gebauer and Boček introduced the so-called velocity slope parameter as a measure of the tendency of the peak to be deformed by EMD [23]. The theoretical dependency of the velocity slope on pH in the BGE revealed that peaks may change their shape from tailing to fronting, thus passing through a transient pH where they become symmetrical. Notably, the authors pointed out that "the point of inversion ..., does not have any reliable simple relation to (the) effective and/or ionic mobilities of the analyte and BGE co-ion". Therefore, the authors finally suggested to abandon the (effective) mobility match rules completely.

The velocity slope parameter depends on the concentration of the BGE. The higher is the concentration of the BGE, the more overloaded it can be with the analyte before the analyte peak becomes EMD-dispersed. To allow for comparisons among different BGEs based solely on their nature (chemical composition), Horká and Šlais [25] introduced the so-called relative velocity slope, $S_{BGE,X}$. Relations between the relative velocity slope, $S_{BGE,X}$, and the velocity slope or the EMD constant, k_{EMD}, are given by the authors in the referenced paper. A symbol S_X was originally used for the velocity slope by Gebauer and Boček, albeit it was later overridden by the

© 2018 WILEY-VCH Verlag GmbH & Co. KGaA, Weinheim

actual meaning of $S_{BGE,X}$ in the literature. We will also use S_X in the actual meaning of $S_{BGE,X}$ herein. The definition of the relative velocity slope was finally refined into a mathematically concise form by Štědrý et al. [26] as (Eq. (1) and the related discussion in the original paper by Štědrý et al. [26] may be misleading. Cf. discussion around eq. (21) in the same paper or eq. (26) in [30] or eq. (45) in [31] in the later papers by the authors)

$$S_X = \lim_{c_A \to 0} \frac{\kappa}{v_A} \left(\frac{dv_A}{dc_A} \right) \tag{13}$$

where c_A is the concentration of the analyte. The parameter S_X is evaluated based on the mere knowledge of the BGE composition and the pK_A values and mobilities of the analyte forms. This made it a highly convenient descriptor of the tendency of the analyte peak to undergo EMD with the following meaning that resembles that of the mobility match rules, eq. (11),

$$\begin{aligned} &S_X > 0 \Rightarrow sharp\ front\ \&\ tailing\ back \\ &S_X < 0 \Rightarrow\ tailing\ front\ \&\ sharp\ back \\ &S_X = 0 \Rightarrow\ symmetric\ peak \end{aligned} \tag{14}$$

1.5 Linear theory of electromigration

A conceptually different approach to the problem of electromigration stems from the linear theory of electromigration (LTEM). Equarion (3) is expressed for each of the N constituents in the system and thus comprises a set of N partial differential equations (PDEs), which is coupled with the set of algebraic eqs. (2). Taking only the first—electromigration—term in Eq. (3), thus, disregarding the diffusion processes, the set of PDEs, eq. (3), can be transformed into a matrix notation as first applied by Poppe [27, 28] in 1990. Štědrý, Gaš et al. extensively developed this idea into LTEM for strong and weak electrolytes later [27, 29, 30]. We completed the theory very recently by extending it to CZE systems with fast equilibria in general, e.g., to EKC, and we are publishing the results in a separate paper in this special issue [6]. Therefore, we refer the reader to that paper for detailed description of LTEM while we summarize a few points relevant for our present discussion below.

The first step in the LTEM consists of expressing the electromigration term in a matrix form,

$$\left(\frac{\partial \vec{C}}{\partial t} \right)_{em} = -\frac{j}{\kappa_{BGE}} \boldsymbol{M} \times \frac{\partial \vec{C}}{\partial x} \tag{15}$$

where $\vec{C} \equiv (c_1, \ldots, c_N)^T$ is a column vector of the concentrations of all constituents, κ_{BGE} is the conductivity of the BGE, and $\boldsymbol{M} \equiv \boldsymbol{M}(\vec{C}(x,t))$ is a certain matrix. It is important to note that matrix $\boldsymbol{M}$ comprises all necessary terms so that Eq. (15) represents the electromigration part of the set of the PDEs, Eq. (3), exactly (we do not account for the diffusion potential in the electromigration term (cf. [6])). Second, matrix $\boldsymbol{M}$, is evaluated at the composition of the BGE resulting in a constant matrix, $\boldsymbol{M}_0 = \boldsymbol{M}(\vec{C}_{\mathrm{BGE}})$. Notice that vector $\vec{C}_{\mathrm{BGE}}$ contains all constituents present in the system including analytes, the concentration of which is set to zero there. Setting the analytes' concentrations to zero in matrix $\boldsymbol{M}_0$ has an important consequence that we will recall later.

Matrix $\boldsymbol{M}_0$ can be understood as a matrix that characterizes the BGE as a homogeneous environment in which analyte and system peaks develop upon injection of a sample plug and voltage application. The velocity of the peaks in such an environment is obtained through diagonalization of the matrix

$$\boldsymbol{M}_0 = \boldsymbol{Q}_R\ \boldsymbol{\Lambda}\, \boldsymbol{Q}_L \tag{16}$$

where $\boldsymbol{Q}_R$ and $\boldsymbol{\Lambda}$ are a matrix of row eigenvectors and a diagonal matrix of eigenvalues of $\boldsymbol{M}_0$, respectively, and $\boldsymbol{Q}_L = (\boldsymbol{Q}_R)^{-1}$. By substituting $\boldsymbol{M}_0$, Eq. (16), for $\boldsymbol{M}$ into Eq. (15), multiplying Eq. (15) by $\boldsymbol{Q}_R$ from the left, and introducing a set of functions $\vec{w}$ defined as

$$\vec{w} = \boldsymbol{Q}_L\ \times \vec{C} \tag{17}$$

the original set of N interrelated PDEs is decoupled into a set of N fully independent linear PDEs, each describing a simple propagation of a single wave,

$$\frac{\partial \vec{w}}{\partial t} = -\frac{j}{\kappa_{BGE}} \begin{bmatrix} \lambda_{0,1} & 0 & 0 \\ 0 & \ddots & 0 \\ 0 & 0 & \lambda_{0,N} \end{bmatrix} \frac{\partial \vec{w}}{\partial x} \tag{18}$$

where $\lambda_{0,i}$ are eigenvalues of the matrix $\boldsymbol{M}_0$. These waves represent the analyte and system peaks in CZE [19]. (Investigation of system peak propagation in CZE is again not the subject of this paper and we shall further focus on the analyte peaks only.)

LTEM provided further insight into the relative velocity slope, S_X. Its analytical expressions are given for strong electrolytes with two co-ions in the BGE [27], univalent weak electrolytes with two co-ions [30], and multivalent electrolytes [31]. Further, it was shown that in systems that contain only strong electrolytes, the value of S_X is equal but opposite in sign to the molar conductivity response. This has an interesting consequence: symmetrical peaks are principally invisible to conductivity detection in such systems. This simple relation does not persist when the analyte constituent becomes a weak electrolyte. The S_X parameter is generally composed of the molar conductivity response, b_X, and a pH-dependent term [31],

$$S_X = -b_x + const * \left(\frac{dpH}{dc_A} \right)_{c_A \to 0} \tag{19}$$

the latter of which may compensate for—but also amplify—the former. The constant in Eq. (19) depends on the nature of both analyte and BGE, albeit it can be shown based on expressions provided in ref. 31 that it approaches zero when the analyte constituent is a strong electrolyte.

The relative velocity slope, S_X, serves as a semi-quantitative estimate of the analyte peak shape within LTEM. The model has been implemented in the PeakMaster software (https://echmet.natur.cuni.cz/Software/PeakMaster) [31] that performs all necessary calculations and displays the

© 2018 WILEY-VCH Verlag GmbH & Co. KGaA, Weinheim

expected electropherogram. The utilization of PeakMaster for inspection of BGEs when using conductivity detection in CZE was proposed by the same group [32].

1.6 First-order nonlinear approximation to LTEM

A significant progress in the theory was made by Hruška in 2012 [8], who introduced a first-order nonlinear term into LTEM. By adopting an assumption that the peaks become immediately fully separated, the author arrived to a set of Burgers' equations,

$$\frac{\partial \tilde{w}_i}{\partial x} = -\frac{j}{\kappa_{BGE}}\left(\lambda_{0,i} + \frac{\partial \lambda_i}{\partial \tilde{w}_i}\tilde{w}_i\right)\frac{\partial \tilde{w}_i}{\partial x} + \delta_i \frac{\partial^2 \tilde{w}_i}{\partial x^2} \tag{20}$$

The equation is expressed in terms of wave-function perturbances,

$$\tilde{w}_i = w_i - w_{i,\mathrm{BGE}} \tag{21}$$

where $w_{i,\mathrm{BGE}}$ is a (constant) value of the original wave-function w_i in the BGE. We refer to this theory as the first-order nonlinear theory of electromigration (NLTEM). An interested reader can find a thorough analysis of NLTEM in the other paper published in this special issue [6]. In Eq. (20), $\lambda_{0,i}$ is the eigenvalue of matrix $\boldsymbol{M}_0$ (cf. Eq. (18)), which corresponds to the mobility of the peak, δ_i is a constant related to the diffusion of the peak, and the $\frac{\partial \lambda_i}{\partial \tilde{w}_i}$ derivative is another constant (evaluated for the composition of the BGE) responsible for the asymmetrical peak distortion that will be discussed later.

The solution to Eq. (20), with an initial condition of an infinitely narrow injected plug, is the so-called Haarhoff-Van der Linde (HVL) function [8]. The HVL function was introduced by Haarhof and Van der Linde as a solution to describe non-ideal (for our purposes, non-ideal conditions can be limited to accounting for the longitudinal diffusion), nonlinear GC [33] under the limiting conditions of injecting a negligible volume of a highly concentrated solute. It may be worth noticing that although both electrophoresis and chromatography are transport processes governed by mass conservation laws, the mathematical formulation of the problem solved by Haarhof and Van der Linde is far away from the governing equations of electrophoresis, Eq. (3). Thus, the application of the HVL solution to the EMD-dispersed peaks in electrophoresis is not obvious, although in 2001, Erny, Bergström, and Goodall made an observation that "the Haarhoff–Van der Linde peak function provides excellent fitting to the shapes of CZE peaks" [34, 35]. We will investigate the mathematical resemblance between the chromatographic and the CZE systems in more detail in the Discussion.

The HVL function can be expressed in either of two parameterizations [36]. The matter is further complicated by the fact that Erny et al. arbitrarily interchanged the spatial and the temporal (x and t) variables in the HVL function [36], while the original Haarhoff and Van der Linde solution applies to the spatial domain only. While using one or the other parameterization as well as switching from the spatial to the temporal domain does not introduce severe practical consequences, the move makes any theoretical discussion unnecessarily difficult. Therefore, we do not provide the HVL function in its parametric form here but stay with its spatiotemporal expression as an explicit solution to Eq. (20) [8],

$$HVL_i\ (x,t) = \frac{A_i}{\sqrt{4\pi\delta_i t}} \frac{\exp\left(-\frac{(x - v_{0,i}t)^2}{4\delta_i t}\right)}{\psi_i\left\{\frac{1}{\exp(\psi_i) - 1} + \frac{1}{2}\left[1 + \mathrm{erf}\left(\frac{x - v_{0,i}t}{\sqrt{4\delta_i t}}\right)\right]\right\}} \tag{22}$$

where A_i is the area of the peak in the spatial domain, i.e., its dimension is mol m^{-2}, $v_{0,i} = \lambda_{0,i}\ E_{BGE}$, and ψ_i is a distortion parameter. We recently introduced the software CEVal [37,38] that allows for easy evaluation of the HVL properties of an experimental peak from an electropherogram.

The HVL function can be viewed as a Gaussian distribution distorted by the denominator term that contains the distortion parameter ψ_i. NLTEM not only succeeded in demonstrating the relation between the HVL function and the EMD-dispersed peaks as suggested by Erny et al., but also revealed physical meaning of parameter ψ_i. To do so, the so-called electromigration mobility parameter was introduced as [8]

$$\mu_{EMD,i} = \frac{\partial \lambda_i}{\partial \tilde{w}_i}\quad W_i \tag{23}$$

In Eq. (23), λ_i is an eigenvalue of matrix $\boldsymbol{M}_0$, so that the term $\frac{\partial \lambda_i}{\partial \tilde{w}_i}$ is the derivative of that eigenvalue with respect to the wave-function disturbance, $\tilde{w}_i$, evaluated from matrix $\boldsymbol{M}_0$ at the composition of the BGE, $\vec{\boldsymbol{C}}_{BGE}$. ΔW_i is a value of this disturbance introduced by the initial conditions. Noticeably, although the wave, $\tilde{w}_i$, develops in time, the quantities $\frac{\partial \lambda_i}{\partial \tilde{w}_i}$ and ΔW_i are fixed by the initial conditions. Consequently, $\mu_{EMD,i}$, is also a constant characteristic for the given BGE and the wave (analyte or system peak), $\tilde{w}_i$.

In the frame of LTEM, the eigenvalue λ_i corresponds to the mobility of the analyte. Thus, Eq. (23) resembles the definitions of the relative velocity slope, S_X, or the assumed linear dependency of the analyte velocity on its own concentration as expressed by the EMD constant, Eq. (12). In their later work concerning electromigration in EKC systems [38, 39], the authors introduced the so-called nonlinear electromigration velocity slope as a generalized measure of EMD for an analyte peak. The parameter is defined as

$$S_{EMD,A} = \frac{\mu_{EMD,A}}{\Delta C_A} \tag{24}$$

where ΔC_A is the injected concentration of the analyte. We will devote more attention to all these parameters further in this paper. As for now, we complete our discussion on NLTEM with the relationship between the electromigration mobility, $\mu_{EMD,i}$, and the distortion parameter of the HVL function, ψ_i, which reads [8],

$$\psi_i = -E_{BGE}\frac{\mu_{EMD,i}}{2\delta_i} \tag{25}$$

© 2018 WILEY-VCH Verlag GmbH & Co. KGaA, Weinheim

Parameter ψ_i is proportional to parameter $a_{3\delta}$ in the δ-parameterization of the HVL function (https://echmet.natur.cuni.cz/Software/CEVal) in the spatial domain (cf. Eq. (22) and refs. 8, 38). Although not explicitly stated in the original paper [8], parameter ψ_i is somewhat normalized per unit length, so that

$$a_{3\delta} = \psi_i \; L \tag{26}$$

where L is a length of the injection plug.

Finally, the HVL function results as a solution to Burgers' equation, Eq. (20), only under the initial condition of an infinitesimally narrow injection plug (the Dirac distribution). A more realistic picture can be obtained when a rectangular plug profile is considered as the initial condition. Under such conditions, the so-called HVLR function results [8]. In contrast to the HVL function, the HVLR function may exhibit a plateau at its maximum that originates from the rectangular initial profile. As the peak develops in time, the plateau shortens until it disappears completely. We will explore transition of an HVLR peak distribution into an HVL peak distribution later in this paper.

2 Theory and Discussion

2.1 From the Linear Theory of Electromigration Approach to Mikker's Equation

LTEM, NLTEM, and Mikker's solution can be considered as the most fundamental approaches to investigating peak development in CZE. We will further refer to Mikkers' solution as the nonlinear electromigration model (NEM), which should not be mistaken for the first-order nonlinear approximation to the linear model of electromigration (NLTEM); we shall always use the NLTEM or NEM acronyms to clearly differentiate between the two.

LTEM provides only positions (and amplitudes, cf. [40]) of system and analyte peaks. NLTEM adds information on peak distribution similarly to NEM. The way NLTEM is formulated, however, seems very different from NEM originally solved by Mikkers. In this section, we provide the missing link between LTEM and NEM. In contrast to the Introduction, in this section, we use numbers as indexes for the constituents (either analytes or BGE components), this allows us to consider more than one analyte in the system and thus extend the theory to co-migrating analytes in our future work.

We consider an electrophoretic system that consists of N_A analytes, constituents 1, 2, …, N_A, and $N - N_A$ constituents of the BGE, constituents $N_A + 1$, …, N. According to LTEM, the analytes occupy N_A of the total of N zones (traveling waves) in the capillary. We base our derivation on the condition that all system zones get immediately separated from all analyte zones. This condition is never completely accomplished in reality. However, it is the same, and in a sense weaker, requirement than the immediate separation of every single zone from each other as adopted by NLTEM. The interaction among analyte zones (but not among system zones or among analyte and system zones) can be preserved due to a special structure of matrix $\boldsymbol{M}_0$ and, consequently, matrices $\boldsymbol{Q}_L$ and $\boldsymbol{Q}_R$.

Each row of matrix $\boldsymbol{M}$ in general, and $\boldsymbol{M}_0$ in particular, corresponds to one PDE describing the spatiotemporal development of one component in the system. Let an A-th component be an analyte. It can be shown (publication with a general proof is in preparation, for special cases cf., e.g., refs. 27, 31, 39) that the A-th row of matrix $\boldsymbol{M}_0$ has always a unique structure consisting of zeros everywhere, except one element, which is equal to the effective mobility of the analyte, $\mu_{eff,\,A}$. After the diagonalization procedure, this effective mobility becomes the eigenvalue stored in matrix $\boldsymbol{\Lambda}$. Although a set of eigenvalues is unordered, we can purposely order diagonal elements of matrix $\boldsymbol{\Lambda}$ in such a way that its A-th row contains the eigenvalue, $\lambda_{0,A} = \mu_{eff,A}$. This row has its counterparts in the A-th rows of matrices $\boldsymbol{Q}_L$ and $\boldsymbol{Q}_R$,

$$\begin{aligned} &(\boldsymbol{Q}_L)_A: \;\; (Q_L)_{Ai} = \delta_{Ai} \;\; = \begin{cases} 1, & i = A \\ 0, & i \neq A \end{cases} \\ &(\boldsymbol{Q}_R)_A: \;\; (Q_R)_{Ai} = \delta_{Ai} \end{aligned} \tag{27}$$

Using Eq. [17], it is seen that the A-th wave-function isomposed as

$$w_A = \sum_{i=1}^{N} (Q_L)_{Ai} c_i \;\; = \sum_{i=1}^{N} \delta_{Ai} c_i \;\; = c_A \tag{28}$$

This allows us to identify the A-th wave-function with the A-th (analyte) concentration profile. However, the same strategy cannot be adopted for system zones for which the corresponding wave function cannot be related to a unique constituent in the system. All elements in the corresponding rows of matrices $\boldsymbol{Q}_L$ and $\boldsymbol{Q}_R$ (cf. Eqs. (27) and (28)) generally differ from zero for system zones.

Above, we borrowed the main ideas of LTEM in order to distinguish the analyte peaks from the system peaks and to show that the analyte peaks are described with a single wave function that can be identified with the concentration profile of the actual analyte. Next, we focus on the development of the concentration profiles of the analytes. In contrast to NLTEM, we will keep the full nonlinearity in the electromigration term, Eq. (3), albeit disregarding the diffusion term, similarly as NEM does.

The primary source of nonlinearity is hidden in the conductivity term in the denominator of the electromigration term, Eq. (3). Thus, the key step in solving this problem is to first find out how conductivity changes with the concentration profile of the analyte inside the analyte peak. This was achieved through utilizing the KRF for strong electrolytes by Mikkers [15] and the generalized KRF for univalent weak electrolytes by Šustáček et al. [21]. The solution for the univalent weak electrolytes further requires that the pH stays constant within the sample zone. LTEM allows us to formulate the solution in a more general way, although we will see that the requirement of a constant pH persists.

The conductivity profile within the sample zone is given by Eq. (4), i.e., it depends on the concentrations of all forms of

© 2018 WILEY-VCH Verlag GmbH & Co. KGaA, Weinheim

all constituents. We express the concentration of every form as

$$c_{i,z} = h_{i,z}\ c_i \tag{29}$$

where $h_{i,z} \equiv h_{i,z}(c_H)$ are coefficients introduced in the context of LTEM [31]. Although not stated explicitly in the original paper, it is seen from Eq. (29) that coefficient $h_{i,z}$ equals the molar fractions of the ionic form $c_{i,z}$ with respect to their constituent, c_i. Conductivity thus takes the form of

$$\kappa = F\left(\sum_{i=1}^{N}\sum_{z=n_i}^{p_i} z\mu_{i,z}h_{i,z}c_i + \mu_H c_H - \mu_{OH}c_{OH}\right) \tag{30}$$

where every constituent concentration, be it a BGE constituent or an analyte, can be expressed in terms of the wave-functions, Eq. (17),

$$c_i = \sum_{j=1}^{N}(Q_R)_{ij}w_j \tag{31}$$

Since we require the system peaks to be separated from the analyte peaks, all system wave-functions, $w_{j>N_A}$, equal zero in the zone(s) of the analyte(s) so that only the terms $j \leq N_A$ remain in the summation, Eq. (31). Simultaneously, $w_{j\leq N_A} = c_j$ applies due to Eq. (28). Thus, we arrive at,

$$\kappa = F\left(\sum_{i=1}^{N}\sum_{z=n_i}^{p_i} z\mu_{i,z}h_{i,z}\left(C_i + \sum_{j=1}^{N_A}(Q_R)_{ij}c_j\right) + \mu_H c_H - \mu_{OH}c_{OH}\right) \tag{32}$$

where C_i is the concentration of the i-th constituent in the BGE.

Up to this point, no approximation has been made apart from the separation of the analyte and system zones. To proceed further toward the form of NEM, Eq. (9), we need to extract the summation over the concentrations of the analytes, c_j, out of the conductivity term. To do so, we split conductivity into two parts,

$$\kappa = \kappa_{BGE} + \sum_{j=1}^{N_A}\kappa_j c_j \tag{33}$$

where

$$\kappa_j = F\sum_{i=1}^{N}\sum_{z=n_i}^{p_i} z\mu_{i,z}h_{i,z}(Q_R)_{ij} \tag{34}$$

The quantity κ_j has a dimension of conductivity per concentration, i.e., Sm^2mol^{-1}. In order to arrive at Eq. (34), we had to assume that pH is constant within the analyte(s) zone(s) and is equal to that of the BGE. This assumption allows us, first, to exclude the H_3O^+ and OH^- ions from the additional term to κ_{BGE}, and second, to fix the coefficients (molar fractions) $h_{i,z}$ to the same values in both the κ_{BGE} and κ_j terms in Eq. (33) (cf. Eq. (32)). In this way, quantity κ_j becomes constant and is defined by the composition of the BGE. We would like to mention explicitly that in this treatment the ionic strength (IS) effects are neglected (as in all of the formerly published approaches).

The effective mobility in the numerator of the electromigration term, Eq. (3), is a secondary source of the nonlinearity. However, the requirement of a constant pH profile along with the neglection of the IS effects essentially fix the effective mobility(ies) of the analyte(s) within the zone to a constant value, too. Thus, the electromigration terms, Eq. (3), form a set of N_A coupled quasilinear partial differential equations for the development of the waves of the analytes

$$\frac{\partial c_i(x,t)}{\partial t} + \frac{\partial}{\partial x}\left(\frac{v_{eff,i}c_i(x,t)}{1+\sum_{j=1}^{N_A}\frac{\kappa_j}{\kappa_{BGE}}c_j(x,t)}\right) = 0 \qquad i = 1,\ldots,N_A \tag{35}$$

where quantities $v_{eff,i}$, κ_j, and κ_{BGE} are all constants given by the BGE environment and the equations are coupled solely by means of the analyte concentrations, c_j.

In the case of only one analyte, the set of equations, Eq. (35), is replaced by a single quasilinear partial differential equation

$$\frac{\partial c_A(x,t)}{\partial t} + \frac{\partial}{\partial x}\left(\frac{v_{eff,A}c_A(x,t)}{1+\frac{\kappa_A}{\kappa_{BGE}}c_A(x,t)}\right) = 0 \tag{36}$$

This equation has to be compared with NEM, Eq. (9). From a mathematical point of view, both equations are the same: the role of NEM constant a in Eq. (9) is played by the ratio $(-\kappa_A/\kappa_{BGE})$. Since κ_{BGE} is always a positive number, the sign of parameter κ_A thus determines whether the peak will be fronting or tailing. Considering strong electrolytes only, it can be shown that this ratio is exactly equal to NEM constant a. However, Eq. (36) is slightly more general than Eq. (9). Adoption of the basic ideas of LTEM allowed us to arrive at Eq. (36) without the need to employ the KRF or any similar conservation law. Thus, we have shown that the assumption of a constant pH is the only requirement to maintain validity of Mikker's solution to NEM, even for systems where any such conservation law is difficult or even impossible to formulate.

2.2 Similarities between zone propagation in chromatography and CZE

Interestingly, a similar kind of equation has been known in LC since 1939 when the first attempts to formulate a mathematical description of the ideal model of chromatography for a single component were carried out by Wicke [41]. In 1943, these efforts were completed by DeVault [42] who arrived at the following equation,

$$\frac{\partial c}{\partial t} + \frac{1-\epsilon}{\epsilon}\frac{\partial q}{\partial t} + u\ \frac{\partial c}{\partial x} = 0 \tag{37}$$

Here, ϵ is the total porosity of the column packing material, u is the velocity of mobile phase, c is the concentration

© 2018 WILEY-VCH Verlag GmbH & Co. KGaA, Weinheim

of the analyte in the mobile phase, and q is the concentration of the analyte in the stationary phase. It took almost 30 years until Rhee et al. gave a rigorous solution to Eq. (37) using the method of characteristics and the shock theory in the special case of a Langmuir isotherm [43].

In the case of a Langmuir isotherm,

$$q = \frac{N_b K c}{1 + K c} \tag{38}$$

Equation (37) takes the form of [43]

$$\frac{\partial c}{\partial t} + \frac{1-\epsilon}{\epsilon}\frac{\partial}{\partial t}\left(\frac{N_b K c}{1 + K c}\right) + u\ \frac{\partial c}{\partial x} = 0 \tag{39}$$

where N_b is the concentration of binding sites in the stationary phase and K is the adsorption constant. We can see that eq. (39) closely resembles NEM, Eq. (9) or (36). The first term $\partial c/\partial t$ is the same in both LC and the NEM equations: it accounts for the accumulation of the analyte in the mobile phase and in the unperturbed BGE, respectively. The second term in Eq. (39) accounts for the accumulation of the analyte in the stationary phase and, from a physical point of view, has no counterpart in CZE. The third term in Eq. (39) and the second term in the NEM model account for the movement of the analyte along the column: by convection in LC and along the capillary due to electrophoresis in CZE, respectively.

It is likely only a matter of chance that the movement of ions in NEM in electrophoresis is described in a way that is mathematically identical to the accumulation of an analyte in a stationary phase under Langmuir isotherm conditions in LC. In spite of this rather provocative resemblance, we did not find any meaningful reinterpretation of the electrophoretic process in terms of the chromatographic one, or vice versa. Any such comparison is particularly uneasy due to the fact that the ratio $(\frac{\kappa_j}{\kappa_{BGE}})$, i.e., parameter $(-a)$ in NEM, that plays a role of the adsorption constant K in LC, Eq. (39), attains both positive and negative values. However, this lucky coincidence allows us to utilize the formalism developed in the field of chromatography and adopt it to CZE.

2.3 Description of the solution to NEM

For a special choice of initial and boundary conditions, i.e., a rectangular-shape sample zone injected into the capillary at time $t = 0$ s, it is possible to find an analytical solution to Eq. (36). The solution is, indeed, identical to that provided earlier by Mikkers [15]. However, due to the aforementioned connection between chromatography and CZE, we can discuss the solution in a more contemporary fashion. Consequently, we will briefly outline the most significant characteristics of the solution itself rather than going into details of the mathematical theory behind it. An interested reader may find more on quasilinear partial differential equations in the following references [44, 45].

It is a significant feature of quasilinear partial differential equations that they allow discontinuities in dependent variables, i.e., concentrations in our case. Even if one starts with a continuous initial condition, a discontinuity in concentration may develop after some time. This discontinuity is called shock in the context of the mathematical theory of quasilinear partial differential equations. A typical solution of NEM, therefore, is not a smooth wave as, e.g., in the case of the NLTEM solution, but rather a discontinuous and only piecewise differentiable function. The discontinuous character of the solution naturally stems from the fact that Eq. (36) omits all diffusional effects.

In the following we will assume a model case with $\kappa_A < 0$, which corresponds to the sharpening front of the peak. The solution is best to explain in terms of an x–t diagram shown in Fig. 2A. (An interesting example of using x–t diagrams for advanced understanding of electrophoretical processes can be found, e.g., in ref. 46 by Gebauer et al. from 1990's.) In Fig. 2B, we present the solution at a fixed time $t = 1$ s (horizontal line in Fig. 2A). A general solution consists of up to three regions (X), (Y), and (Z). Region (Y) is a trivial case of zero concentration, i.e., a region not yet reached by or already left by the analyte peak. In contrast to a continuous solution, the peak distribution does not formally spread to

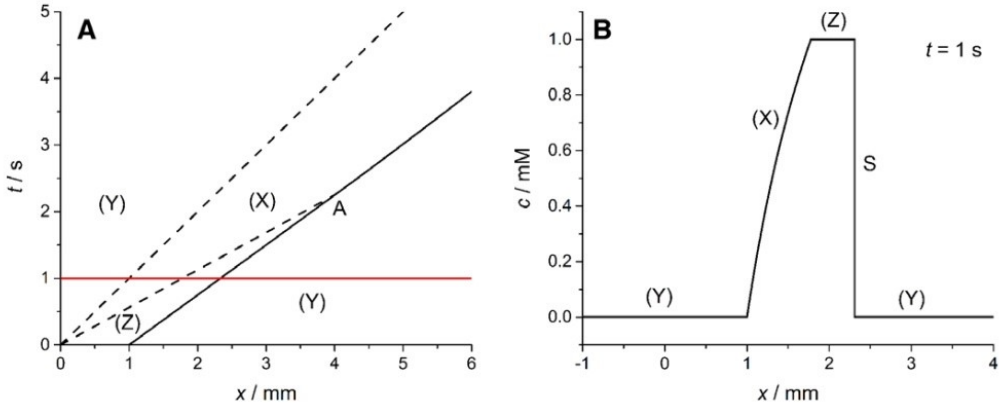


Figure 2. A schematic x–t diagram (panel A) and the related concentration profile (panel B). Data for $\kappa_A < 0$, rectangular initial sample plug ranging from 0 to 1 mm. The concentration profile is depicted at time 1 s (red horizontal line in panel A). Point A in panel A depicts the critical time, t_A, when the region (Z) disappears. Lines (X), (Y), and (Z) in panel B corresponds to the respective regions in panel A; line S in panel B is the shock. See text (Section 2.3 Description of the solution to NEM) for explanation of the regions (X), (Y), (Z).

© 2018 WILEY-VCH Verlag GmbH & Co. KGaA, Weinheim

infinity but is constrained by the two, left dashed and right solid, lines in the x–t diagram (equivalent to region δ in Fig. 1). Region (Z) can be viewed as a portion of the initial injection plug that has so far survived the EMD process. As EMD continues to act on the peak, this region narrows as indicated by the dashed diagonal line in the x–t diagram, which defines region (X). For coordinates (x, t) lying inside region (X) the analytical formula for concentration of the analyte reads

$$c_A\ (x,t) = \frac{\kappa_{\mathrm{BGE}}}{\kappa_A}\ \left(\sqrt{\frac{t v_{eff,A}}{x}} - 1\right) \tag{40}$$

Notice, that the concentration has a units of mol/m^3 as expected due to the units of the quantity κ_A, Eq. (34). When compared to the original solution [15, 17], it can be noticed that an extra term "$\Delta l_0(\frac{c_B^{S*}}{c_B^S} - 1)$" appears therein for the case of spatially tailing peaks. This term, however, does not follow from the mathematical solution to NEM. It was artificially introduced to account for a presumed stacking of the sample zone due to a mismatch in the conductivities of the injected plug and the BGE. This effect can be seen as an interaction of the sample wave function with the injection system wave function, which is purposely omitted herein.

At a certain time, t_A, indicated by point A in Fig. 2A, the smooth concentration profile catches up with the shock boundary and the concentration plateau (Z) disappears. Because the shock boundary S is not penetrable for the analyte, the front edge of region (X) cannot overtake it. Instead, they both join together. Velocities of both edges of region (X), $v_{\mathrm{bottom}}^{(\mathrm{X})}$ (the left dashed line in Fig. 2A) and $v_{\mathrm{top}}^{(\mathrm{X})}$ (the diagonal dashed line in Fig. 2A), as well as that of the shock boundary S, v_{S} (the right solid line in Fig. 2A), are summarized in Table 1. The ordering of the velocities is always $v_{\mathrm{bottom}}^{(\mathrm{X})} < v_{\mathrm{S}} < v_{\mathrm{top}}^{(\mathrm{X})}$ for our case of $\kappa_A < 0$ and $v_{\mathrm{top}}^{(\mathrm{X})} < v_{\mathrm{S}} < v_{\mathrm{bottom}}^{(\mathrm{X})}$ for the alternative case of $\kappa_A > 0$. Notice that $v_{\mathrm{bottom}}^{(\mathrm{X})} = v_{eff,A}$ for the entire separation process. This point thus migrates with the expected mobility of the analyte in the BGE.

It can be shown that the velocity of the shock, v_{S}, is fully equivalent to the velocity of the sharp moving boundary as results from the MBE theory, Eq. (8), under the therein treated conditions of strong electrolyte ions. Finally, Eq. (33) clearly shows that inside the analyte zone, conductivity is directly proportional to the analyte concentration under constant pH conditions. Since the velocity is the inverse of conductivity, the assumption of the velocity be directly proportional to the analyte concentration expressed by the EMD constant, k_{EMD},

Table 1. Velocities of both edges of the region (X) as well as of the shock boundary S. cf. Fig. 2

	$(0, t_A)$	(t_A, ∞)
$v_{\mathrm{bottom}}^{(\mathrm{X})}$	$v_{eff,A}$	$v_{eff,A}$
$v_{\mathrm{top}}^{(\mathrm{X})}$	$\frac{v_{eff,A}}{(1+\frac{\kappa_A}{\kappa_{\mathrm{BGE}}} c_{A,0})^2}$	—
v_{S}	$\frac{v_{eff,A}}{1+\frac{\kappa_A}{\kappa_{\mathrm{BGE}}} c_{A,0}}$	$v_1[1 - \frac{c_{A,0}}{(\frac{\kappa_{\mathrm{BGE}}}{\kappa_A} + c_{A,0})\sqrt{\frac{t}{t_A}}}]$

Eq. (12), can only be approximate even in the simplest systems. As long as pH effects are negligible, validity of such approximation is constrained by a condition of $\frac{|\kappa_A|}{\kappa_{\mathrm{BGE}}} c_A << 1$ as can be seen from Eq. (41) below.

2.4 Comparison between NEM and NLTEM

We completely discarded the diffusion effects in NEM, while keeping the full nonlinearity of electromigration under the assumption of a constant pH profile. Diffusion effects and pH effects, on the other hand, are partially covered by NLTEM, at the expense of approximating nonlinearity by a first-order Taylor expansion term only. In this section, we will focus on the relation between the NLTEM and the NEM models.

When the analyte concentration is small enough, i.e., $\frac{|\kappa_A|}{\kappa_{\mathrm{BGE}}} c_A << 1$, we can expand the denominator in NEM, Eq. (36), into a Taylor series and keep only the first two terms,

$$\begin{aligned} &\frac{\partial}{\partial x}\left(\frac{v_{eff,A} c_A(x,t)}{1+\frac{\kappa_A}{\kappa_{\mathrm{BGE}}} c_A(x,t)}\right) \\ &\cong \frac{\partial}{\partial x}\left[v_{eff,A} c_A(x,t)\left(1 - \frac{\kappa_A}{\kappa_{\mathrm{BGE}}} c_A(x,t) + \ldots\right)\right] \\ &= \left(v_{eff,A} - 2 v_{eff,A}\frac{\kappa_A}{\kappa_{\mathrm{BGE}}} c_A(x,t)\right)\ \frac{\partial c_A(x,t)}{\partial x} \end{aligned} \tag{41}$$

This expression is to be compared with the corresponding term in NLTEM, Eq. (20). Due to the unique properties of the analyte zone (cf. Section 2.1 From the Linear Theory of Electromigration Approach to Mikker's Equation), the $\frac{\partial \lambda_A}{\partial \tilde{w}_A}$ derivative in Burgers' equation can be expressed as

$$\frac{\partial \lambda_A}{\partial \tilde{w}_A} = \left(\frac{\partial \mu_{A,eff}}{\partial c_A} - 2\frac{\mu_{A,eff}}{\kappa_{\mathrm{BGE}}}\frac{\partial \kappa}{\partial c_A}\right) \tag{42}$$

which yields,

$$\begin{aligned} &\frac{j}{\kappa_{BGE}}\left(\lambda_{0,A} + \frac{\partial \lambda_A}{\partial \tilde{w}_A}\tilde{w}_A\right) \\ &= \left[v_{eff,A} + \left(\frac{\partial v_{eff,A}}{\partial c_A} - 2\frac{v_{eff,A}}{\kappa_{\mathrm{BGE}}}\frac{\partial \kappa}{\partial c_A}\right) c_A(x,t)\right]\ \frac{\partial c_A(x,t)}{\partial x} \end{aligned} \tag{43}$$

Now we can approach comparison of Eq. (41), representing NEM, and Eq. (43), representing NLTEM. Obviously, the first terms in the parentheses, Eqs. (41) and (43), are equal. The remaining terms in the parentheses are not equal because the two equations are based on slightly different approximations. Particularly, the restriction of a constant pH is not limiting NLTEM, although NLTEM accounts only for the first-order approximations of the related dependencies. If we apply the same requirement of a constant pH to NLTEM, the term $\frac{\partial \mu_{eff,A}}{\partial c_A}$ in Eq. (43) disappears and the derivative $\frac{\partial \kappa}{\partial c_A}$ turns into κ_A.

This analysis shows that under the assumption of a constant pH, NLTEM is—up to diffusion-related effects—a first-order approximation to NEM. If the requirement of a constant pH profile within the sample zone cannot be fulfilled, NEM loses its validity and the full nonlinearity of the solution

© 2018 WILEY-VCH Verlag GmbH & Co. KGaA, Weinheim

cannot (as yet) be handled. Then, NLTEM is the only approximation to the full nonlinear solution currently available.

2.5 The dynamics of EMD

The critical time, t_A, point A in Fig. 2A, when the top of the peak, region (*Z*), can be easily calculated from the initial width of the injection plug and the difference in the velocities v_S and v_{top},

$$t_A = \frac{L}{|v_{\text{top}} - v_{\text{S}}|} \tag{44}$$

where L is the length of the sample plug. In 1990's, the critical time was formulated by Gebauer et al. [47, 48]. In that paper, the authors also considered readjustment of the analyte concentration, which occurs when the analyte leaves the injection zone and is caused by conductivity mismatch between the injection zone and the zone of unperturbed BGE. Equation (44), with the quantities v_{top} and v_S obtained from Table 1, does not take this readjustment into account (cf. also discussion below Eq. (40)). After the critical time has been reached, the concentration at the shock boundary starts to decline. Table 1 shows that the velocity, v_s, depends on the concentration at the shock boundary and, consequently, the shock boundary slows down, reaching the velocity $v_{eff,A}$ after an infinite time, $\lim_{t\to\infty} v_{\text{s}} = v_{eff,A}$ (when the peak simultaneously becomes infinitely dispersed).

In the case of a rectangular initial sample zone, the solution to NLTEM is the HVLR function while in the case of an infinitely narrow initial sample zone, the solution is the HVL function (cf. Section 1.6 First-order nonlinear approximation to LTEM). In spite of the fact that the initial condition of a rectangular pulse is much closer to the real experimental conditions, it became a common practice to assign the HVL distribution to the EMD-dispersed peaks in CZE (cf. *ibid*). As a matter of fact, the HVLR function becomes overparametrized upon disappearance of its initial plateau region (corresponding to region (*Z*) in Fig. 2), and thus cannot be used for fitting standard experimental peaks. On the other hand, we did not succeed in providing a direct mathematical proof of a presumed convergence of the HVLR distribution to the HVL distribution with increasing time.

Instead, we show in Fig. 3 a schematic *x*–*t* diagrams for two individual peaks evolved from the rectangular initial sample zones. The two cases differ in the width L of the initial sample plugs, but both plugs have the same area. This means that the value of the product of initial concentration and width, $c_{A,0}L$, is preserved. It is seen that for a series of peaks with a given area it holds that from the point when both peaks become triangular, indicated by point (A1), the *x*–*t* diagrams overlap. The overlapping *x*–*t* diagrams mean that the shapes of both peaks are exactly the same. This suggests that two peaks of the same area, albeit of different initial widths, are indistinguishable from each other after the initial concentration plateau of the wider peak disappears. We can generalize this observation to all peaks of a given area,

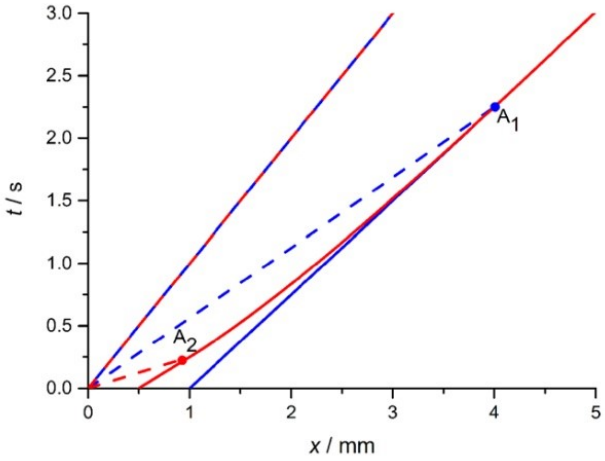


Figure 3. Schematic *x*–*t* diagrams evolved from rectangular initial sample plug of different widths $L_1 = 2L_2$, but the same area $c_{A,0|1}\ L_1 = c_{A,0|2}\ L_2$. Blue lines correspond to a rectangular initial sample plug ranging from 0 to 1 mm, whereas red lines correspond to a rectangular initial sample plug ranging from 0 to 0.5 mm. The former (blue) *x*–*t* diagram is identical to that depicted in Fig. 2. Point A1 is the point A in panel A in Fig. 2, i.e., the critical time t_A for the wider peak. Point A2 is the critical time t_A for the narrower peak.

including an infinitely narrow initial sample zone corresponding to the Dirac initial distribution. In the frame of the above discussion (cf. 2.4 Comparison between NEM and NLTEM) it is reasonable to expect that the convergence of peaks predicted by NEM can serve as an indirect justification of the convergence of the HVLR distribution to the HVL distribution. The critical time, t_A, Eq. (44), is then an estimate of the time when the peak takes the shape of the HVL function.

In order to provide more justification for our statements about the HVLR to HVL convergence, we used Simul 5, a simulation freeware for CE developed in our laboratory (https://echmet.natur.cuni.cz/Software/Simul) [49]. The two-component BGE is composed of a 6 mM strong univalent base and a 12 mM weak univalent acid with pK_a 7. The sample contains one analyte, which is a strong base, dissolved in the BGE. The electrophoretic mobilities of the BGE constituents are: $\mu_{\text{base}} = 20 \cdot 10^{-9}\ \text{m}^2\text{V}^{-1}\text{s}^{-1}$, $\mu_{\text{acid}} = -40 \cdot 10^{-9}\ \text{m}^2\text{V}^{-1}\text{s}^{-1}$. The electrophoretic mobility of the analyte is: $\mu_{\text{analyte}} = 10 \cdot 10^{-9}\ \text{m}^2\text{V}^{-1}\text{s}^{-1}$. The area of all peaks was set to 1 mM mm.

In order to establish a criterion whether a peak is well described by the HVL function, we took advantage of the fact that parameter $a_{3\delta}$ of the HVL function is fully set by the initial conditions and thus should result in the same value irrespectively of the spatiotemporal development of the peak (cf. Section 2.7 Measuring the extent of EMD). We monitored parameter $a_{3\delta}$ obtained by fitting the HVL function to the peak distribution propagating through the capillary until the value of this parameter leveled out. This point in time was chosen as the time when the HVLR function converged to the HVL function. A representative example of this procedure is depicted in Fig. 4B. A comparison of the HVLR to HVL

© 2018 WILEY-VCH Verlag GmbH & Co. KGaA, Weinheim

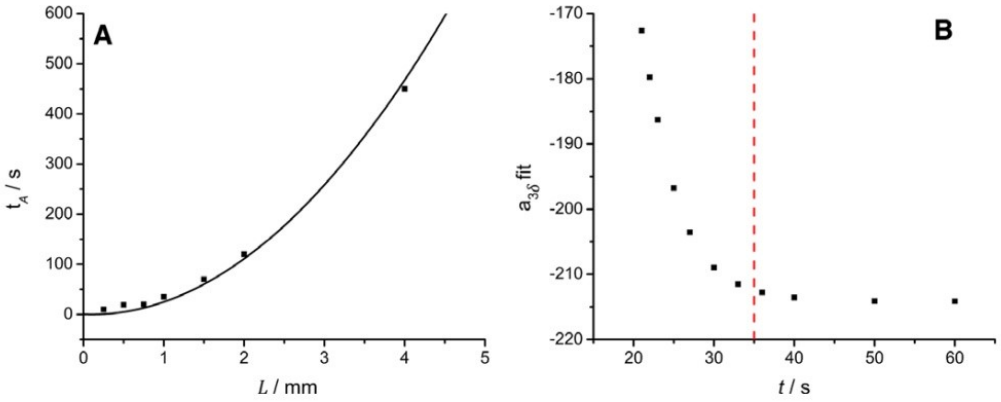


Figure 4. Panel A) A comparison between observed (points) and predicted (line) critical times, t_A, of the HVLR to HVL convergence. Points obtained by means of computer simulation, *cf.* panel B and text (Section 2.5 The dynamics of EMD). Line calculation based on NEM, Eq. (44). Panel B) A representative example of convergence of the $a_{3\delta}$ parameter to a constant value. Initial sample plug width of 1 mm (the same conditions as in Fig. 2). $a_{3\delta}$ parameter was obtained by applying HVL fit on consecutive simulated peak profiles as the peak was developing in the capillary. Red dashed vertical line indicates visual reading of the HVLR to HVL convergence point, i.e., the critical time, t_A, at $L = 1$ **mm** in panel A.

convergence times obtained this way with their predicted values by eq. (44) is given in Fig. 4A. Excellent agreement was observed between the predictions and the simulations.

It is, however, important to recall that Eq. (44) applies only under the assumption of a constant pH profile. Otherwise, NEM may underestimate or overestimate the extent of electromigration dispersion, if $\frac{\partial \mu_{eff,A}}{\partial c_A}$ and $-2\frac{\mu_{eff,A}}{\kappa_{BGE}}\frac{\partial \kappa}{\partial c_A}$ have the same or opposite signs, respectively, cf. Eq. (43). It may be anticipated that our discussion actually provides a basis for correcting NEM for these effects. Unfortunately though, this is not the case and we did not find a way to provide a solid estimate about the time of the HVLR to HVL convergence if the preconditions for the validity of NEM, Eq. (36), are not satisfied.

2.6 The effective mobility

The effective mobility of the peak is a typical characteristic of its electromigration. Nevertheless, the idea of the "peak mobility" has no physical meaning since the velocity of the concentration distribution must be distinguished from the velocity of the molecules the distribution consists of. This possibly not particularly intuitive phenomenon is well explained in the case of chromatography, cf. Chapter 7 in ref. 45. Thus, the question is not what the mobility of the peak is, but how an observed velocity of a certain fragment of the peak distribution relates to the effective mobility of the analyte.

Equation (8) showed that the self-sharpening boundary in MBE, equivalent to the shock boundary in CZE, moves with the effective velocity of the analyte inside its own plug. This can be utilized in MBE measurements for the determination of the effective mobilities of the constituents and their forms provided that the conductivity (electric field) can be determined inside the analyte zone adjacent to the self-sharpening boundary [5]. Although the shock velocity, v_S, behaves in the same way in CZE, the same strategy is not applicable here due to the gradual deceleration of the shock starting from the critical time, t_A. Instead, the velocity v_{bottom} was shown to equal the effective velocity of the analyte in the BGE. Determination of the actual point corresponding to this velocity is, however, hindered by diffusion.

The best currently available approximation to that point is provided by NLTEM. Equation (22) reveals that the effective velocity, $v_{eff,A}$, can be observed as one of its fitting parameters when applied to the peak distribution (typically by fixing the variable x at the detector position and fitting over time as the independent variable). It can be shown that if the parameterized HVL function [36, 38] is applied to the peak distribution in the time domain without special consideration, as is the usual practice, the resulting a_1 parameter still provides the sought after position that corresponds to the effective velocity, $v_{eff,A}$. The only natural requirement is that the peak distribution has not changed within the time it takes the peak to pass through the detector.

Two more points are worth noticing. First the NEM concentration distribution, Eq. (40), results in a concave profile for tailing peaks and a convex profile for fronting peaks in the x domain (cf. Fig. 1). As the peak passes through the detector, the fronting/tailing perception interchanges but—rather interestingly—so does the concave/convex character of the NEM distribution. The HVL distribution, on the other hand, is perfectly anti-symmetrical with virtually convex tail in both tailing and fronting versions. Therefore, the HVL function can be expected to better fit the fronting peaks (in both the spatial and the temporal domain). In our experience, highly overloaded tailing peaks often resemble the NEM distribution Eq. (40) more closely, than the HVL distribution.

Second, the point of the peak distribution that moves with the velocity $v_{bottom} = v_{eff,A}$ differs in its starting position for tailing and fronting peaks. The former originates from the rear boundary of the sample plug, while the latter from the front boundary (in the spatial domain). Thus, peaks fronting

© 2018 WILEY-VCH Verlag GmbH & Co. KGaA, Weinheim

in the capillary (i.e., tailing in the detector trace) "reach" the detector by the distance of the injection plug earlier than expected. Although this distance is likely negligible in a classical CE setup, the fact that it is the product of $c_{A,0}L$ that governs the extent to which the peak is subjected to EMD-distortion advises us to prefer narrower injection plugs of higher concentration compared to the opposite possibility when detection limit is an issue and the effective mobility of an analyte is to be determined.

2.7 Measuring the extent of EMD

The dependency of the velocity inside the analyte zone on the presence of the analyte itself is characterized by the term $\frac{j}{\kappa_{BGE}} \frac{\partial \lambda_A}{\partial \bar{w}_A} = \frac{j}{\kappa_{BGE}} \frac{\partial \lambda_A}{\partial c_A}$. Notice that we did not replace variable λ_A with the effective mobility of the analyte, $\mu_{eff,A}$ in the derivative. Although the wording "derivative of eigenmobility with respect to analyte concentration c_i" was used in the original paper [8], the term "eigenmobility" should be understood strictly in the sense of the eigenvalue λ_i, not the actual mobility, $\lambda_{0,i}$, which then equals $\mu_{eff,A}$ in case of analyte zones. Equation (42) shows that the derivative consists of two contributions.

First, the actual effective mobility of the analyte may vary if the molar fractions of the analyte forms do not stay constant within the sample zone. This can be caused by pH changes in case of weak electrolyte analytes, as discussed in the Introduction (Section 1.4 Weak electrolytes and mobility slope measures). Alternatively, the same effect can be caused by any equilibria such as encountered, e.g., in EKC. This was clearly demonstrated by means of a theoretical analysis of the $S_{EMD,A}$ parameter accompanied with experiments and computer simulations in NLTEM, even for a fully dissociated analyte interacting with a neutral chiral selector [39, 40]. This additionally supports Svensson's notion about acid–base equilibria being not particularly different from complex formation equilibria in general [4] (cf. Section 1.2 Moving boundary electrophoresis). On the other hand, we failed in our attempts to extend NEM to general EKC systems. Such generalization would require that not only pH but also the molar fractions of all complexed forms stay constant within the sample plug, which (as yet) turned out not to be reasonably justifiable even in the simplest EKC systems.

Second, the electric field, which the analyte is exposed to, may vary due to changes in conductivity in the analyte zone. This, in turn, can be caused by the simple replacement of the BGE (co)-ions with the analyte ions, and possibly also by ongoing acid–base or general complexation equilibria. The former case is handled by NEM, Eq. (36). Then, the extent of EMD can be estimated from parameter κ_A, which can be linked to the mobility-match rules and prescribes a linear dependency of the velocity of the analyte peak distribution on the analyte concentration as discussed earlier. In the latter case of ongoing acid-base or complexation equilibria, the $\frac{\partial \kappa}{\partial c_A}$ derivative in Eq. (42) may not be constant and NEM can be invalidated.

All these contributions to EMD can be generally both synergic or antagonistic. Attempts have been made by several authors to find an appropriate descriptor of a tendency of an analyte peak to undergo EMD that would handle all these effects (cf. Section 1.4 Weak electrolytes and mobility slope measures and Section 1.6 First-order nonlinear approximation to LTEM). We suggest parameter $a_{3\delta}$ along with the $\frac{\partial \lambda_A}{\partial c_A}$ derivative as the best candidates. They both can be calculated based on the given combination of analyte and BGE from NLTEM. Consequently, though, the extent to which these two parameters reflect the reality depends on how close the first-order nonlinear approximation adopted by NLTEM to that reality is.

After the critical time, t_A, elapses, parameter $a_{3\delta}$ should be conserved in time and it controls the asymmetrical distortion of the peak. Therefore, the distortion itself stays constant in time as well, albeit the peak broadens and gradually diminishes. The sign of parameter $a_{3\delta}$ indicates whether a tailing or fronting peak results and its magnitude reveals how severe the distortion is. The parameter further depends on the sample load and the diffusion effects, and thus provides a more realistic picture of the final peak distribution compared to the parameters that are based on velocity slopes only.

The $\frac{\partial \lambda_A}{\partial c_A}$ derivative, on the other hand, is characteristic to the given combination of analyte and BGE and it embodies—to the first order approximation—the dependency of the analyte velocity on its own concentration in the BGE. Noticeably, the derivative is equivalent to the derivative $(\frac{dv_A}{dc_A})_{c_A \to 0}$, which forms the basis for the various "S" parameters, yet it is free of any additional effects. Therefore, the measure of EMD in a sample zone is best characterized by the $\frac{\partial \lambda_A}{\partial c_A}$ derivative, whereas the extent to which EMD manifests itself in the peak shape is given by parameter $a_{3\delta}$.

3 Concluding remarks

In the first part of this paper, we reviewed several approaches to understanding the dynamics of band shape (peak shape) development in CZE, then provided a thorough discussion on the theories and their outcomes in the second part. It was shown that NEM, as introduced by Mikkers et al. for strong electrolytes in 1979, can be extended to all ampholytic compounds provided that the pH profile remains constant within the sample plug, equal to that in the BGE. This was achieved through finding a connection between NEM and LTEM, the latter introduced by Štědrý et al.. A remarkable, yet likely accidental, mathematical resemblance between CZE and LC under the conditions of a constant pH profile and Langmuir isotherm, respectively, was additionally revealed. This resemblance allowed us to describe the outcome of NEM in a more modern fashion in the so-called x–t diagrams.

The x–t diagrams showed that, under a constant pH profile approximation, two peaks originating from two injection plugs of different plug lengths, L, although the same areas (i.e., different concentrations, $c_{0,A}$, so that the total sample load $c_{0,A}L$ is preserved) become indistinguishable from each

© 2018 WILEY-VCH Verlag GmbH & Co. KGaA, Weinheim

other after a certain "critical time", t_A. This suggests that the so-called HVLR peak distribution, that results from NLTEM for the realistic initial condition of a rectangular injection plug, should converge to the so-called HVL distribution that results from the same theory albeit under an infinite narrow injection plug approximation. The critical time, t_A, of the convergence can be predicted under the constant pH profile approximation, and it is believed that the HVLR to HVL convergence is preserved beyond this approximation, although the critical time is not known a priory in this case. These considerations provide a justification for using the HVL function to describe the peak distribution in CZE. In this way, the point of the peak distribution that moves with the mobility exactly equal to the effective mobility of the analyte in the BGE in question is determined.

If the constant pH profile approximation is not satisfied within the sample peak or additional equilibria take place, such as in EKC, the mobility of that specific point of the HVL distribution does not change. Instead, asymmetry of the distribution is affected. The asymmetry is additionally affected by a possible change in conductivity inside the analyte zone. We suggest two other parameters, $\frac{\partial \lambda_A}{\partial c_A}$ and $a_{3\delta}$, that result from NLTEM as the best candidates to describe these effects, altogether referred to as electromigration dispersion. These parameters depend on both of the $\frac{\partial \kappa}{\partial c_A}$ and $\frac{\partial \mu_{eff,A}}{\partial c_A}$ derivatives, which both are generally functions of pH in the simple CZE systems and may be functions of other complexation equilibria in general EKC systems. The $\frac{\partial \lambda_A}{\partial c_A}$ derivative serves as a measure of EMD in a sample zone in a given BGE, whereas the $a_{3\delta}$ parameter provides a measure of the extent to which EMD manifests itself in the absolute peak shape.

We are especially thankful to prof. Gyula Vigh, Texas A&M University, for his initiation of this research as well as his enduring interest in it, which resulted in hours of discussions and his reviewing the final version of this manuscript. We also thank Dr. Petr Gebauer, Ústav analytické chemie Akademie věd České republiky, Czech Republic, for providing us with a copy of the historical paper by Weber [2]. *This work has been supported by Czech Science Foundation, grant numbers 15–18424Y and 18–11776S, Charles University Grant Agency, grant no. GAUK 116217, and Charles University Research Centre, grant no. UNCE/SCI/014.*

The authors have declared no conflict of interest.

4 References

[1] Gaš, B., Štědrý, M., Kenndler, E., *Electrophoresis* 1997, *18*, 2123–2133.

[2] Kohlrausch, F., *Ann. Phys.* 1897, *62*, 209–239.

[3] Hartley, G.S., Moilliet, J. L., *Proc. R. Soc. London A* 1933, *140*, 141–158.

[4] Svensson, H, *Acta Chem. Scand.* 1948, *2*, 841–855.

[5] Alberty, R. A., *J. Am. Chem. Soc.* 1950, *72*, 2361–2367.

[6] Malý, M., Dovhunová, M., Dvořák, M., Gerlero, G. S., Kler, P. A., Hruška, V., Dubský, P., Generalized model of the linear theory of electromigration and its application to the electrokinetic chromatography: Theory and software PeakMaster 6 – next generation, Submitted to this special issue.

[7] Dubský, P., Dvořák, M., Ansorge, M., *Anal. Bioanal. Chem.* 2016, *408*, 8623–8641.

[8] Hruška, V., Riesová, M., Gaš, B., *Electrophoresis* 2012, *33*, 923–930.

[9] Mosher R.A., Saville D.A., Thormann W., Radola B.J. (Ed.), *The Dynamics of Electrophoresis*, VCH Verlagsgesellschaft GmbH, Weinheim 1992.

[10] Foret F., Křivánková L., Boček P., Radola, B.J. (Ed.), *Capillary Zone Electrophoresis*, VCH Verlagsgesellschaft GmbH, Weinheim 1993.

[11] Tiselius A., *Nova Acta Regiae Soc. Sci. Ups* 1930, Ser IV 7, *4*, 1–107.

[12] Weber, H., *Sitz. Preuss. Akad. Wiss.*, 1897, 936–946.

[13] Henry, D.C., Brittain, J., *J. Chem. Soc. Faraday Trans.* 1933, *29*, 798–815.

[14] Dole, V.P., *J. Am. Chem. Soc.* 1945, *67*, 1119–1126.

[15] Mikkers, F. E. P., Everaerts, F. M., Vergheggen, T. P. E. M., *J. Chromatogr.* 1979, *169*, 1–10.

[16] Thormann, W., *Electrophoresis* 1983,*4*, 383–390.

[17] Mikkers, F. E. P., *Anal. Chem.* 1999, *71*, 522–533.

[18] Gaš, B., Kenndler, E., *Electrophoresis* 2004, *25*, 3901–3912.

[19] Foret, F., Fanali, S., Ossicini, L., Boček, P., *J. Chromatogr. A* 1989, *470*, 299–308.

[20] Šustáček, V., Foret F., Boček P., *J. Chromatogr. A* 1991, *545*, 239–248.

[21] Xu, X., Kok, W. Th., Poppe, H., *J. Chromatogr. A* 1996, *742*, 211–227.

[22] Gebauer, P., Boček, P., *Anal. Chem.* 1997, *69*, 1557–1563.

[23] Hruška, V., Gaš, B., *Electrophoresis* 2007, *28*, 3–14.

[24] Dismukes, E. B., Alberty, R. A., *J. Am. Chem. Soc.* 1954, *76*, 191–197.

[25] Horká, M., Šlais, K., *Electrophoresis* 2000, *21*, 2814–2827.

[26] Štědrý, M., Jaroš, M., Gaš, B., *J. Chromatogr. A* 2002, *960*, 187–198.

[27] Poppe, H., *J. Chromatogr.* 1990, *506*, 45–60.

[28] Poppe, H., *Anal.Chem.* 1992, *64*, 1908–1919.

[29] Štědrý, M., Jaroš, M., Včeláková, K., Gaš, B., *Electrophoresis* 2003, *24*, 536–547.

[30] Štědrý, M., Jaroš, M., Hruška, V., Gaš, B., *Electrophoresis* 2004, *25*, 3071–3079.

[31] Jaroš, M., Hruška, V., Štědrý, M., Zusková, I., Gaš, B., *Electrophoresis* 2004, *25*, 3080–3085.

[32] Jaroš, M., Soga, T., van de Goor, T., Gaš, B., *Electrophoresis* 2005, *26*, 1948–1953.

[33] Haarhoff, P. C., Van der Linde, H. J., *Anal. Chem.* 1966, *38*, 573–582.

[34] Enry, G. L., Bergström, E. T., Goodall, D. M., *Anal. Chem.* 2001, *73*, 4862–4872.

[35] Erny, G. L., Bergström, E. T., Goodall, D. M., *J. Chromatogr. A* 2002, *959*, 229–239.

© 2018 WILEY-VCH Verlag GmbH & Co. KGaA, Weinheim

[36] Dubský, P., Dvořák, M., Müllerová, L., Gaš, B., *Electrophoresis* 2015, *36*, 655–661.

[37] Dubský, P., Ördögová, M., Malý, M., Riesová, M., *J. Chromatogr. A* 2016, *1445*, 158–165.

[38] Hruška, V., Svobodová, J., Beneš, M., Gaš, B., *J. Chromatogr. A* 2012, *1267*, 102–108.

[39] Beneš, M., Svobodová, J., Hruška, V., Dvořák, M., Zusková, I., Gaš, B., *J. Chromatogr. A* 2012, *1267*, 109–115.

[40] Hruška, V., Štědrý, M., Včeláková, K., Lokajová, J., Tesařová, E., Jaroš, M., Gaš, B., *Electrophoresis* 2006, *27*, 4610–4617.

[41] Wicke, E., *Kolliod Z.* 1939, *86*, 295–313.

[42] DeVault, D., *J. Am. Chem. Soc.* 1943, *65*, 532–540.

[43] Rhee, H.-K., Aris, R., Amundson, N. R., *Philos. Trans. R. Soc. London Ser A* 1970, *267*, 419–455.

[44] Rhee, H.-K., Aris, R., Amundson, N. R., *First-Order Partial Differential Equations – II. Theory and Application of Hyperbolic Systems of Quasilinear Equations*, Prentice-Hall, Englewood Cliffs, N. J. 1989.

[45] Guiochon G., Fellinger, A., Shirazi, D. G., Katti, A. M., *Fundamentals of preparative and nonlinear chromatography* 2nd ed., Elsevier Inc., San Diego 2006.

[46] Gebauer, P., Deml, M., Pospíchal, J., Boček, P., *Electrophoresis* 1990, *11*, 724–731.

[47] Gebauer, P., Thormann, W., Boček, P., *J. Chromatogr.* 1992, *608*, 47–57.

[48] Křivánková, L., Gebauer, P., Thormann, W., Mosher, R.A., Boček, P., *J. Chromatogr.* 1993, *638*, 119–135.

[49] Hruška, V., Jaroš, M., Gaš, B., *Electrophoresis* 2006, *27*, 984–991.

© 2018 WILEY-VCH Verlag GmbH & Co. KGaA, Weinheim

Publikace VI

The dynamics of band (peak) shape development in capillary zone electrophoresis in the case of two co-migrating analytes: the displacement and the tag-along effects

Martin Dvořák, Michal Kalus, Magda Dovhunová, Pavel Dubský, Bohuslav Gaš

Electrophoresis 2019, submitováno 21.6.2019, elps.201900225



The dynamics of band (peak) shape development in capillary zone electrophoresis in the case of two co-migrating analytes: the displacement and the tag-along effects

Journal:	*ELECTROPHORESIS*
Manuscript ID	Draft
Wiley - Manuscript type:	Research Paper
Date Submitted by the Author:	n/a
Complete List of Authors:	Dvorak, Martin; Charles University Faculty of Science, Physical and Macromolecular Chemistry Kalus, Michal; Charles University Faculty of Science, Physical and Macromolecular Chemistry Dovhunová, Magda; Charles University Faculty of Science, Physical and Macromolecular Chemistry Dubsky, Pavel; Charles University Faculty of Science, Physcal and Macromolecular Chemistry Gas, Bohuslav; Charles University Faculty of Science, Physical and Macromolecular Chemistry
Keywords:	capillary electrophoresis, co-migration, chromatography, displacement effect, tag-along effect

SCHOLARONE™
Manuscripts

The dynamics of band (peak) shape development in capillary zone electrophoresis in the case of two co-migrating analytes: the displacement and the tag-along effects

Martin Dvořák, Michal Kalus, Magda Dovhunová, Pavel Dubský*, Bohuslav Gaš

Charles University, Faculty of Science, Department of Physical and Macromolecular Chemistry, Prague, Czech Republic

* Corresponding author: Mgr. Pavel Dubský, Ph.D., Charles University, Faculty of Science, Albertov 6, CZ-128 43 Prague 2, Czech Republic

E-mail: pavel.dubsky@natur.cuni.cz

Keywords: capillary electrophoresis; co-migration; chromatography; displacement effect; tag-along effect

Total number of words: 7213

For Peer Review

Abstract

Peak shapes in electrophoresis are often distorted from the ideal Gaussian shape due to disturbing phenomena, of which the most important is electromigration dispersion. It is caused be a particular nonlinearity of electromigration – when the velocity of the separated analyte is dependent on its own concentration. This causes a typical triangular deformation of the separated peaks. Even more interesting is when the velocity of the separated analyte is dependent on the concentration of co-analytes. The consequence is a mutual influence of the analytes couples which distorts both analyte zones and causes much more complicated peak shapes, at least at the initial stages of separation. We utilize the nonlinear theory of electromigration, which is formulated analogously to the nonlinear theory of chromatography, for the thorough analysis of electromigration peak shapes. A special attention is devoted to the displacement and the tag-along effects, which have the analogy in chromatography.

For Peer Review

1 Introduction

Migration of ions in capillary electrophoresis is described by a set of partial differential equations (PDEs), which reads [1]

$$\frac{\partial c_i(x,t)}{\partial t} = \left(\frac{\partial c_i(x,t)}{\partial t}\right)_{\text{em}} + \left(\frac{\partial c_i(x,t)}{\partial t}\right)_{\text{diff}}$$

$$\left(\frac{\partial c_i(x,t)}{\partial t}\right)_{\text{em}} = -\frac{\partial}{\partial x}\sum_{z=n_i}^{p_i}\left(\frac{j}{\kappa}\mu_{i,z}c_{i,z}(x,t)\right) \qquad (1)$$

$$\left(\frac{\partial c_i(x,t)}{\partial t}\right)_{\text{diff}} = \frac{\partial}{\partial x}\sum_{z=n_i}^{p_i}\left(D_{i,z}\frac{\partial c_{i,z}(x,t)}{\partial x} - \frac{j_{\text{diff}}(x,t)}{\kappa(x,t)}\mu_{i,z}c_{i,z}(x,t)\right)$$

where x is the axial coordinate in the separation channel, t is time, c_i is the total (analytical) concentration of an i-th constituent in the system, n_i and p_i are the most negative and the most positive, respectively, ionic forms the constituent can produce, $c_{i,z}$ are concentrations of these individual forms, $D_{i,z}$ and $\mu_{i,z}$ are their diffusion coefficients and signed electrophoretic mobilities, respectively, j is the current density, and κ and j_{diff} are the (local) conductivity and diffusion current density, respectively. The conductivity is expressed as

$$\kappa(x,t) = F\left(\sum_i\sum_{z=n_i}^{p_i} z_{i,z}\mu_{i,z}c_{i,z}(x,t) + \mu_H c_H(x,t) - \mu_{OH}c_{OH}(x,t)\right) \qquad (2)$$

where F is the Faraday constant, the first sum goes over all constituents in the system, and indexes H and OH stand for H_3O^+ and OH^- ions, respectively. The diffusion current density is expressed as

For Peer Review

$$j_{\text{diff}}(x,t) = -F\left(\sum_i \sum_{z=n_i}^{p_i} z_{i,z} D_{i,z} \frac{\partial c_{i,z}(x,t)}{\partial x} + D_H \frac{\partial c_H(x,t)}{\partial x} - D_{OH} \frac{\partial c_{OH}(x,t)}{\partial x}\right) \quad (3)$$

In eqs. (1) - (3), we assume constant mobilities and diffusion coefficients, i.e., we neglect ionic strength effects. Second, we consider only acid-base equilibria in the system. We discuss the form of PDEs with general equilibria in CZE, such as complexation equilibria, elsewhere [2]. The limitation of our discussion to the acid-base equilibria in this paper is motivated by the fact that the theory of the dynamics of band (peak) shape development in the case of two co-migrating analytes – as we are about to discuss herein – cannot be extended to general equilibria as yet.

The individual PDEs in the set, eq. (1), are coupled to each other through the conductivity term, κ, and the diffusion current density term, j_{diff}, and the entire set of PDEs is further coupled with a set of algebraic equations describing the acid-base equilibria present in the system. This leads to an inherently nonlinear problem, the solution to which has not been found in a closed form. Several strategies have been applied to find an approximate solution to these equations with different initial conditions corresponding to different modes of electrophoresis. Capillary zone electrophoresis (CZE) is indisputably one of prominent importance in analytical chemistry. The initial conditions in CZE match the experimental setup where the entire capillary is filled with a homogenous background electrolyte (BGE) except for a short injection plug, which consists of analytes, and, possibly, modified concentrations of BGE constituents. Any constituent of the sample plug which is not a BGE constituent is mathematically equivalent to an analyte.

These initial conditions lead to a propagation of certain waves through the system, which exhibit themselves as system peaks or analyte peaks in the detector trace [3]. Amplitudes of these waves can be decomposed into components that originate from the physical concentration distribution functions of the individual constituents, $c_i(x,t)$ [4]. In this context, a peak of the analyte is the only peak that has a nonzero component originating from the concentration distribution of this analyte. Consequently, the

For Peer Review

corresponding wave-function can be identified with the physical concentration distribution of the analyte (cf. discussion around eq. (28) in ref. [5]). This allows us to avoid the abstract language of propagating waves in CZE and to speak of a propagation of an analyte peak, when focused on analytes.

We summarized various approaches to solving the problem of analyte peak propagation in CZE in our previous paper [5]. Starting with the basic theory of moving boundary electrophoresis, an existence of two fundamental types of boundaries in electrophoresis is revealed in general: i) a shock, self-sharpening boundary and ii) a dispersed, fronting or tailing boundary. Both types of boundaries develop in a single peak of an analyte, one type on front and the other type at back of the peak. This manifests as the electromigration dispersion (EMD) of the peak. (We purposely neglect the case of possibly a perfectly symmetrical peak. This allows us to simplify the discussion, whereas an absolutely zero EMD would require precisely tuned conditions barely encountered in a real experiment.)

Supposing all analytes are strong electrolytes and considering only the electromigration term, the term "em" in eq. (1), Mikkers et al. [6] and later also Thormann [7] found a solution to the concentration distribution within the dispersed boundary for a single analyte peak propagating in a virtually homogeneous environment of the BGE. Gebauer and Boček showed that the same solution applies to univalent weak electrolytes in the so-called safe pH region [8], and we extended the applicability of the solution to general weak electrolytes, provided that pH within the analyte peak does not change and stays equal to that of the BGE [5]. Any of these setups leads to a single PDE for the analyte concentration distribution, which can be solved analytically. On the one hand this solution neglects diffusion, albeit it takes the nonlinear nature of electrophoresis into account on the other hand. We refer to this solution as to the nonlinear electromigration model (NEM).

Also considering the electromigration term only, Poppe [9, 10] adopted a strategy of solving the set of PDEs, eq. (1), as an eigenvalue problem, where a certain characteristic matrix is first formulated for

For Peer Review

the given CZE system, the eignevalues of which equal velocities of the waves propagating through the system and the corresponding eigenvectors provide information on amplitudes of the waves and their relation to the physical concentration distribution functions of the individual constituents, $c_i(x,t)$. The approach has been extensively developed later by Štědrý, Gaš et al. [11, 12, 13] and generalized beyond the mere acid-base equilibria in our group recently [2]. The theory provides number of all (analyte and system) peaks in the system, their exact positions and approximate composition, however, all nonlinearity in the system is discarded and information on concentration distributions (peak shapes) is lost. The extent of EMD can be expressed only in terms of a single number [14 - 17], or the peak shapes can be approximated using an iterative computational strategy based on the knowledge of the eigenvector compositions [10]. We refer to this model as to the linear theory of electromigration (LTEM).

The disadvantage of losing information on peak shapes in LTEM was overcome by Hruška et al. who extended LTEM with a first-order approximation to the nonlinearity built in the set of PEDs, eq. (1) [1]. We refer to this model as to the nonlinear theory of electromigration (NLTEM). NLTEM approximates the complete set of PDEs, eq. (1), including the diffusion term, by a Taylor series. Only the first two terms of the Taylor series are taken into account and other simplifications are made on the way to the solution, however the solution is found in a closed form. In contrast to NEM, NLTEM provides a smooth peak concentration distribution in the form of the so-called Haarhoff-Van der Linde (HVL) function [18], which has been shown to describe the actual peak concentration distribution in CZE very well [19, 20].

All of the existing models listed above adopt an approximation of an immediate separation of all waves in CZE, i.e., they assume independent migration of analyte (and system) peaks from the very beginning of the separation process. Co-migration of analytes and the conditions inside a cluster of overlapping peaks have apparently not been discussed in CZE till now.

For Peer Review

This is in contrast to chromatography, where considerable effort has been put into solving the problem of co-eluting peaks, motivated mostly by the needs of preparative chromatography. A solution to the ideal model of two-solute chromatography was found already in 1945 by Glueckauf [21]. The solution was presented in a more rigorous treatment by Rhee et al. in 1970 [22]. These theoretical efforts were completed by Guiochon et al. in 1989 [23]. The theory is summarized in several review papers [24 - 26]. Chromatography, as well as electrophoresis, comprises a transport problem that is generally described by a set of PDEs of the same type, yet different structure, as that given in eq. (1). The chromatographic equations are formulated in a general way that requires an adsorption isotherm, which the analytes obey on the given stationary phase, to be supplied to them. A (competitive) Langmuir isotherm is typically considered.

The solution to the chromatographic equations was found, at the expense of neglecting the diffusion, in a piecewise continuous form. The column space (x-axis) is divided into several regions in which one, both or none of the analytes (solutes) exist and their distributions within these regions are described by individual (continuous) functions. The border points of these regions move in time along characteristic curves depicted in the so-called x-t diagram (cf. Figure 1 in this paper). The regions may appear and disappear as the separation process evolves. A horizontal cut in the x-t diagram provides the solution at the given time along the x axis (inside the column). A vertical cut provides the solution at the given point in the x axis within time (detector trace).

Two fundamental phenomena, the displacement effect and the tag-along effect [27], have been described in chromatographic systems with nonlinear convex upward isotherms, such as the competitive Langmuir isotherm at high solute concentrations. These effects are attributed to “the competition of the closely eluting components for access to the stationary phase and involvement in the retention mechanism” (cited from ref. [27]).

For Peer Review

The displacement effect describes a situation when the slower (more retained) analyte tends to displace the faster (less retained) analyte ahead of the slower analyte's zone. The retention of the slower analyte in a mixture with the faster analyte on the stationary phase is thermodynamically favourable [27], so that the faster analyte speeds up, while it slows down again as it escapes the mixed band. This is accompanied by a discontinuity in the concentration profile of the faster analyte at the front boundary of the slower analyte, where the faster analyte's concentration increases abruptly. Consequently, a "stacked" zone of higher concentration of the faster analyte is formed and pushed forward ahead of the mixture of the two solutes.

The tag-along effect is caused by the faster analyte that, when in excess, does not leave enough binding sites for the slower one. Thus the slower analyte speeds up, yet it cannot overcome the faster analyte so it tags along with it inside the mixed band. Simultaneously, it escapes the mixed band sluggishly, which leads to a formation of a tailing plateau behind the mixture of the two solutes. The displacement effect is found advantageous in (semi)preparative chromatography [28 - 31] since it yields larger amount of the pure component of the faster peak in the presence of an excess of the slower peak than would be expected based on their individual retention factors. Revealing the inner structure of a cluster of two not completely separated peaks is additionally helpful in understanding their actual analytical resolution [32 - 34].

Poppe noticed in 1992 [10] that "the theories as developed on nonlinear chromatographic transport … are also applicable to electrophoresis". Simultaneously though, he only focused on the case of isolated sample and system zones leaving "the more complicated phenomena when different zones still interact for later investigations". This approach lead to the development of LTEM and a unified approach to investigating system peaks in both electrophoresis and chromatography [35]. Noticeably, the HVL function resulting from the NLTEM theory in electrophoresis for a single-peak concentration distribution was first introduced in the context of an overloaded sample in nonlinear gas chromatography [18]. On the other

For Peer Review

hand, we are not aware of an actual work that would solve the problem of interacting zones in electrophoresis till now.

In the cited review paper [5], we compared mutual relationships among the NEM, LTEM, and NLTEM theories in electrophoresis and showed that NEM can be in principle extended to more than one analyte using the concept of the eigenvectors introduced within LTEM. Simultaneously, we discussed that the resulting PDEs rather surprisingly resemble those describing chromatographic separations with Langmuir isotherm. Under the simplification that: i) only analyte peaks co-migrate for a certain period of time and they do not interact with system peaks from the very beginning of the separation process; ii) pH is constant throughout the capillary, i.e., analytes do not change their dissociation states within their own peak(s); iii) diffusion (along with the diffusion current density) is neglected altogether; the following set of PDEs describes the propagation of analyte peaks in electrophoresis

$$\frac{\partial c_i(x,t)}{\partial t} + \frac{\partial}{\partial x}\left(\frac{\tilde{v}_i c_i(x,t)}{1 + \sum_{j=1}^{N_A} \frac{\kappa_j}{\kappa_{\mathrm{BGE}}} c_j(x,t)}\right) = 0 \qquad (4)$$

where i stands for analyte constituents only and the constituents are indexed so that the 1st up to the N_A-th constituents are analyte constituents, $\tilde{v}_i$ is the (effective) velocity of the i-th analyte in the given BGE and κ_j is a quantity defined in ref. [5]. The quantity κ_j is calculated using the LTEM and can be regarded as a partial derivative of κ with respect to c_j at $c_j \to 0$. In this paper, we implement eq. (4) for the thorough analysis of the mutual interaction between two comigrating analytes in the initial stages of the separation process.

For Peer Review

2 Materials and Methods

2.1 Chemicals

All used chemicals were of analytical-grade purity. Tris(hydroxymethyl)aminomethane (TRIS), (R)-(-)-2-Fluoro-α-methyl-4-biphenylacetic acid (flurbiprofen, FLU), (S)-(+)-2-(6-Methoxy-2-naphthyl)propionic acid (naproxen, NAP), and dimethyl sulfoxide anhydrous (DMSO) were purchased from Sigma-Aldrich (Prague, Czech Republic). Hydrochloric acid (HCl) (35%) was purchased from Lachema a.s. (Brno, Czech Republic). Sodium hydroxide (NaOH) for rinsing the capillary was purchased from Agilent Technologies (Waldbronn, Germany). IUPAC buffers, pH 7.000 and 9.012 (Radiometer, Copenhagen, Denmark), were used for calibration of the pH meter.

2.2 Instrumentation and Software

Rowapur and Ultrapur water purification system (Watrex, San Francisco, USA). Syringe filters (Sartorious, Goettingen, Germany), pore size 45 μm. OHM 220 pH meter instrument (Radiometer, Denmark). ^{3D}CE capillary electrophoresis system operated with the ChemStation software (Agilent Technologies, Waldbronn, Germany). Fused-silica capillaries of 50 μm ID and 375 μm OD (Polymicro Technologies, Phoenix, AZ, USA). Simul 5 Complex [36, 37], PeakMaster 6 [2] and CEVal [38] freeware developed in our laboratory. MS Excel and Wolfram Mathematica 8.0 (Wolfram, Oxfordshire, United Kingdom) for NEM calculations. Origin Pro 2016 (OriginLab corporation) and GIMP 2.10.8 (GNU Licence) for presentation of figures.

2.3 Experimental conditions

BGE: TRIS / HCl (20 mM / 10mM), pH 8.08. Sample: (1 mM FLU, 1 mM NAP, 0.04% DMSO) in BGE. All solutions were prepared from the Ultrapur water and filtered through the syringe filters prior to use. Capillary length (total / effective): 47.2 / 38.7 cm. Capillary preconditioning: deionized water (10 min),

For Peer Review

0.1 M NaOH (10 min), deionized water (10 min). Capillary flush prior each measurement: BGE (3 min). Temperature: 25°C. Detection: diode-array detector, 220 nm and 250 nm. Signal decomposition procedure described in Supporting information. Injection: hydrodynamic, 12 mbar × 5 s (~1.1 mm injection plug width). Voltage: 20 kV (42.38 kV/m electric field intensity). Mobility of electroosmotic flow (EOF): 63.5×10^{-9} $m^2V^{-1}s^{-1}$ (experimentally determined).

2.4 NEM calculations and Simulations

Electrophoretic mobilities of BGE constituents corrected for the ionic strength (IS) of the BGE: 26.73×10^{-9} $m^2V^{-1}s^{-1}$ (TRIS), 74.80×10^{-9} $m^2V^{-1}s^{-1}$ (HCl). IS corrections of pKa constants of TRIS an HCl resulted as negligible. Effective electrophoretic mobilities of analytes determined in the given BGE with software CEval: 20.6×10^{-9} $m^2V^{-1}s^{-1}$ (FLU), 20.8×10^{-9} $m^2V^{-1}s^{-1}$ (NAP). κ_{BGE}: 97.99×10^{-3} S/m. κ_1 (FLU): -11.223×10^{-3} (S/m)/(mol/m^3), κ_2 (NAP): -11.038×10^{-3} (S/m)/(mol/m^3).

NEM calculation, Figures Figure 2-**Figure 4**: Sample composition: 1 mM FLU, 1 mM NAP. TRIS and HCl concentrations in the sample are not an input parameter to NEM. Nevertheless, the NEM model behaves as if the composition of the sample was such that it would invoke system zones with exclusively zero amplitudes. This corresponds to a sample composed of 18.64 mM TRIS and 6.64 mM HCl. Injection plug width: 3 mm. Electric field intensity: 39.53 kV/m.

Simulation, Figure 4: Sample composition: 1 mM FLU, 1 mM NAP, 18.64 mM TRIS, 6.64 mM HCl. Capillary length: 80 mm. Grid points: 64000. Peak edge width: 0.01mm. Injection site: 15 mm. Electric field intensity: 39.523 kV/m. EOF mobility: 20.6×10^{-9} $m^2V^{-1}s^{-1}$. The artificially introduced EOF enables simulations in shorter capillary length and does not affect the form of the solution in the x-domain.

Calculations for Figure 5: Sample composition: 1 mM FLU, 1 mM NAP, 20.00 mM TRIS, 10.00 mM HCl. TRIS and HCl concentrations apply to Simul only. Injection plug width: 1.1 mm. Electric field

For Peer Review

intensity: 42.381 kV/m. EOF mobility: $63.52\times10^{-9}m^2V^{-1}s^{-1}$. In Simul: Capillary length: 472 mm. Grid points: 377600 (a novel in-development computational core of Simul was used that allows for extraordinary high grid point numbers). Peak edge width: 0.01mm. Injection site: 13.55 mm. Detector position: 400 mm.

3 Results and discussion

3.1 Description of the solution for two co-migrating analytes

In the case of two analytes, eq. (4) reduces to the following pair of coupled quasilinear partial differential equations

$$\frac{\partial c_1(x,t)}{\partial t}+\frac{\partial}{\partial x}\left(\frac{\tilde{v}_1 c_1(x,t)}{1+\frac{\kappa_1}{\kappa_{\mathrm{BGE}}}c_1(x,t)+\frac{\kappa_2}{\kappa_{\mathrm{BGE}}}c_2(x,t)}\right)=0$$
$$\frac{\partial c_2(x,t)}{\partial t}+\frac{\partial}{\partial x}\left(\frac{\tilde{v}_2 c_2(x,t)}{1+\frac{\kappa_1}{\kappa_{\mathrm{BGE}}}c_1(x,t)+\frac{\kappa_2}{\kappa_{\mathrm{BGE}}}c_2(x,t)}\right)=0 \qquad (5)$$

Since these equations as well as the general eq. (4) represent a generalization of the original NEM model for a single analyte [5], we keep the NEM acronym when referring to the theory described in this paper. The resemblance of eqs. (5) with the governing equations of chromatography with the competitive Langmuir isotherm allows us to adapt the mathematical formalism originally developed in chromatography [39, 40] and find a solution to eqs. (5) for a practically relevant choice of initial and boundary conditions in electrophoresis. Although the adaptation of a solution from chromatography to electrophoresis is not a straightforward task, we leave its complete description aside and focus on the final solution and its properties in this paper. We refer an interested reader to ref. [39, 40] for detailed information on quasilinear partial differential equations.

For Peer Review

The initial and boundary conditions correspond to a rectangular-shape sample zone of width x_0 injected into the beginning of the capillary at time $t = 0$,

$$\begin{aligned} &c_1(x,0) = c_1^0,\ c_2(x,0) = c_2^0 \text{ for } 0 \le x \le x_0 \\ &c_1(x,0) = 0,\ c_2(x,0) = 0 \text{ for } x > x_0 \\ &c_1(0,t) = 0,\ c_2(0,t) = 0 \text{ for } t > 0 \end{aligned} \qquad (6)$$

Eqs. (6) prescribe that both analytes migrate in the same direction towards the positive x values and that the beginning of the capillary coincides with the beginning of the sample plug. The parameters $\frac{\kappa_i}{\kappa_{BGE}}$ in eqs. (5) take the same role as the adsorption constant, K, in chromatography under the Langmuir isotherm conditions [5]. In contrast to chromatography, which makes only positive values of K meaningful, the parameters κ_i can attain either positive or negative values in electrophoresis. This gives rise to three qualitatively different solutions to eqs. (5): i) both analyte peaks fronting, ii) both analyte peaks tailing, and iii) the peak of the slower analyte fronting and the peak of the faster analyte tailing. Whether the peak of an analyte is fronting or tailing is predetermined by the sign of κ_i [5]. There is no formal difference between anions and cations as analytes in electrophoresis. The initial and boundary conditions, eqs. (6), require that the analytes move in the positive direction along the x axis, so the applied voltage is required to change its polarity upon switching from cations to anions, and vice versa.

We present the solution to eqs. (5), under the conditions (6), through the corresponding x-t diagram (Figure 1) and resulting concentration profiles at four separation times covering the whole separation process (Figure 2). All curves in the figures were constructed using formulas given in Supporting information. Please notice that the x-t diagram (Figure 1) is displayed in a schematic way using an arbitrary scale – i.e. not quantitatively matching the model electropherograms (Figure 2) – for better readability. This scaling does not affect any aspect of the solution we are discussing below. We confine

For Peer Review

our practical illustrations to the case of $\kappa_1 < 0$ and $\kappa_2 < 0$, i.e. both analyte peaks tailing in the detector domain. Similar figures for the other case of $\kappa_1 > 0$ and $\kappa_2 > 0$ can be found in Supporting information. The third case of $\kappa_1 < 0$ and $\kappa_2 > 0$ is not discussed because it would require a separate mathematical treatment that goes beyond the limits of a single paper. Moreover, this case seems to be of low practical relevance because it implies that two analytes of very similar mobilities – so that their co-migration time is significant – exist, one with a positive and the other with a negative contribution to the zone conductivity. However, this can most likely happen only if $(\kappa_1 < 0) \cong 0$ and $(\kappa_2 > 0) \cong 0$ which results in a pair of symmetric Gaussian peaks with only a minor influence on each other.

As the electromigration process starts, the originally rectangular injection plug develops into a profile with a dispersive boundary (D) at one side and a shock boundary $S_{(S)}$ at the other side, see Figure 2. These two boundaries form later, when the two analytes get separated, the corresponding boundaries of the single-analyte zones, e.g. in our configuration of $\kappa_1 < 0$ and $\kappa_2 < 0$, the boundary (D) forms a dispersive tail, which belongs to the slower analyte (1), and the shock front $S_{(S)}$ belongs to the faster analyte (2). In the other configuration of $\kappa_1 > 0$ and $\kappa_2 > 0$, Figure 1 and Figure 2 become somewhat mirrored (cf. Supplementary information), and the two boundaries swap their positions. In order to be able to discuss both cases of i) $\kappa_1 < 0$ and $\kappa_2 < 0$ and ii) $\kappa_1 > 0$ and $\kappa_2 > 0$ at the same time, we will refer to the analyte/peak located at the dispersive side of the migrating plug as the analyte/peak D, and that located at the shock-boundary side as the analyte/peak S. Simultaneously, we keep referring the slower analyte/peak with index 1 and the faster one with index 2 (according to their positions inside the capillary). Thus: i) $1 \equiv D$ and $2 \equiv S$ and ii) $1 \equiv S$ and $2 \equiv D$, respectively.

Another shock boundary $S_{(D)}$ is located inside the cluster of the two analyte peaks. It can be viewed as a shock boundary of the peak D through which the analyte S escapes the zone of mixed analytes. Up to three regions of a constant composition, denoted by (Z), (R) and (V) in figures Figure 1 and Figure 2,

For Peer Review

can be further recognized. The region (Z) retains the composition of the initially injected sample plug. The regions (R) and (V) consist of pure analytes S and D, respectively, as they are becoming separated. The concentration of the analyte S in the region (R) and that of the analyte D in the region (V) is always higher and lower, respectively, than their concentrations in the injection plug, the region (Z). Technically, another region (Y) of a constant composition exists, which however represents a trivial case of a region of zero concentrations of analytes, i.e. a region not yet reached or already escaped by the analytes. The regions of constant nonzero composition have temporary character as they get finally vanished due to EMD. This is especially true for the constant region (R), which disappears soon after it is formed. Finally, the region (DS), which forms the dispersive boundary of the peak S, and an intermediate region of mixed analytes, region (SD), both exhibiting smooth concentration profiles, exist in the solution. Concentrations of analytes in the individual regions are given by formulas presented in Supporting information.

The solution is described by velocities of several characteristic points of the concentration profile along with some critical times, the formulas for which are summarised in Supporting information. Each velocity corresponds to a particular curve in the x-t diagram, Figure 1, and each critical time to a point where a pair of these curves intersects. The characteristic velocity points regarding peak D are: the point where the dispersive boundary rises from the baseline velocity $v_{\mathrm{bottom}}^{(D)}$ (blue dashed curve), the point where the dispersive region (D) turns into the plateau region (V), as long as the region (V) exists velocity $v_{\mathrm{top}}^{(D)}$ (blue dotted curve), the front shock boundary of the peak D velocity $v_{\mathrm{S_{(D)}}}$ (blue solid curve). Those for the peak S are: the point where the dispersive boundary of the peak S rises from the baseline; this point is identical to the left edge of the region (SD) before the two peaks get separated or the left edge of the region (DS) after the two peaks get separated velocity $v_{\mathrm{bottom}}^{(S)}$ (red dashed curve), the point where the region (SD) touches the region (Z), as long as the region (Z) exists, or where the region (DS) touches the region (R), as long as the region (R) exists velocity $v_{\mathrm{top}}^{(S)}$ (red dotted curve), and finally, the shock boundary of the peak S velocity $v_{\mathrm{S_{(S)}}}$ (red solid curve). Then, the critical points (times) occur when: the

For Peer Review

region (Z) disappears t_z (red dotted curve crosses blue solid curve), the region (R) disappears t_R (red dotted curve coincides with red solid curve), the region (SD) disappears and the two analytes (peaks) get separated t_P (red dashed curve crosses blue solid curve), and finally, the region (V) disappears t_V (blue dotted curve coincides with blue solid curve).

3.2 Displacement effect and tag-along effect

Because of the close mathematical resemblance between NEM and the ideal model of chromatography with Langmuir isotherm, similar phenomena are observed in liquid chromatography and in capillary electrophoresis.

The displacement effect in electrophoresis manifests as the formation of the region (R), i.e., an increased concentration of the analyte S in its own zone as it separates from the injection zone (Z). (Specifically, the displacement effect as described herein must not be confused with a displacement of ions of BGE from an analyte band in electrophoresis). Similarly to chromatography, the analyte S additionally experiences a discontinuity in its concentration profile at the shock boundary $S_{(D)}$. In chromatography, the displacement effect is attributed to an act of speeding up the faster analyte by the presence of the slower analyte. Similar reasoning can be used in electrophoresis in the case of negative values of κ_i. It does not hold applicable to the other case of $\kappa_i > 0$, though. Instead, the displacement effect is easy to explain in terms of changes in the electric field occurring in the zone of the analytes compared to the BGE. If $\kappa_i < 0$, the intensity of electric field in regions (Z), (R) and (Y) satisfies $E_{(Z)} > E_{(R)} > E_{(Y)}$, whereas if $\kappa_i > 0$, then $E_{(Z)} < E_{(R)} < E_{(Y)}$. In both cases leads the ordering of intensities of electric field to a stacking condition for the analyte S. The system thus virtually behaves as if the analyte D displaced the analyte S out of the mixed zone. More descriptive illustrations can be found in Supporting information.

The extent of the displacement effect can be quantitatively characterized by the ratio Σ_D,

For Peer Review

$$\Sigma_D \stackrel{\text{def}}{=} \frac{c_S^{(R)}}{c_S^{(Z)}} \equiv \frac{c_S^{(DS)}}{c_S^{(SD)}} \quad (7)$$

where $c_S^{(Z)}$, $c_S^{(R)}$, $c_S^{(DS)}$ and $c_S^{(SD)}$ are concentrations of the analyte S in the respective regions at the discontinuity, shock boundary $S_{(D)}$ (cf. Figure 3). The same ratio serves for the description of the extent of the displacement effect in chromatography [27]. The parameter Σ_D can be calculated from the NEM model at any stage of the separation process (until the two peaks get completely separated). We provide the formula in Supporting information. Assuming that the analytes have similar effective mobilities, it can be shown (cf. Supporting information) that $\Sigma_D$is governed by the ratio of the initial concentrations,

$$\mu_{\text{eff},1} \cong \mu_{\text{eff},2} : \Sigma_D \approx 1 + \frac{c_D^0}{c_S^0} \quad (8)$$

where $\mu_{\text{eff},i}$ are the (constant) effective mobilities of the i-th analyte in the given BGE, and c_D^0 and c_S^0 are the initial concentrations of the analytes D and S, respectively. The displacement effect is more pronounced in the case of an excess of the analyte D over the analyte S. On the other hand, the displacement effect is suppressed if the injected concentration of the analyte S predominates that of the analyte D, as expected. Eq. (8) again has its direct counterpart in chromatography, where loading factors, i.e., the ratio of the sample size to the column saturation capacity, states in place of the initial concentrations c^0 [27].

The tag-along effect refers to tagging along of the analyte D with the analyte S so that the analyte D leaves the region of mixed analytes, the regions (Z) or (SD), only sluggishly. This results in a long and low concentration plateau, the region (V), in the concentration profile of the analyte D. The explanation of the

For Peer Review

tag along effect goes in a similar way as that of the displacement effect, and we provide it in Supporting information.

The width of the concentration plateau, $\Delta x_{(V)}$ in Figure 3, grows linearly in time (cf. Supporting information). The highest rate of its broadening is achieved when the analyte S predominates the analyte D,

$$\lim_{c_S^0 \to \infty} \Delta x_{(V)} = \lim_{c_D^0 \to 0} \Delta x_{(V)} = (\tilde{v}_2 - \tilde{v}_1)t \qquad (9)$$

while the opposite applies when the analyte D predominates the analyte S,

$$\lim_{c_S^0 \to 0} \Delta x_{(V)} = \lim_{c_D^0 \to \infty} \Delta x_{(V)} = 0 \qquad (10)$$

Since the position where the dispersive region (D) of the analyte D starts to rise from the baseline, the point $x_{(D)}$ in Figure 3, moves with a constant velocity, $x_{(D)} = \tilde{v}_D t$ (cf. Supplementary information and ref. [5]), we can use it as a reference point and characterize the extent of the tag-along effect by a dimensionless constant Σ_{TA},

$$\Sigma_{TA} \stackrel{\text{def}}{=} \frac{\Delta x_{(V)}}{x_{(D)}} \qquad (11)$$

Σ_{TA} can be calculated from the NEM model (cf. Supplementary information). In accordance with eqs. (9) and (10), it results,

For Peer Review

$$\lim_{c_S^0 \to \infty} \Sigma_{TA} = \lim_{c_D^0 \to 0} \Sigma_{TA} = \frac{\mu_{eff,2} - \mu_{eff,1}}{\mu_{eff,D}} \quad (12)$$

where $\mu_{eff,i}$ are effective mobilities of the given analyte in the BGE, and

$$\lim_{c_S^0 \to 0} \Sigma_{TA} = \lim_{c_D^0 \to \infty} \Sigma_{TA} = 0 \quad (13)$$

respectively. We defined the measure of the tag-along effect differently than it is expressed in chromatography [27]. Nevertheless, the limits, eqs. (9) and (10), lead to the same conclusion as discussed in the context of chromatography in ref. [27].

Finally, we shall discuss two more effects closely related to the displacement and the tag-along effects that show how the initial conditions influence the form of the solution to eq. (2) at times when the two peaks have already got separated and migrate independently of each other. We will use Figures Figure 1 and **Figure 3** for this discussion and we refer the reader to Figures S6 and S4 in Supporting information for a more illustrative example.

At time t_P, when the analytes D and S get separated, the concentration profile of the analyte D consists of only two regions, (D) and (V). The point indicated as $x_{(D)}$ in Figure 3, develops from the edge of the injection plug. The trajectory of this point as well as the development of the entire region (D) are not influenced by the presence of the analyte S, cf. Figure 1. Therefore, the concentration profile of the analyte D inside the region (D) is given by the same function that also describes the concentration profile at the dispersive boundary of a single-analyte solution. The form of this function is independent of the initial conditions, i.e., it depends neither on the initial concentration of the analyte nor the initial width of the sample plug (cf. region (X) in ref. [5] and Supporting information). The only difference between the region (X) of the single-analyte solution and the region (D) of the two-analyte solution is that the

For Peer Review

concentration profile of the analyte D in the region (D) rises until it reaches the value of the concentration $c_D^{(V)}$, whereas in its single-analyte solution counterpart, the concentration profile of the single analyte in the region (X) in ref. [5], ends at the initial concentration $c_D^0 > c_D^{(V)}$. The region (V) forms a flat concentration profile of the single analyte D and at times higher than t_P it can be regarded as an analogue to the region (Z) of the single-analyte solution, i.e., the injected sample plug not yet smeared out by EMD.

Thus, at times higher than t_P, the entire concentration profile of the analyte D is identical to a single-analyte solution that would develop from a hypothetical rectangular sample plug of the single analyte D, yet with an initial concentration $c_D^{(V)} < c_D^0$ and an initial width $x_0' = x_0 \frac{c_D^0}{c_D^{(V)}} > x_0$. Note that the initial width x_0' is prescribed by the mass conservation, such that the area of the hypothetical initial rectangular sample plug is the same as the area of the analyte D in the actual initial rectangular sample plug, i.e., $x_0' c_D^{(V)} = x_0 c_D^0$. We discussed in ref. [5] that two peaks of an analyte which both develop from an initially rectangular sample plug of a given area, but possibly differ in their initial widths (and initial concentrations), become indistinguishable from each other after the initial concentration plateau, the region (X) in ref. [5], of the wider peak disappears. This corresponds to time t_V when the concentration plateau (V) disappears in the case of the peak D. We can conclude that at times higher than t_V the shape and position of the peak of analyte D, which migrates at the dispersive edge of the injection plug, is in no way affected by its co-migration with another analyte S during the early stage of the separation process.

The peak S, on the contrary, is influenced on both of its sides. The displacement effect acts at the shock boundary $S_{(S)}$, and the dispersive boundary (SD) migrates under the influence of the peak D till the separation time, t_P, cf. red dashed line in Figure 1. Unfortunately, the shape of the peak S is expressed as an implicit function in the NEM model (cf. Supporting information), which makes it impossible to decide how the initial co-migration with the analyte D affects the final shape of the peak S. Nevertheless, the model allows us to conclude that the point $x_{(S)}$, Figure 3, moves with a velocity that is higher ($\kappa_i < 0$) or

For Peer Review

lower ($\kappa_i > 0$) than the expected velocity $\tilde{v}_S$ in the BGE, until the two peaks get separated (cf. Supplementary information). It was discussed in our previous paper [5] that the point $x_{(S)}$ serves as an indicator of the effective velocity (mobility) of the analyte and can be best approached through an HVL fit when the according to NLTEM (recall that NEM – in contrast to NLTEM – neglects diffusion altogether). Thus – supposing that the HVL distribution applies to the peak S – the peak becomes virtually shifted towards lower ($\kappa_i < 0$) or higher ($\kappa_i > 0$) times under the influence of the co-migrating component D. This conclusion amends the NLTEM model, which cannot see such an effect because it assumes immediate separation of all system zones (including the analyte zones) [5].

3.3 Computer simulation and experimental verification

We compare the calculated electropherograms predicted by NEM with computer simulations carried out by Simul 5 software [41, 42]. Simul 5 is a freeware developed in our laboratory that provides a precise numerical solution to electromigration continuity equations. We present a comparison between the NEM solution and simulation at two separation times, which belong to time intervals $(0,t_Z)$ and (t_R,t_P), in Figure 4. The electropherograms are depicted in x-domain, i.e. as they appear inside the capillary. Naproxen (NAP) and flurbiprofen (FLU) were used as model analytes in a TRIS/Hydrochloric acid BGE of pH 8.08. Both analytes are weak univalent acids with pKa 4.19 and pKa 4.33, FLU and NAP, respectively, cf. ref. [43]. The analytes are thus fully dissociated and their degree of dissociation does not change over the sample plug in the given BGE. Effective electrophoretic mobilities of both analytes in the given BGE were measured in a devoted experiment and are summarized together with electrophoretic mobilities of BGE constituents in Materials and methods section. Electrophoretic mobilities of all constituents (including analytes) are valid for the actual ionic strength (IS) of the BGE and no direct IS correction was applied during the simulation. Other simulation conditions are provided in Materials and methods section.

For Peer Review

The simulation conclusively proves that NEM is capable of capturing all kinds of peak distortions related to co-migration of two analytes in CZE. Specifically, the NEM solution predicts the striking increase in concentration of analyte 2 (NAP) at the front of the migration plug, i.e. the displacement effect, Figure 4 A) and C). The displacement effect is less pronounced in simulation (and reality) compared to the NEM model due to diffusion. Further, the NEM solution predicts correctly that the slope of concentration profile of analyte 2 (NAP) is lower to the left (the region (SD)) and higher to the right (the region (DS)) from the shock boundary $S_{(D)}$. Finally, the NEM solution provides an explanation for the bump on the concentration profile of analyte 1 (FLU), which is observed in the simulated electropherogram (see Figure 4 D) around 367 mm). This bump clearly corresponds to a diffusion-smeared concentration plateau (V), also known as the tag-along effect, which is visible in the NEM electropherogram (compare Figure 4 D)).

Finally, we demonstrate that electropherograms obtained in real experiment agree well with the predictions made by NEM. We take an advantage of the fact that the analytes NAP and FLU have different absorption coefficients at 220 nm and 250 nm. This allows us to decompose the signal of highly overlapping peaks (zones) of FLU and NAP into the signal traces of the individual analytes. The signal decomposition procedure is described in Supporting information. The experimental electropherogram (after signal decoupling and normalization) is shown in Figure 5 along with profiles obtained for the same experimental conditions by Simul 5 and the NEM model. This time, both simulation and NEM calculation are performed in the time domain, i.e. as a detector trace. We see a perfect agreement between the simulated electropherogram and the electropherogram predicted by NEM, which indicates that the NEM model approximates the full numerical solution of the related PDEs correctly. On the other hand, the front (NAP) shock boundary $S_{(S)}$ is slightly shifted towards higher times in the experiment. We have not found a reason for this slight shift, which must be caused by some higher-order bias not captured by the theory. Otherwise though, the measured electropherogram exhibits all the characteristic features predicted by NEM.

For Peer Review

4 Concluding remarks

In the recent paper by us [5] we have shown a tight analogy between nonlinear models describing a separation process in chromatography and electrophoresis. The analogy is not absolute and fails in the case of weak electrolytes when their dissociation is not complete. However, for fully dissociated analytes, or at least for the constant pH along the separation channel (neglecting pH effects), the thorough analysis by means of the nonlinear models can bring a lot of information and understanding. The present paper analysed electromigration of two fully dissociated analytes, which in the initial stages of separation influence each other. The analysis has revealed that the two most important phenomena – the displacement and the tag-along effects – are common both for nonlinear chromatography and electrophoresis, though their description is partly based on rather different phenomena. The comparison of the nonlinear model of electromigration with numerical computer solution of the original continuity equations has proved almost perfect agreement. As the models are very close to the physical reality, it was not surprising that the experimental verification confirmed fully the predicted phenomena.

Acknowledgements

We are especially thankful to prof. Gyula Vigh, Texas A&M University, for his initiation of this research as well as his enduring interest in it, which resulted in hours of discussions and his reviewing the final version of this manuscript.

The support of the Czech Science Foundation, Grants No. 18-11776S, Grant Agency of Charles University, Grant No. 116217 are gratefully acknowledged.

All authors declare no conflicts of interest.

For Peer Review

5 References

[1] Hruška, V., Riesová, M., Gaš, B., *Electrophoresis* 2012, *33*, 923–930.

[2] Malý, M., Dovhunová, M., Dvořák, M., Gerlero, G.S., Kler, P.A., Hruška, V., Dubský, P., *Electrophoresis* 2019, *40*, 683–692.

[3] Gaš, B., Kenndler, E., *Electrophoresis* 2004, *25*, 3901–3912.

[4] Hruška, V., Štědrý, M., Včeláková, K., Lokajová, J., Tesařová, E., Jaroš, M., Gaš, B., *Electrophoresis* 2006, *27*, 4610–4617.

[5] Dvořák, M., Dubský, P., Dovhunová, M., Gaš, B., *Electrophoresis* 2019, *40*, 668–682.

[6] Mikkers, F. E. P., Everaerts, F. M., Vergheggen, T. P. E. M., *J. Chromatogr.* 1979, *169*, 1–10.

[7] Thormann, W., *Electrophoresis* 1983, *4*, 383–390.

[8] Gebauer, P., Boček, P., *Anal. Chem.* 1997, *69*, 1557–1563.

[9] Poppe, H., *J. Chromatogr.* 1990, *506*, 45–60.

[10] Poppe, H., *Anal.Chem.* 1992, *64*, 1908–1919.

[11] Štědrý, M., Jaroš, M., Gaš, B., *J. Chromatogr. A* 2002, *960*, 187–198.

[12] Štědrý, M., Jaroš, M., Včeláková, K., Gaš, B., *Electrophoresis* 2003, *24*, 536–547.

[13] Štědrý, M., Jaroš, M., Hruška, V., Gaš, B., *Electrophoresis* 2004, *25*, 3071–3079.

[14] Xu, X., Kok, W. Th., Poppe, H., *J. Chromatogr. A* 1996, *742*, 211–227.

[15] Gebauer, P., Boček, P., *Anal. Chem.* 1997, *69*, 1557–1563.

[16] Gebauer, P., Borecká, P., Boček, P., *Anal. Chem.* 1998, *70*, 3397-3406.

[17] Horká,M. , Šlais, K., *Electrophoresis* 2000, *21*, 2814–2827.

[18] Haarhoff, P. C., Van der Linde, H. J., *Anal. Chem.* 1966, 38, 573–582.

[19] Enry, G. L., Bergström, E. T., Goodall, D. M., *Anal. Chem.* 2001, *73*, 4862–4872.

For Peer Review

[20] Erny, G. L., Bergström, E. T., Goodall, D. M., *J. Chromatogr.* A 2002, *959*, 229–239.

[21] Glueckauf, E., *Proc. Roy. Soc.* 1946, A186, 35-57.

[22] Rhee, H.-K., Aris, R., Amundson, N. R., *Trans. Roy. Soc.* 1970, A267, 419-455.

[23] Golshan-Shirazi, S., Guiochon, G., *J. Phys. Chem.* 1989, 93, 4143-4157.

[24] Lin, B., Ma, Z., Golshan-Shirazi, S., Guiochon G., *J. Chromatogr.* 1990, *500*, 185-213.

[25] Guiochon, G., *J. Chromatogr. A* 2002, *965*, 129–161.

[26] Rajendran, A., *J. Chromatogr. A* 2012, *1250*, 227– 249.

[27] Guiochon, G., Golshan-Shirazi, S., *Chromatographia* 1990, *30*, 613-617.

[28] Newburger, J., Guiochon, G., *J. Chromatogr.* 1989, *484*, 153-166.

[29] Newburger, J., Guiochon, G., *J. Chromatogr.* 1990, *523*, 63-80.

[30] Felinger, A., Guiochon, G., *J. Chromatogr.* 1992, *591*, 31-45.

[31] Siitonen, J., Sainio, T., *Chem. Eng. Sci.* 2015, *122*, 436–451.

[32] Schoenmakers, P. J., Strasters, J. K, Bartha, A., *J. Chromatogr.* 1988, *458*, 355–370.

[33] Dose, E. V., Guiochon, G., *Anal. Chem.* 1990, *62*, 174–181.

[34] Dvořák, M., Svobodová, J., Dubský, P., Riesová, M., Vigh, G., Gaš, B., *Electrophoresis* 2015, *36*, 646–654.

[35] Poppe, H., *J. Chromatogr. A* 1999, *831*, 105–121.

[36] Hruška, V., Beneš, M., Svobodová, J., Zusková, I., Gaš, B., *Electrophoresis* 2012, *33*, 938-947.

[37] Svobodová, J., Beneš, M., Hruška, V., Ušelová, K., Gaš, B., *Electrophoresis* 2012, *33*, 948-957.

[38] Dubský, P., Ördögová, M., Malý, M., Riesová, M, *J. Chromatogr. A* 2016, *1445*, 158–165.

[39] Rhee, H.-K., Aris, R., Amundson, N. R., First-Order Partial Differential Equations – II. Theory and Application of Hyperbolic Systems of Quasilinear Equations, Prentice-Hall, Englewood Cliffs, N. J. 1989.

For Peer Review

[40] Guiochon, G., Felinger, A., Shirazi, D. G., Katti, A. M., *Fundamentals of preparative and nonlinear chromatography 2nd ed.*, Elsevier Inc., San Diego 2006.

[41] https://echmet.natur.cuni.cz/Software/Simul

[42] Hruška, V., Jaroš, M., Gaš, B., *Electrophoresis* 2006, *27*, 984-991

[43] Riesová, M., Svobodová, J., Ušelová, K., Tošner, Z., Zusková, I., Gaš, B., *J. Chromatogr. A* 2014, *1364*, 276-288

For Peer Review

Figure 1: A schematic *x*-*t* diagram displayed in arbitrary units assuming $\boldsymbol{\kappa_1 < 0}$ and $\boldsymbol{\kappa_2 < 0}$. The diagram covers characteristic features of the solution to eq. (5). Blue and red lines indicate migration of characteristic points in the concentration profile of the slower (1) and the faster (2) analyte, respectively. Solid: the shock boundaries; Dashed: the points where the dispersive boundaries rise from the baseline; Dotted: the points where the dispersive boundaries reach the temporary plateau zone ($\boldsymbol{V}$), ($\boldsymbol{Z}$) or ($\boldsymbol{R}$). Shadow bracketed letters indicate regions of characteristic concentration profiles, shadow dashed arrows point to these regions into the zoomed area. Green letters indicate critical points (times) where the solution changes qualitatively, green solid arrows point to these points into the zoomed area. Letters at the time axis indicate time cuts as they correspond to the individual panels in Figure 2 (illustrative example only; the order of the regions matches that as depicted in Figure 2 but their widths – in $\boldsymbol{x}$ axis – do not). Cf. Figure 2 and text for more details on the characteristic concentration profiles regions and critical time points.

Figure 2: The solution to eq. (5). Concentration profiles calculated for a real system with composition given in Materials and methods section. Initial sample width: 3 mm; Individual panels display the solution at four separation times: A) 7 s, B) 450 s, C) 12000 s and D) 20000 s. The separation times are schematically indicated on the time axis in Figure 1. Bracketed letters indicate regions of characteristic concentration profiles, cf. Figure 1 and text. Blue and red concentration profiles correspond to the slower (1) and the faster (2) analyte, respectively, and $S_{(D)}$ and $S_{(S)}$ are the respective shock boundaries.

Figure 3: Characteristic parameters used for quantification and discussion of the displacement and the tag along effect are indicated in black letters. Points, where these parameters are to be read from the concentration profiles are indicated with squares. The two-side arrow marks the width of the plateau region (V). Data identical to Figure 2, panel B), 450 s.

For Peer Review

Figure 4: Comparison of simulated electropherograms and electropherograms predicted by NEM in x-domain (inside the capillary). Panels A) and C) predicted by NEM and simulated, respectively, concentration profiles at 7 s. Panels B) and D) those at 450 s. Blue and red concentration profiles: analyte 1 (FLU) and analyte 2 (NAP), respectively. NEM data identical to Figure 2. Simulation conditions given in Materials and methods section.

Figure 5: Experimental (A), simulated (B), and predicted by NEM (C), concentration profiles of FLU (blue line) and NAP (red line). Experimental and simulation conditions described in Materials and methods section. Experimental signals of individual analytes (FLU and NAP) obtained by signal decomposition at two different wavelengths (procedure described in Supporting information).

For Peer Review

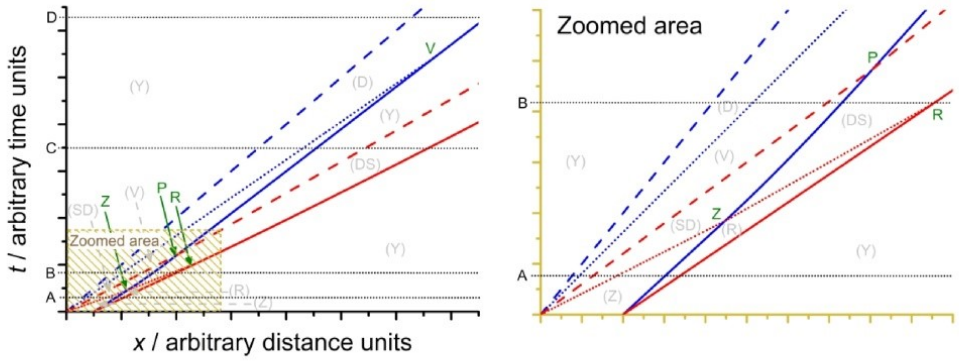


Figure 1: A schematic x-t diagram displayed in arbitrary units assuming $\kappa_1<0$ and $\kappa_2<0$. The diagram covers characteristic features of the solution to eq. (5). Blue and red lines indicate migration of characteristic points in the concentration profile of the slower (1) and the faster (2) analyte, respectively. Solid: the shock boundaries; Dashed: the points where the diffuse boundaries rise from the baseline; Dotted: the points where the diffuse boundaries reach the temporary plateau zone (V), (Z) or (R). Shadow bracketed letters indicate regions of characteristic concentration profiles, shadow dashed arrows point to these regions into the zoomed area. Green letters indicate critical points (times) where the solution changes qualitatively, green solid arrows point to these points into the zoomed area. Letters at the time axis indicate time cuts as they correspond to the individual panels in Figure 2 (illustrative example only; the order of the regions matches that as depicted in Figure 2 but their widths – in x axis – do not). Cf. Figure 2 and text for more details on the characteristic concentration profiles regions and critical time points.

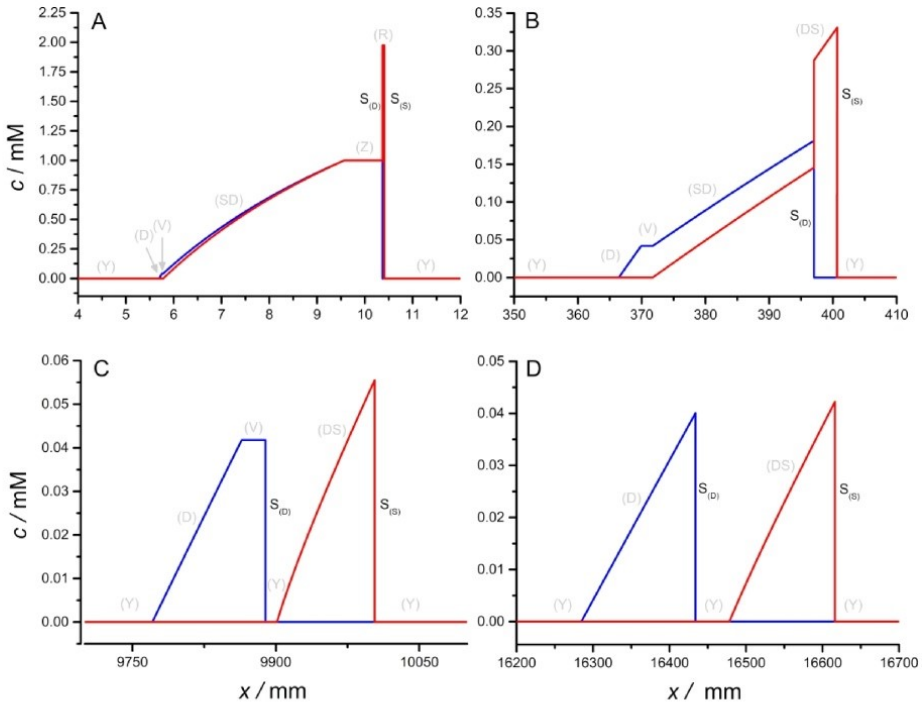


Figure 2: The solution to eq. (5). Concentration profiles calculated for a real system with composition given in Materials and methods section. Initial sample width: 3 mm; Individual panels display the solution at four separation times: A) 7 s, B) 450 s, C) 12000 s and D) 20000 s. The separation times are schematically indicated on the time axis in Figure 1. Bracketed letters indicate regions of characteristic concentration profiles, cf. Figure 1 and text. Blue and red concentration profiles correspond to the slower (1) and the faster (2) analyte, respectively, and S(D) and S(S) are the respective shock boundaries.

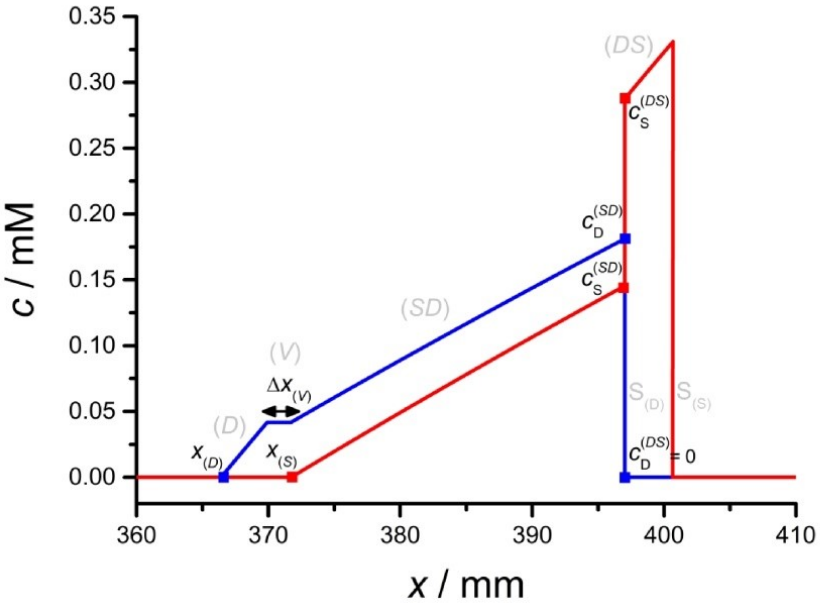


Figure 3: Characteristic parameters used for quantification and discussion of the displacement and the tag along effect are indicated in black letters. Points, where these parameters are to be read from the concentration profiles are indicated with squares. The two-side arrow marks the width of the plateau region (V). Data identical to Figure 2, panel B), 450 s.

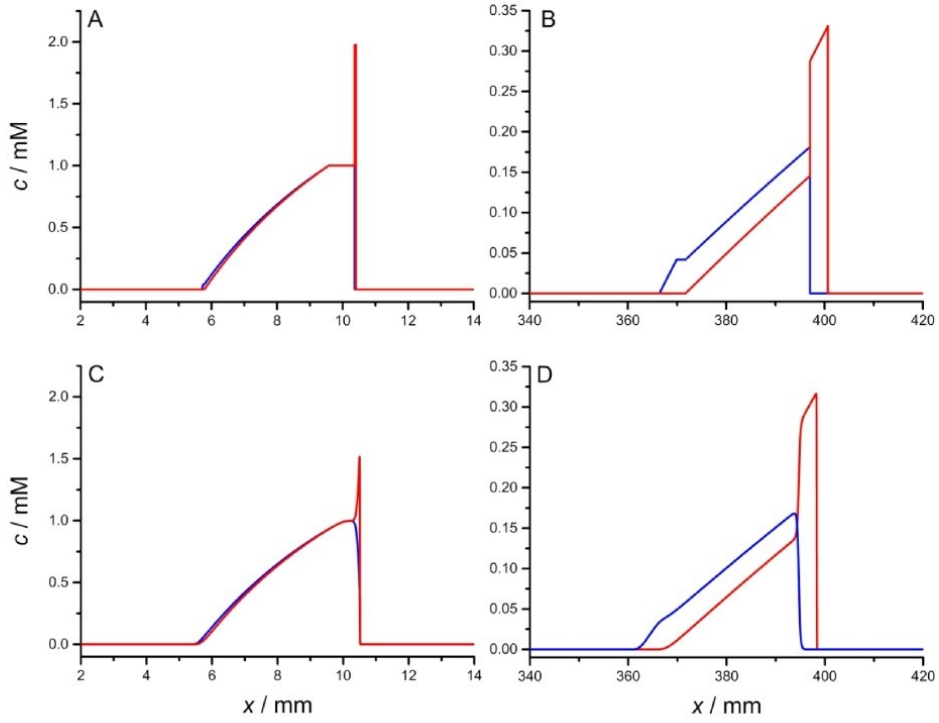


Figure 4 Comparison of simulated electropherograms and electropherograms predicted by NEM in x-domain (inside the capillary). Panels A) and C) predicted by NEM and simulated, respectively, concentration profiles at 7 s. Panels B) and D) those at 450 s. Blue and red concentration profiles: analyte 1 (FLU) and analyte 2 (NAP), respectively. NEM data identical to Figure 2. Simulation conditions given in Materials and methods section.

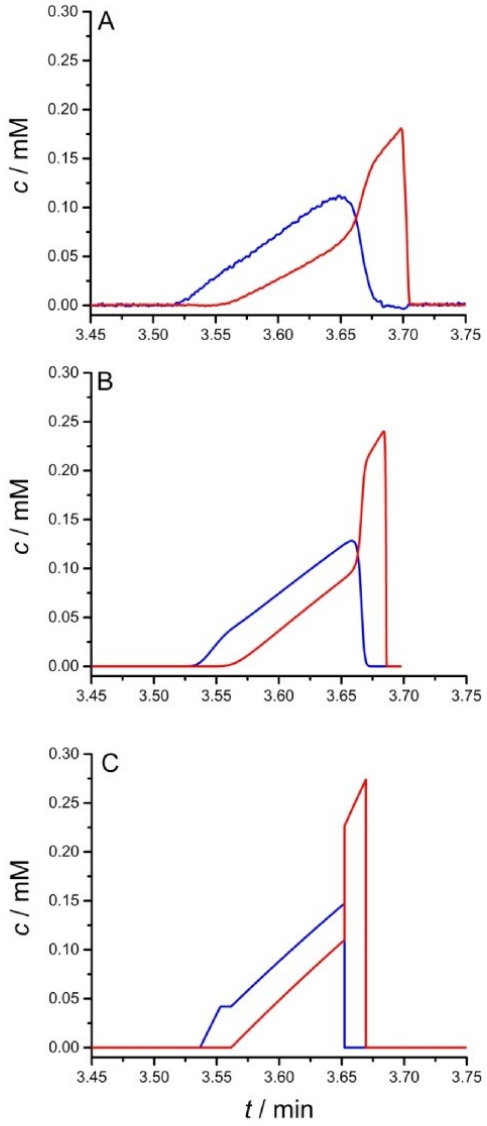


Figure 5: Experimental (A), simulated (B), and predicted by NEM (C), concentration profiles of FLU (blue line) and NAP (red line). Experimental and simulation conditions described in Materials and methods section. Experimental signals of individual analytes (FLU and NAP) obtained by signal decomposition at two different wavelengths (procedure described in Supporting information).

5 Závěr

Předkládaná disertační práce se ve své první části věnuje problematice vyhodnocení experimentálních elektroferogramů a jejich interpretaci. V rámci této disertační práce byla navržena nová veličina pro objektivní kvantifikaci rozsahu separace dvojice píků v kapilárních a kolonových separačních metodách, nazvaná ekvivalentní rozlišení. Definice ekvivalentního rozlišení je zobecněním dobře známého a běžně používaného vztahu pro rozlišení dvojice identických píků s Gaussovým rozdělením koncentračních profilů. Ekvivalentní rozlišení dobře popisuje rozsah separace i v případě, kdy píky mají značně odlišné plochy. Hodnota ekvivalentního rozlišení 1,5 přitom odpovídá dvojici píků, které jsou odděleny až na základní linii. Dále byla navržena metoda pro získání parametrů HVL funkce, která je založena na geometrických vlastnostech HVL funkce a nevyžaduje provádění nelineární regrese. Tím značně usnadňuje a urychluje vyhodnocení experimentálních elektroferogramů.

Druhá část disertační práce byla zaměřena na zobecnění a rozšíření současných aproximativních modelů kapilární elektroforézy. Model NLTEM, což je analyticky řešitelný nelineární model kapilární elektroforézy zahrnující příspěvky jak elektromigrace, tak difúze, byl rozšířen tak, aby plně zahrnul komplexační rovnováhy a umožnil popis kapilární elektromigrační chromatografie. Rozšířený model NLTEM byl implementován do programu PeakMaster 6, který umožňuje získat téměř okamžitou a přitom velmi přesnou předpověď výsledku kapilárně elektroforetického experimentu. Správnost rozšířeného modelu NLTEM a programu PeakMaster 6 byla ověřena porovnáním předpovědí programu PeakMaster 6 a elektroferogramů získaných numerickým řešením úplných elektroforetických rovnic kontinuity a rovnic chemické rovnováhy v programu Simul. Byla pozorována velmi dobrá shoda mezi předpovědí programu PeakMaster 6 a numerickým řešením.

Dále byl diskutován vztah mezi modelem NLTEM a modelem NEM, který na rozdíl od NLTEM sice nezahrnuje difúzi, ale zato umožňuje podstatně přesnější popis elektromigrační disperze. Bylo ukázáno, že po vypuštění příspěvku difúze v modelu NLTEM a za předpokladu konstantní hodnoty pH v celé kapiláře, představuje NLTEM aproximaci prvního řádu k modelu NEM. Model NEM byl následně rozšířen tak, aby umožnil popis vzájemné komigrace libovolného počtu analytů. Pro speciální případ dvou

komigrujících analytů bylo nalezeno řešení tohoto modelu. Byla diskutována formální podobnost modelu NEM a ideálního modelu chromatografie s Langmuirovou izotermou. Pozornost byla věnována deformacím píků analytů, displacement efektu a tag along efektu, které jsou důsledkem vzájemné interakce mezi píky analytů. Bylo podáno teoretické vysvětlení jejich vzniku a uvedeny vztahy mezi intenzitou těchto deformací a počátečními koncentracemi analytů, respektive jejich elektroforetickými mobilitami. Správnost rozšířeného modelu NEM byla ověřena porovnáním elektroferogramu vypočteného podle NEM, elektroferogramu získaného numerickým řešením elektroforetických rovnic kontinuity a rovnic chemické rovnováhy v programu Simul a experimentálního elektroferogramu. Experimentální a nasimulovaný elektroferogram vykazovaly všechny charakteristické znaky a deformace předpovězené modelem NEM.

Přílohy

Seznam publikací

1. A nonlinear electrophoretic model for PeakMaster: Part IV. Electromigration dispersion in systems that contain a neutral complex-forming agent and a fully charged analyte. Experimental verification
Martin Beneš, Jana Svobodová, Vlastimil Hruška, **Martin Dvořák**, Iva Zusková, Bohuslav Gaš
Journal of Chromatography A 2012, *1267*, 109 - 115

2. Applicability and limitations of affinity capillary electrophoresis and vacancy affinity capillary electrophoresis methods for determination of complexation constants
Martin Dvořák, Jana Svobodová, Martin Beneš, Bohuslav Gaš
Electrophoresis 2013, *34*, 761-767

3. Generalized model of electromigration with 1:1 (analyte:selector) complexation stoichiometry: Part I. Theory
Pavel Dubský, Ludmila Müllerová, **Martin Dvořák**, Bohuslav Gaš
Journal of Chromatography A 2015, *1384*, 142 – 146

4. Equivalent peak resolution: Characterization of the extent of separation for two components based on their relative peak overlap
Martin Dvořák, Jana Svobodová, Pavel Dubský, Martina Riesová, Gyula Vigh, Bohuslav Gaš
Electrophoresis 2015, *36*, 646-654

5. Determination of the correct migration time and other parameters of the Haarhoff-van der Linde function from the peak geometry characteristics
Pavel Dubský, **Martin Dvořák**, Ludmila Müllerová, Bohuslav Gaš
Electrophoresis 2015, *36*, 655 – 661

6. Affinity capillary electrophoresis: the theory of electromigration
Pavel Dubský, **Martin Dvořák**, Martin Ansorge
Analytical and Bioanalytical Chemistry 2016, *408*, 8623 – 8641

7. Generalized model of the linear theory of electromigration and its application to electrokinetic chromatography: Theory and software PeakMaster 6 – Next Generation
Michal Malý, Magda Dovhunová, **Martin Dvořák**, Gabriel S. Gerlero, Pablo A. Kler, Vlastimil Hruška, Pavel Dubský
Electrophoresis 2019, *40*, 683 - 692

8. The dynamics of band (peak) shape development in capillary zone electrophoresis in light of the linear theory of electromigration
Martin Dvořák, Pavel Dubský, Magda Dovhunová, Bohuslav Gaš
Electrophoresis 2019, *40*, 668 – 682

9. The dynamics of band (peak) shape development in capillary zone electrophoresis in the case of two co-migrating analytes: the displacement and tag along effects
Martin Dvořák, Michal Kalus, Pavel Dubský, Magda Dovhunová, Bohuslav Gaš
Electrophoresis 2019, submitováno 21.6.2019, elps.201900225

Seznam konferenčních příspěvků

Postery

1. Generalized Resolution: the Correct Way to Comparably Describe Separation of Nonidentical or Distorted Peaks
Martin Dvořák, Jana Svobodová, Pavel Dubský, Martina Riesová, Bohuslav Gaš
ITP 2013 – 20th International Symposium on Electro- and Liquid Phase- Separation Techniques, říjen 2013, Tenerife, Španělsko

2. Effective Mobility of Analytes as a Function of pH in Capillary Electrophoresis Dual Selector Separation Systems
Martin Dvořák, Ludmila Müllerová, Pavel Dubský, Bohuslav Gaš
ITP & LACE 2014 – 21th International Symposium on Electro- and Liquid Phase-Separation Techniques, 20th Latin-American Symposium on Biotechnology, Biomedical, and Industrial Applications of Capillary Electrophoresis and Microchip Technology, říjen 2014, Natal, Brazílie

3. Interaction of Two Analytes in Capillary Electrophoresis: Nonlinear Effects
Martin Dvořák, Pavel Dubský, Gyula Vigh
HPLC 2016 – 44th International Symposium on High-Performance Liquid Phase Separations and Related Techniques, červen 2016, San Francisco, USA

Literatura

[1] Kohlrausch, F., *Ann. Phys.* 1987, *62*, 209-239

[2] Kanoatov, M., Cherney, L. T., Krylov, S. N., *Anal. Chem.* 2014, *86*, 1298-1305

[3] Mironov, G. G., Okhonin, V., Gorelsky, S. I., Berezovski, M. V., *Anal. Chem.* 2011, *83*, 2364-2370

[4] Štědrý, M., Jaroš, M., Gaš, B., *J. Chromatogr. A* 2002, *960*, 187-198

[5] Štědrý, M., Jaroš, M., Včeláková, K., Gaš, B., *Electrophoresis* 2003, *24*, 536-547

[6] Štědrý, M., Jaroš, M., Hruška, V., Gaš, B., *Electrophoresis* 2004, *25*, 3071-3079

[7] Poppe, H., *J. Chromatogr. A* 1990, *506*, 45-60

[8] Poppe, H., *Anal. Chem.* 1992, *64*, 1908-1919

[9] Horká, M., Šlais, K., *Electrophoresis* 2000, *21*, 2814-2827

[10] Hruška, V., Riesová, M., Gaš, B., *Electrophoresis* 2012, *33*, 923-930

[11] Haarhoff, P. C., Van der Linde, H. J., *Anal. Chem.* 1966, *38*, 573-582

[12] Erny, G. L., Bergström, E. T., Goodall, D. M., Grieb, S., *Anal.Chem.* 2001, *73*, 4862-4872

[13] Erny, G. L., Bergtsröm, E. T., Goodall, D. M., *J. Chromatogr. A* 2002, *959*, 229-239

[14] Hruška, V., Svobodová, J., Beneš, M., Gaš, B., *J. Chromatogr. A* 2012, *1267*, 102-108

[15] Hruška, V., Jaroš, M., Gaš, B., *Electrophoresis* 2006, *27*, 984-991

[16] Mosher, R. A., Dewey, D., Thormann, W., Saville, D. A., Bier M., *Anal. Chem.* 1989, 61, 362-366

[17] Breadmore, M. C., Quirino, J. P., Thormann, W., *Electrophoresis* 2009, 30, 570-578

[18] Bercovici, M., Lele, S.K., Santiago, J.G., *J. Chromatogr. A* 2009, 1008-1018

[19] Mikkers, F. E. P., Everaerts, F. M., Vergheggen, T. P. E. M., *J. Chromatogr.* 1979, *169*, 1-10

[20] Mikkers, F. E. P., *Anal. Chem.* 1999, *71*, 522-533

[21] Xu, X., Kok, W. T., Poppe, H., J. Chromatogr. A 1996, *742*, 211-227

[22] Le Saux, T., Varenne, A., Gareil. P., *Electrophoresis* 2005, *26*, 3094-3104

[23] Desty, D. H., *Proceedings of the second symposium organized by the Gas Chromatography Discussion Group under the auspices of the Hydrocarbon Research Group of the Institute of Petroleum and the Koninklijke Nederlandse Chemische Verenging,* held at the Royal Tropical Institute, Amsterdam, 19-23 May 1958; Butterworths Scientific, London 1958

[24] Snyder, L. R., Kirkland, J. J., Glajch, J. L., *Practical HPLC*, druhé vydání, John Wiley & Sons, Inc., New York 1991, strany 86 - 108

[25] Schoenmakers, P. J., Strasters, J. K., Bartha, A., *J. Chromatogr.* 1988, *458*, 355-370

[26] Dose, E. V., Guiochon, G., *Anal. Chem.* 1990, *62*, 174-181

[27] Hruška, V., Beneš, M., Svobodová, J., Zusková, I., Gaš, B., *Electrophoresis* 2012, *38*, 938-947

[28] Kapitola <621>, United States Pharmacopeia 34, 2011, United States Pharmacopeia Convention, ISBN 37-692-5390-6

[29] DeVault, D., *J. Am. Chem. Soc.* 1943, *65*, 532-540

[30] Rhee, H.-K., Aris, R., Amundson, N. R., *Philos. Trans. R. Soc. London Ser A* 1970, *267*, 419-455

[31] Glueckauf, E., *Proc. Roy. Soc.*1946, *A186*, 35-57

[32] Golshan-Shirazi, S., Guiochon, G., *J. Phys. Chem.* 1989, 93, 4143-4157